THE MICROBIAL ECOLOGY OF NITROUS OXIDE PRODUCTION IN MARINE ENVIRONMENTS: LINKING COMMUNITY DYNAMICS TO ECOSYSTEM PROCESSES

by

Brett Douglas Jameson
B.Sc., Dalhousie University, 2016

A Dissertation Submitted in Partial Fulfillment of the
Requirements for the Degree of

DOCTOR OF PHILOSOPHY

in the School of Earth and Ocean Sciences

THE MICROBIAL ECOLOGY OF NITROUS OXIDE PRODUCTION IN MARINE ENVIRONMENTS: LINKING COMMUNITY DYNAMICS TO ECOSYSTEM PROCESSES

by

Brett Douglas Jameson
B.Sc., Dalhousie University, 2016

Supervisory Committee

Dr. S. Kim Juniper (Ocean Networks Canada; University of Victoria, Department of Biology and School of Earth & Ocean Sciences)
Co-supervisor

Dr. Catherine J. Stevens (University of Victoria, School of Earth & Ocean Sciences)
Co-supervisor

Dr. Roberta C. Hamme (University of Victoria, School of Earth & Ocean Sciences)
Departmental Member

Dr. Caren C. Helbing (University of Victoria, Department of Biology)
Outside Member

Dr. Damian S. Grundle (Bermuda Institute of Ocean Sciences)
External Member

Dr. Réal Roy (University of Victoria, Department of Biology)
Additional Member

Abstract

Nitrous oxide (N_2O) is an increasingly abundant, atmospheric trace-gas that contributes to climate change and stratospheric ozone depletion. Marine environments act as a net source of N_2O to the atmosphere at global scales resulting from the combined microbial processes of nitrification and denitrification. Considerable effort has been directed toward understanding the environmental drivers of N_2O production and consumption in the ocean over the past few decades. However, comparatively little is known about the ecological mechanisms that facilitate N_2O cycling in marine environments and how this relates to environmental variability. This research attempts to resolve some of these knowledge gaps by leveraging modern molecular tools and biogeochemical rate measurements to identify links between microbial community dynamics and N_2O production across a wide range of marine environments.

The first data chapter considers Saanich Inlet, a seasonally anoxic fjord located on Vancouver Island, Canada, as a model oxygen deficient zone for investigating patterns of microbial community assembly in relation to variable N_2O production rates across spatial and temporal redox gradients. Network analysis of prokaryote 16S rRNA amplicon sequences delineated discrete community subnetworks that were structured around several putative keystone taxa and displayed contrasting water column distributions and roles in N_2O cycling. Keystone taxa implicated in coupled carbon, nitrogen, and sulfur cycling were prominent in the low-oxygen subnetwork and correlated well with N_2O production from denitrification in waters demonstrating net N_2O consumption. Conversely, oxycline subnetworks were characterized by keystone aerobic heterotrophs that correlated with nitrification rates and water column N_2O accumulation. This work presents a first assessment of the relationships between microbial community interaction networks and N_2O cycling rate processes in the ocean.

The remainder of this dissertation focuses on N_2O cycling in sediment environments, which can act as net sources or sinks of N_2O at local scales. The third chapter resolves an important data gap with respect to N_2O fluxes from continental margin sediments underlying the northeast subarctic Pacific (NESAP) oxygen deficient zone, a previously unstudied environment with respect to N_2O cycling. This work reports the first sub-millimeter resolution porewater N_2O profiles in offshore sediments and employs a profile interpretation model to demonstrate that these environments are a considerable source of N_2O to the water column. Finally, experimental manipulations provided evidence that upwelling conditions can stimulate N_2O production and efflux from continental shelf sediments.

Chapter Four builds on this work by adapting this procedure for work at low N_2O concentrations to quantify the N_2O sink capacity of minimally impacted mangrove sediments. Molecular data collected from both the mangrove and NESAP continental margin sediments was then used to identify relationships between microbial community dynamics and sediment N_2O source/sink status. Mangrove N_2O sinks had higher abundances and expression levels of 'atypical' N_2O reductases (*nosZII*), suggesting that net N_2O consumption in nitrogen-limiting systems may be driven by non-denitrifying N_2O scavengers. *NosZII* was associated with taxonomic groups implicated in dissimilatory nitrate reduction to ammonium (DNRA), a prominent nitrogen conservation pathway in nitrogen-limiting systems. N_2O source sediments from the NESAP contained higher abundances of putative ammonia oxidizing Archaea and were associated with elevated expression levels of typical *nosZI* variants, suggesting likely contributions from nitrification and denitrification.

Table of Contents

List of Tables

List of Figures

Acknowledgements

In some sense this section has been the most challenging for me to write. This is not for lack of inspiration, but it is difficult to find adequate words to describe the level of gratitude I have for the people who have made this accomplishment possible. With that being said, I will try my best.

To my supervisor, Kim Juniper, thank you for taking a chance on me and for your countless hours of guidance. There are few people in this world that have had as profound and lasting impact on me as you have; I am a better person for having had the opportunity to learn from your example. Thank you to my co-supervisor, Catherine Stevens, for offering not only your wisdom and expertise, but also your friendship. Your constant support has lightened the burden of graduate school in more ways than I can name. To my friend and mentor, Damian Grundle, your faith in my abilities has been a consistent source of confidence for me and your presence has filled this journey with much joy. I would certainly not be where I am today without the time and resources you invested in my development.

I would also like to express my heartfelt appreciation and respect for the remainder of my committee members. Thank you to Roberta Hamme for including me in regular lab discussions, and for always making time to meet with me. Your insights and thought-provoking questions have expanded my understanding of our oceans and always encourage me to think deeper. To Réal Roy, thank you for the many hours of conversation and for the stimulating discussions on the mysteries of the microbial realm. Your passion for science and capacity for knowledge is inspirational, and you carry yourself with a light-heartedness that is infectious to those around you. Thank you also to Caren Helbing for your mentorship, generosity, and attentiveness. The time I spent learning from you and your lab has equipped me with an invaluable skillset and has changed the way I view scientific inquiries of the biological world. To my committee as a whole, studying under your guidance has been one of the greatest privileges of my lifetime.

A massive thank you also goes out to the other members of the Juniper Lab. To Sheryl Murdock, thank you for putting up with all my questions and for all the time you dedicated toward helping me in the lab. To Moronke Harris, thank you for being the realest one around. You breathed life into the department when you arrived on campus and have helped to construct a supportive

environment for everyone that calls SEOS home. To the remainder of the SEOS department, thank you for the community you have provided and for filling the journey with laughs and good times.

I would also like to take this opportunity to thank all the funding agencies and institutions that have made this work possible, including the University of Victoria, the Bermuda Institute of Ocean Sciences, the National Sciences and Engineering Research Council, the Canadian Healthy Oceans Network, and Ocean Networks Canada. Thank you to the many private donors for who have provided financial support, including the M.A. & D.E. Breckenridge, Donald Wagg, Alexander & Helen Stafford McCarthy Muir, and Alfred & Adriana Potvin scholarship funds. A thank you also goes out to the captains and crew of the CCGS John P. Tully, E/V Nautilus, and Strickland research vessels for facilitating and assisting with field work.

To my west coast family, including Sam van Ginkel, Justin Bryksa, Eric Taylor, Danny Olliver, Jarred Aasen, and Christian Wiebe, thank you for providing a place of refuge away from all the madness. A very special thank you goes out to Nicholas Sargeant and Sasha Goatley, who opened their hearts and their home to me in my darkest of days. To my absolute boys (whomst I adore), thank you for keeping me grounded and connected to my authentic self, and for always reminding me where I came from. Witnessing each of you move through life is a daily source of inspiration.

Last but certainly not least, I would like to thank my entire family back home for all that they have given me. To my parents Doug and Brenda, thank you for always believing in the best in me despite my early attempts to prove you otherwise. You provided a loving and nurturing home, and gave me the space I needed to explore myself and find my passion. Finally, to my sisters Haylee (a.k.a Lil Jame) and Michelle (a.k.a Chelle Dawg), thank you for your unconditional love and support, and for always being there for me when I need you.

This has been the ride of a lifetime, thank you all for tagging along.

As you were,

Jame

Dedication

This dissertation is lovingly dedicated to my parents, Doug and Brenda, for whom I have the utmost respect and admiration. Your unwavering support has made achieving this dream possible and has strengthened my resolve in times of doubt.

It is also dedicated to the many who have come before me and to the many who will follow.

“If I have seen further than others, it is by standing upon the shoulders of giants”

-Sir Isaac Newton

Chapter 1: Introduction

1.1 Nitrous Oxide in the Marine Environment

Nitrous oxide (N_2O) is an increasingly abundant, ozone-depleting greenhouse gas with an atmospheric warming potential that is roughly 300 times more potent than carbon dioxide over a 100-year timeframe (Arias et al., 2021; Jain et al., 2000). Atmospheric concentrations have risen by more than 20 per cent since the industrial revolution, with the most rapid growth observed over the previous five decades (Table 1.1 IPCC 2021 global N2O budget.; IPCC, 2021; Prinn et al., 2018; Tian et al., 2020). Although a proportion of the annual emissions can be attributed to fossil fuel combustion and industrial processes, the majority results from microbial metabolic activities in terrestrial, freshwater, and marine environments (Table 1.1; IPCC, 2021; Tian et al., 2020). Most studies of biogenic N_2O production have focused on terrestrial systems, with added emphasis placed on agricultural soils that contribute disproportionately to anthropogenically-driven N_2O emissions (Table 1.1). Increasing effort has been directed in recent years toward aquatic environments, as empirical observations and biogeochemical models continue to highlight their importance to regional and global N_2O budgets (Arévalo-Martínez et al., 2015a; Freing et al., 2012; Ji et al., 2018). Current estimates suggest a combined source of 4.4 Tg-N yr^{-1} from open oceans and coastal regions that accounts for approximately 25% of total annual emissions (Table 1.1).

The biological production of N_2O in the ocean occurs when microbial communities catalyze transformations of fixed nitrogen substrates across environmental gradients (Fig. 1.1). N_2O is produced as a by-product of ammonia oxidation by nitrifying bacteria and archaea in the presence of oxygen, and as a metabolic intermediate of the denitrification pathway under suboxic

and anoxic conditions (Bange et al., 2010). The reduction of N_2O to dinitrogen gas (N_2) during the final step of denitrification is the only known biological sink for N_2O, and can drive pronounced

Table 1.1 IPCC 2021 global N_2O budget.

A comprehensive list of global anthropogenic and natural N_2O sources, and natural N_2O sinks averaged over the 1980s, 1990s, 2000s, and the period from 2007-2016. Uncertainties are given in parentheses and correspond to the range of source/sink estimates. Table was reproduced from IPCC (2021) and Tian et al. (2020). Emissions totals are bolded for anthropogenic, natural, and overall sources. Observed growth rates and inferred stratospheric sinks are also bolded.

	AR6 1980-1989 (Tg-N yr^{-1})	AR6 1990-1999 (Tg-N yr^{-1})	AR6 2000-2009 (Tg-N yr^{-1})	AR6 2007-2016 (Tg-N yr^{-1})
	Anthropogenic sources			
Fossil fuel combustion and Industry	0.9 (0.8 to 1.1)	0.9 (0.9 to 1.0)	1.0 (0.8 to 1.0)	1.0 (0.8 to 1.1)
Agriculture (incl. aquaculture)	2.6 (1.8 to 4.1)	3.0 (2.1 to 4.8)	3.4 (2.3 to 5.2)	3.8 (2.5 to 5.8)
Biomass and biofuel burning	0.7 (0.7 to 0.7)	0.7 (0.6 to 0.8)	0.6 (0.6 to 0.6)	0.6 (0.5 to 0.8)
Wastewater	0.2 (0.1 to 0.3)	0.3 (0.2 to 0.4)	0.3 (0.2 to 0.4)	0.4 (0.2 to 0.5)
Inland water, estuaries, coastal zones	0.4 (0.2 to 0.5)	0.4 (0.2 to 0.5)	0.4 (0.2 to 0.6)	0.5 (0.2 to 0.7)
Atmospheric nitrogen deposition on ocean	0.1 (0.1 to 0.2)	0.1 (0.1 to 0.2)	0.1 (0.1 to 0.2)	0.1 (0.1 to 0.2)
Atmospheric nitrogen deposition on land	0.6 (0.3 to 1.2)	0.7 (0.4 to 1.4)	0.7 (0.4 to 1.3)	0.8 (0.4 to 1.4)
Other indirect effects from CO2, climate and land-use change	0.1 (–0.4 to 0.7)	0.1 (–0.5 to 0.7)	0.2 (–0.4 to 0.9)	0.2 (–0.6 to 1.1)
Total anthropogenic	**5.6 (3.6 to 8.7)**	**6.2 (3.9 to 9.6)**	**6.7 (4.1 to 10.3)**	**7.3 (4.2 to 11.4)**
	Natural sources and sinks			
Rivers, estuaries, and coastal zones	**0.3 (0.3 to 0.4)**	**0.3 (0.3 to 0.4)**	**0.3 (0.3 to 0.4)**	**0.3 (0.3 to 0.4)**
Open oceans	**3.6 (3.0 to 4.4)**	**3.5 (2.8 to 4.4)**	**3.5 (2.7 to 4.3)**	**3.4 (2.5 to 4.3)**
Soils under natural vegetation	5.6 (4.9 to 6.6)	5.6 (4.9 to 6.5)	5.6 (5.0 to 6.5)	5.6 (4.9 to 6.5)
Atmospheric chemistry	0.4 (0.2 to 1.2)	0.4 (0.2 to 1.2)	0.4 (0.2 to 1.2)	0.4 (0.2 to 1.2)
Surface sink	–0.01 (–0.3 to 0)	–0.01 (–0.3 to 0)	–0.01 (–0.3 to 0)	–0.01 (–0.3 to 0)
Total natural	**9.9 (8.5–12.2)**	**9.8 (8.3–12.1)**	**9.8 (8.2–12.0)**	**9.7 (8.0–12.0)**
Total source	**15.5 (12.1 to 20.9)**	**15.9 (12.2 to 21.7)**	**16.4 (12.3 to 22.4)**	**17.0 (12.2 to 23.5)**
Observed growth rate			**3.7 (3.7 to 3.7)**	**4.5 (4.3 to 4.6)**
Inferred stratospheric sink			**12.9 (12.2-13.5)**	**13.1 (12.4–13.6)**

undersaturation in some anoxic and suboxic water columns (Bange, 2008). Hotspots of N_2O production and sea-air effluxes are commonly observed in waters of highly productive

oceanographic regions, such as mesoscale eddies and oxygen minimum zones (OMZs) associated with eastern boundary upwelling systems (**Error! Reference source not found.**) (Arévalo-Martínez et al., 2015; Grundle et al., 2017; Ji et al., 2018). In these environments, high rates of organic matter remineralization drive steep redox gradients, rapid nitrogen cycling, and high N_2O production yields from nitrification and denitrification.

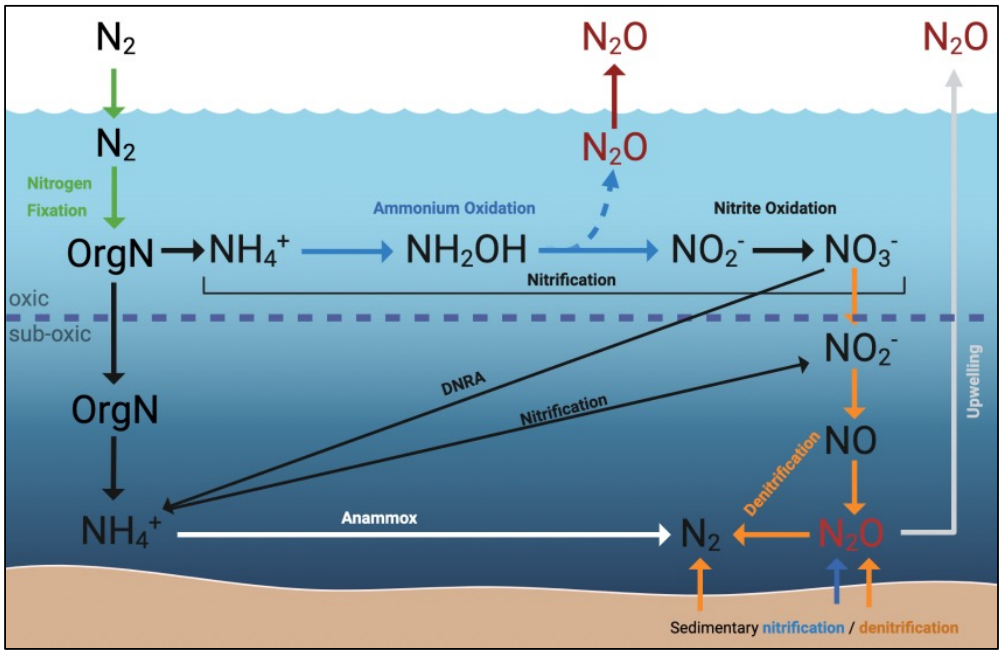

Fig. 1.1 The marine nitrogen cycle.

Core redox reactions responsible for biogeochemical nitrogen cycling in marine water columns and sediments. Pathways are color coded, with emphasis placed on metabolic pathways leading to N_2O production and consumption. Figure was modified from Arrigo (2005) and Sollai et al. (2015) and created in BioRender.

Estimates of net N_2O emissions from marine ecosystems are still associated with a large degree of uncertainty despite attracting substantial interest from the scientific community (Bange et al., 2019). This is, in part, a consequence of limited data coverage across marine environments and an incomplete understanding of the environmental and biological factors that regulate N_2O cycling by microbial organisms. As a result, how the marine N_2O cycle will respond to combined

anthropogenic forcing including upper ocean stratification, ocean deoxygenation, and eutrophication remains uncertain. Evidence suggest that marine OMZs are increasing in extent and severity in recent decades, which may be expected to increase N_2O production globally (Codispoti, 2010; Crawford & Peña, 2013; Paulmier & Ruiz-Pino, 2009; Stramma et al., 2008). However, some models predict reductions in net oceanic N_2O emissions caused by stratification-induced decreases in organic matter export and vertical mixing (Battaglia & Joos, 2018; Landolfi et al., 2017; Martinez-Rey et al., 2015). Accurate projecting of future N_2O emissions scenarios will require better constraints on present day N_2O fluxes and a robust understanding of how microbial communities respond to environmental variability, and how community dynamics regulate the balance between N_2O production and consumption across a broad range of marine ecosystems.

1.2 N_2O production pathways

1.2.1 Nitrification

Nitrification describes the oxidation of ammonia (NH_3) to nitrate (NO_3^-) by the combined activities of chemolithotrophic ammonia oxidizing bacteria and archaea (AOB and AOA), and nitrite (NO_2^-) oxidizing bacteria (NOB). The production of N_2O from nitrification is linked to the first step, whereby NH_3 is oxidized to NO_2^- via hydroxylamine (NH_2OH) as a metabolic intermediate (**Error! Reference source not found.**) (Bange et al., 2010; Kozlowski et al., 2016). Previous studies suggest a role for nitric oxide (NO) as a precursor to N_2O formation in both AOA and AOB, albeit through different mechanisms (Kozlowski et al., 2016; Martens-Habbena et al., 2015). During bacterial ammonia oxidation, a membrane-bound NH_3 monooxygenase enzyme complex (AMO) catalyzes the hydroxylation of NH_3 to NH_2OH which is followed by the subsequent oxidation of NH_2OH to NO_2^- by hydroxylamine oxidoreductase (HAO) (Sayavedra-

Soto & Arp, 2011). The prevailing view for AOB, based largely on *Nitrosomonas europea* cultures, suggested that N_2O production results from incomplete oxidation of NH_2OH by HAO, whereby nitric oxide (NO) arises as a by-product and is subsequently reduced to N_2O by respiratory NO-reductases (Caranto & Lancaster, 2017; Stein, 2011). However, recent work on purified HAO enzymes suggests that NO is the primary intermediate product preceding the formation of NO_2^- by abiotic means or by way of a presently unknown enzymatic step (Caranto & Lancaster, 2017). Under this model, the subsequent formation of N_2O arises abiotically through chemodenitrification, or enzymatically via NO reduction during nitrifier denitrification.

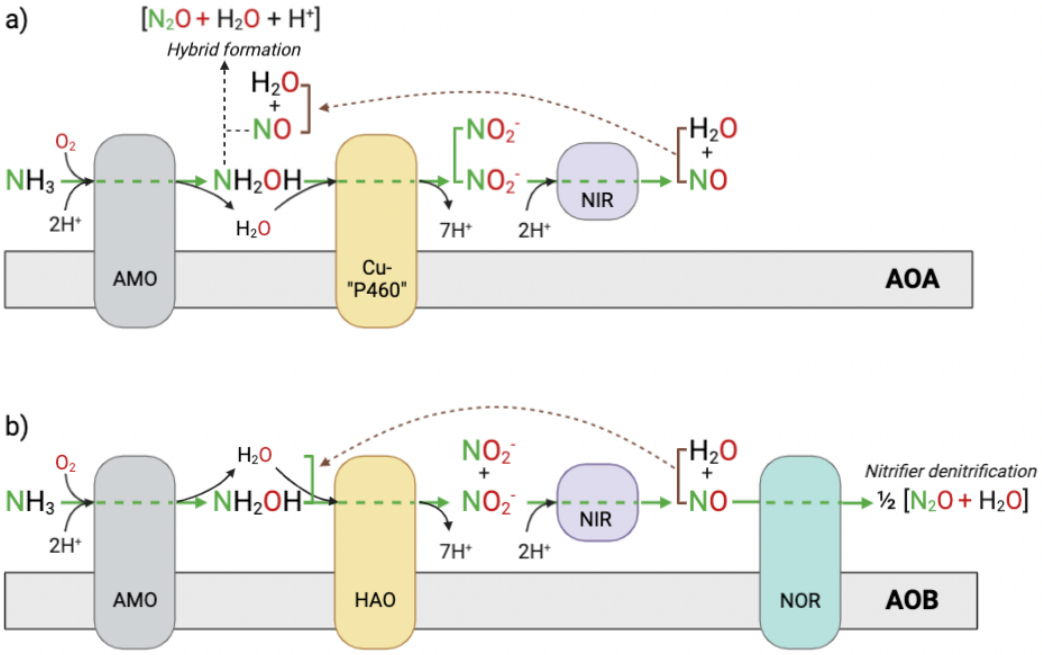

Fig. 1.2 Ammonia oxidation by AOA and AOB.

Simplified ammonia oxidation pathways by (a) ammonia-oxidizing Archaea (AOA) and (b) Bacteria (AOB) showing core enzymes and nitrogen transformations. Panel (a) depicts hybrid N_2O formation hypothesized for AOA. Panel (b) shows the prevailing view of enzymatic N_2O production by AOB involving reduction of NO_2^- to N_2O via nitrifier denitrification. AMO, ammonia monooxygenase; Cu-P460, tetraheme cytochrome c protein P460; HAO, hydroxylamine dehydrogenase; NIR, nitrite reductase; NOR, nitric oxide reductase. Figure adapted from Kozlowski et al. (2016)

Ammonia oxidation by AOA is also mediated through an AMO enzyme complex, yet the absence of homologous HAO sequences in the genomes of known AOA suggests a different mechanism of N_2O production (**Error! Reference source not found.**) (Tourna et al., 2011; Vajrala et al., 2013; Walker et al., 2010). This is supported by isotopic signatures of Archaea-produced N_2O which suggest a hybrid mode of formation that involves both NO and NH_2OH (Jung et al., 2014; Kozlowski et al., 2016; Stieglmeier et al., 2014; Trimmer et al., 2016). In contrast to AOB, NO appears to be generated from the reduction of NO_2^- by AOA nitrite reductases (*nirK*) as a means of driving NH_2OH oxidation to NO_2^- (Kozlowski et al., 2016). Indeed, AOA growth rates are inhibited in culture in the presence of NO-scavenging compounds, a finding that is not replicated for known AOB (Kozlowski et al., 2016; Martens-Habbena et al., 2015). Whether N_2O formation occurs enzymatically via some undetermined mechanism or abiotically has yet to be empirically determined (Kozlowski et al., 2016). Regardless of the precise mechanisms involved, elevated N_2O yields from nitrification are observed under oxygen-limiting conditions for both AOA and AOB (Frame & Casciotti, 2010; Hink et al., 2017; Löscher et al., 2012).

Marine nitrification was originally thought to be performed primarily by AOB affiliated with the β- and γ-proteobacteria until the isolation of *Nitrosopumilus maritimus* SCM1 from seawater aquariums provided the first evidence of archaeal ammonia oxidation (Könneke et al., 2005; Ward, 2002; Wuchter et al., 2006). Since then, AOA genes have been detected ubiquitously throughout terrestrial and aquatic environments and may represent as much as 30% of all marine microbes (Alves et al., 2018; Hatzenpichler, 2012). It is now generally accepted that ammonia oxidation is dominated by AOA in marine environments (Beman et al., 2012; Lam et al., 2009; Wuchter et al., 2006).

1.2.2 Denitrification

Heterotrophic denitrification (or canonical denitrification) is a respiratory process performed by facultative anaerobes capable of utilizing oxidized nitrogen substrates as terminal electron acceptors during organic matter oxidation (Devol, 2008; Knowles, 1982). Although much of the previous work has focused on this mode of denitrification, several chemolithotrophic bacteria have been described with the capacity to couple denitrification to sulfide or elemental sulfur oxidation (Murillo et al., 2014; Shah et al., 2019; Walsh et al., 2009). In both cases, the stepwise reduction of NO_3^- to dinitrogen gas (N_2) follows a defined order of reactions that lead to the production of N_2O as an obligatory free intermediate (**Error! Reference source not found.**) (Devol, 2008). These reactions are mediated by four well-studied enzyme complexes that are distributed broadly across the prokaryote phylogenetic tree and found ubiquitously throughout the environment (Graf et al., 2014; Wei et al., 2015; Zumft, 1997). Studies of natural populations also indicate that the denitrification pathway is highly modular, with many organisms possessing only a partial compliment of the genes required for complete denitrification (Graf et al., 2014).

Denitrification generally begins with the reduction of NO_3^- to NO_2^- by nitrate reductase enzymes (NAR), although the first step alone does not constitute 'denitrification' in a technical sense (Knowles, 1982; Zumft, 1997). The transformation of fixed nitrogen from its bioavailable form to gaseous form occurs during the reduction of NO_2^- to NO by nitrite reductases (NIR), which is further reduced to N_2O and N_2 by nitric oxide- and nitrous oxide reductases (NOR and NOS, respectively) (**Error! Reference source not found.**). Consequently, the net flux of N_2O from denitrification in any given environment is governed by the balance between its production and subsequent consumption. Oxygen thresholds for the onset of denitrification are not well constrained, but it is generally accepted that complete denitrification is favoured under anoxic and suboxic conditions ($O_2 < 5$ μmol L^{-1}) (Codispoti et al., 2001). However, evidence suggests that

enzymatic sensitivities to dissolved O_2 are highly variable across the denitrification pathway, with NOS enzymes demonstrating the lowest tolerance to the presence of O_2 (Bonin et al., 1989; Conrad, 1996).

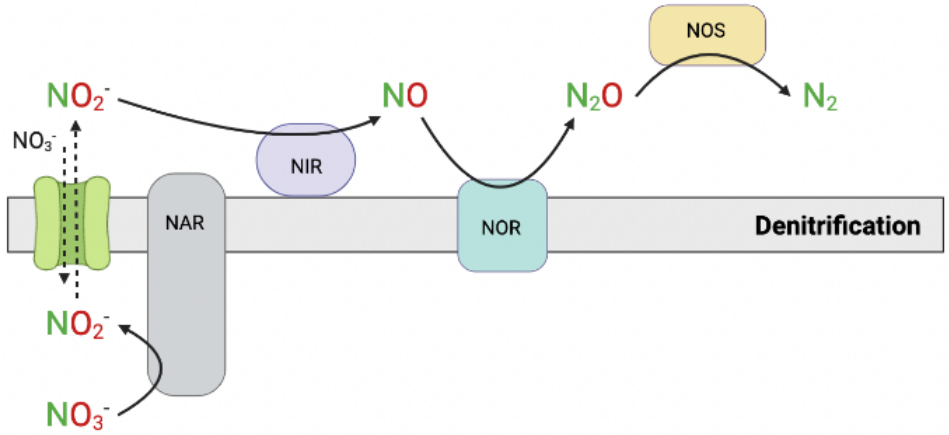

Fig. 1.3 Heterotrophic denitrification pathway.

The complete heterotrophic denitrification pathway highlighting the stepwise reduction of NO_3^- to N_2 gas by respiratory reductase enzymes. NAR, nitrate reductase; NIR, nitrite reductase; NOR, nitric oxide reductase; NOS, nitrous oxide reductase. Figure adapted from Robertson & Groffman, (2015).

1.3 N_2O in marine environments

1.3.1 N_2O in the water column

Approximately half of global oceanic N_2O production is attributable to open ocean water columns that are generally well oxygenated while the remaining half occurs in hypoxic and suboxic waters (Codispoti, 2010). Despite suggestions of a negligible or even absent N_2O source within the surface mixed layer, active N_2O production from reductive and oxidative pathways has been detected in surface waters of the mid-latitude North Atlantic (Ji & Ward, 2017). Surface N_2O concentrations outside of equatorial and coastal upwelling regions trend towards slight supersaturation, with considerable regional and seasonal variability in both the direction and magnitude of net N_2O fluxes (**Error! Reference source not found.**). (Suntharalingam &

Sarmiento, 2000; Yang et al., 2020). Poor spatiotemporal data coverage across large swaths of the ocean has complicated estimates of the contributions of global open ocean and surface waters to atmospheric N_2O emissions. Regardless, most oceanic N_2O is produced at subsurface depths where restricted ventilation and elevated O_2 demand from the oxidation of organic matter drives decreases in dissolved O_2 concentrations (Freing et al., 2012).

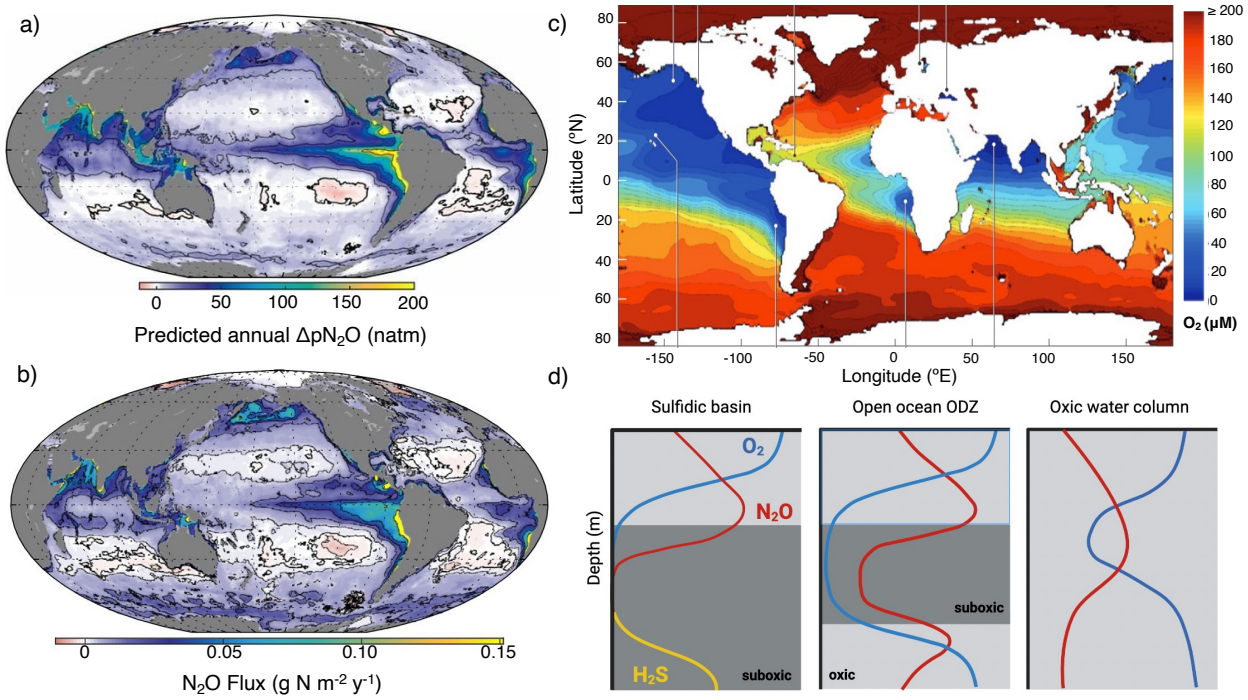

Fig. 1.4 Global oceanic N_2O and O_2 distributions.

Predicted global surface ΔpN_2O (a), surface N_2O fluxes (b), and ocean interior O_2 concentrations at the depth of the O_2 minimum (c). Panel d contains idealized water column N_2O, O_2, and H_2S profiles for sulfidic basins, open ocean ODZs, and oxygenated water columns. Panels a-b were adapted from Yang et al. (2020) (Figs 1 and 3, respectively). Panel (c) was modified from Wright et al. (2012).

In water columns that remain oxygenated throughout, subsurface N_2O maxima generally coincide with the NO_3^- maximum and O_2 minimum (**Error! Reference source not found.**d; Bange, 2008). Positive correlations between N_2O excess (ΔN_2O), apparent oxygen utilization (AOU) and NO_3^- concentrations in these regions implicate nitrification as the dominant N_2O

production pathway across most of the global ocean (Nevison et al., 2003; Yoshinari, 1976). Indeed, a recent study suggested that nitrification accounts for as much as 80% of the total oceanic N_2O production across open ocean and OMZ water columns (Ji et al., 2018). The distribution of N_2O in oxygenated deep waters below 2000 m follows a water mass age gradient, with *in situ* production from nitrification driving increasing concentrations moving from the North Atlantic Ocean to the North Pacific Ocean (Bange & Andreae, 1999; Toyoda et al., 2019). However, this production is small relative to that which occurs within the upper water column, and air-sea N_2O fluxes are relatively insensitive to variability in deep-ocean N_2O content (Suntharalingam & Sarmiento, 2000).

N_2O profiles from suboxic OMZs, hereafter referred to as oxygen deficient zones (ODZs), demonstrate a two-peak structure characterized by distinct N_2O maximums at the upper and lower redox boundaries (Fig. 4d; Bange, 2008). Coupled nitrification and partial denitrification near the base of the oxycline results in high N_2O production rates and supersaturations, while N_2O concentrations within the ODZ core are generally depleted as a result of net N_2O consumption. In these regions, vertical transport of N_2O supersaturated subsurface waters during upwelling leads to exceptionally high surface N_2O anomalies that contribute disproportionately to global N_2O fluxes (Fig. 4a-b; Arévalo-Martínez et al., 2015; Cohen & Gordon, 1979; Yang et al., 2020). Relative contributions of nitrification versus denitrification to N_2O production in ODZs vary regionally and with depth along the redox gradient, but recent work suggests that denitrification dominates total N_2O production in some open ocean ODZs (Ji et al., 2018). In contrast, N_2O production in coastal anoxic basins is typically dominated by nitrification as a result of elevated benthic ammonium fluxes and tight coupling between N_2O production and consumption in suboxic and anoxic waters (Capelle et al., 2018; Ji et al., 2020; Westley et al., 2006).

1.3.2 N_2O in sediments

Marine sediments are active sites of carbon and nitrogen cycling that are often characterized by shallow oxygen penetration depths and high microbial cell densities (Devol, 2015; Schmidt et al., 1998). Unlike the water column, where redox gradients span tens to hundreds of metres, anoxic conditions in sediments are generally detected within the top few millimeters (**Error! Reference source not found.**) (Devol & Christensen, 1993; Wang et al., 2014). Considerable effort has been directed toward quantifying N_2O production in marine sediments and subsequent atmospheric fluxes in easily accessible coastal systems. A recent review estimated a combined global efflux of 0.15 to 0.91 Tg N_2O-N yr^{-1} from estuarine, intertidal, and vegetated coastal environments (Murray et al., 2015). Coastal and near shore sediments can be a significant source of N_2O to the atmosphere at local scales, especially when organic carbon and dissolved inorganic nitrogen (DIN) levels are high.

Nitrification and denitrification as sources of N_2O have been demonstrated in marine sediments with high DIN loads (Bauza et al., 2002; Meyer et al., 2008; Usui et al., 2001). However, the current literature on N_2O production in sediments is biased toward highly populated and anthropogenically disturbed estuarine and coastal regions of Europe and Asia (Murray et al., 2015). Systems with low dissolved inorganic nitrogen (DIN) loads, including minimally impacted coastal mangroves and temperate estuaries, can act as net N_2O sinks (Foster & Fulweiler, 2016; Maher et al., 2016). The geographic extent of these sinks and their relevance to global or even regional N_2O budgets are not well known, and the literature bias toward anthropogenically disturbed systems may lead to an overestimation of the contributions of sediments to atmospheric N_2O emissions (Murray et al., 2015). Further to this, the literature on sedimentary N_2O production reflects a larger bias towards easily accessible coastal and near shore sediments of the inner continental shelf. The collective result is an incomplete account of sedimentary N_2O sinks and a

dearth of information regarding N_2O cycling processes in outer continental margin and continental slope sediments.

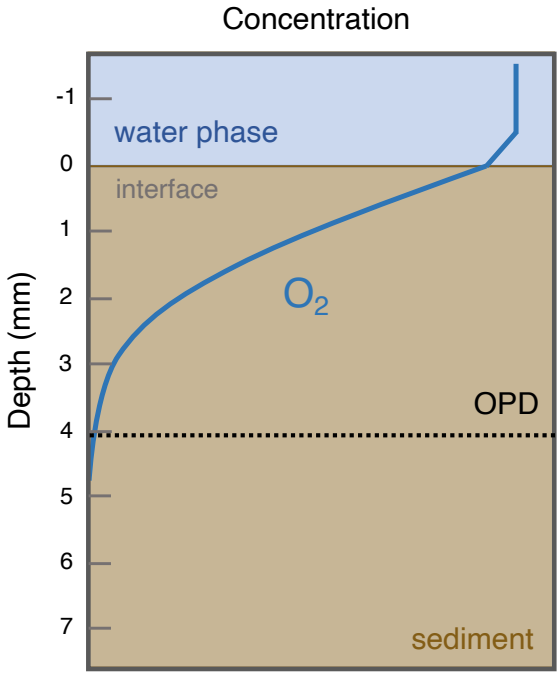

Fig. 1.5 Sediment porewater O_2 profile.

Idealized sediment porewater O_2 profile in permeable coastal sediments highlighting a shallow oxygen penetration depth (OPDs). Brown and blue shading represents sediment and water phases, respectively. The sediment-water interface is also highlighted.

1.4 The Microbial Ecology of N_2O cycling

Microorganisms, although small in size, are responsible for the vast majority of marine primary productivity and mediate all biogeochemical cycles (Whitman et al., 1998). Estimates of microbial cell abundances in marine water columns range from approximately 10^5 to 10^6 cells per ml of seawater, while cell counts in sediments can exceed those of the overlying seawater by up to three orders of magnitude (Porter & Feig, 1980; Schmidt et al., 1998; Sogin et al., 2006). Each millilitre of seawater (or sediment) thus contains a community of thousands of co-evolving taxa

that participate in a complex network of ecological interactions and are tightly coupled to a dynamic chemical and physical environment. Ecosystem function in a broad sense is an emergent property of the cumulative set of these interactions, which occur at small spatial scales but exert control over the global state of the oceans and atmosphere (Falkowski et al., 2008). However, identifying mechanistic links between large-scale biogeochemical processes such as N_2O cycling and microbial community dynamics remains one of the foremost challenges in the field of environmental microbiology (Fuhrman, 2009; Rocca et al., 2015).

1.4.1 Meta-omics, meta-organisms, and metabolic niches

The application of meta-omics to surveys of natural microbial communities has resulted in a growing awareness, throughout the prokaryotic phylogenetic tree and across a broad range of environments, of enzyme-encoding functional genes responsible for mediating core biogeochemical cycles (Graf et al., 2014; Sunagawa et al., 2015). Functional genes of this sort demonstrate predictable distribution patterns across environmental gradients, such that the metabolic potential of a microbial community can be inferred by taking inventories of relevant genes, transcripts, or proteins (Bertagnolli & Stewart, 2018; Hawley et al., 2014; Stewart et al., 2012). Further to this, individual microorganisms can be classified into functional groups based on the presence or absence of specific functional genes. Environmental variables thus define various metabolic niches, with each community effectively acting as a meta-organism that, taken cumulatively, contains all the requisite metabolic machinery required to carry out the given processes (Bertagnolli & Stewart, 2018; Hawley et al., 2014). This is especially true for marine oxygen deficient zones (ODZs), where sharp redox gradients constrain both the taxonomic identity and metabolic potential of microbial constituents, and the character of key biogeochemical transformations.

Robust patterns of microbial niche differentiation have since led to conceptual models that describe coupled metabolic exchanges between key players in ODZ carbon, nitrogen, and sulfur cycles (Hawley et al., 2014, 2017; Wright et al., 2012). Inferences regarding the roles of specific microorganisms in regulating the transformations that result in N_2O production can be made based on the relationships between environmental variables, experimentally derived rate measurements, and pools of relevant biomolecules (Callbeck et al., 2018; Sun et al., 2021; Trimmer et al., 2016). In some studies, functional gene abundances have proved useful for predicting both environmental variability and experimentally derived rate measurements for nitrifying and denitrifying processes (Louca et al., 2016a; Trimmer et al., 2016). However, the meta-organism paradigm provides limited insight into the mechanisms that drive microbial community assembly at high taxonomic resolutions. Furthermore, the mechanisms by which ecosystem function emerges from the complex network of biogeochemical and ecological interactions between individual organisms, populations, and functional groups remain obscure.

1.4.2 The role of microbial community structure

Investigations of the ecology of individual microorganisms may be hampered by the recent emphasis on functional redundancy in microbial communities. Functional redundancy describes the existence of multiple taxa that can perform the same set of metabolic processes and implies that changes in the underlying community structure are inconsequential for ecosystem function (Louca et al., 2018; Louca et al., 2016b; Louca et al., 2016c). It is important to reiterate that environmental variables influence biogeochemical processes by regulating the synthesis and activity of microbial enzymes within individual cells, and by regulating the growth of populations over space and time. So called ‘functionally redundant’ organisms can exhibit variable substrate preferences, enzymatic efficiencies, or sensitivities to environmental factors (Bayer et al., 2016;

Jung et al., 2022; Santoro et al., 2017). These findings challenge definitions of functional redundancy that are based solely on metabolic potential and argue for a holistic approach to investigations of ocean biogeochemistry that considers both metabolic and ecological dynamics.

A limited body of evidence suggests that variability in N_2O production and consumption rates tracks variability in microbial community structure at taxonomic and functional levels. For example, the N_2O sink capacity of European agricultural soils appears to be mediated largely by a single clade of N_2O-reducing bacteria (Jones et al., 2014). Similarly, variability in N_2O emissions from global wetlands has been linked to several genera of AOA from the Thaumarchaeota phylum (Bahram et al., 2022). Despite these advances, the level of taxonomic resolution that is relevant to discussions of ecosystem function with respect to the biogeochemical processes that lead to N_2O production remains largely uncertain. Culture-independent, species- and strain-level resolution can now be approximated, as a result of improvements to high-throughput sequencing technologies and data processing tools that have reduced error (Callahan et al., 2016; Edgar, 2016; Johnson et al., 2019). Yet this new capability has only recently seen application in elucidating microbial community dynamics in the environment, especially in relation to niche-specialization, ecological interactions, and element cycling in the ocean (Auladell et al., 2019, 2022).

1.5 Motivation for research

The metabolic pathways that lead to N_2O production provide a tractable set of well-described processes that are well suited for investigations into the microbial ecology of biogeochemical cycling in the ocean. Progress to this end is contingent on multidisciplinary research programs that consider both biogeochemical rate processes and microbial community dynamics across a broad range of environments and biological organizations. This dissertation leverages environmental characterizations, rate estimates, and modern molecular tools to elucidate

robust relationships between microbial community structure and N_2O cycling in marine water columns and sediments.

In Chapter Two, I evaluate the importance of keystone microbial taxa in modulating N_2O production and consumption across vertical and temporal redox gradients in seasonally anoxic Saanich Inlet using network analysis of prokaryote 16S rRNA gene sequences and ^{15}N-tracer incubations. In Chapter Three, I attempt to fill an important data gap in the global N_2O cycle by providing the first estimates of N_2O production and efflux from continental margin sediments underlying the northeast subarctic Pacific (NESAP) ODZ. This chapter also presents an improved method for quantifying N_2O cycling rate processes in surface sediments that involves sub-millimeter resolution profiling of porewater N_2O concentrations and previously developed profile interpretation models. Chapter Four builds on the work presented in Chapter Three by applying the methods outlined to evaluate the N_2O sink capacity of sediments from a minimally impacted coastal mangrove stand. I extend this work further in Chapter Four by using mangrove and NESAP sediments as a comparative basis for elucidating functional and taxonomic correlates of microbial N_2O source or sink status. Chapter Five concludes the dissertation with a synthesis of the central findings, a brief discussion of the relevance of these findings within a broader context, and suggestions for future research.

Chapter 2: Network analysis of 16S rRNA sequences suggests microbial keystone taxa contribute to marine N_2O cycling

Citation:

Jameson, B. D., Murdock, S. A., Ji, Q., Stevens, C. J., Grundle, D.S., & Juniper, S. K. (2023). Network analysis of 16S rRNA sequences suggests microbial keystone taxa contribute to N_2O cycling. *Communications Biology* **6**, 212.

2.1 Abstract

The mechanisms by which large-scale microbial community function emerges from complex ecological interactions between individual taxa and functional groups remain obscure. We leveraged network analyses of 16S rRNA amplicon sequences obtained over a seven-month timeseries in seasonally anoxic Saanich Inlet (Vancouver Island, Canada) to investigate relationships between microbial community structure and water column N_2O cycling. Taxa separately broadly into three discrete subnetworks with contrasting environmental distributions. Oxycline subnetworks were structured around keystone aerobic heterotrophs that correlated with nitrification rates and N_2O supersaturations, linking N_2O production and accumulation to taxa involved in organic matter remineralization. Keystone taxa implicated in anaerobic carbon, nitrogen, and sulfur cycling in anoxic environments clustered together in a low-oxygen subnetwork that correlated positively with nitrification N_2O yields and N_2O production from denitrification. Close coupling between N_2O producers and consumers in the anoxic basin is indicated by strong correlations between the low-oxygen subnetwork, PICRUSt2-predicted nitrous oxide reductase (*nosZ*) gene abundances, and N_2O undersaturation. This study implicates keystone taxa affiliated with common ODZ groups as a potential control on water column N_2O cycling and provides a theoretical basis for further investigations into marine microbial interaction networks.

2.2 Introduction

Linking the dynamics of complex marine microbial communities to ecosystem-scale biogeochemical processes is one of the foremost challenges in the field of microbial ecology (Fuhrman, 2009; Graham et al., 2016). The application of high-throughput gene sequencing and meta-omics to surveys of marine microbial communities has resulted in a growing awareness of the ubiquity, throughout the microbial phylogenetic tree and across a broad range of environments, of enzyme-encoding functional genes responsible for mediating core biogeochemical cycles (Graf et al., 2014; Sunagawa et al., 2015). Functional genes of this sort co-vary strongly with environmental variables, leading to an emerging view of microbial communities as meta-organisms rather than assemblages of interacting taxa (Louca et al., 2018; Louca et al., 2016c). From a biogeochemical point of view, proximal, abiotic controls on rate processes can now be seen as shaping genomes, transcriptomes and proteomes across environmental gradients, rather than simply modulating inputs and outputs from microbial black boxes (Hawley et al., 2014; Louca et al., 2016b; Stewart et al., 2012). This is especially true for marine oxygen deficient zones (ODZs) and sulfidic basins, where sharp redox gradients constrain the taxonomic identity and metabolic potential of microbial constituents, as well as the character of key biogeochemical transformations (Hawley et al., 2014; Ulloa et al., 2012; Wright et al., 2012). Robust patterns of metabolic niche differentiation have since led to the development of conceptual models that describe coupled metabolic interactions between key players across vertical redox gradients (Hawley et al., 2014, 2017). However, from an ecological point of view, the meta-organism paradigm provides limited insight into the mechanisms that drive community assembly at the taxonomic level, and how ecosystem function arises from a complex network of biogeochemical and ecological interactions between individual taxa.

Ecosystem function is an emergent phenomenon that results from the cumulative set of metabolic and ecological interactions that characterize dynamic and co-evolving microbial communities in the environment (Falkowski et al., 2008). These interactions occur at the microscopic level and involve countless individual taxa with diverse functional capacities and taxonomic affiliations. Individual cells, strains, or functional groups within a community can influence each other through multiple mechanisms, including mutualistic cross-feeding (Goldford et al., 2018), resource competition (MacLean et al., 2005), the production of public goods (Drescher et al., 2014) or allelopathic compounds (Leão et al., 2012), and many others (Cordero & Polz, 2014). Unfortunately, ecological interactions of this sort are difficult to characterize given the cryptic nature of natural microbial community dynamics. Complicating matters further is the fact that the vast majority of microbial organisms remain uncultured, and thus taxonomically and functionally ambiguous. Fortunately, improvements to high-throughput sequencing technologies and data processing tools combined with novel statistical approaches have allowed researchers to study patterns of microbial community assembly in unprecedented detail (Bálint et al., 2016; Callahan et al., 2016; Johnson et al., 2019).

Network analyses applied to the study of complex microbial communities has resulted in a corpus of literature documenting spatiotemporal co-occurrence patterns amongst microbial community members across a wide range of terrestrial and aquatic ecosystems (Barberán et al., 2012; Murdock et al., 2021; Steele et al., 2011). These tools go beyond traditional assessments of biodiversity and community structure by utilizing pairwise correlations between individual taxonomic units to identify core community members and assess co-occurrences between individual taxa. Although the mechanisms driving specific co-occurrences cannot be discerned from network analyses alone, parallel information on rate processes and environmental variables

can help generate testable hypotheses regarding putative ecological interactions responsible for driving ecosystem function (Wright et al., 2012). This is a potentially fruitful line of investigation, given recent progress in linking microbial community structure to large-scale ecosystem processes such as carbon export, nitrogen fixation, and denitrification (Guidi et al., 2016; Jones et al., 2014; Wang et al., 2021). A holistic approach to the study of marine biogeochemical processes that encapsulates the internal complexity of entire communities may also help to elucidate ecological controls that have been previously overlooked by a reductionist focus on protein-encoding functional genes.

Empirical and computational studies suggest that microbial communities contain keystone members, defined as highly connected taxa that exert considerable influence over community structure and function irrespective of their abundances across space and time (Banerjee et al., 2018). Keystone taxa can exist independently or may also be part of keystone guilds comprising several taxa of similar niche-preferences and functional properties (Jones et al., 2014). More importantly, keystone taxa may exert influence over ecosystem processes directly, such as through the production or utilization of shared metabolites (Li et al., 2017), or indirectly by modulating the broader community structure (Herren & McMahon, 2018). This evidence suggests that ecological interactions between functionally diverse microorganisms may underly more subtle relationships between microbial community structure and ecosystem function.

The microbial production and consumption of nitrous oxide (N_2O) is a timely area of focus for investigating links between microbial community dynamics and ecosystem processes. Nitrous oxide is currently the third most important greenhouse gas behind CO_2 and methane and is the predominant ozone-depleting substance emitted in the 21st century (Arias et al., 2021; Ravishankara et al., 2009). Current models estimate that marine ecosystems account for 10 to 53%

of the annual global N_2O emissions, leaving much to be learned about the drivers of spatiotemporal variability (Bange et al., 2019). In the marine environment, N_2O is produced primarily as a by-product of ammonium oxidation or as a free-intermediate in the sequential reduction of nitrate and nitrite to dinitrogen gas (N_2) during heterotrophic or sulfide-driven denitrification (Bange et al., 2010). Elevated rates of production from both pathways are observed near the boundaries of marine oxygen deficient zones (ODZs) and anoxic basins where oxidative and reductive processes are closely coupled in space and time (Arévalo-Martínez et al., 2015; Babbin et al., 2015; Ji et al., 2015). Conversely, the reduction of N_2O to N_2 by organisms possessing N_2O-reductases is the only confirmed biological sink for N_2O and can drive N_2O concentrations toward undetectable levels in some anoxic water masses (Bange, 2008; Devol, 2008). Nitrous oxide cycling is thus the product of distributed metabolic networks that involve syntrophic interactions between important players in the biogeochemical cycling of carbon, nitrogen and sulfur, with net fluxes likely determined by a complex interplay between environmental and biological factors.

Saanich Inlet is a well-studied, seasonally euxinic fjord located on Vancouver Island, Canada that is characterized by extreme seasonal shifts in water column redox gradients driven by cycles of primary production and physical mixing (Anderson & Devol, 1973; Gargett et al., 2003; Grundle et al., 2009). The inlet is further distinguishable from open ocean ODZs by its restricted depths (~225 m maximum) and the presence of sulfidic bottom water throughout much of the year (Anderson & Devol, 1973; Capelle et al., 2018; Emerson et al., 1979). However, the reliable transition between periods of water column stagnation and bottom water anoxia, and oxygenation of the deep basin following deep water renewal provides a unique opportunity to explore links between biogeochemical rate processes and microbial community dynamics under changing redox conditions (Michiels et al., 2019; Soetaert et al., 2022). Furthermore, studies focusing on microbial

community dynamics in easily accessible anoxic basins with reliable sulfide accumulation are useful for understanding trajectories in coastal systems experiencing increases in the frequency of bottom water hypoxia and transient sulfidic conditions (Breitburg et al., 2018; Lavik et al., 2009; Schunck et al., 2013). Previous work in Saanich Inlet suggests that N_2O production is driven by ammonium oxidation at oxycline depths, with substantial contributions from reductive processes near the base of the oxycline during periods of bottom-water anoxia and in the deep basin following renewal events (Capelle et al., 2018; Ji et al., 2020). However, little is currently known about the role of keystone taxa, and ecological interactions more broadly, in mediating N_2O-cycling rate processes across marine redox gradients.

This study combines high-throughput sequencing of microbial 16S rRNA amplicons, *in situ* rate measurements, and environmental characterizations collected in Saanich Inlet over a bi-monthly timeseries between April and October 2018. This study leverages network and multivariate statistical analyses to separate co-occurring taxa into discrete subnetworks with contrasting ecological distributions and roles in water column N_2O cycling. Oxycline subnetworks were correlated with nitrification rates and N_2O supersaturations and contained keystone taxa implicated in aerobic organic matter remineralization, including members of the ubiquitous SAR11 group. Members of the low-oxygen subnetwork demonstrated a preference for anoxic and N_2O-undersaturated waters and contained keystone taxa belonging to groups associated anaerobic carbon, nitrogen, and sulfur cycling such as SUP05. Taxa identified as potential keystones belonged to groups found throughout global ODZs and anoxic basins, thus providing a theoretical basis for further investigations into the importance of ecological interactions in regulating marine N_2O production and accumulation.

2.3 Methods

2.3.1 Field sampling

Sampling was conducted bimonthly on the *MSV John Strickland* at a single location in Saanich Inlet (48° 37.53'N, 123° 29.91'W) on 5 April, 14 June, 02 August, and 25 October 2018 (**Error! Reference source not found.**). The specifics of the sampling campaign, including chemical analyses and ^{15}N-labeled tracer experiments to measure N_2O production rates from NH_4^+ oxidation and NO_3^- reduction, have been detailed in Ji et al. (2020). Environmental proxies for N_2O production processes considered in the statistical analyses included dissolved O_2, N_2O saturation, as well as NO_3^- + NO_2^- and NH_4^+ concentrations. N_2O saturation was defined as the N_2O excess, which is calculated from the concentrations difference between measured and expected equilibrium values with respect to the atmosphere. Seston samples for DNA sequencing were also obtained from the six discrete sampling depths (75, 90, 100, 110, 130, and 160 m) by filtering 5 L of seawater onto 0.2 μm Sterivex™ filters (Merck) by peristalsis. Samples designated for DNA extraction were immediately placed on dry ice, transferred to a -80°C freezer later the same day, and stored for 6-12 months prior to extraction.

2.3.2 DNA extractions and high-throughput sequencing

Nucleic acids were extracted according to Crump et al. (1999) with the modifications suggested by Huber et al. (2002) and Sogin et al. (2006). Sterivex filters were thawed, cut into strips, and placed in clean 2 mL microcentrifuge tubes containing 1 mL of DNA extraction buffer (1.5 M NaCl, 0.1 M Na-EDTA [pH 8.0], 0.1 M Tris-HCl [pH 8.0], 0.1 M NaH_2PO_4 [pH 8.0], and 5% cetyltrimethylammonium bromide; 0.2 μm filtered, autoclaved). Each tube was aliquoted with 20 μl of Proteinase K (10 mg/ml) and 40 μl of lysozyme (50 mg/ml) and then taken through three freeze-thaw cycles of 15 mins at -80°C and 5 mins at 37°C. Following the final freeze step, tubes

were incubated at 37°C for 30 mins prior to addition of 50 µl sodium dodecyl sulfate (SDS; 20%; 0.2 µm filtered and autoclaved) and incubation in a water bath at 65°C for 120 mins. Tubes were then filled with phenol:chloroform:isoamyl alcohol (P:C:I; 25:24:1) to a final volume of ~2 ml, vortexed, and centrifuged (3000 rpm) for 5 mins. The aqueous layer was transferred to a new 2 ml tube and the P:C:I addition, spin-down, and transfer steps were repeated a second time. DNA was precipitated by adding 0.6 volumes of molecular grade isopropopanol (99.5%), mixing gently, and incubating at room temperature for 2 hours. Samples were then centrifuged (13,000 rpm) for 30 mins, washed with 1 ml of ethanol (70%), dried, and eluted in 150 µl of TE buffer (10 mM Tris-HCl [pH 8.0]; 1 mM Na-EDTA [pH 8.0]; 0.2 µl filtered, autoclaved). A sterile, blank Sterivex filter was included in each round of extractions, and the resulting material was carried through the PCR validation steps to ensure no contaminants were introduced during the extraction process. DNA extracts were cleaned using a QIAquick® PCR purification kit and DNA concentrations in cleaned extracts were quantified on a NanoDrop™ One Microvolume UV-Vis Spectrophotometer (Thermo Scientific).

The presence of target genes (16S rRNA) was verified by polymerase chain reaction (PCR) of genomic DNA (gDNA) using primers targeting the bacterial V6-V8 variable regions described by Comeau et al. (2011) (Table 2.2). PCR was conducted in 20 µl reaction volumes containing 4.0 µl 5X Green GoTaq™ reaction buffer (Promega), 2.0 µl dNTPs mixture diluted to final concentrations of 2.0 mM each (Thermo Scientific), 1.0 µl each of 2.0 µM forward and reverse primer (Eurofins Scientific), 10.8 µl UltraPure™ DNase/RNase-Free water (Invitrogen), 0.2 µl GoTaq™ DNA polymerase (Promega) and 1.0 µl template DNA. Thermal cycling began with an initial denaturation at 94°C for 120 s, followed by 30 cycles of denaturation at 94°C for 30s, annealing at 55°C for 45 s, extension at 72°C for 120 s, and terminated following a final

extension at 72°C for 600 s. Bacterial and archaeal 16S rRNA genes were selected for sequencing from raw extracts using the same universal primer sets on an Illumina MiSeq at the Integrated Microbiome Resource (Dalhousie University, Halifax, Canada) using 2 x 300 bp paired-end V3 chemistry (https://imr.bio/protocols.html) (Comeau et al., 2011). Final amplicon read lengths were 437 and 445 bp for Bacteria and Archaea, respectively. Bacterial 16S rRNA gene sequences were obtained from all samples, while archaeal sequences were obtained in 18 of 24 samples.

Demultiplexed reads were trimmed of primer-binding sequences using Cutadapt and reads with no primer match were discarded (Martin, 2011). Trimmed reads were then processed in USEARCH v11 to generate amplicon sequence variant (ASV) count tables (Edgar, 2010). Bacterial and Archaeal 16S gDNA reads were merged using the *fastq_mergepairs* command with maximum allowable mismatches in the overlapping region (*fastq_maxdiffs*) set to 20 and the minimum percent ID of alignment (*fastq_pctid*) left on the default setting of 90. The trimmed and merged reads were then quality-filtered using a maximum expected error threshold (*fastq_maxee*) of 1.0 and ASV denoising was conducted on dereplicated sequences using UNOISE3 (Edgar, 2016). Singletons were removed and ASV tables were constructed with the *usearch_global* command using a similarity threshold of 99%. Since the denoising algorithm recovers the majority of true sequences in the sample, the 99% identity cut-off is fixed to allow for 1% error in the underlying reads believed to be generated by sequencing and PCR errors. Taxonomies for 16S rDNA ASVs were inferred from the silva_nr_132 reference database in Mothur v1.42.3 (Appendix A) (Quast et al., 2013; Schloss et al., 2009).

2.3.3 Statistics and reproducibility

Unless otherwise stated, statistical analyses and additional data-processing steps were conducted in the R Statistical Environment and followed best practices for the handling of

compositional data (Gloor et al., 2017; R Core Team, 2019). Imputation of zero-values was performed using Bayesian multiplicative replacement in the zCompositions package and read counts were converted to centred-log ratios (clr) prior to downstream analyses (Palarea-Albaladejo & Martín-Fernández, 2015). Patterns of microbial community assembly were assessed using non-metric multidimensional scaling (NMDS) based on Aitchison distance matrices calculated across samples using the vegan package (Dixon, 2003). The *envfit* function was used to test for significant effects of environmental parameters on microbial community dissimilarity. We considered dissolved inorganic nitrogen concentrations (NH_4^+, NO_3^-, NO_2^-), dissolved O_2 concentrations, water column N_2O saturations (ΔN_2O), temperature, and salinity as potential predictors of microbial community structure.

Co-occurrence patterns between taxa with putative roles in N_2O production and the rest of the microbial community ASVs were explored using proportionality analysis within the propr package (Quinn et al., 2017). ASV tables were trimmed to select taxa that occurred ≥ 10 times in at least 10% of samples prior to network-level analyses to improve interpretability and minimize the risk of spurious correlations. Pairwise interactions between individual taxa with rho values greater than 0.60 were plotted using Cytoscape v3.9.0 and network topological indices were calculated using the NetworkAnalyzer tool (Shannon et al., 2003). Relationships between microbial community structure and rate processes were then assessed using weighted gene correlational network analysis (WGCNA) performed with the WGCNA package (Langfelder & Horvath, 2008). The signed adjacency measure was first calculated for each pair of features (ASVs) by raising the absolute value of their pairwise correlation coefficients to a soft-thresholding power of 8 to maximize the scale-free topology fit. Hierarchical clustering of taxa into discrete subnetworks was completed using a minimum module size threshold of 20 and a

dissimilarity threshold of 0.3. Pearson correlation coefficients and corresponding *p*-values are reported for correlations between sample traits, subnetwork eigengenes, and individual ASVs (Appendix B). Subnetwork membership and intranetwork connectivity measures are also reported for each ASV and were used in further analyses to assess broad relationships between ASV connectivity and importance with respect to N_2O production rates.

Links between individual taxa and N_2O production processes inferred from WGCNA were then confirmed using sparse partial least squares regression (sPLSR), implemented in the MixOmics package (Rohart et al., 2017). The advantage of sPLSR is that it is capable of modeling highly dimensional datasets with multiple noisy and collinear variables, making it a useful method for exploring relationships between two continuous datasets when the total number of variables greatly outnumbers the number of discrete observations (Cao et al., 2008). This method combines dimension reduction and variable selection in a one-step modelling procedure, thus greatly improving interpretability over the standard PLSR approach. The final model was built after tuning based on Leave One Out cross-validation to determine the optimal number of latent components and variables for inclusion. Data sparsification is achieved by introducing a LASSO penalization to reduce the number of original variables used to construct the latent components. Pearson correlations between selected ASVs and sample traits were visualized in a clustered heatmap using a complete Euclidean distance method.

2.3.4 Detecting putative keystone taxa

The potential role of keystone taxa in mediating N_2O production and accumulation was explored by leveraging 'propr' network topological indices to determine if taxa selected as important predictors of rate processes scored high on keystone measures. High node (ASV) degree, closeness centrality, and betweenness centrality were considered as indicators of microbial

keystone taxa according to the recommendations of previous studies (Banerjee et al., 2016, 2018; Berry & Widder, 2014; Heijden & Hartmann, 2016). Whereas node degree represents the number of edges (associations) a particular ASV shares with others in the network, closeness centrality measures the average distance of each node to other nodes in the network. In contrast, betweenness centrality calculates the extent to which a particular node lies on the shortest path between two adjacent nodes (Berry & Widder, 2014).

2.3.5 Community functional gene predictions

Bacterial community functional compositions were predicted using PICRUSt2 version 2.4.1 with the default settings to assess relationships between predicted *nosZ* gene abundances and water column N_2O saturations (Douglas et al., 2020; Langille et al., 2013). Briefly, ASVs were placed within a reference phylogeny based on 20,000 16S sequences from the Integrated Microbial Genomes database by multiple sequence alignment using HMMER (https://www.hmmer.org), optimal positioning of ASVs using EPA-ng (Barbera et al., 2019), and phylogenetic tree reconstruction using GAPPA (Czech & Stamatakis, 2019). The nearest-sequenced taxon index (NSTI) was calculated for each ASV and taxa with NSTI values less than 2.0 were excluded from downstream analyses. Less than 1% of bacterial ASVs (43 of 4674) were removed following quality filtering. Prediction of gene family abundances (including KEGG orthologues) was then conducted across samples using the Castor R package (Louca & Doebeli, 2018). Predicted abundances of KEGG orthologues corresponding to the *nosZ* gene were then selected from the model output.

2.4 Results

2.4.1 Microbial community structure

Amplicon sequencing generated 818,133 paired-end microbial 16S rRNA gene sequence reads across 24 samples. A total of 469,628 bacterial and 211,767 archaeal reads remained following sequence merging and quality filtering, resulting in 168 archaeal and 2814 bacterial non-singleton amplicon sequence variants (ASVs). Mean amplicon lengths were 437 and 445 bp for bacterial and archaeal sequences, respectively. The total number of merged reads for each sample following quality control are reported in Table 2.3.

The Saanich Inlet microbial community was well-stratified in April and demonstrated stark shifts in bacterial community structure across depth-dependent redox gradients (**Error! Reference source not found.**). Members of the SAR11 α-proteobacteria dominated bacterial sequence reads between 75 and 100 m (~35%), along with high abundances of Rhodobacterales (9-27%) and Flavobacteriales (4-9%). These groups decreased in prominence with depth along the oxycline, collectively accounting for <1% of sequence reads below the anoxic interface (130 and 160 m). ASVs belonging to the SUP05 γ-proteobacteria showed contrasting distributions, with maximum values observed in the lower oxycline and anoxic basin between 110 and 160 m (39-41%). Other prominent taxa of the low-oxygen communities included members of the Marinimicrobia (2-4%), Ectothiorhodospirales (6-11%), and Desulfobacterales (0.3-6%). Members of the *Nitrospina* genus within the order Nitrospinales also reached peak relative abundances of 1-1.5% in the lower oxycline and anoxic basin samples despite pronounced vertical stratification of individual ASVs.

Archaeal sequence reads were dominated by Thaumarchaeota ASVs that mapped to two genera within the *Nitrosopumilaceae* family (**Error! Reference source not found.**b). A single

Nitrosopumilus-like ASV (ARCH1) accounted for 56-86% of all archaeal sequences and was uniformly distributed across

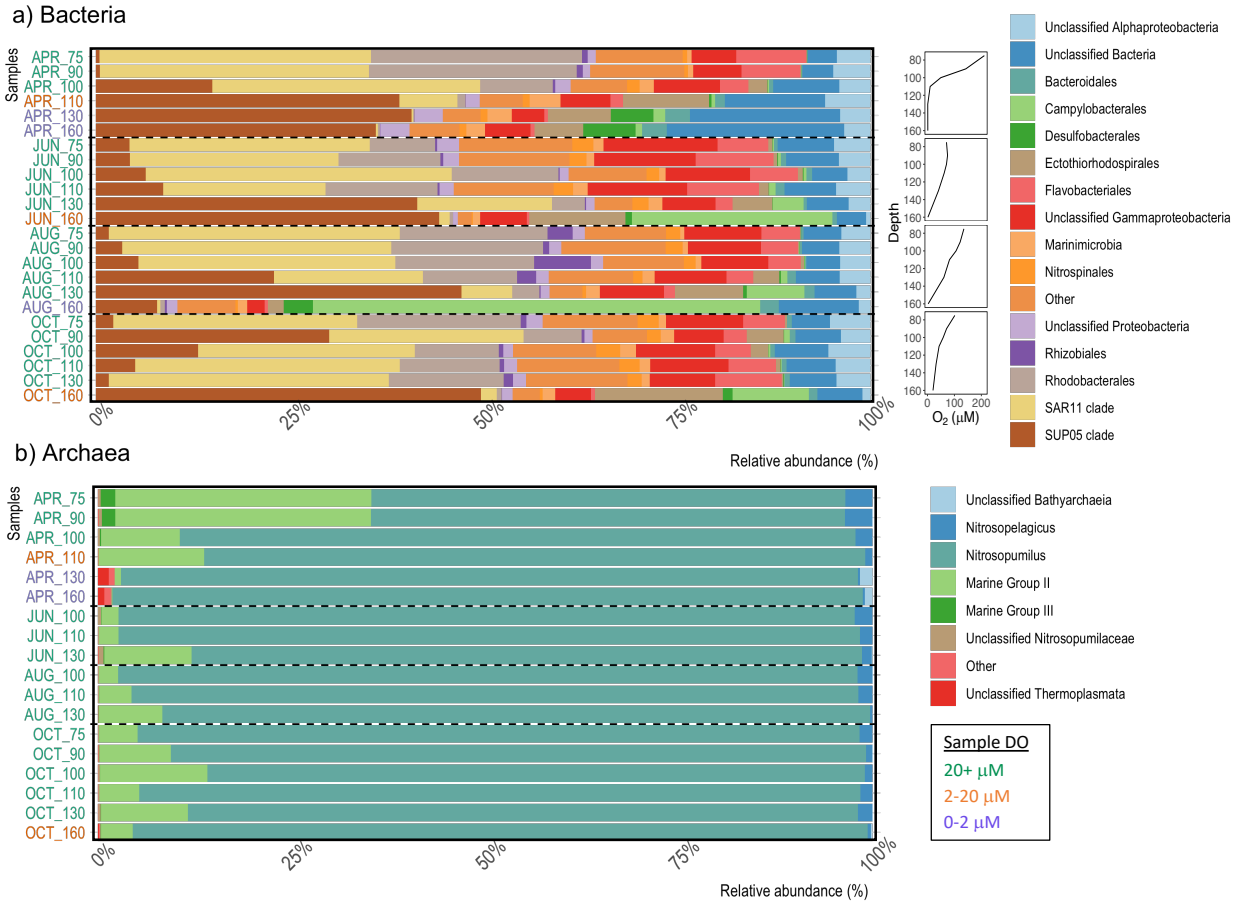

Fig. 2.1 Community composition barplots.

Relative abundances of a) Bacteria and b) Archaea ASVs in Saanich inlet seston samples**.** Dissolved oxygen profiles for each sampling period are reported in panel a) Samples were obtained from Saanich inlet between April and October 2018. Sample labels on the vertical axes correspond to sampling month and water column depth. Vertical axis labels are color coded according to *in situ* dissolved oxygen concentrations.

water column depths and sampling dates (**Error! Reference source not found.**b). Lower oxycline and anoxic basin samples were characterized by increases in the abundance of a second, low-oxygen *Nitrosopumilus* ecotype (ARCH3) with maximum values of over 25% of *Nitrosopumilaceae* reads between 110 and 160 m alongside ASVs belonging to the *Bathyarchaeia*

and Thermoplasmata. In contrast, thaumarchaeotal communities of the upper oxycline contained higher abundances of *Nitrosopelagicus*-like variants (**Error! Reference source not found.**, **Error! Reference source not found.**). Members of the Marine Group II (MGII) and Marine Group III (MGIII) Euryarchaeota also reached peak relative abundances in upper oxycline samples (~33% and 2%, respectively), and decreased precipitously with depth (**Error! Reference source not found.**b).

At least three discrete renewal events were detected at variable depths prior to sampling in June, August, and October, resulting in substantial changes to water column redox gradients and microbial community structures across renewal depths (Ji et al., 2020). Renewal events prior to June and August sampling impacted midwater depths between 75 and 150 m, while October renewal was associated with oxygenation of the deep basin below 160 m. Increases in dissolved O_2, NO_3^-, and N_2O concentrations across renewal depths were associated with elevated abundances of SAR11, *Rhodobacteraceae* and *Flavobacteraceae* ASVs in addition to vertical homogenization of the Archaeal community (**Error! Reference source not found.**). These events were generally accompanied by decreases in the relative abundance of SUP05, Marinimicrobia, Ectothiorhodospirales, and Desulfobacterales ASVs at deeper renewal depths and upward transport to 75 and 90 m ostensibly resulting from uplift of anoxic basin waters and subsequent mixing with renewal waters. Progressive increases in the prevalence of ASVs belonging the Campylobacterales were also detected at 130 and 160 m between April and August. Campylobacterales reads were dominated by a single *Arcobacter* ASV that accounted for between 25% and 57% of total bacterial reads at 160 m in June and August, respectively. Conversely, *Nitrospina* ASVs increased in relative abundance with time throughout much of the water column,

with peak values of approximately 3% occurring at mid depth in October despite variable depth-related trends between sampling dates.

Clustering of bacterial and archaeal communities via non-metric multidimensional scaling (NMDS) followed water column N_2O saturations (ΔN_2O), with samples from undersaturated waters grouping together closely (**Error! Reference source not found.**). Envfit analysis implicated NO_3^- concentrations as the strongest predictor of community structure for both bacterial ($r^2 = 0.82$, $p = 0.001$) and archaeal ($r^2 = 0.77$, $p = 0.001$) ASVs. Secondary predictors for both domains included dissolved O_2 concentrations, NH_4^+ concentrations and ΔN_2O. The influence of dissolved O_2 on NMDS ordinations was stronger for bacterial communities ($r^2 = 0.70$, $p = 0.001$) than for archaeal communities ($r^2 = 0.65$, $p = 0.001$), while ΔN_2O showed greater influence over archaeal community structure ($r^2 = 0.65$, $p = 0.001$ for Archaea versus $r^2 = 0.57$, $p = 0.001$ for Bacteria). In contrast, the influence of NH_4^+ concentration was similar between the bacterial ($r^2 = 0.69$, $p = 0.001$) and archaeal domains ($r^2 = 0.71$, $p = 0.002$). Temperature and salinity were also implicated as potential drivers of community structure, although correlational strengths were lower in comparison to other variables ($r^2 = 0.47$-0.52, $p = 0.001$-0.015).

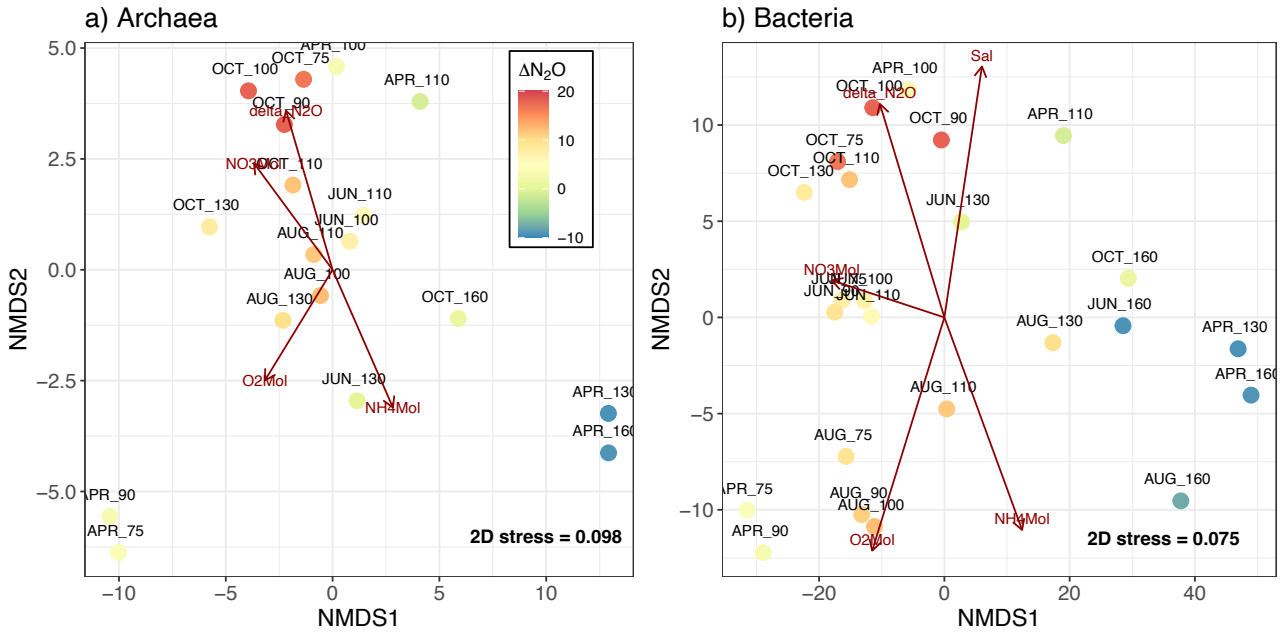

Fig. 2.2 Archaea and Bacteria NMDS biplots.

Nonmetric multidimensional scaling (NMDS) ordinations for a) Archaea and b) Bacteria communities. NMDS analyses were conducted using Aitchison distances between samples calculated using clr-transformed ASV tables. Significant environmental predictors of community dissimilarity were calculated using *envfit* and the corresponding vectors are represented by red arrows.

2.4.2 N_2O-cycling community networks

Two separate network-level analyses were performed on the combined, centred-log ratio (clr) transformed bacterial and archaeal ASV tables to explore patterns of community assembly and relationships between community interaction networks and N_2O cycling. A total of 38 archaeal and 324 bacterial ASVs were included in the network-level analyses following removal of low abundance taxa to improve interpretability and minimize the risk of spurious correlations (Table 1). First, we used proportionality analyses to define a community co-occurrence network of interacting taxa with absolute rho values > 0.60 (**Error! Reference source not found.**). These results were then compared with those obtained through weighted gene correlational network analysis (WGCNA) of the same dataset to identify core community members and elucidate links

between microbial community structure and N_2O production processes. Relationships between entire community subnetworks and N_2O production were assessed by correlating subnetwork eigengenes with relevant sample traits (environmental variables and measured rates). The potential role of community structure in mediating water column N_2O-cycling was explored by evaluating relationships between ASV subnetwork membership, intranetwork connectivity (K_{in}) and ASV importance in predicting rate processes and water column N_2O saturations (ΔN_2O).

Table 2.1 Correlations between SNET eigengenes and sample traits.

Pairwise Pearson's correlation coefficients are reported with corresponding *p*-values (in parentheses) for relationships between subnetwork (SNET) eigengenes and sample traits relevant to N_2O production. N_2O production rates from NH_4^+ oxidation and NO_3^- reduction are symbolized by black arrows

		Environmental variables				**Rate processes**			
SNET	Taxa	O_2	ΔN_2O	NO_3^-+NO_2^-	NH_4^+	Nitrification	$NH_4^+ \rightarrow N_2O$	$NO_3^- \rightarrow N_2O$	N_2O yield
1	135	**-0.75 (3e-04)**	**-0.65 (0.004)**	**-0.89 (9e-07)**	**0.72 (8e-04)**	-0.42 (0.08)	0.21 (0.40)	**0.61 (0.007)**	**0.55 (0.02)**
2	77	0.36 (0.10)	**0.71 (0.001)**	**0.74 (4e-04)**	**-0.73 (6e-04)**	0.44 (0.07)	-0.078 (0.80)	-0.32 (0.20)	**-0.49 (0.04)**
3	150	**0.83 (2e-05)**	**0.52 (0.03)**	**0.83 (2e-05)**	**-0.63 (0.005)**	0.38 (0.10)	-0.25 (0.30)	**-0.64 (0.004)**	**-0.49 (0.04)**

***** Statistically significant correlations ($p < 0.05$) are bolded.

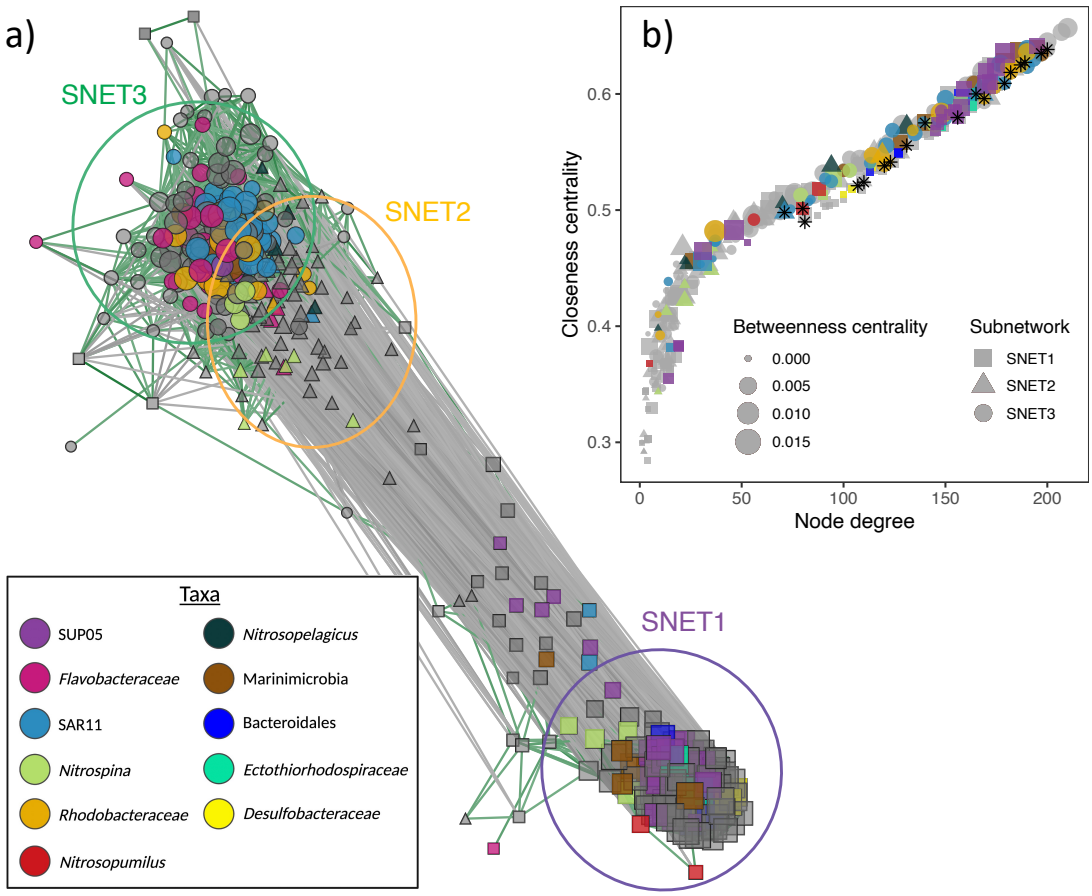

Fig. 2.3 Prokaryote co-occurrence network.

Co-occurrence network depicting interactions between bacterial and archaeal ASVs in the Saanich Inlet microbiome. In panel a), grey lines depict negative covariance and green lines depict positive covariance with $\rho > |0.60|$. Node size represents intranetwork connectivity (K_{in}) and shapes indicate subnetwork assignments determined by WGCNA. Squares, triangles and circles represent taxa belonging to SNET1, SNET2, and SNET3, respectively and are highlighted by coloured circles. Taxonomic assignments are represented by coloured nodes. Panel b) depicts relationships between node (ASV) degree, closeness centrality, and betweenness centrality determined through analysis of the propr network. Individual ASVs implicated by sPLSR (**Error! Reference source not found.**) as important predictors of rate processes and ΔN_2O are indicated (*) in panel b.

WGCNA clustered microbial ASVs into three discrete subnetworks (SNETs 1-3) containing 135, 77, and 150 ASVs, respectively (Table 2.1). These results were largely congruent with those identified through proportionality analyses, with taxa separating broadly into three primary clusters according to their subnetwork assignments identified through WGCNA (**Error! Reference source not found.**). SNET1 was inversely correlated with dissolved O_2 (r = -0.75, p =

3 x 10^{-4}), ΔN_2O (r = -0.65, p = 0.004), and [NO_3^- + NO_2^-] (r = -0.89, p = 9 x 10^{-7}), and positively correlated with N_2O production from NO_3^- reduction (r = 0.61, p = 0.007) as well as N_2O yields from nitrification (r = 0.55, p = 0.02) (**Error! Reference source not found.**, Table 2.1). A total of 81 SNET1 ASVs demonstrated significant positive correlations to rates of N_2O production from NO_3^- reduction (r = 0.47-0.75, p <0.05), while 52 ASVs correlated significantly with N_2O yields from nitrification (r = 0.47-65, p <0.05) (Appendix B). ASV membership to SNET1 was strongly correlated to ASV importance in predicting both N_2O production rates and nitrification yields, and inversely correlated with ΔN_2O (**Error! Reference source not found.**). Although SNET1 membership was also positively correlated with ASV importance in predicting rates of N_2O production from NH_4^+ production, taxa-specific correlations were generally weak and insignificant (**Error! Reference source not found.**, Appendix B).

SNET2 and SNET3 represented nested subnetworks that displayed overlapping niche distributions and similar relationships to environmental parameters and process rates (**Error! Reference source not found.**, Table 2.1). SNET2 was most strongly correlated to ΔN_2O (r = 0.71, p = 0.001) and [NO_3^- + NO_2^-] (r = 0.75, p = 3 x 10^{-4}), but was not significantly related to dissolved O_2 concentrations. In contrast, SNET3 demonstrated significant positive correlations to dissolved O_2 (r = 0.83, P = 2 x 10^{-5}), [NO_3^- + NO_2^-] (r = 0.83, p= 2 x 10^{-5}), and ΔN_2O (r = 0.52, p= 0.03). Positive correlations observed between SNET2 and SNET3 and nitrification rates were not statistically significant at the subnetwork level (r = 0.44 and 0.38, p = 0.07 and 0.10, respectively) (Table 1). Regardless, 25 bacterial ASVs were detected with significant associations to nitrification rates (r = 0.47-0.65, p < 0.05) and a strong positive correlation between ASV importance in predicting nitrification rates and ASV membership in SNET2 and SNET3 (**Error! Reference source not found.**, Appendix B). ASV membership in SNET2 and SNET3 was also

strongly associated with water column ΔN_2O values, with a total of 42 ASVs demonstrating strong positive correlations (r = 0.60-0.89, p <0.001).

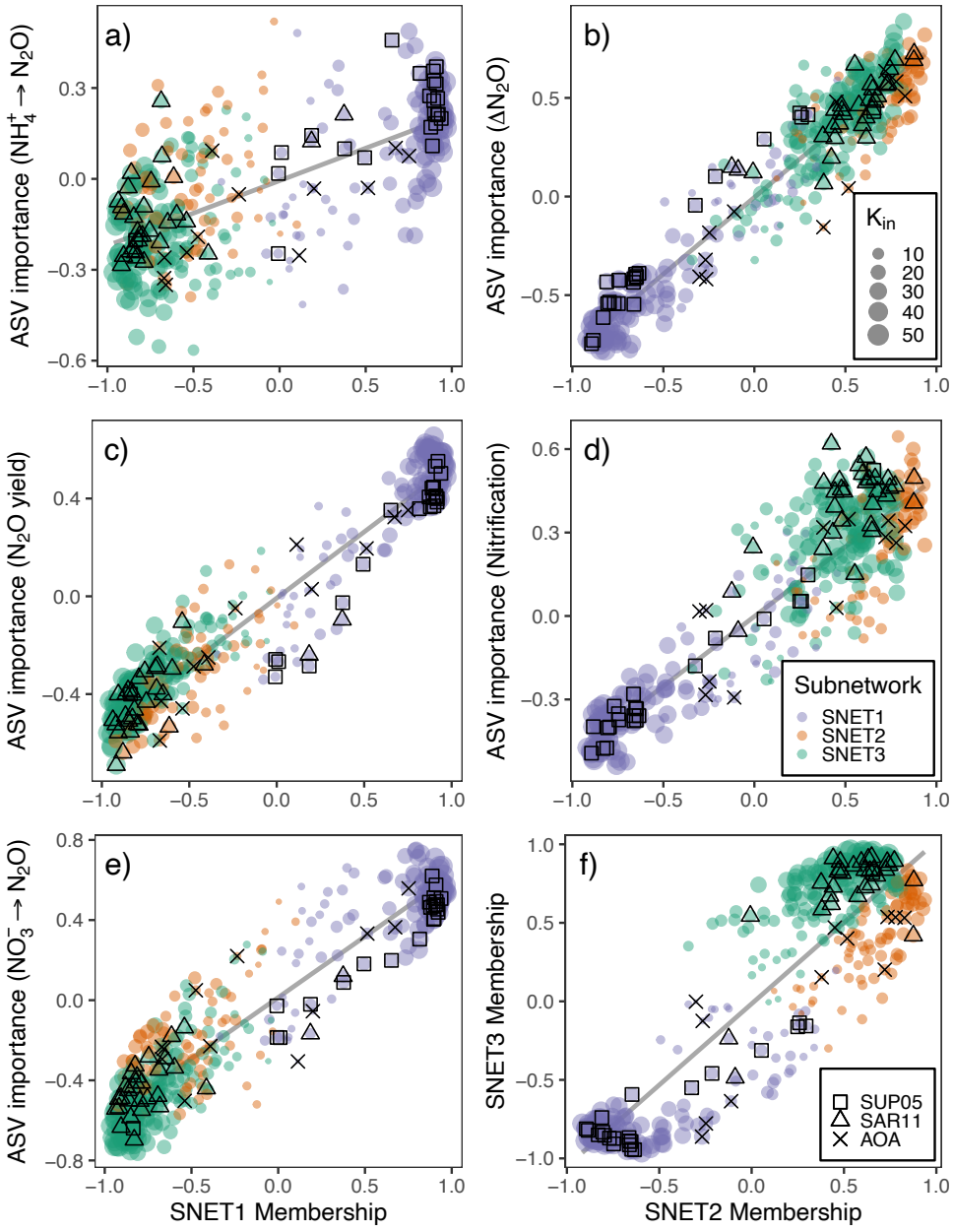

Fig. 2.4 Subnetwork membership vs. correlation strength.

Relationships between ASV subnetwork memberships and ASV importance in predicting various N_2O cycle proxies. Left panels depict relationships between SNET1 memberships and ASV importance in predicting a) rates of N_2O production from NH_4^+ oxidation, c) N_2O yields from nitrification, and e) rates of N_2O production from NO_3^- reduction. Right panels depict relationships between SNET2 memberships and

b) ΔN_2O, d) nitrification rates, and f) SNET3 memberships. ASV importance corresponds to the Pearson coefficients calculated for pairwise correlations between microbial ASVs and sample traits. Colours correspond to community subnetworks inferred from WGNA and bubble size indicates degree of intranetwork connectivity (K_{in}) for each ASV. Black squares, crosses, and triangles denote ASVs belonging to the SUP05 clade, the Nitrosopumilaceae family, and SAR11 clade, respectively.

2.4.3 Keystone taxa linked to N_2O production processes

Network inferences were extended further by utilizing network topological indices of the propr covariance network to identify putative keystone taxa amongst core community members that correlated strongly with rate processes and water column N_2O saturations (ΔN_2O) (Quinn et al., 2017). High node (ASV) degree, closeness centrality, and betweenness centrality were considered as indicators of potential keystone status for microbial ASVs (Banerjee et al., 2018, 2018; Berry & Widder, 2014; Heijden & Hartmann, 2016).

Core community taxa in SNET1 that correlated significantly with rates of N_2O production from NO_3^- reduction included highly connected members of the *Desulfobacteraceae*, *Ectothiorhodospiraceae*, Bacteroidales, and the SUP05 clade (**Error! Reference source not found.**, Appendix B). Other prominent ASVs related to N_2O production from NO_3^- reduction in SNET1 included members of the *Nitrosopumilus* and *Nitrospina* genera ($r = 0.51$-0.59, $p < 0.027$), as well as several unclassified members the α- and γ-proteobacteria, and Marinimicrobia. Core community members that correlated significantly with elevated nitrification rates and ΔN_2O belonged primarily to the SAR11 clade (11 of 25 ASVs) in addition to variants from the *flavobacteraceae* and MG II Euryarchaeota, which were generally well connected in SNET2 and SNET3 (**Error! Reference source not found.**, Appendix B). Additional taxa with high levels of connectivity in SNET2 and SNET3 that correlated strongly with ΔN_2O and demonstrated positive associations with nitrification rates included four *Nitrosopelagicus*-like variants, and several *Rhodobacteraceae* and *Verrucomicrobiae* ASVs.

Microbial taxa that correlated well with N_2O production rates, nitrification rates, and ΔN_2O generally scored high on network topological indices of keystone status (**Error! Reference source not found.**b). However, several highly connected ASVs suggested by WGCNA as potentially important with respect to N_2O cycling were not classifiable below the class level and many were classifiable only at the kingdom level (Appendix B). Furthermore, results of the WGCNA demonstrating correlations between individual ASVs and rate processes are difficult to interpret given the large number of taxa implicated. In attempt to circumvent this issue, a sparse partial least squares regression (sPLSR) model was fit to predict sample traits from clr-transformed microbial ASV tables. The sPLSR analysis elucidated robust taxa-specific links between individual ASVs and N_2O production processes by introducing a LASSO penalization to remove taxa with negligible effects (Cao et al., 2008). The final model was built using two latent components and a total of 60 microbial ASVs that separated broadly into four primary clusters (**Error! Reference source not found.**).

Cluster 1 contained eight bacterial and four archaeal ASVs, all of which belonged to SNET1 and correlated positively with N_2O production from NO_3^- reduction (r = 0.38 – 0.60) (Appendix C). The strongest taxon-specific correlations to rates of N_2O production from NO_3^- reduction (r > 0.50) were observed for ASVs that also correlated well with N_2O yields from nitrification (r = 0.38 – 0.60), which included *Nitrosopumilus* and SUP05 variants in addition to members of the Desulfobacterales, Marinimicrobia, Bathyarchaeia, and Thermosplasmata. In contrast, a subset of nine bacterial taxa within Cluster 4 demonstrated strong correlations to ΔN_2O (r = 0.62-0.78) and moderate correlations to nitrification rates > 0.30 (**Error! Reference source not found.**). Taxa in this subcluster were also positively associated with dissolved O_2 and NO_3^- + NO_2^- concentrations. ASVs included three SAR11 variants, three *Rhodobacteraceae* variants

(including one *Amylibacter* ASV), one member of the *Puniceicoccaceae* (Verrucomicrobia MB11C04 Marine Group), and unclassified members of the α-proteobacteria and Marinimicrobia. Cross-referencing these results with those of the network analyses shows that individual ASVs implicated by sPLSR as strongest predictors of N_2O cycling rate were also implicated as potential keystone taxa with high closeness centrality and node degree (**Error! Reference source not found.**b, **Error! Reference source not found.**).

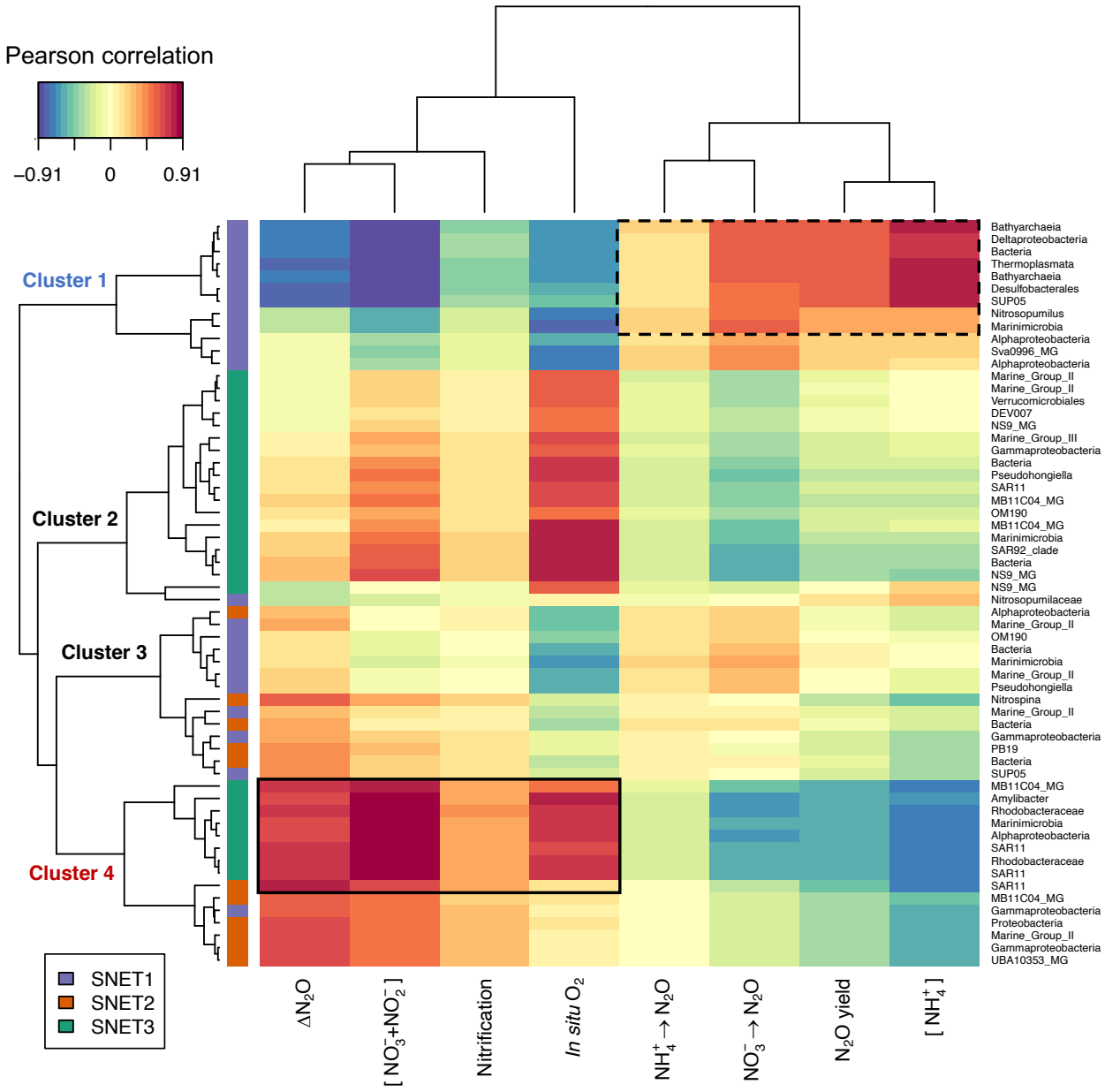

Fig. 2.5 sPLSR clustered heatmap (CIM).

Relationships between prokaryotic amplicon sequence variants (ASVs), relevant environmental variables and process rates. N_2O production rates from NH_4^+ oxidation and NO_3^- reduction are symbolized by black arrows. Pairwise correlation coefficients between ASVs and sample traits were calculated using a two-component sPLS regression model and are presented as a clustered heatmap. Taxa with correlations to nitrification rates > 0.30 are indicated by solid black lines and taxa with correlations to N_2O production from NO_3^- reduction > 0.50 are indicated by dashed lines. Hierarchical clustering of variables was achieved using a complete Euclidean distance method. ASV subnetwork assignments determined through WGCNA are indicated by coloured rectangles on the vertical axis dendrogram. Taxonomic labels correspond to the lowest level of classification determined for each ASV through alignment with the SILVA database.

2.5 Discussion

Spatiotemporal trends in microbial community structure were largely consistent with literature surveys of the Saanich Inlet water column over the seasonal stratification cycle (Michiels et al., 2019; Zaikova et al., 2010). Vertical stratification of key microbial taxonomic groups was also in agreement with patterns of redox-driven niche partitioning observed in open ocean ODZs and other coastal anoxic basins (Ulloa et al., 2012; Wright et al., 2012). Given the extensive body of existing literature documenting patterns of microbial community composition across water column redox gradients and the well-characterized seasonal succession patterns observed in Saanich Inlet, subsequent discussion is directed toward key microbial players and community interaction networks implicated in N_2O cycling.

The Saanich Inlet archaeal community was dominated by thaumarchaeotal ASVs belonging to the *Nitrosopumilaceae* family, a highly supported monophyletic clade that contains all known members of the ammonium oxidizing archaea (AOA) (Alves et al., 2018). The majority of putative AOA sequences belonged to a single *Nitrosopumilus*-like ASV, which displayed broad water column distributions throughout the sampling period. This variant clustered together in SNET1 alongside two additional *Nitrosopumilus*-like ecotypes that were enriched in samples from the lower oxycline and anoxic basin. Members of the *Nitrosopumilus*-like ecotype are widely distributed across marine ecosystems, suggesting a role as generalists possessing broad environmental tolerances (Hu et al., 2019; Müller et al., 2018; Reji et al., 2019a). *Nitrosopumilus*-like variants have been reported to dominate AOA communities in oxygen depleted waters of other sulfidic basins, including the Baltic and Black Seas, and in ODZ waters of the Eastern Tropical South Pacific (Labrenz et al., 2010; Sollai et al., 2019; Stewart et al., 2012). Recent work has demonstrated oxygen production by *Nitrosopumilus maritimus* cultures as a means of supporting

ammonium oxidation under anoxic conditions, indicating the presence of unique cellular machinery for maintenance during periods of severe oxygen limitation (Kraft et al., 2022). In contrast, putative AOA variants related to the *Nitrosopelagicus* genus, which belong to the previously delineated water column group A (WCA) clade (Santoro et al., 2015, 2017), clustered together in SNET2 and were most prevalent at oxycline depths. Previous surveys of oxygen deficient water columns have also demonstrated a preference of WCA-type AOA for oxygenated, epipelagic waters, suggesting that low-oxygen adaptation may not be universally distributed across all AOA clades (Lu et al., 2019; Muck et al., 2019; Sollai et al., 2019).

Inferences based on experimentally derived rate measurements used in this study and relationships between ΔN_2O and apparent oxygen utilization indicate that N_2O production in Saanich Inlet is dominated by ammonium oxidation across oxycline depths (Capelle et al., 2018; Ji et al., 2020). Similar to previous work in Saanich Inlet, sequences related to known ammonium oxidizing bacteria were not detected, suggesting that ammonium oxidation is predominantly mediated by AOA (Hawley et al., 2014). However, associations between biological variables and rates of N_2O production from ammonium oxidation were generally weak despite a significant correlation between the low-oxygen subnetwork (SNET1) and nitrification N_2O yields. Consistent with previous work, a substantial drop-off in overall nitrification rates was observed at O_2 concentrations less than 1 μmol L^{-1} resulting in low overall N_2O production rates despite extremely high molar N_2O yields (**Error! Reference source not found.**a) (Bristow et al., 2016; Ji et al., 2020). In contrast, maximum rates of N_2O production from NH_4^+ oxidation were measured at 160 m in October under suboxic conditions (O_2 < 20 μmol L^{-1}) following renewal of the deep basin (**Error! Reference source not found.**a) (Ji et al., 2020). Injection of oxygen to the deep basin

combined with high NH_4^+ concentrations in this case appears to have stimulated nitrification and the associated production of N_2O at relatively high yields.

Closer analysis of the data following removal of the October outlier point revealed a linear dependence of N_2O production rates from ammonium oxidation on overall nitrification rates (**Error! Reference source not found.**b). Furthermore, nitrification end products (NO_3^- + NO_2^-) and N_2O supersaturations were strongly associated with SNET2 and SNET3 communities (oxycline subnetworks hereafter), which contained distinct *Nitrosopelagicus*-like and *Nitrosopumilus*-like ecotypes. Water column N_2O accumulation in Saanich Inlet thus appears driven primarily by *Nitrosopumilus*- and *Nitrosopelagicus*-like AOA variants at low to moderate yields across oxycline depths, with low-O_2 *Nitrosopumilus*-like ecotypes dominating the high-yield production of N_2O near the anoxic boundary and in the deep basin following oxygen renewal. However, putative nitrifying taxa (AOA or NOB) were not implicated by sPLSR or WGCNA as significant predictors of nitrification rates. There was also no apparent systematic variation in nitrification rates associated with dissolved O_2 or NH_4^+ concentrations (**Error! Reference source not found.**), suggesting that alternative mechanisms may be responsible for regulating variability in nitrification rates, and thus N_2O accumulation across oxycline depths.

Consideration of community-wide dynamics showed that core community members belonging to oxycline subnetworks demonstrated stronger relationships to both nitrification rates and ΔN_2O. Putative keystone taxa linked to nitrification rates belonged primarily to groups previously affiliated with the heterotrophic remineralization of organic matter, including the SAR11 α-proteobacteria, *Rhodobacteraceae, Flavobacteriaceae,* and MGII Euryarchaeota. These results were largely substantiated by the sPLSR analysis, which implicated prominent members of the SAR11 clade, *Rhodobacteraceae*, and *Puniceicoccaceae* (Verrucomicrobia) as important

predictors of ΔN_2O and nitrification rates. Members of the SAR11 clade are found ubiquitously throughout the global ocean and across ODZ redox boundaries, and generally possess streamlined genomes adapted for aerobic growth on dissolved organic carbon under oligotrophic conditions (Giovannoni, 2017; Tsementzi et al., 2016). Conversely, groups affiliated with the Verrucomicrobia, *Rhodobacteraceae*, *Flavobacteriaceae*, and MGII Euryarchaeota are commonly observed in association with phytoplankton blooms and may act as specialist consumers of various phytoplankton-derived carbon substrates (Bakenhus et al., 2017; Cardman et al., 2014; Orellana et al., 2022; Teeling et al., 2016). The presence of proteorhodopsins in MGII metagenomes also suggests the potential for photoheterotrophic growth within the euphotic zone for this particular group (Pereira et al., 2019).

Interestingly, taxa affiliated with many of these groups have been identified as keystone community members across a wide range of aquatic systems, further highlighting the importance of common aerobic heterotrophs in maintaining community stability and facilitating ecosystem function (Banerjee et al., 2018). For example, *Rhodobacteraceae* groups can form mutualistic cross-feeding relationships with pelagic diatoms whereby remineralized ammonium stimulates carbon fixation (Zecher et al., 2020). Similarly, co-culture experiments using *Synechococcus and Roseobacter* populations have demonstrated that interactions between marine phototrophs and heterotrophs are stabilized over time through mutualistic nutrient cycling that involves leakage and subsequent remineralization of organic matter (Christie-Oleza et al., 2017). Recent work has indicated that marine AOA also exude considerable amounts of labile dissolved organic matter, and that these exudates may support the growth requirements of auxotrophic heterotrophs such as SAR11 (Bayer et al., 2019). Indeed, regeneration of ammonium or urea from dissolved organic matter has been proposed as a potential mode of metabolic coupling between marine AOA and

SAR11 based on metaproteomic surveys of the Saanich Inlet water column (Hawley et al., 2014). This is consistent with previous studies that have linked ammonium and nitrite oxidation rates to organic matter export and remineralization in marine water columns (Kalvelage et al., 2013; Santoro et al., 2021). These results collectively suggest that nitrification may be modulated through cross-feeding interactions with common aerobic heterotrophs occupying diverse niche spaces across oxycline depths.

Appreciable rates of N_2O production from NO_3^- reduction (hereafter denitrification), on the other hand, were primarily restricted to suboxic and anoxic depths, and were associated with putative keystone taxa belonging to the low-oxygen subnetwork. Prominent SUP05 ASVs were highly connected within the low-oxygen subnetwork and demonstrated robust taxa-specific correlations to N_2O production rates in both the WGCNA and sPLSR analyses. This is consistent with the role of SUP05 as core community taxa linking the biogeochemical cycling of nitrogen and sulfur in oxygen depleted environments (Hawley et al., 2014; Stewart et al., 2012; Walsh et al., 2009). Members of the SUP05 clade are abundant and active members of microbial communities across marine redox boundaries even in the absence of detectable levels of hydrogen sulfide and have been implicated as important drivers of autotropic denitrification coupled to sulfide and elemental sulfur oxidation (Callbeck et al., 2018, 2021; Canfield et al., 2010). Several mechanisms have been proposed to explain the persistence of SUP05 in sulfide-free waters, including intracellular storage of elemental sulfur or particle-associated micro-niches (Bianchi et al., 2018; Callbeck et al., 2021; Shah et al., 2019). Metagenomic and metaproteomic surveys of marine ODZs and coastal anoxic basins also indicate that the majority of SUP05 variants lack the metabolic machinery required to reduce N_2O to dinitrogen gas (N_2), leading to further speculation about a potential role in water column N_2O production (Hawley et al., 2014; Murillo et al., 2014;

Walsh et al., 2009). Given that SUP05 also appear as the only organisms in Saanich Inlet to express consecutive denitrification genes, these results provide further evidence that SUP05 acts as an important mediator of N_2O production from denitrification (Hawley et al., 2014).

Several additional ASVs were also implicated as potential keystone taxa with significant links to N_2O production from denitrification, including members of the Marinimicrobia, Bathyarchaeia, *Ectothiorhodospiraceae*, Desulfobacterales, and Thermoplasmata. Whether these relationships reflect direct contributions to denitrification processes, ecological interactions with denitrifying taxa, or overlapping niche-preferences remains to be determined. Genes encoding components of the denitrification pathway are spread ubiquitously throughout the prokaryote domains with many taxa possessing only a partial compliment of those required for complete denitrification, making it difficult to identify putative functional groups based on 16S rRNA sequences alone (Graf et al., 2014). Furthermore, a considerable proportion of highly connected ASVs within the low-oxygen subnetwork were not classifiable below the phylum or class level, leaving much to be learned about the taxonomic affiliations and functional potentials of many potential core community members. Approximately half of the total denitrification proteins detected in Saanich Inlet belong to taxa other than SUP05 (Hawley et al., 2014), indicating potential contributions to N_2O production facilitated by extracellular exchange of metabolic intermediates between modular components of the denitrification pathway. For example, two low-oxygen SAR11 ecotypes were detected in SNET1, and recent analysis of single-cell genomes from the ETNP has uncovered novel ODZ variants that contribute to nitrogen loss processes via respiratory nitrate reduction (Tsementzi et al., 2016).

As noted previously, elevated rates of N_2O production from denitrification were observed at depths depleted of nitrate and nitrite and were likely augmented by substrate enrichment

following tracer additions (Ji et al., 2020). However, putative nitrite-oxidizing bacteria (NOB) from the *Nitrospina* genus consisted of several low-O_2 ecotypes that were well-connected in the low-oxygen subnetwork alongside low-oxygen AOA ecotypes and correlated significantly with rates of N_2O production from denitrification. This correlation with denitrification supports previous reports of ecotype-specific metabolic interactions between AOA and NOB across depth-dependent environmental gradients and suggests the potential for N_2O production at lower oxycline depths driven by coupled nitrification-denitrification (Mincer et al., 2007; Parada & Fuhrman, 2017; Reji et al., 2019b). Surveys of the Eastern Tropical North Pacific (ETNP) reported enrichment of novel *Nitrospina*-like variants at the upper ODZ boundary and within the ODZ core coinciding with relatively high rates of nitrite oxidation coupled to nitrate reduction (Peng et al., 2015; Sun et al., 2021). Measurable rates of nitrification were also detected at sub-micromolar oxygen concentrations during the sampling period (Ji et al., 2020), and active ammonium and nitrite oxidation has been demonstrated in ODZ waters at oxygen concentrations as low as 5 nmol L^{-1} (Bristow et al., 2016; Ji et al., 2020). Regardless, taxa belonging to the low-oxygen subnetwork generally displayed strong negative correlations with water column ΔN_2O, and appreciable rates of N_2O production from denitrification were generally concomitant with pronounced N_2O undersaturation (Ji et al., 2020). As a result, N_2O production near the anoxic interface appears off-set by close coupling with N_2O consumption processes. Tight metabolic coupling between distributed elements of the denitrification pathway in Saanich Inlet may explain the low water column N_2O concentrations and surface N_2O fluxes relative to open ocean ODZs (Capelle et al., 2018).

Several of the core community members identified in the low-oxygen subnetwork belong to taxonomic groups containing ODZ representatives that possess atypical N_2O reductases, such

as the *Ectothiorhodospiraceae, Arcobacteraceae*, and Bacteroidales (Bertagnolli et al., 2020; Hawley et al., 2017). PICRUSt2 predictions of bacterial *nosZ* gene abundances based on 16S rRNA sequences were negatively correlated with ΔN_2O (**Error! Reference source not found.**), supporting previous reports of elevated *nosZ* activity within the Saanich Inlet deep basin (Hawley et al., 2014). Organisms possessing the atypical *nosZ* variant are commonly associated with higher N_2O affinities and lower O_2 sensitivities, and also typically lack additional genes in the denitrification pathway (Bertagnolli et al., 2020; Sanford et al., 2012; Yoon et al., 2016). A conceptual model describing mutualistic N_2O-cycling interactions has already been proposed in which N_2O produced by SUP05 is used by *nosZ*-harbouring Marinimicrobia ecotypes to store polysulfide and regenerate H_2S (Hawley et al., 2017). In contrast, atypical *nosZ* in the Bacteroidia class has been linked to particle-associated N_2O consumption while members of the *Arcobacter* genus in Saanich Inlet have been implicated in sulfide-driven denitrification (Bertagnolli et al., 2020; Callbeck et al., 2019; Fernández-Gómez et al., 2013). Atypical *nosZ* genes have also been identified in members of the *Ectothiorhodospiraceae*, a group generally associated with sulfide oxidation in anoxic environments (Beman & Carolan, 2013; Bertagnolli et al., 2011, 2020). Given the inability of SUP05 in Saanich Inlet to reduce N_2O, these results indicate that N_2O consumption may be mediated through cross-feeding relationships involving diverse N_2O-reducing organisms that occupy varying ecological niches (Hawley et al., 2014; Louca et al., 2016a).

The analyses presented here provide statistical support for the presence of distributed metabolic networks mediating N_2O production and consumption in low-oxygen and sulfidic environments, and implicate additional groups involved in anaerobic sulfur cycling as potential keystone taxa. ASVs belonging to the *Desulfobacteraceae* family, for example, may supply sulfide to denitrifying organisms by coupling heterotrophic carbon oxidation to sulfate reduction (Canfield

et al., 2010; Rabus et al., 2015). Metabolic coupling between chemolithotrophic denitrifiers and heterotrophic sulfate reducers may also help to explain the presence of detectable N_2O production rates from denitrification observed under well-oxygenated conditions following deep water renewal (Ji et al., 2020). Appreciable rates of N_2O production from reductive processes were detected at oxycline depths with O_2 concentrations as high as 70 μmol L^{-1} following summer and fall renewal events and were concomitant with high relative abundances of taxa from the low-oxygen subnetwork resulting from uplift of anoxic basin waters. Taxa from the low-oxygen subnetwork thus appear to serve as a net N_2O sink during periods of stable water column stratification yet maintain the capacity to respond rapidly to fresh inputs of terminal electron acceptors following renewal events, even under aerobic conditions. Re-supply of oxygen and fixed nitrogen species following deep-water renewal events therefore has the potential to simultaneously stimulate rates of N_2O production from all pathways and impede N_2O reduction within the deep basin, and may contribute to the elevated surface N_2O fluxes typically observed over fall months (Capelle et al., 2018).

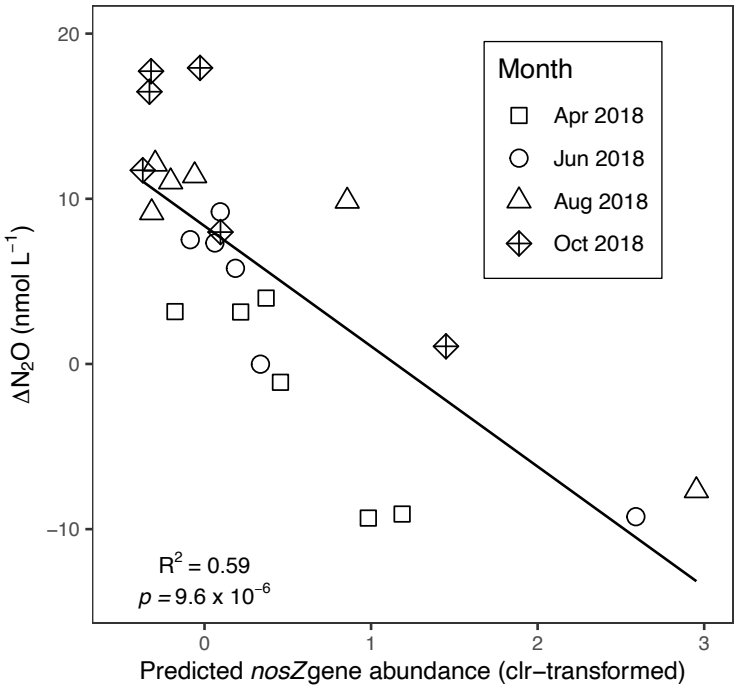

Fig. 2.6 PICRUSt2-predicted *nosZ* abundances.

Relationship between water column ΔN_2O (nmol L^{-1}) and PICRUSt2-predicted bacterial *nosZ* gene abundances. *NosZ* gene abundances were inferred from the predicted KEGG orthologues across all 24 samples using bacterial 16S rRNA amplicon sequences as input to the PICRUSt2 algorithm.

It is important to reiterate that specific findings obtained in a dynamic anoxic fjord that experiences both sulfide accumulation and transient oxygenation of the deep basin may not be extrapolatable to permanent open ocean ODZs. However, many of the interactions reported herein are centered around microbial constituents found ubiquitously throughout other sulfidic basins and open ocean ODZs, suggesting that similar relationships may be important determinants of microbial rate processes in other oxygen deficient marine systems. Regardless, interpreting the underlying nature of specific co-occurrences revealed by network analyses is challenging, as interactions between taxa may reflect several ecological, environmental, or stochastic mechanisms. This is complicated further by the functional ambiguities associated with molecular marker profiling of natural microbial communities. Although improvements to the taxonomic resolution provided by shotgun metagenomics surveys may permit a more detailed assessment of microbial

community interaction networks from a functional perspective, this would not eliminate the need to verify presumed ecological interactions empirically. A comprehensive view of how ecosystem function emerges from the cumulative influences of environmental variability and microbial community dynamics will require careful experimentation guided by exploratory analyses to better understand the mechanisms that drive ecological interactions and co-evolution between microbial taxa over space and time.

2.6 Acknowledgements

This research was supported by the Canadian Healthy Oceans Network, the University of Victoria, the Bermuda Institute of Ocean Sciences, and an NSERC CGS-M award. Field operations and laboratory analyses were partially supported by German Research Foundation (DFG) grants GR4721/2-1, MA6297/3-1) to D. Grundle and Christa Marandino (GEOMAR Helmholtz Centre for Ocean Research Kiel). I would like to thank co-author Dr. Qixing Ji for performing the stable-isotope incubations and providing the rate and environmental data. I would like to thank Captain Ken Brown and the crew of the MSV John Strickland for their valued assistance with field operations. I would also like to thank Dr. Roberta Hamme, Erinn Raftery (UVic), and Amy Maas (BIOS) for their assistance with oxygen measurements. Finally, we would like to thank Alan Roberts and Dr. Sheryl Murdock for their guidance on the statistical analyses and Drs. Roberta Hamme and Caren Helbing for their valued comments on early manuscript drafts.

2.7 Article Supplementary Tables and Figures

Table 2.2 Supplement: 16S rRNA primer sequences.

Primer sequences used to target the V6-V8 variable regions of the bacterial and archaeal 16S rRNA gene for high-throughput sequencing on Illumina MiSeq at the Integrated Microbiome Resource at Dalhousie University (https://imr.bio/protocols.html).

Primer sequences	Forward Primer	Reverse Primer
Bacteria (B969F/BA1406R)	ACGCGHNRAACCTTACC	ACGGGCRGTGWGTRCAA
Archaea (A956F/A1401R)	TYAATYGGANTCAACRCC	CRGTGWGTRCAAGGRGCA

Table 2.3 Supplement: Total read counts.

Total read counts are reported for bacterial and archaeal 16S rRNA gene amplicon reads in each sample following quality control and paired-end read merging. Depths and dates of sampling are recorded in addition to sample IDs.

Sample ID	Date	Depth	Bacteria	Archaea
APR_75	05-Apr-18	75	20125	8416
APR_90	05-Apr-18	90	17675	16455
APR_100	05-Apr-18	100	16185	15640
APR_110	05-Apr-18	110	19691	10423

APR_130	05-Apr-18	130	19928	8940
APR_160	05-Apr-18	160	12103	14636
JUN_75	14-Jun-18	75	15136	NA
JUN_90	14-Jun-18	90	14149	NA
JUN_100	14-Jun-18	100	16442	9224
JUN_110	14-Jun-18	110	15668	4873
JUN_130	14-Jun-18	130	26512	9230
JUN_160	14-Jun-18	160	19616	NA
AUG_75	02-Aug-18	75	9268	NA
AUG_90	02-Aug-18	90	7160	NA
AUG_100	02-Aug-18	100	10180	4271
AUG_110	02-Aug-18	110	10516	4391
AUG_130	02-Aug-18	130	21470	6912
AUG_160	02-Aug-18	160	7322	NA
OCT_75	25-Oct-18	75	13483	18683
OCT_90	25-Oct-18	90	13754	13005
OCT_100	25-Oct-18	100	25608	16961
OCT_110	25-Oct-18	110	17409	10915
OCT_130	25-Oct-18	130	12452	22826
OCT_160	25-Oct-18	160	15320	8355

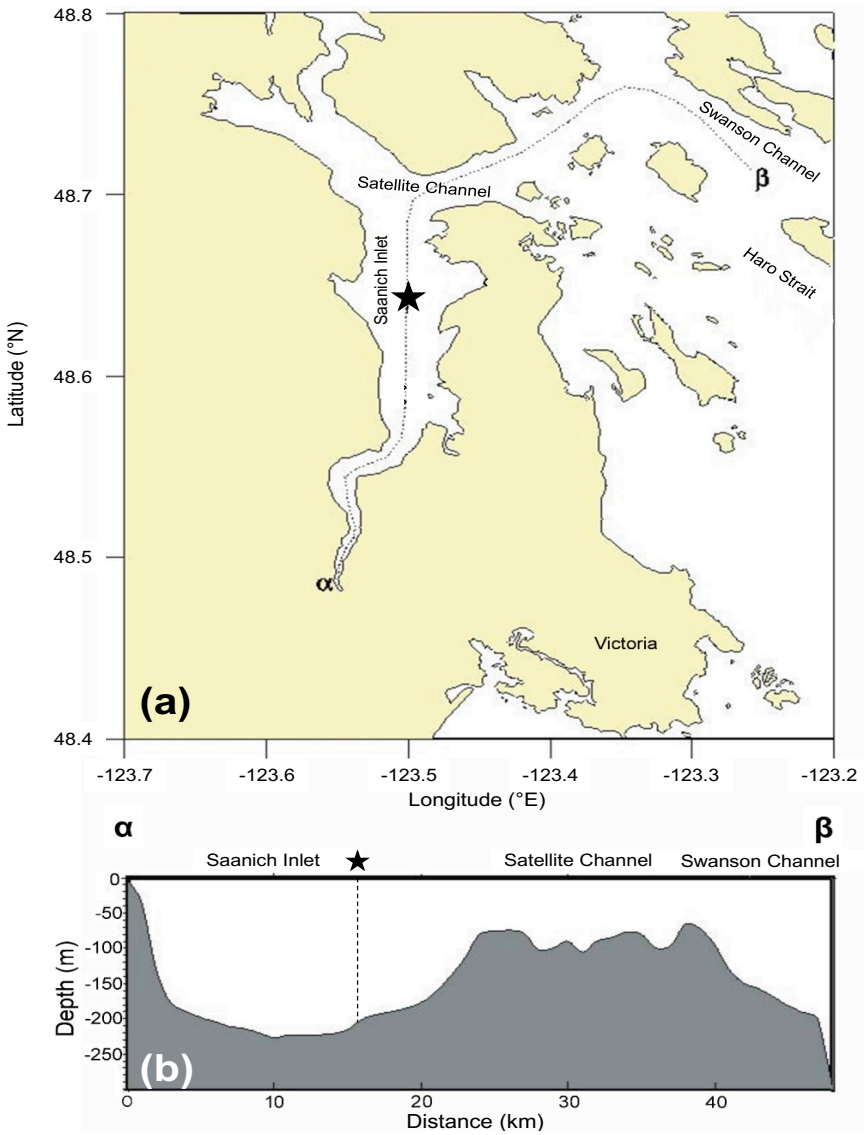

Fig. 2.7 Supplement: Map of Saanich Inlet, B.C., Canada.

Includes bathymetric cross section traversing the central deep basin and shallow sill located at Satellite Channel (b). Cross section in panel b follows the dashed transect line depicted in panel a. Sampling location is indicated by a star in both panels (48°47.707'N, 123°29.927'W). Figure adapted from Ji et al. (2020) Supplementary material.

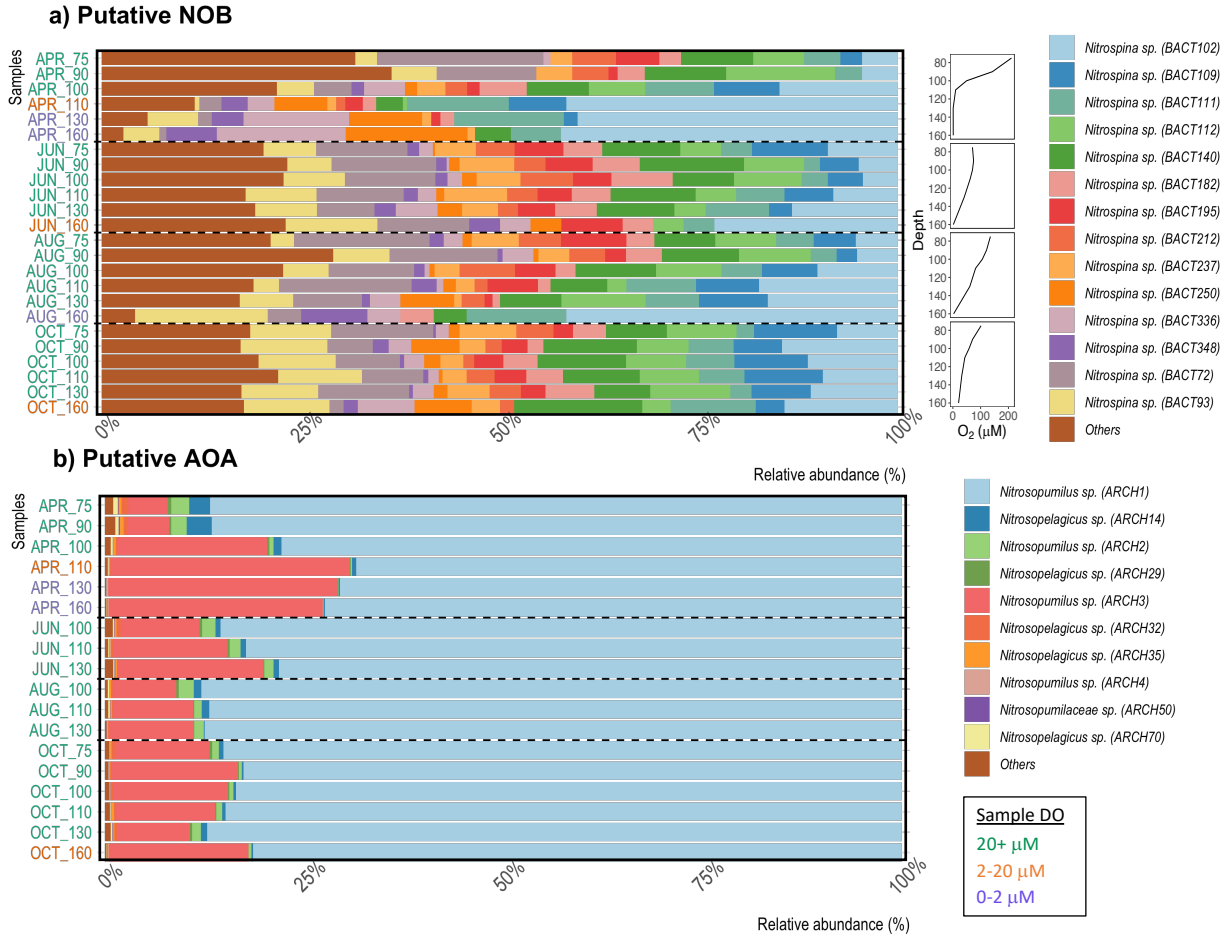

Fig. 2.8 Supplement: NOB and AOA community composition.

Relative abundances of a) putative nitrite-oxidizing Bacteria (NOB) and b) putative ammonium-oxidizing Archaea (AOA) ASVs in seston samples obtained in Saanich Inlet. Dissolved oxygen profiles for each sampling period are reported in panel a). Samples were obtained from Saanich inlet between April and October 2018. Sample labels on the vertical axes correspond to sampling month and water column depth.

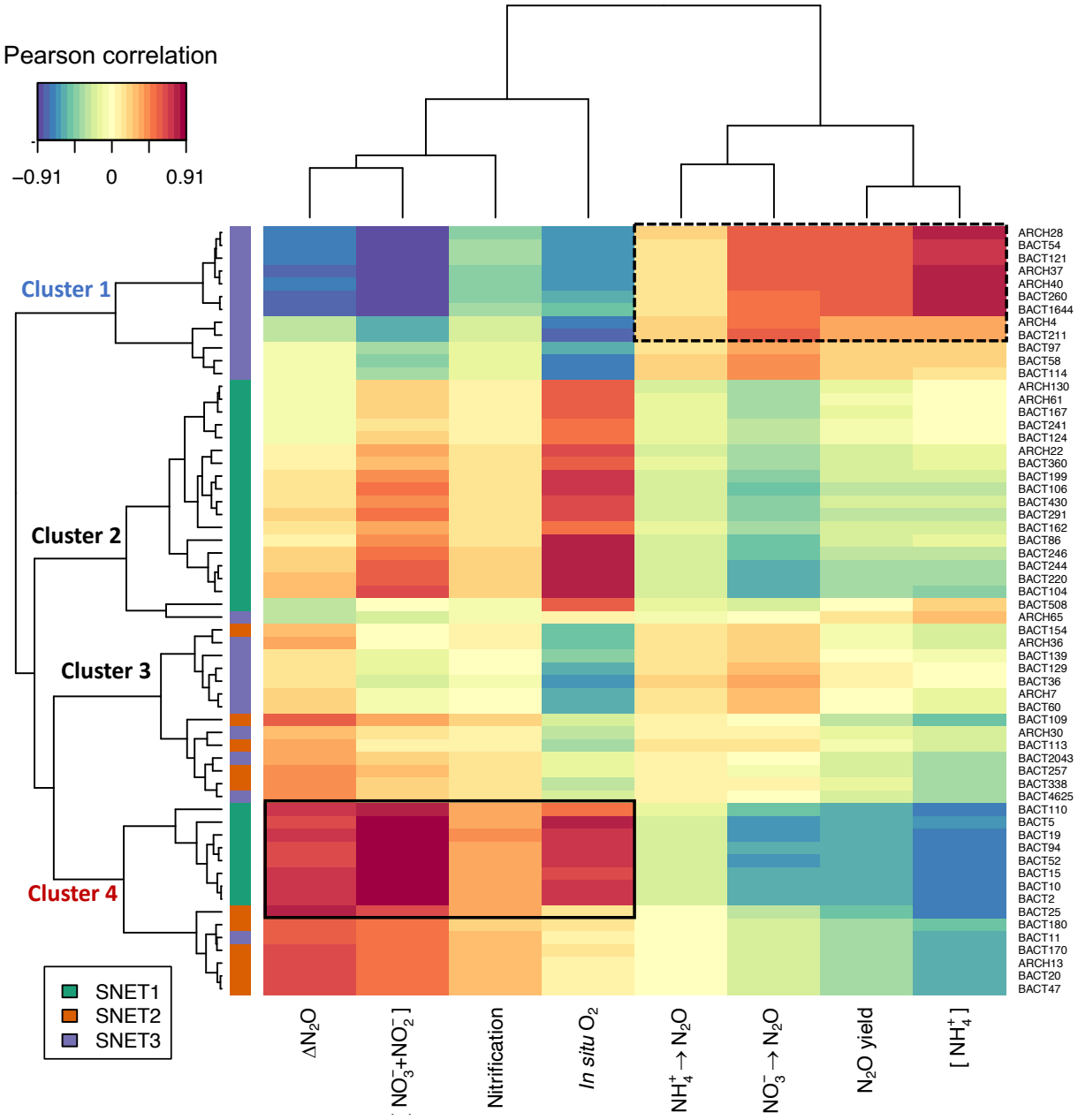

Fig. 2.9 Supplement: PLSR CIM with ASV identifiers.

Relationships between prokaryotic amplicon sequence variants (ASVs), relevant environmental variables and process rates. N_2O production rates from NH_4^+ oxidation and NO_3^- reduction are symbolized by black arrows. Pairwise correlation coefficients between ASVs and sample traits were calculated using a two-component sPLS regression model and are presented as a clustered heatmap. Taxa with correlations to nitrification rates > 0.30 are indicated by solid black lines and taxa with correlations to N_2O production from NO_3^- reduction > 0.50 are indicated by dashed lines. Hierarchical clustering of variables was achieved using a complete Euclidean distance method. ASV subnetwork assignments determined through WGCNA are indicated by coloured rectangles on the vertical axis dendrogram. This figure was reproduced from **Error! Reference source not found.** in the main text but replaces row names with microbial ASV identifiers.

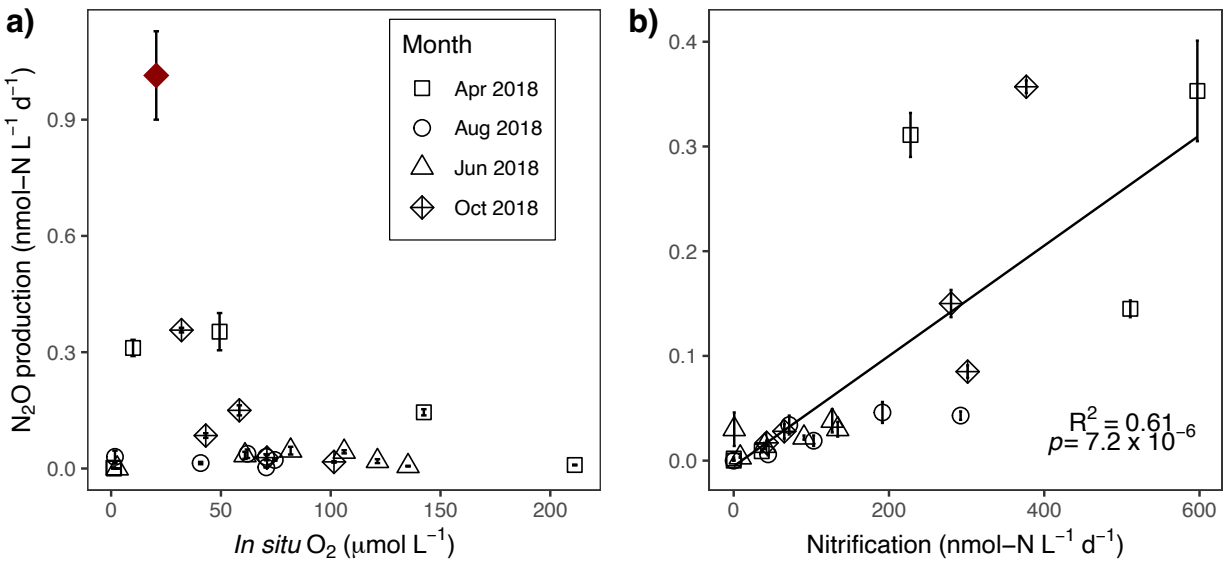

Fig. 2.10 Supplement: N_2O production rates.

Scatterplots showing relationships between rates of N_2O production from NH_4^+ oxidation (nmol-N L^{-1} d^{-1}) and a) *in situ* dissolved O_2 concentrations (μmol L^{-1}) and b) nitrification rates (nmol-N L^{-1} d^{-1}). Linear regression in panel B was conducted following removal of the outlier point highlighted in red in panel A. Reproduced from data reported in Ji et al. (2020). Error bars represent ± SD.

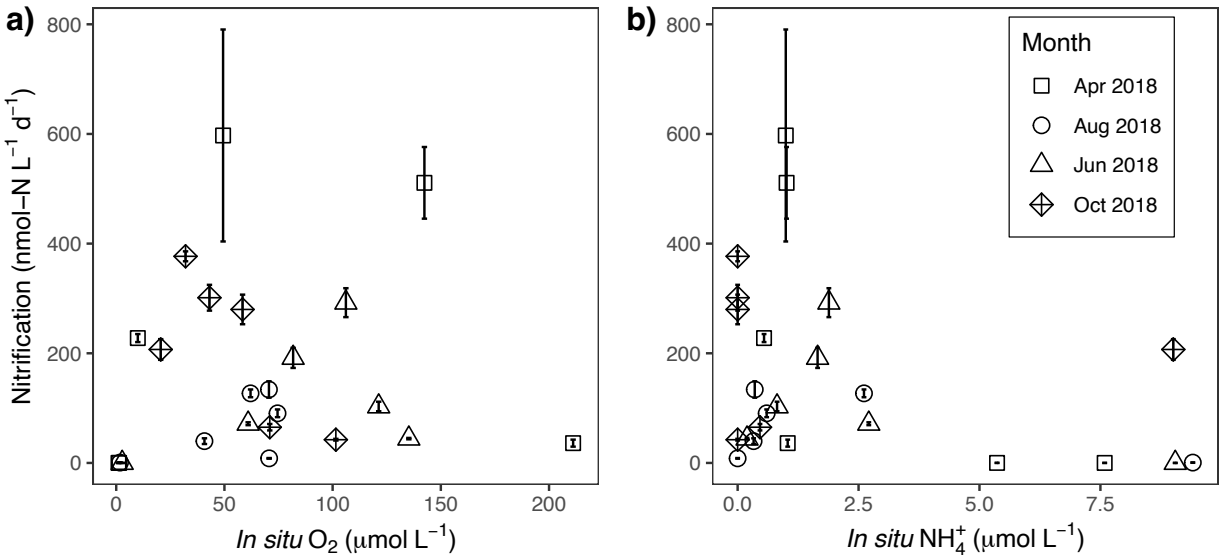

Fig. 2.11 Supplement: Nitrification rates.

Scatterplots showing relationships between nitrification rates (nmol-N L^{-1} d^{-1}) and a) *in situ* dissolved O_2 concentrations (μmol L^{-1}) and b) *in situ* dissolved NH_4^+ concentrations (μmol L^{-1}). Reproduced from data reported in Ji et al. (2020). Error bars represent ± SD.

Chapter 3: Continental margin sediments underlying the NE Pacific oxygen minimum zone are a source of nitrous oxide to the water column

Citation:

Jameson, B. D., Berg, P., Grundle, D. S., Stevens, C. J., & Juniper, S. K. (2021). Continental margin sediments underlying the NE Pacific oxygen minimum zone are a source of nitrous oxide to the water column. *Limnology and Oceanography Letters*, *6*(2), 68-76.

3.1 Abstract

Continental margin sediments are important sites of marine nitrogen cycling and potential contributors to atmospheric N_2O emissions. Trace level N_2O microsensors were employed to measure vertical N_2O profiles at sub-millimeter resolutions in intact cores from outer continental margin sediments underlying the NE Pacific oxygen minimum zone. Application of mathematical modelling to porewater profiles estimated depth-dependent rates of N_2O production and fluxes to the overlying water along a transect of diminishing bottom water oxygen concentrations. Net sediment efflux was observed at all sites on the outer continental margin, with a mean value of ~524 nmol m^{-2} d^{-1}. N_2O efflux increased with decreased oxygen penetration depth in sediments. Enhanced N_2O production and efflux were obtained when outer continental shelf sediments were experimentally exposed to lower bottom-water O_2 concentrations, to simulate upwelling conditions. These results underline the need for further investigation of the drivers of N_2O production in continental margin sediments, and the relative importance of these environments to the global N_2O budget.

3.2 Introduction

Nitrous oxide (N_2O) is an important and increasingly abundant atmospheric trace gas which, in the troposphere, has a per mol atmospheric warming potential that is up to 340 times that of CO_2 over a 100-year timespan (Bange, 2008; IPCC, 2021). N_2O also survives transport to the stratosphere where it contributes to ozone depletion (IPCC, 2021). In terrestrial and aquatic environments, N_2O is produced by nitrifying bacteria and archaea, and both produced and consumed by denitrifying bacteria. Recent estimates indicate that the global ocean acts as a net source of N_2O to the atmosphere, amounting to approximately 25% of the combined 15.8 TgN-N_2O yr^{-1} of natural and anthropogenic emissions (IPCC, 2021). Elevated N_2O production rates and atmospheric fluxes are often associated with productive oceanographic regions, such as eastern boundary upwelling systems and mesoscale eddies, where high rates of organic matter decomposition drive steep redox gradients and rapid nitrogen cycling in subsurface waters and sediments (Arévalo-Martínez et al., 2015; Grundle et al., 2017). However, modelled estimates of global oceanic flux have high degrees of uncertainty, partially attributable to sparse observational data coverage across marine environments (Bange et al., 2019). Indeed, studies have primarily focused on water column oxygen minimum zones (OMZs) and estuarine systems (Freing et al., 2012; Murray et al., 2015), leaving data gaps over large portions of the global ocean.

Comparatively little effort has been directed at investigating N_2O cycling in offshore sediments and in relation to the availability of dissolved O_2 in bottom waters. Continental margin sediments are important regions of organic carbon deposition, fueled by high primary production in overlying shelf waters (Huettel et al., 2014). The remineralization of organic matter in surface sediments results in shallow oxygen penetration depths (Devol, 2015), and facilitates tight spatial coupling of nitrification and denitrification at the sedimentary oxycline (Devol & Christensen,

1993; Seitzinger & Giblin, 1996; Devol, 2015). This highlights the potential contributions of sedimentary processes to N_2O cycling on the continental margin.

The Northeast Subarctic Pacific Ocean (NESAP) is characterized by an intermediate depth OMZ (~400 – 1100 m) that impinges on continental slope sediments off the coasts of British Columbia, Washington and Oregon (Crawford & Peña, 2013),and N_2O concentrations in the OMZ core can exceed 50 nmol L^{-1} (Fenwick & Tortell, 2018). *In situ* production of N_2O has been attributed to water column nitrification, based on N_2O excess (ΔN_2O) versus apparent oxygen utilization (AOU) relationships, and the fact that water column dissolved O_2 concentrations in the OMZ core (~10 μmol L^{-1}) remain above the hypothesized threshold for the onset of denitrification (Grundle et al., 2012; Capelle & Tortell, 2016; Fenwick & Tortell, 2018). However, the status of sediments underlying the NESAP OMZ as sources or sinks of N_2O to the water column has not been investigated. Previous research in the region has confirmed both nitrification and denitrification activity in shelf and slope sediments, with denitrification fueled by nitrate supplied from the overlying water column and from sedimentary nitrification (Devol & Christensen, 1993; Belley et al., 2016) .

N_2O originating in subsurface waters in this area can be emitted to the atmosphere following episodic upwelling and other vertical mixing processes (Capelle & Tortell, 2016), presenting a potential conduit linking N_2O cycling in sediments with sea surface N_2O emissions. In addition, the exposure of shelf sediments to low-O_2 waters during upwelling events or through longer-term shoaling of the upper OMZ may have undescribed impacts on sediment N_2O production and efflux. Dissolved O_2 concentrations below 45 μmol L^{-1} have been observed in bottom waters on the Vancouver Island continental shelf between 200 and 100 m depth during the

summer upwelling season, and long-term declines in O_2 concentrations on the continental shelf have been observed in previous decades (Crawford & Peña, 2013).

This study reports the first measurements of submillimeter-scale N_2O porewater profiles, depth- distributed production rates, and vertical fluxes in offshore sediments using trace-level N_2O microsensors and mathematical modelling. The numerical profile interpretation procedure, PROFILE (Berg et al., 1998), was used to model N_2O production rates and sediment effluxes in relation to O_2 consumption and bottom water O_2 availability. These results demonstrate substantial sedimentary N_2O production in the NESAP, and highlight the potential contribution of continental margin sediments to water column N_2O accumulation and sea-to-air emissions.

3.3 Methods

3.3.1 Field sampling

Field operations were conducted off the west coast of Vancouver Island, Canada between 29 September and 04 October 2019. All data are available through Scholars Portal Dataverse (Jameson et al., 2020). A multicorer was used to collect replicate sediment cores (i.d = 9.8 cm; length = 52.0 cm) from three sampling stations (200, 475, and 850 m depth) positioned along a transect of increasing depth and diminishing bottom water O_2 concentrations (**Error! Reference source not found.**). The two deeper stations (475 and 850 m) were within the portion of the upper continental slope that is influenced by the OMZ, whereas the shallowest station (200 m) represented the more oxygenated outer continental shelf. Bottom water characteristics were measured at each station using a CTD rosette (SBE 43, Sea-Bird Electronics), and bottom water samples were obtained from 5 – 10 m above the seafloor in 2.8-L Niskin bottles. Bottom water was immediately transferred to an N_2-flushed reservoir using ¾ inch Tygon tubing and stored in the shipboard cold room.

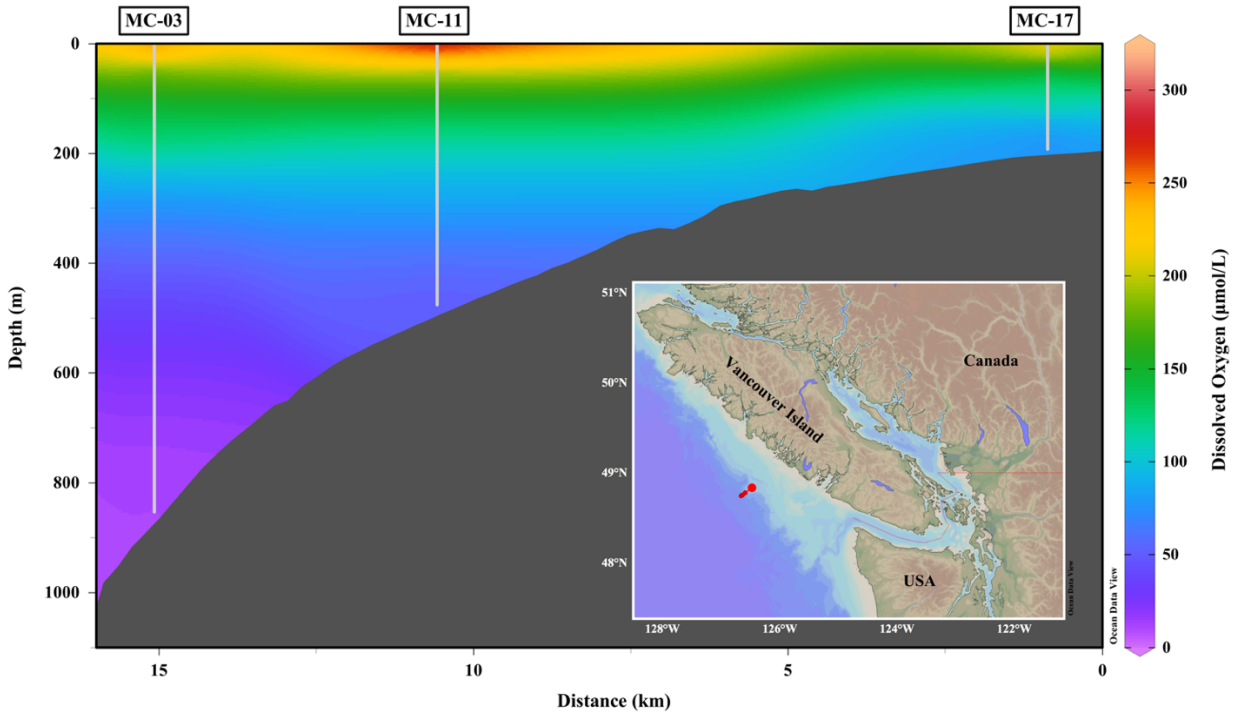

Fig. 3.1 Clayoquot slope sampling transect

Includes map of locations selected for multi-core sediment sampling and bathymetric cross-section of water column dissolved O_2 concentrations. Samples were collected on Clayoquot Slope in the Northeast Pacific between 29 September – 2 October 2019. White lines on the depth-section plot indicate the locations of water column profile and multi-core operations. This figure was created in Ocean Data View using the Data-Interpolating Variational Analysis (DIVA) tool. The interpolation was performed using CTD cast data from 4 stations, including the three sediment sampling locations labelled above and one off-shelf deep CTD cast station not shown (no sediments were collected at this station).

3.3.2 Incubation procedures and upwelling experiment

Triplicate sediment cores from each sampling location for 24-36 hours were incubated under near *in situ* temperature and dissolved O_2 conditions to re-establish steady-state conditions prior to sediment profiling. Sediment cores were sealed with ~1.5 L of bottom-water headspace using acrylic caps fitted with water circulation ports and magnetic stir bars to facilitate continuous water flow and headspace mixing (Belley et al., 2016). Core tubes were connected in line to a peristaltic pump and an oxygen-control reservoir (13.25 L high-density polyethylene; neoprene lid gasket) using 5/8 inch Masterflex Precision Pump Tubing (Cole-Parmer, Montreal, CAN). Water

circulation ports, an O_2 measurement port, and a gas control port were fitted into the reservoir lid (**Error! Reference source not found.**). The same setup was used to incubate three additional cores from the 200 m station in low-O_2 water obtained from 475 m depth, to examine how N_2O flux in outer continental shelf sediments might respond to exposure to low-O_2 water during upwelling events. The experiment simulated dissolved O_2 concentrations observed by Ocean Networks Canada (ONC) in continental shelf bottom waters in the region during the summer upwelling season(Crawford & Peña, 2013). During the upwelling season, low-O_2 bottom waters can propagate across the shelf to the outer coast of Vancouver Island and are regularly detected at the ONC Folger Deep node at 98 m depth (ONC, 2020).

The peristaltic pump continuously circulated water from the reservoir through the core tubes at a flow rate of ~50 mL min^{-1}. Steady-state dissolved O_2 concentrations in the headspace water were maintained by bubbling either N_2 gas or medical-grade compressed air (Praxair, Mississauga, ON) into the reservoir through the gas control port using an aquarium air stone. Monitoring of O_2 concentrations at regular intervals (2 – 4 hrs) in the reservoir was accomplished using a Fibox 4 Trace O_2 meter; and in individual core tubes with pre-fitted O_2 Sensor Spots using a Fibox Polymer Optical Fiber attachment (PreSens, Regensburg, DE). Temperature in the reservoir was recorded continuously using an RBRduet T.D Dual Channel Logger (RBR Ltd., Ottawa, ON).

In-situ bottom water dissolved O_2 ranged from 10 to 77 μmol L^{-1}, temperatures ranged from 4.0 to 6.9 °C, while salinity ranged from 34.0 to 34.3 (PSS-78) (Table 2.1). All sediment cores were incubated at a mean temperature of 8.2 (± 0.6) ºC, over the final 8 hours of incubation. Mean O_2 concentrations during the same timeframe were 132.5 (± 15.4), 32.3 (± 0.9), 32.8 (± 6.8),

and 13.9 (± 4.3) μmol L^{-1}, respectively, for the 200 m control, 200 m upwelling experiment, 475 m and 850 m sediment core incubations (Supporting Information, Table 2.2).

Table 3.1 Clayoquot slope sampling information.

Sampling stations, dates, locations and environmental characteristics. Temperature, Salinity, and O_2 values are for bottom water at the depth of sediment core collection. OPD = mean oxygen penetration depth in initial profiles (± SE, n = 3), defined as the depth at which porewater O_2 reaches suboxic levels (O_2 < 5 μmol L^{-1}).

Station	Date	Lat (N)	Long (W)	Depth (m)	Temp (°C)	Salinity (PSS-78)	Bottom O_2 (μmol L^{-1})	Porosity (%)	OPD (mm)
MC-17	2019-09-28	48° 49.86	126° 28.99	200	6.9	34.0	77	56 ± 11	4.2 ± 1.1 [C] 1.3 ± 0.2 [U]
MC-11	2019-10-01	48° 46.66	126° 35.30	475	5.4	34.1	47	53 ± 3	1.8 ± 0.2
MC-03	2019-10-02	48° 45.26	126° 38.31	850	4.0	34.3	10	81 ± 2	0.9 ± 0.1

[C] *OPDs measured in 200 m control cores.*
[U] *OPDs measured in 200 m upwelling experiment cores.*

3.3.3 Microelectrode profiles

Porewater N_2O and O_2 concentration profiles were measured in post-incubation cores, and in initial cores immediately following sampling (**Error! Reference source not found.**). The latter was to ensure that post-incubation profiles were not artifacts of the incubation procedure. Profiles were obtained using Clark-type N_2O and O_2 microelectrodes with respective detection limits less than 20 nmol L^{-1} and 0.3 μmol L^{-1}, and sensor tip diameters of 500 μm and 200 μm (Unisense, Aarhus, DK). All sensors were calibrated in a CAL300 chamber by two-point calibration according to manufacturer instructions. The O_2 sensor was calibrated in a zero-oxygen solution and in air-saturated water, correcting O_2 concentration of air-saturated water for temperature and salinity (Garcia & Gordon, 1992; Garcia & Gordon, 1993). The N_2O sensor was calibrated in bottom water flushed with N_2 and 15.6 ppmv N_2O gas standards, and N_2O

concentrations in enriched standards were calculated using the N_2O solubility coefficients table (Weiss & Price, 1980).

Microelectrodes were mounted on a Unisense MM33 motorized micromanipulator and adjusted to the sediment interface prior to profiling. Discrete measurements were made at 500 μm steps, starting at 1000 μm above the sediment interface and terminating once consistent zero values were reached. N_2O and O_2 profiles were measured separately, and sensors were left to equilibrate at each measurement depth in accordance with individual sensor response times (25 and 5 seconds, respectively).

3.3.4 PROFILE interpretations and statistical analyses

Porewater profiles from post-incubation cores were used to model depth-dependent production/consumption rates and sediment fluxes using the numerical profile interpretation procedure PROFILE described by Berg et al. (1998). Sediment porosities were determined in each incubated core according to Dalsgaard et al. (2000), for use in the PROFILE model. Oxygen penetration depths (OPD), defined as the depth at which porewater O_2 fell to less than the suboxic level of 5 μmol L^{-1} (Belley et al., 2016), were estimated in each core following linear interpolation between individual data points. Concentration profile measurements, sediment fluxes and OPDs are all reported as means (± SE, n = 3).

All statistical analyses were conducted in the R statistical environment (R Core Team, 2019), and all datasets were tested for normality using Shapiro-Wilks tests. Where assumptions of linearity or normality were violated, the response variable was natural-log transformed. To determine the potential drivers of N_2O flux variability, a multiple regression model was fit to N_2O fluxes using the paired O_2 fluxes and OPDs as predictor variables. Finally, a separate linear

regression model was fit relating individual OPDs and bottom water (headspace) O_2 concentrations.

3.4 Results

3.4.1 Porewater concentration profiles

Mean OPDs were deepest in the control cores from 200 m depth, where natural bottom water O_2 concentrations were highest, and shallowest in the 850 m cores from the OMZ core (Table 3.1, **Error! Reference source not found.**). Natural log-transformed OPDs were positively correlated with bottom water (headspace) O_2 concentrations ($R^2_{adj} = 0.46$, $p < 0.01$). Pronounced subsurface N_2O maxima were observed coinciding with down-core transitions to suboxic conditions in cores from the 200 m upwelling experiment, 475 m, and 850 m; while the 200 m control sediments showed relatively consistent concentrations in the top 3 mm (**Error! Reference source not found.**). Maximum porewater N_2O concentrations ranged from 57 (± 10) in the 200 m control sediments to 116 (± 20) nmol L^{-1} in the 475 m sediments. In the cores from 200 m depth, porewater N_2O concentrations were higher in experimental (simulated upwelling) cores (78 ± 16 nmol L^{-1}) than in controls (57 ± 10 nmol L^{-1}).

3.4.2 PROFILE interpretations

Modelled concentration profiles for both N_2O and O_2 provided good fits ($R^2 > 0.98$) to the mean profiles (**Error! Reference source not found.**). Maximum net N_2O production rates coincided with zones of O_2 consumption in surface sediments for all core incubations and increased with diminishing bottom water O_2 concentrations. Maximum N_2O production rates in the 200 m sediments increased from 0.046 to 0.290 nmol cm^{-3} d^{-1} between the control and upwelling cores, while increasing from 0.221 to 0.348 nmol cm^{-3} d^{-1} between the 475 m and 850

m cores. Single zones of net consumption coincided with declines in porewater N_2O concentrations in anoxic layers for both 200 m

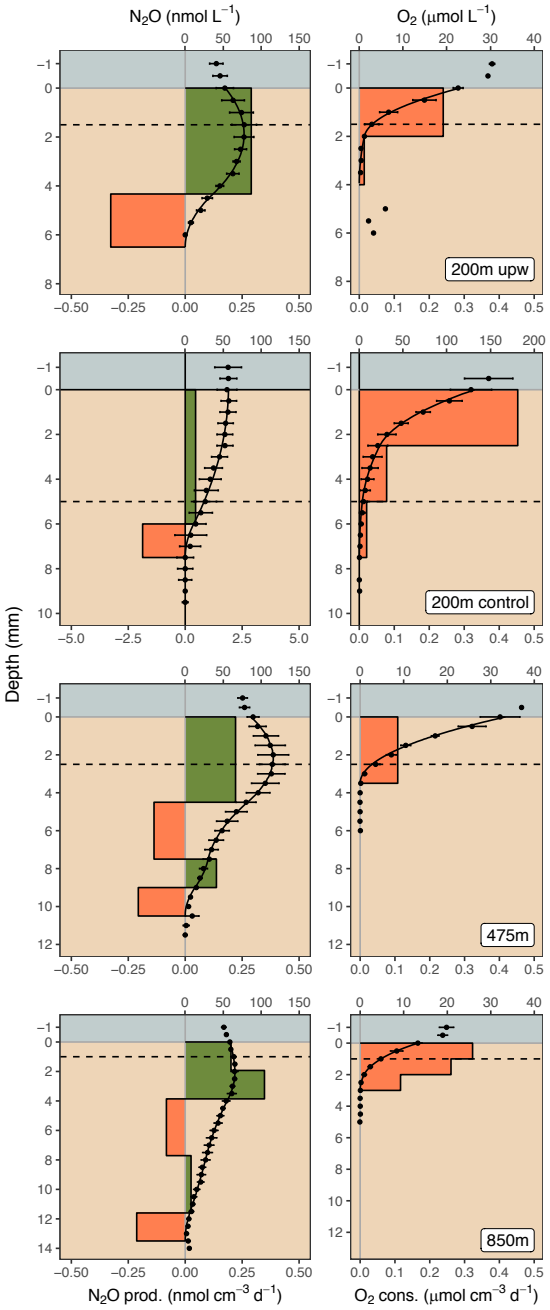

Fig. 3.2 PROFILE model outputs.

Depth-distribution of N_2O production and O_2 consumption zones modelled from mean porewater concentration profiles in post-incubation cores. Solid black lines are modelled concentration profiles and

individual points represent measured porewater concentrations (± SE) for the 200 m control (n = 2), 200 m control, 475 m, and 850 m cores (n = 3). Dashed lines represent OPD in the mean profile. Green and red boxes represent zones of production and consumption, respectively. In each panel, the scale on the upper horizontal axes corresponds to pore water concentrations, while the lower axis corresponds to rates of production and consumption. Note 1000 factor difference in units between N_2O panels (nmol cm^{-3} d^{1} and nmol L^{-1}) and O_2 panels (µmol cm^{-3} d^{-1} and µmol L^{-1}), and the change in scale for the O_2 concentration axis in the 200 m control profiles.
incubations. In the 475 and 850 m sediments, secondary zones of net N_2O production of smaller

magnitude were present in deeper anoxic layers (**Error! Reference source not found.**).

3.4.3 Sediment fluxes

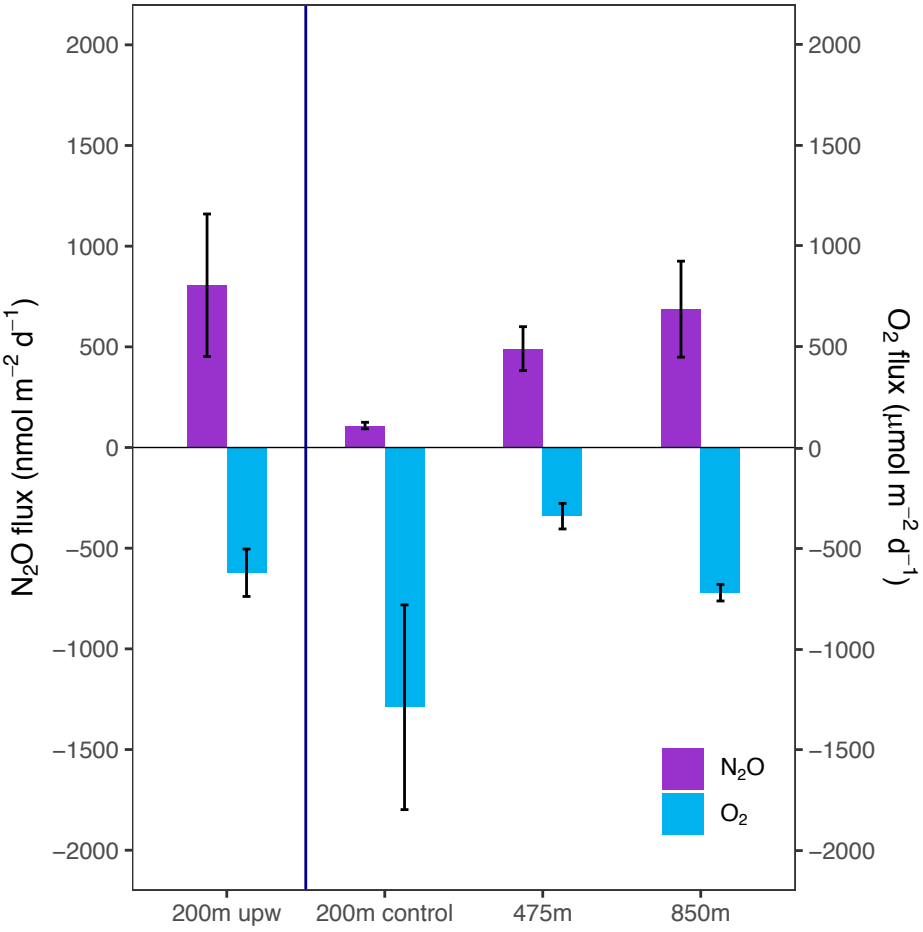

Fig. 3.3 Modelled N_2O and O_2 fluxes.

Values represent mean fluxes (± SE) estimated from individual concentration profiles using the PROFILE model for the 200 m control (n = 2), 200 m upwelling, 475 m, and 850 m cores (n = 3). Note the 1000 factor difference in units between N_2O fluxes (nmol m^{-2} d^{1}) and O_2 fluxes (µmol m^{-2} d^{-1}).

Sediment N_2O effluxes were positive for all sampling locations (**Error! Reference source not found.**). Mean N_2O effluxes were lowest in the 200m control cores (109 ± 28 nmol m^{-2} d^{-1}) and increased five-fold to a maximum of 806 (± 613) nmol m^{-2} d^{-1} in the 200 m upwelling cores. Mean N_2O effluxes for the 475 m and 850 m cores were comparable at 456 (± 248) and 687 (± 413) nmol m^{-2} d^{-1}, respectively. OPD and O_2 flux accounted for approximately 66% of the variability in natural log-transformed N_2O fluxes ($R^2_{adj} = 0.66$, $p < 0.01$). In separate, non-linear exponential models, N_2O efflux was inversely correlated with OPD ($R^2_{adj} = 0.31$, $p = 0.035$) but was not significantly correlated with O_2 flux (**Error! Reference source not found.**a). Total O_2 consumption estimates ranged from 341 (± 110) to 965 (± 640) μmol m^2 d^{-1} and did not show any discernable trends.

3.5 Discussion

This study provides a first examination of N_2O cycling in continental margin sediments of the NESAP, and implicate these environments as net N_2O sources to the overlying water column. Downcore, subsurface N_2O maxima and zones of highest production rates generally corresponded to zones of O_2 consumption, implicating ammonium oxidation as an important production pathway. N_2O production from ammonium oxidation under low-O_2 conditions is the result of incomplete oxidation of the metabolic intermediate, hydroxylamine (Kozlowski et al., 2016), and exponential increases in N_2O production have been demonstrated below 30 μmol L^{-1} O_2 in OMZ waters of the eastern tropical North Pacific (Trimmer et al., 2016). Potential contributions from denitrification are also indicated by the extension of N_2O production zones below the OPD. Denitrification can also proceed under suboxic conditions, and partial denitrification leading to N_2O accumulation has been attributed to the higher O_2 sensitivity of the N_2O-reductase enzyme (Spiro, 2012). Further work will be needed to evaluate the relative

contributions of nitrification and denitrification to N_2O production in offshore sediments, and how this balance may be related to environmental factors.

The negative correlation of N_2O efflux and OPD observed here (**Error! Reference source not found.**a) suggests that N_2O efflux may be influenced by diffusion distance between zones of production and the sediment surface. To test this, the sensitivity of N_2O efflux to N_2O source depth was modelled by applying Fick's First Law of Diffusion to a hypothetical dataset constrained by the porewater profiling results. Holding sediment diffusivity and porosity constant, the effect of N_2O concentration gradient strength ($\frac{dC}{dX}$) on diffusive fluxes was estimated by varying the N_2O source depth and N_2O source concentrations (**Error! Reference source not found.**b). Since subsurface N_2O maxima observed in this study coincided with suboxic sediment depths, the range of N_2O source depths was set to encompass the range of mean OPDs across all incubations. Source concentrations were within the range of those observed in NESAP sediment cores. These results demonstrate the degree to which N_2O efflux can be influenced by source depth and the resulting strength of concentration gradients, and suggest that there may be a critical OPD beyond which little N_2O can reach the sediment surface unless there are large increases in N_2O production (**Error! Reference source not found.**b).

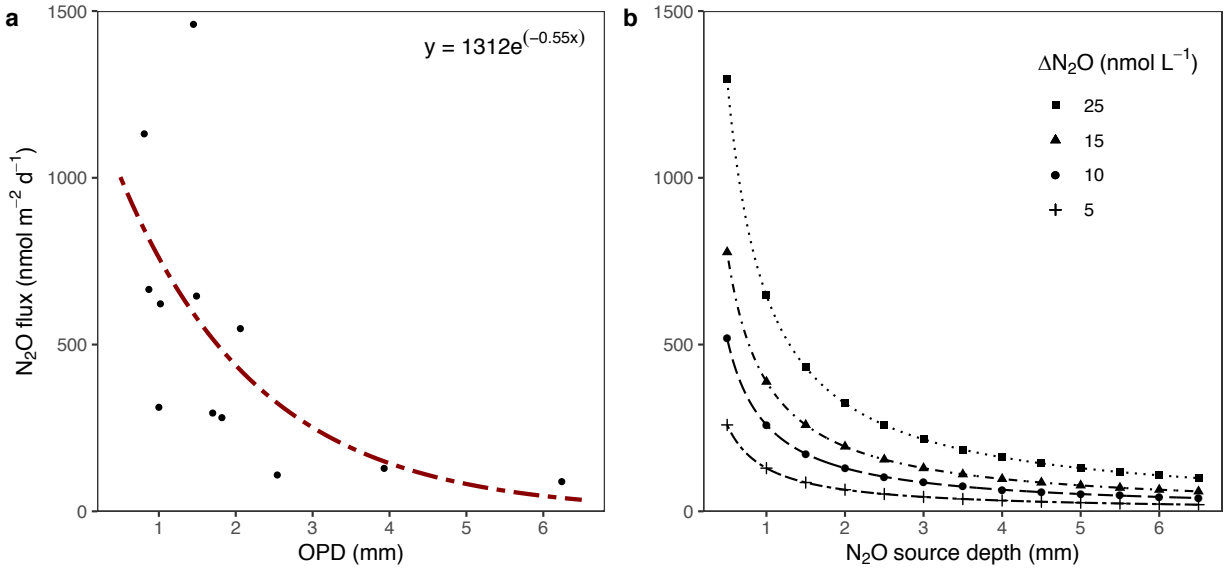

Fig. 3.4 N2O efflux as a function of oxygen penetration depth (OPD).

A) Efflux (nmol m^{-2} d^{-1}) and OPD (mm) values were determined from measured porewater concentrations in individual cores, pooled across all incubations. The correlation is statistically significant ($R^2_{adj} = 0.31$, $p = 0.035$). B) Modelled analysis of the sensitivity of N_2O efflux to N_2O source depth and change in N_2O concentration between the sediment surface and the subsurface N_2O source (ΔN_2O). For each ΔN_2O value, N_2O effluxes (nmol m^{-2} d^{-1}) were calculated from varying N_2O source depths (mm) using Fick's First Law of Diffusion, and holding the sediment diffusivity and porosity constant.

Results of the simulated upwelling experiment suggest that low-O_2 events can increase N_2O efflux from shelf sediments, through shoaling of the OPD and a rapid metabolic response of N_2O-producing organisms. Bottom-water hypoxia can extend over large portions of the continental shelf during the upwelling season, as low-O_2 water from the offshore OMZ propagates inshore (Grantham et al., 2004). Since upwelling events in the NE Pacific are also associated with large increases in sea surface N_2O emissions (Capelle & Tortell, 2016), this creates a possible link between sediment N_2O production and the atmosphere. This also emphasizes the need for additional research into the effects of long-term OMZ shoaling (Crawford & Peña, 2013) on sedimentary N_2O production.

The estimates of N_2O efflux presented here are generally an order of magnitude lower than those reported for intertidal estuarine sediments (Murray et al., 2015). The higher N_2O production rates and sediment efflux in estuaries can be attributed to increased organic matter

supply, DIN concentrations, and temperatures (Middelburg et al., 1995; Murray et al., 2015). However, there is considerable spatial and temporal variability in the magnitude and direction of reported N_2O fluxes in estuarine sediments (Murray et al., 2015). This variability has been linked, in part, to DIN availability, with net N_2O consumption by denitrification commonly observed when NO_3^- and NO_2^- are sufficiently low (Foster & Fulweiler, 2016; Jensen et al., 1984). The global median NO_3^- concentration for estuarine systems is approximately 50 μmol L^{-1} (Murray et al., 2015), and much of the work on sedimentary N_2O production has focused on eutrophic estuaries, where NO_3^- concentrations can exceed 500 μmol L^{-1} (Sanders et al., 1997). In contrast, bottom water NO_3^- plus NO_2^- concentrations for the sampling sites in September 2019 ranged from 30.19 to 44.84 μmol L^{-1} (Table 2.2). As well, Capelle and Tortell (2016) report NO_3^- plus NO_2^- values for the NE Pacific water column that are all below 50 μmol L^{-1}.

Other measurements of N_2O flux in subtidal and offshore sediments have used whole-core squeezing (Usui et al., 1998) or sealed-core incubations (Townsend-Small et al., 2014), both of which limit their use for constraining N_2O effluxes. Porewater concentration profiles obtained from whole-core squeezing have poor depth resolution and large depth assignment uncertainties (Bender et al., 1987), which can mask small-scale gradients near the sediment interface and bias subsequent flux estimates. Continuous declines in dissolved O_2 during sealed-core incubations could potentially lead to changes in OPD, and cause shifts toward net N_2O consumption as oxygen-limitation becomes more severe (Barnes & Upstill-Goddard, 2018). Further, the N_2O efflux estimates are likely conservative, as it was not possible to account for bioturbation-enhanced sediment diffusivity (Aller & Aller, 1992; Berg et al., 2001). Holding porewater concentrations constant, any increase in diffusivity would increase modelled rate estimates and associated N_2O effluxes (Berg et al., 1998)

Using data from all stations, a daily flux of 524 ± 122 nmol N_2O m^{-2} d^{-1} (n = 12) from the sediment to the overlying water column was calculated. By comparison, average sea-to-air N_2O flux for the world ocean is approximately 1030 nmol N_2O m^{-2} d^{-1} (Grundle et al., 2012; Ciais et al., 2013), while similar estimates for the Vancouver Island continental margin range from negative efflux prior to summertime upwelling, to a positive efflux of ~7600 nmol N_2O m^{-2} d^{-1} (Grundle et al., 2012; Capelle & Tortell, 2016; Fenwick & Tortell, 2018). These comparisons underlie the potential importance of continental margin sediments as sources for oceanic N_2O flux to the atmosphere, as well as the need to better constrain regional sources, especially in areas where permanent or temporary low-O_2 conditions enhance conditions for N_2O production in water columns and sediments.

3.6 Conclusions

This study present the first estimates of submillimeter-scale porewater N_2O concentration profiles, depth-distributed production rates, and vertical fluxes in offshore sediments that combine trace-level N_2O microsensor measurements and mathematical modelling. This method provides an improved approach to constraining sediment N_2O cycling in deep-water sediments under steady-state conditions, and requires minimal sediment disturbance. The PROFILE model also allows for an assessment of the vertical positioning of N_2O production zones in relation to sediment oxyclines and the seawater interface. This study has highlighted the importance of continental margin sediments as sources of N_2O to the regional water column in the NE Pacific Ocean, and shown the importance of bottom water O_2 concentrations in modulating N_2O production and effluxes. The results of the simulated upwelling experiment also suggest a dynamic response of N_2O-producing microbes to transient changes in dissolved O_2. Upwelling events may thus contribute additionally to atmospheric N_2O emissions by stimulating sediment N_2O efflux into the water column, a

proportion of which may ventilate to the atmosphere as the water masses continue to shoal. These underline the need for further research into the spatial and temporal variability of N_2O production in continental margin sediments, and their relative importance to the global N_2O budget.

3.7 Acknowledgments

This research was supported by the National Sciences and Engineering Research Council (NSERC), Canadian Healthy Oceans Network (CHONe), Ocean Networks Canada (ONC), the University of Victoria, and the Bermuda Institute of Ocean Sciences (BIOS). I would like to thank the Snelgrove Lab and Memorial University of Newfoundland, especially Vanessa Reid and Alessia Ciraolo, who provided the equipment for sediment core incubations and assisted with sample collection and incubation experiments. I would also like to thank Dr. Steve Mihaly for his assistance with deck operations, as well as the Captain and crew of the CCGS John P. Tully. Thank you to Drs. Roberta Hamme and Réal Roy, as well as all co-authors for their valued input on the first manuscript drafts, and to Dr. Peter Berg for providing instruction on the PROFILE model.

3.8 Article Supplementary Material

Table 3.2 Supplement: Water column chemical properties

Water column chemical properties for the Vancouver Island continental slope region. Data were obtained from the Department of Fisheries and Oceans Water Properties website. All data were collected between September 1-2, 2019. Available data includes dissolved O_2, phosphate (PO_4^{3-}) and nitrate plus nitrite ($NO_3^- + NO_2^-$). Means (± SD) are calculated for separate depth bands that are similar to the sediment sampling depths at the outer continental shelf (188.60 – 198.60 m), upper continental slope (495.20 – 496.30 m), and OMZ core (742.90 – 989.60 m).

Date	Lat (N)	Long (W)	Bottom Depth	Sample Depth	PO_4^{3-}	$NO_3^- + NO_2^-$
2019-09-01	48° 29.43	126° 07.07	198	188.60	2.45	36.09
2019-09-02	48° 39.14	126° 23.38	770	199.00	1.99	30.55
2019-09-02	49° 03.51	127° 01.14	955	198.60	2.12	30.19
2019-09-01	48° 18.95	126° 26.74	1500	197.80	2.23	32.05
2019-09-02	48° 28.70	126° 43.05	1593	198.70	2.12	31.63
2019-09-01	48° 25.98	126° 13.68	1250	198.60	2.08	30.72
			Mean	**196.88**	**2.16**	**31.87**
			SD	**4.08**	**0.16**	**2.18**
2019-09-02	48° 39.14	126° 23.38	770	496.20	2.82	40.97
2019-09-02	49° 03.51	127° 01.14	955	495.20	2.91	41.51
2019-09-01	48° 18.95	126° 26.74	1500	495.60	2.71	41.26
2019-09-02	48° 28.70	126° 43.05	1593	495.30	2.98	41.23
2019-09-01	48° 25.98	126° 13.68	1250	496.30	2.93	41.16
			Mean	**495.72**	**2.87**	**41.23**

			SD	**0.51**	**0.11**	**0.19**
2019-09-02	48° 39.14	126° 23.38	770	757.30	3.03	43.67
2019-09-02	49° 3.51	127° 01.14	955	958.70	3.27	44.56
2019-09-01	48° 18.95	126° 26.74	1500	742.90	3.07	44.01
2019-09-01	48° 18.95	126° 26.74	1500	989.40	3.17	44.89
2019-09-02	48° 28.70	126° 43.05	1593	743.10	3.13	44.02
2019-09-02	48° 28.70	126° 43.05	1593	989.60	3.21	44.84
			Mean	**863.50**	**3.14**	**44.33**
			SD	**127.38**	**0.09**	**0.50**

Table 3.3 Supplement: Sediment core incubation conditions.

Mean incubation temperatures and dissolved O_2 concentrations (± SD) calculated from measurements obtained at 1-2 hr intervals over the final 8 hours of incubation.

Incubation	Mean Temp (°C)	Mean DO (μmol L^{-1})
200m control	8.42 ± 0.50	126.0 ± 12.7
200m upwelling	8.50 ± 0.24	32.3 ± 0.9
475m	7.10 ± 0.87	32.8 ± 6.8
850m	8.73 ± 0.64	13.9 ± 4.3

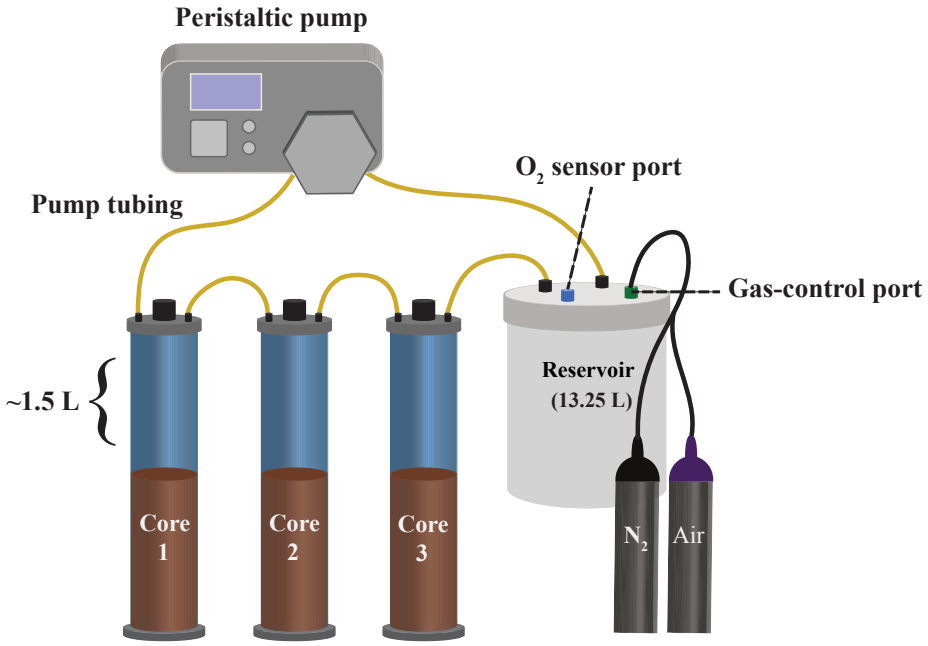

Fig. 3.5 Supplement: Schematic of core incubation and oxygen-regulation system

Water was continuously circulated from the oxygen-control reservoir through the sequence of core tubes using a peristaltic pump. Water flow direction was reversed every ~4 hours, and the middle core was rotated out at the midway point. Adjustments to incubation O_2 concentrations were performed by bubbling gas through the gas-control port using aquarium air stones.

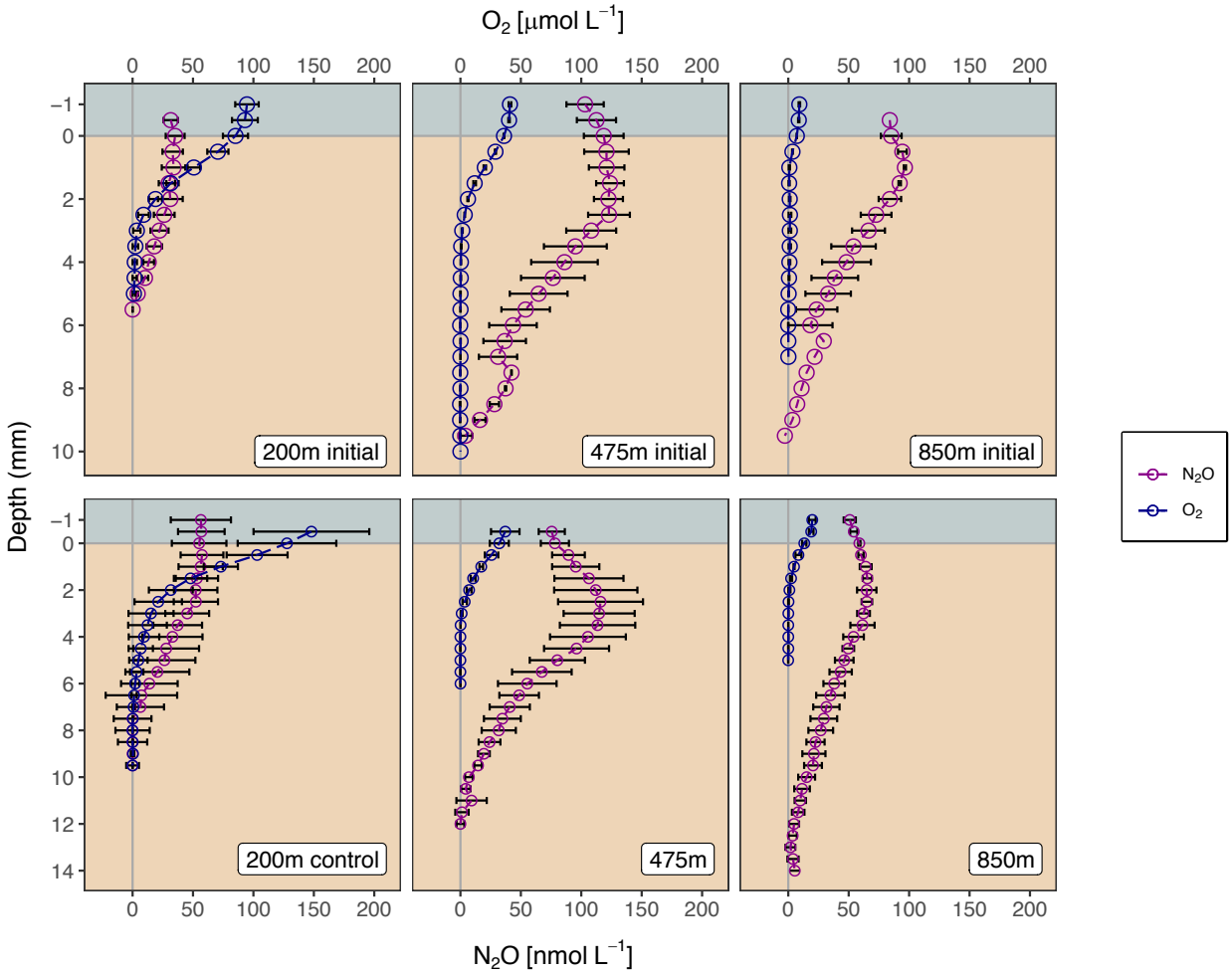

Fig. 3.6 Supplement: Porewater concentration profiles.

Top panels - representative initial vertical profiles of pore-water dissolved O_2 (µmol L^{-1} ± SE) and N_2O (nmol L^{-1} ± SE) obtained in replicate cores from 200m, 475m and 850m sampling locations (n = 3, 3, and 2) immediately after coring operations. Lower panels – corresponding profiles from incubated cores, taken at the end of the incubation period (n = 3). Pore-water analyte concentrations were determined using Clark-type microelectrodes (Unisense, DK) with detection limits of 20 nmol l^{-1} and 0.3 µmol L^{-1} for N_2O and O_2 sensors, respectively. Cores selected for initial profiling were not included in the core incubation experiments.

Chapter 4: The magnitude and direction of N_2O flux from marine sediments is linked to the community structure and gene expression of atypical *nosZII*-type reductases

Citation:

Jameson, B. D., Lopez, M. L. D., Bonderud, M., Stevens, C. J., Juniper, S. K., Helbing, C. C. & Grundle, D. S. (*Unpublished manuscript*). The magnitude and direction of N_2O flux from marine sediments is linked to the community structure and gene expression of atypical *nosZII*-type reductases.

4.1 Abstract

Knowledge of the ecological mechanisms that regulate N_2O cycling in marine sediments lags that of water column environments and terrestrial soils, leaving much to be learned about how microbial community dynamics relate to the direction and magnitude of sediment N_2O fluxes. The present study leverages trace-level microsensors and profile interpretation modelling to assess the N_2O sink capacity of microbial communities in minimally impacted Bermudian mangrove sediments. Mangrove sediments were then compared with sediments from the NESAP outer continental margin to understand variability in microbial community dynamics between sedimentary N_2O sources and sinks. Mangrove sediments demonstrated net N_2O uptake across all incubations, with fluxes ranging from -0.22 ± 0.15 to -0.30 ± 0.26 μmol m^{-2} d^{-1} in control and DIN-amended sediments and reaching maximum values of -0.94 ± 0.28 μmol m^{-2} d^{-1} in N_2O-amended sediments. Targeting of bacterial *nosZI* and *nosZII* gene clusters for quantification of gene and transcript copy abundances indicated higher abundance and activity of 'atypical' *nosZII*-type N_2O reducers in mangrove sediments. Parallel sequencing of 16S rRNA genes suggests that *nosZII* in mangrove sediments may be linked to organisms involved in dissimilatory nitrate reduction to ammonium. Archaeal communities in NESAP sediments were dominated by putative AOA, suggesting ammonia oxidation likely contributes to N_2O effluxes. These results suggest that *nosZII*-type organisms may act as important N_2O scavengers in nitrogen-limited mangrove sediments.

4.2 Introduction

Nitrous oxide (N_2O) is an increasingly abundant, ozone depleting greenhouse gas produced and consumed by microbe-mediated metabolic processes in soils, and in freshwater and marine water columns and sediments. N_2O is produced as a by-product of ammonia oxidation in the presence of oxygen, and as an obligatory intermediate of the denitrification pathway under oxygen-limiting conditions. Elevated rates of N_2O production and accumulation are generally observed in suboxic waters where high N_2O yields from both pathways coincide with the inhibition of N_2O consumption by suboxic levels of dissolved oxygen (Arévalo-Martínez et al., 2015; Babbin et al., 2015). Much of the present literature on marine N_2O cycling is focused on suboxic and anoxic water columns that contribute disproportionately to atmospheric N_2O emissions (Tian et al., 2020; Yang et al., 2020). Redox gradients in these environments span tens to hundreds of meters, allowing for high-resolution assessments of biogeochemical rates, microbial community dynamics, and relationships between the two (Bertagnolli & Stewart, 2018; Ji et al., 2015; Sun, 2021). Investigations of a similar sort are more challenging in sediment environments, where shallow oxygen penetration depths (OPDs) drive sharp redox gradients that span just a few millimeters (Devol, 2015).

Coastal and continental shelf sediments can be considerable sources of N_2O at local scales when dissolved inorganic nitrogen (DIN) levels are high (Allen et al., 2011; Barnes & Owens, 1999; Jameson et al., 2021). Current estimates from estuarine, intertidal, and coastal vegetated environments such as salt marshes and mangrove stands suggest a combined global efflux of 0.15 to 0.91 Tg N_2O-N yr^{-1} (Murray et al., 2015). Contributions from nitrification and denitrification to total N_2O production have been demonstrated in mangrove sediments that act as net sources to the water column and atmosphere (Allen et al., 2007; Bauza et al., 2002; Muñoz-Hincapié et al., 2002).

However, observations of N_2O cycling in nearshore sediments in general are biased toward highly populated and anthropogenically disturbed regions of Europe and Asia, potentially leading to overestimations of the relative contributions of coastal and estuarine environments to global N_2O budgets (Murray et al., 2015).

Systems with low DIN loads, as seen in some coastal mangroves and temperate estuaries, can act as net N_2O sinks (Foster & Fulweiler, 2016; Maher et al., 2016). Benthic sediments of these systems bring reducing environments near the water column and atmosphere, allowing for net N_2O consumption when metabolic precursors are limited. Previous work suggests that some sediments can switch rapidly from N_2O sinks to N_2O sources when exposed to sufficient DIN enrichment (Maher et al., 2016; Muñoz-Hincapié et al., 2002). This is consistent with porewater profile observations of increased subsurface N_2O production following incubation under elevated NH_4^+ or NO_3^- concentrations (Meyer et al., 2008; Nielsen et al., 2009). However, such experiments typically enrich DIN concentrations to millimolar ranges and thus may not accurately reflect the response of minimally impacted systems to more modest eutrophication scenarios. Furthermore, variability in the magnitude and duration of nutrient enrichment in natural systems can be expected to differentially affect microbial community structure over a range of timescales with likely consequences for the direction and magnitude of sediment N_2O fluxes.

Surveys of soil and sediment microbial communities reveal stark contrasts in denitrifier community composition at the functional and taxonomic levels across natural DIN and organic matter gradients (Wallenstein et al., 2006; Xie et al., 2020). Genomic surveys have also shown the denitrification pathway to be highly modular and that many organisms do not possess the full genetic machinery required to perform complete denitrification. High-throughput sequencing of environmental samples has delineated two primary clades of N_2O-reductase genes (*nosZ*) (Jones

et al., 2013; Orellana et al., 2014; Sanford et al., 2012). Organisms that possess the clade I *nosZ* variant (*nosZI*, or 'typical' *nosZ*) are more likely to carry the full denitrification gene compliment, while clade II *nosZ* variants (*nosZII*, or 'atypical' *nosZ*) are associated with genomes that lack upstream pathway components (Bertagnolli et al., 2020; Sanford et al., 2012).

Observations suggest that N_2O-reducing microbial populations in marine microbiomes are dominated by atypical *nosZII* variants (Bertagnolli et al., 2020), and that these organisms may act as important N_2O scavengers across a wide range of environments (Jones et al., 2013, 2014; Sun et al., 2021). This is consistent with previous work that suggests denitrification N_2O yields are affected by variability in denitrifier community structure in terrestrial soils (Cavigelli & Robertson, 2000; Jones et al., 2014). However, comparatively little is presently known about the factors that govern the distribution and activity of *nosZI*- and *nosZII*-type reductases in marine sediments or their influence on benthic N_2O cycling. Further to this, the broader relationships between microbial community dynamics and N_2O source or sink status remain understudied in marine sediments, especially in offshore and minimally impacted coastal systems.

Recent advances in trace-level microsensor technology now facilitate porewater N_2O profiling at sub-millimeter resolutions and nanomolar concentration ranges (Damgaard et al., 2020; Jameson et al., 2021). Depth-stratified N_2O production and consumption rates, as well as vertical fluxes, can be accurately estimated from porewater profiles under steady-state conditions through the application of profile interpretation models (Berg et al., 1998; Jameson et al., 2021). These methods present a preferred means of quantifying N_2O cycling rate processes in sediment environments and may be useful for shedding light on the role of microbial community structure in regulating the direction and magnitude of N_2O flux across the surface.

Building on previous research, the present reports on depth-stratified N_2O production rates, consumption rates, and sediment-seawater fluxes in sediments of a minimally impacted mangrove stand using whole-core incubations, trace-level N_2O microsensors, and applied numerical modelling (Jameson et al., 2021). First, the N_2O sink capacity of Bermudian mangrove sediments was evaluated under ambient conditions and modest increases in seawater N_2O and DIN concentrations. The results presented suggest that the N_2O sink capacity of minimally impacted mangrove sediments may be resilient against short-term N_2O and DIN enrichment. Molecular data obtained from mangrove sediments were then contrasted with those obtained in N_2O source sediments of the Northeast Subarctic Pacific (NESAP) outer continental slope to better understand relationships between microbial community dynamics and N_2O fluxes. N_2O sinks sediments from the Bermudian mangroves were associated with high abundances and expression levels of atypical *nosZII*-type reductases, and lower abundances of putative ammonia oxidizing organisms. In contrast, archaeal communities in N_2O source sediments were dominated by putative ammonia oxidizing Archaea and demonstrated increased expression levels of typical *nosZI-type* reductases.

4.3 Methods

4.3.1 Field sampling

Field sampling and incubation experiments for the present took place between 28 October and 01 November 2020 in a mangrove stand in Ferry Reach, Bermuda, and between 29 September and 04 October 2019 in the NE Subarctic Pacific Ocean (NESAP) (**Error! Reference source not found.**). Mangrove sediments were collected in Pyrex mini-core tubes (i.d. = 3 cm, length = 10 cm) at low tide from a mangrove stand, placed in cylindrical aluminum blocks, and carefully transported approximately 200 m to an outdoor flume mesocosm at the Bermuda Institute of Ocean

sciences (**Error! Reference source not found.**). Sediment interface levels were adjusted to ~2 mm below the edge of the core tube prior to submersion to prevent water stagnation over the sediment interface. Core tubes were then submerged in a 1,500 L mesocosm tank with continuous seawater flow drawn from Ferry Reach and acclimated for 4-8 hours before the start of each incubation period. Cylindrical blocks were used to elevate the core tube housing within 50 cm of the water-air interface so that profile measurements could be made directly in the flume without disturbing the samples.

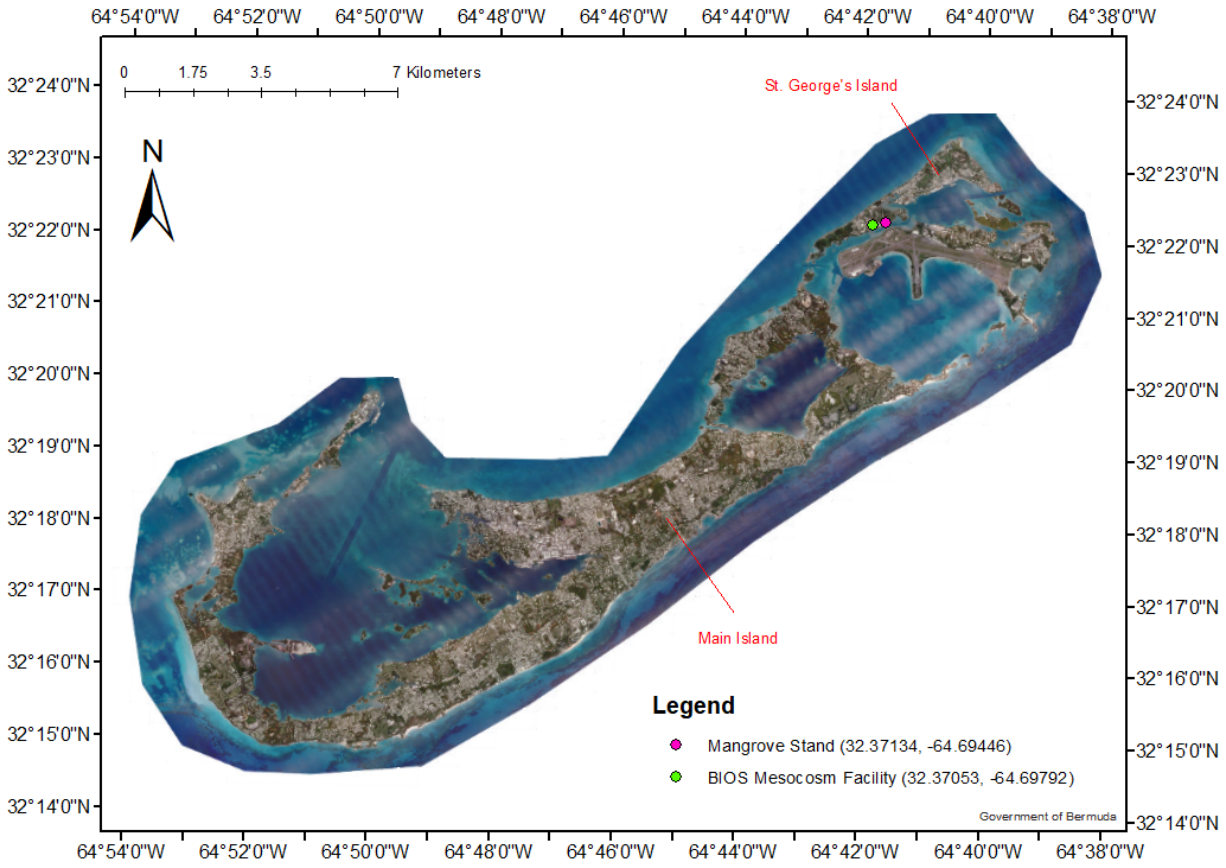

Fig. 4.1 Map of Bermuda.

Map depicts the location of the Bermuda Institute of Ocean Sciences mesocosm facility (green circle) and the Ferry Reach mangrove stand used as a sediment sampling site (red circle). Sediment core sampling and

incubation experiments took place between 28 October and 01 November, 2021. Figure was created by Moronke Harris.

Details of the 2019 NESAP sediment sampling campaign are reported in Jameson et al. (2021) and include a full description of the sampling methodologies and incubation procedures. Briefly, NESAP upper continental slope and outer shelf sediments were sampled across a depth-dependent gradient of decreasing bottom water O_2 (depth = 200 – 850 m; O_2 = 10 – 77 μmol L^{-1}) and incubated under near *in situ* temperature and dissolved O_2 concentrations. A separate experiment involving incubation of outer shelf course from 200 m under reduced O_2 concentrations using water from 475 m was performed to test responses to simulated upwelling conditions. N_2O production rates and vertical fluxes were quantified according to similar protocols detailed below. Subsequent discussion of experimental design, incubation procedures, and microprofile measurements thus focuses on the mangrove experiments conducted.

4.3.2 Experimental design and incubation procedures

Four separate incubation experiments were conducted on each of four consecutive days using sediment cores sampled at the same location. After acclimation, freshly collected sediment cores were incubated for 8-10 hours under variable nutrient regimes. Incubations were performed during dark periods to avoid confounding effects of light. Experimental manipulations including DIN and N_2O additions were performed by submerging one aluminum block in a 6 L polyethylene chamber that was partially submerged in the flume tank to create a semi-enclosed system while maintaining consistent water temperatures. For the first experiment, four replicate sediment cores were incubated under elevated N_2O conditions by bubbling 1.5 ppmv N_2O gas (in zero-air carrier gas) into the incubation chamber through an aquarium air stone, to a final concentration of 30-32 nmol L^{-1} (~5x atmospheric enrichment). Continuous bubbling of N_2O throughout the experiment ensured N_2O saturation and promoted continuous water circulation. The final three incubation

experiments involved amendment of treatment cores with DIN to obtain concentrations of: 1) 50 μmol L^{-1} KNO_3, 2) 50 μmol L^{-1} NH_4Cl, and combined 50 μmol L^{-1} KNO_3 and 50 μmol L^{-1} NH_4Cl. For experiments involving DIN amendments, 8 sediment cores were randomly split in to 4-core treatment and control groups, with the exception of the NH_4Cl amendment experiment where one of the control cores was damaged during transport to the flume. Continuous bubbling of atmospheric air through an aquarium air stone prevented water stagnation in incubations amended with DIN. Seawater incubation temperatures ranged from 23.7 to 25.2 °C across all experiments.

4.3.3 Microelectrode profiles

Porewater N_2O and O_2 profiles were obtained at sub-millimetre resolutions using Clarke-type microelectrodes with manufacturer stated detection limits of <25 nmol L^{-1} and 300 nmol L^{-1}, and sensor tip diameters of 500 and 200 μm, respectively (Unisense). Sensors were calibrated prior to each measurement period by two-point calibration according to manufacturer instructions. Briefly, zero-point N_2O and O_2 calibration standards were made fresh daily in 20 mL crimp-sealed vials by bubbling N_2 gas in filtered seawater for at least 15 mins. The vials were then sealed in plastic bags and secured within the flume to ensure equilibrium with flume temperature prior to calibration. N_2O-enriched standards were prepared in a CAL300 calibration chamber (Unisense) immediately prior to calibration by bubbling 1.5 ppmv N_2O gas into flume seawater for 10 minutes. High-point O_2 calibration values were obtained by bubbling atmospheric air into the calibration chamber for 10 minutes to ensure saturation. The final concentrations of air-saturated and N_2O-enriched standards were calculated using the solubility coefficients tables of Garcia & Gordon, (1992; 1993) and Weiss & Price (1980).

Following calibration, microelectrodes were mounted on a Unisense MM33 motorized micromanipulator and sensor tips were manually adjusted to the sediment-water interface.

SensorTrace Suite Profiling software (Unisense) was used to control the sensor tip position and log sensor output during profiling. Discrete porewater N_2O and O_2 concentrations were estimated at 500 and 200 μm depth intervals, respectively, starting one mm above the sediment interface and concluding after two or more consecutive zero values were recorded. At each measurement depth, O_2 sensors were allowed to acclimate for 5 seconds while the longer response time of the N_2O sensor necessitated a 25-second acclimation period. All profile measurements were made directly in the flume to minimize sediment disturbance and ensure continuity between incubation and measurement conditions.

Duplicate porewater N_2O profiles were measured in each mini core yielding a total of 8 profile replicates per experimental group. Dissolved O_2 profiles were not obtained in post-incubation cores given the considerable time constraints associated with repeated N_2O profiling. Instead, a separate O_2 profile dataset obtained from separate experiments that took place between 24 and 27 October 2019 in the same mangrove stand. Briefly, fresh sediment cores were collected daily in quadruplicate at low tide and monitored in the flume over a daily light-dark cycle. Dissolved O_2 profiles obtained at 4 hr intervals over dark periods were used as context for understanding general porewater O_2 distributions and sediment O_2 consumption rates in the mangrove sediment system.

4.3.4 Sensor drift corrections

Amperometric microelectrodes such as the ones described in this dissertation are prone to baseline signal drift over time. For large concentration ranges, such as those seen in dissolved O_2 profiles that cover ranges from saturation to anoxia, the signal drift component is negligible over the course of a single measurement period and can be ignored. However, when working within concentration ranges that border on the detection limits of the sensors, the signal drift

component can account for a considerable portion of the measured concentration range. In such cases, repeated re-calibration of the sensors between profiles is time consuming, limiting the number of replicates that can be profiled in an experiment period. This section details the method I developed for modelling and correcting for baseline drift in porewater N_2O profiles when baseline signal drift over time is approximately linear (**Error! Reference source not found.**).

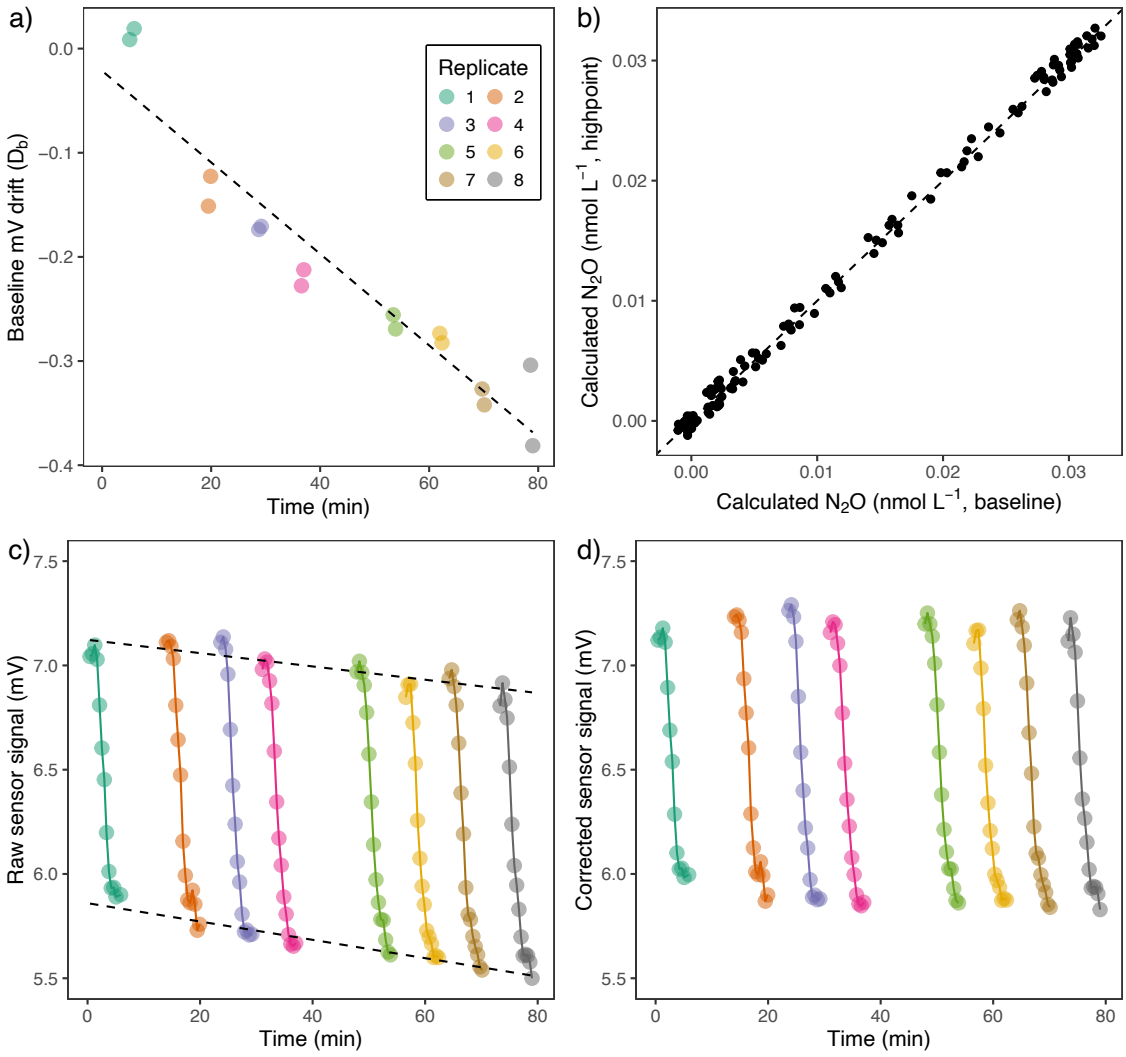

Fig. 4.2 Outline of sensor drift correction procedure.

Figure shows (a) the linear regression of sensor baseline drift (D_b) on time (mins), (c) the raw sensor signals for individual profile replicates over time prior to drift correction, (d) the drift-corrected sensor signals. Panel (b) depicts the linear regression of drift-corrected N_2O concentrations (nmol L^{-1}) obtained from independent models of sensor signal drift over time using both baseline (0 nmol L^{-1}) and highpoint

sensor readings (R^2_{adj} = 0.997, p < 0.0001). Dashed lines in panel (b) represent linear fits to drift in the sensor baseline (lower) and highpoint (upper) readings. Data shown are for profiles obtained in N_2O-amended cores (~33 nmol L^{-1}).

The drift correction method requires two to three replicate zero measurements at the bottom of each porewater profile (indicated by constant mV readings), which are used to fit the original model (**Error! Reference source not found.**a). For experiments with significant sensor offset (assessed if the baseline signal changed significantly over time), the degree of offset from the original sensor baseline is calculated according to Equation 1,

$$D_b = mV_b - b \quad (1)$$

where mV_b equals the sensor signal readout at the bottom of the profile (assuming N_2O = ~0 nmol L^{-1}) and b is the y-intercept of the original calibration curve (equal to the mean sensor signal measured in zero calibration standard). A linear model is then fit using the calculated offset (D_b) as the dependent variable and time as the independent variable, which is used to predict the drift component of the sensor signal (D) across all measurements. The drift-corrected sensor signal (mV_c) for a given measurement is thus calculated using Equation 2,

$$mV_c = mV_t - D_t \quad (2)$$

where mV_t represents the raw sensor signal in millivolts at measurement interval t and D_t represents the predicted drift component.

The validity of the drift corrections was assessed by performing a separate drift-correction for profiles obtained from cores amended with 30 nmol L^{-1} N_2O using measurements obtained at the top of the profile above the sediment interface and diffusive boundary layer (**Error! Reference source not found.**b). This was possible since continuous bubbling of N_2O standard throughout the incubation and measurement periods ensured N_2O concentrations were constant at ~33 nmol L^{-1}. A scatterplot of corrected N_2O concentrations shows a near 1:1 correlation between the two

independently derived drift corrections (Fig. 4.2b). These results validate the assumption the sensor drift is entirely y-intercept offset and that the slope of the relationship between N_2O concentration and raw sensor signal (or gain) remains constant, which permits the application of the initial calibration curve to drift-corrected sensor signals. A difference in the magnitude of sensor drift over time at either end of the calibration range would indicate a change in the slope of the calibration curve and thus necessitate frequent re-calibration.

4.3.5 PROFILE interpretations

Drift-corrected porewater N_2O profiles were used as input to model depth-dependent production rates, consumption rates, and vertical fluxes across all replicate profiles using the PROFILE model described by Berg et al. (1998). Separate models, using the mean porewater concentration profiles shown in **Error! Reference source not found.**, were also run to visualize production and consumption profiles for each experimental grouping, and to assess consistency between 1) mean flux estimates averaged across individual profiles, and 2) flux estimates obtained from a single model run of the mean profile. A mean sediment porosity (±SD) of 0.82 ± 0.03 was determined for the top 5 mm of sediments in 2 out of 4 mini-cores from each experimental group (n = 16) according to Dalsgaard et al., (2000) and used for parameterization of the PROFILE models. Diffusivities of N_2O in water at fixed temperature and salinities used in the model were obtained from Tamimi et al. (1994). Oxygen penetration depth was defined as the depth at which dissolved O_2 decreased below the 5 μmol L^{-1} suboxic threshold and was estimated in all replicate profiles (n = 67) following linear interpolation between profile points (Belley et al., 2016). Dissolved oxygen profiles showed a high degree of consistency across all replicate profiles. As a result, eight dissolved O_2 profiles were selected at random from the total pool of replicates as a representative subsample for PROFILE modelling of sediment O_2 consumption rates using the

same porosity estimate listed above and O_2 diffusivities reported by (Ramsing and Gundersen, 1994).

4.3.6 Nucleic acid extractions and cDNA synthesis

Samples for nucleic acid extraction were obtained from the top 0.5 cm of sediment immediately following porewater profiling using 50 mL Falcon tubes for both the NESAP slopes (all cores) and Bermuda mangroves experiments (2/4 cores). For the NESAP slopes sediments, initial samples were obtained from separate cores immediately following sampling. Sediment RNA samples were preserved in RNAlater (~1:10 sample to preservative ratio) and then stored at -80°C. DNA samples were flash-frozen immediately following sampling and the stored at -80°C until extraction in the lab. Total genomic DNA (gDNA) was extracted from ~700 mg of wet sediment using a DNeasy® PowerSoil® kit (Qiagen, Germany) according to manufacturer instructions. DNA extracts were purified prior to downstream analyses using QIAquick® PCR purification columns (Qiagen, Germany) to remove PCR inhibitors and other impurities. DNA concentrations in cleaned extracts were then quantified using a NanoDrop™ One Microvolume UV-Vis Spectrophotometer (Thermo Scientific, USA). In contrast, total RNA was extracted from 2.0 to 5.0 g of wet sediment using a RNeasy® PowerSoil® Total RNA kit (Qiagen, Germany) with the following modification. Thawed sediment samples were centrifuged for 15 min at 2,500 x g and RNA later was decanted. Sediments were then washed three times with 10 mL PBS buffer by briefly vortexing and then centrifuged for 10 minutes at 2,500 x g. RNA integrity was assessed using a Qubit™ RNA IQ Assay Kit and total RNA concentrations were determined using a Qubit™ RNA High Sensitivity Assay Kit (Invitrogen, USA). Before cDNA synthesis, removal of co-extracted genomic DNA was achieved by treating samples with ezDNase™ enzyme according to manufacturer instructions (Invitrogen, USA). A total of 200 ng RNA input was used for

standardized cDNA synthesis using a High-Capacity cDNA Reverse Transcription Kit with RNase Inhibitor (Applied Biosystems, USA).

Validation of nosZI and nosZII assays

Published primer sets by Henry et al. (2006) and Jones et al. (2013) were used for quantitative real-time polymerase chain reaction (qPCR) analysis with SYBR Green I chemistry to quantify *nosZI* and *nosZII* gene (gDNA) and transcript (cDNA) copy numbers, respectively (Table 4.1). First, databases of 399 *nosZI* and 315 *nosZII* sequences from cultured organisms were downloaded from the FunGene Repository (http://fungene.cme.msu.edu/). *In silico* validation of the assays was performed by mapping primer sets to consolidated *nosZI* and *nosZII* sequences in Geneious Prime v.2023.0 to assess the coverage and specificity (https://www.geneious.com). Laboratory assay validation was achieved following the modified workflow proposed by Langlois et al. (2021). Primer specificity was assessed using cleaned DNA extracts from a broad range of environmental samples (soil, freshwater, marine) and *Pseudomonas aeruginosa* quantitative gDNA (strain PAO1-LAC; American Type Culture Collection) as a positive control for the *nosZI* primer set. Quantitative gDNA was not available for cultured organisms that possess the *nosZII* variant. The fragment size (in bp) of the resulting PCR amplicons was assessed through electrophoresis in 1% agarose gel, and amplicons were sent for Sanger sequencing to confirm amplification of target genes. Lastly, gBlocks® synthetic DNA fragments (Integrated DNA Technologies, USA) dilutions of the target amplicons were used to construct standard curves and assess sensitivity. Amplification efficiencies for *nosZI* and *nosZII* assays were assessed based on the slope of the constructed standard curves (Fig. 4.7; Table 4.2).

A baseline amplification signal was detected at low copy numbers for *nosZI* and *nosZII* assays, and was indicated by lack of signal attenuation below four copies per reaction in the five-

fold dilution series. A continuous limit of detection (LOD_{cont}) was established to ensure that the signal detected in environmental samples was above background noise (Table 4.2). A certain degree of background noise is expected for qPCR assays targeting bacterial genes, as contamination of common laboratory reagents by prokaryote DNA is often unavoidable (Salter et al., 2014). Three of 39 samples exhibited C_q values above the baseline threshold for the *nosZII* assay and were removed prior to downstream analyses. These samples corresponded to cDNA samples from the NESAP continental margin and demonstrated unusually low 16S rRNA and nosZI transcript copy numbers, suggestive of poor-quality samples. Furthermore, all samples that were below the baseline threshold were from different experimental groupings.

4.3.7 qPCR analyses of environmental samples

The integrity of extracted gDNA and cDNA was assessed with the IntegritE-DNA™ assay targeting a conserved region of the plant chloroplast genome (Veldhoen et al., 2016; Hobbs et al., 2019) and with a TaqMan probe-based assay targeting a conserved region of the bacterial 16S rRNA gene (Table 4.1; Ritalahti et al., 2006). Probe-based qPCR reactions were carried out in 15 μL reaction volumes using two μL of purified gDNA or cDNA, 700 nM forward and reverse primer, 100 nM TaqMan probe, and 1X of QIAcuity Probe Master Mix (QIAGEN). All thermal cycling steps were performed in a Bio-Rad CFX96 (Bio-Rad) thermocycler. The following TaqMan thermocycler profile was used for all probe-based assays: initial denaturation at 95°C for 9 min followed by 50 cycles of denaturation at 95°C for 15 s, annealing at 64°C for 30 s, and extension at 72°C for 30 s. Successful amplification of endogenous plant chloroplast and bacteria DNA contained within the samples confirms that the recovered nucleic acids are viable and inhibitory compounds have been sufficiently removed.

Quantifications of *nosZI* and *nosZII* copy numbers were carried out in 15 µL reaction volumes consisting of two µL of purified gDNA or cDNA, 700 nM forward and reverse primer, and 2X of SensiFAST SYBR® No-ROX mix (Bioline). Eight replicates each of two µL UltraPure™ DNase/RNase-Free water (Invitrogen) and two µL synthetic target DNA (20 copies/reaction) of the appropriate DNA sequence (Integrated DNA Technologies) were used as non-template and positive controls, respectively. The SYBR Green I thermal cycling profiles for *nosZI* assays were performed with initial denaturation at 95°C for 9 minutes, followed by 50 cycles of denaturation at 95°C for 15s, annealing at 64°C for 30s, and extension at 72°C for 30s. Thermal cycling conditions for the *nosZII* assays were modified such that annealing and extension were performed at 54°C and 80°C, respectively. Concentrations of *nosZ* gene and transcript copies (copies g^{-1}) were extrapolated from C_q values using the previously generated standard curves. Absolute *nosZI* and *nosZII* copy numbers were normalized to 16S rRNA copy numbers (gDNA or cDNA) and *nosZII* ratios were expressed as the ratio of *nosZII* copies to total nosZ copies (*nosZI* + *nosZII*).

4.3.8 High-throughput sequencing and sequence data processing

Cleaned raw gDNA extracts were sent to the Integrated Microbiome Resource (Dalhousie University, Halifax, Canada) for sequencing of bacterial and archaeal 16S rRNA genes on an Illumina MiSeq using 2 x 300 bp paired-end V3 chemistry and universal primers targeting the V6-V8 variable regions (Table 4.1) (https://imr.bio/protocols.html). Demultiplexed forward and reverse reads were trimmed of primer binding sequences using Cutadapt (Martin, 2011) and processed according to standardized protocols in QIIME2 (v2022.8) (https://www.qiime2.org). Reads were merged with VSEARCH (Rognes et al., 2016) using a minimum overlap length of 50 bp and then filtered using a quality score threshold of 20. Denoising of filtered reads into amplicon

sequence variants (ASVs) was achieved using QIIME-Deblur (Amir et al., 2017; Bolyen et al., 2019). Bacterial and archaeal ASV counts were tabulated and ASV sequences were assigned taxonomic IDs using a naïve Bayesian classifier trained against the Silva reference database (version 138) (Quast et al., 2013). Inverse Simpson diversity indices were calculated separately for bacterial and archaeal communities in each sample using the 'qiime diversity alpha' command.

4.3.9 Statistical analyses

All statistical analyses and data visualizations were conducted in the R Statistical Environment (R Core Team, 2019). N_2O flux and *nosZ* gene/transcript abundance datasets were tested for normality and homogeneity of variance using Shapiro-Wilks and Levine's tests, respectively. Variability in N_2O fluxes, and *nosZ* gene copy and transcript abundances between sample groupings were then tested for statistical significance using one-way ANOVA and Tukey-Kramer post-hoc tests. Variability in inverse Simpson diversity group means was assessed for significance using a Kruskal-Wallis rank sum test and pairwise comparisons were evaluated using Wilcoxon rank sum tests with a Benjamini-Hochberg correction for multiple comparisons. Finally, non-metric multidimensional scaling ordinations of bacterial communities in NESAP continental slopes samples were performed to assess patterns of community dissimilarity across slope depth and between pre- and post-incubation sediments.

4.4 Results

4.4.1 PROFILE interpretations

Oxygen penetration depths (OPDs) were highly consistent across replicate sediment cores and consecutive sampling days, ranging between 1.2 and 2.8 mm with a mean (± SD, n = 67) of 2.0 ± 0.4 mm (**Error! Reference source not found.**8). Mean seawater N_2O concentrations for the

control and DIN-amended incubations was 15 ± 2 nmol L^{-1} (Fig. 4.3). N_2O concentrations decreased with depth in all control, N_2O amended, and NH_4Cl-amended sediments, and generally reached zero values between 4 to 6 mm (**Error! Reference source not found.**; **Error! Reference source not found.**9).

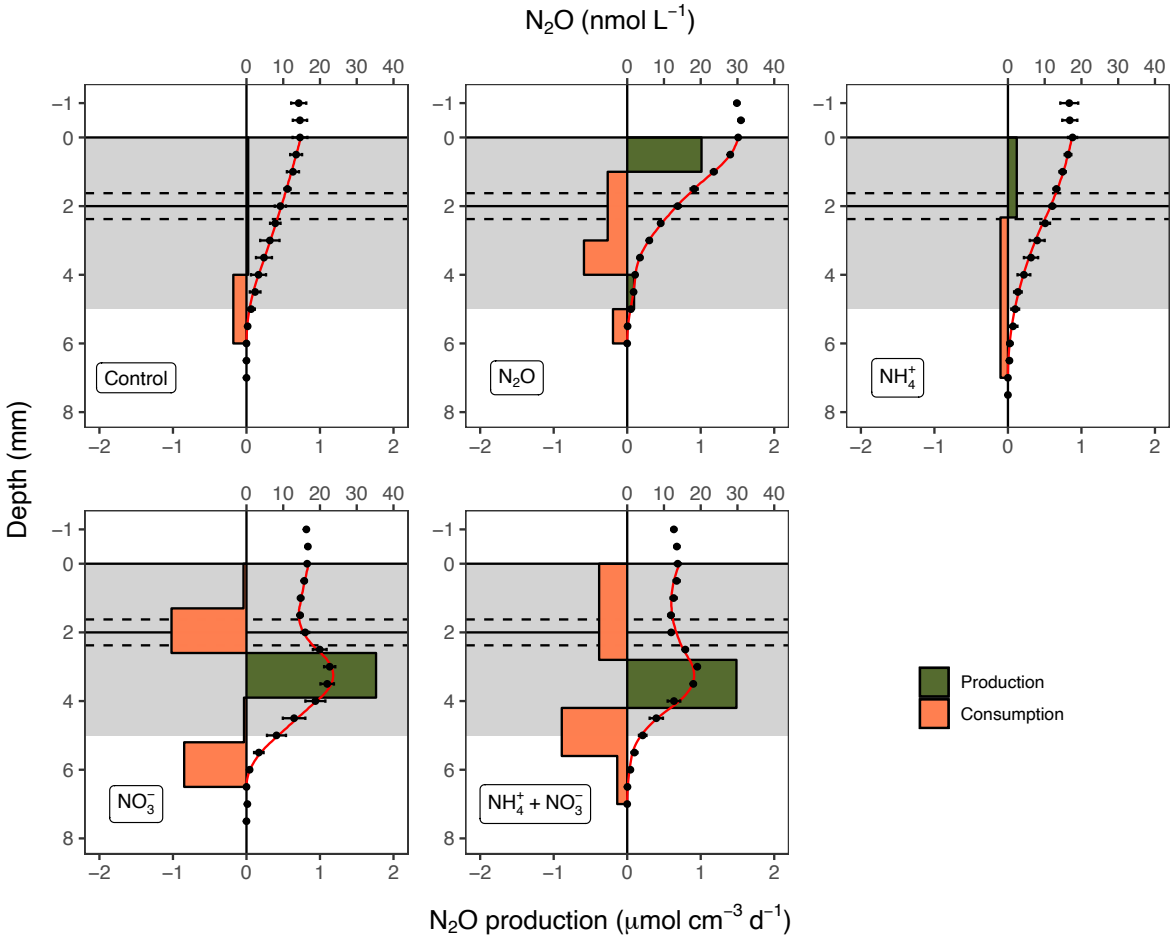

Fig. 4.3 Depth-stratified N_2O production & consumption rates.

N_2O production and consumption rates (µmol-N_2O cm^{-3} d^{-1}) were modelled from mean porewater N_2O concentration profiles in post-incubation cores. Solid red lines represent the modelled concentration profiles and individual points correspond to measured porewater N_2O concentrations (nmol L^{-1}). Green and red boxes correspond to zones of N_2O production and consumption, respectively. Solid and dashed horizontal lines denote the mean OPD ± SD, respectively. Grey shading highlights the sample section depth for nucleic acids analyses.

Depth-stratified N_2O consumption rates ranged from 0.10 to 0.18 μmol-N_2O cm^{-3} d^{-1} for control and NH_4Cl-amended cores, and increased to a maximum of 0.59 μmol-N_2O cm^{-3} d^{-1} in N_2O-amended cores (**Error! Reference source not found.**). Subsurface N_2O maxima ranging from 17.6 to 32.7 nmol L^{-1} were detected below oxycline depths across all cores amended with NO_3^- following an initial decrease in concentrations between the sediment surface and the base of the oxycline (**Error! Reference source not found.**; **Error! Reference source not found.**9). Subsurface N_2O maxima were associated with zones of net N_2O production (~1.49 to 1.76 μmol-N_2O cm^{-3} d^{-1}) positioned between net N_2O consumption zones (-0.13 to 1.02 μmol-N_2O cm^{-3} d^{-1}). Zones of slight net N_2O production were estimated in the top few mm for several individual and mean profiles (Fig. 4.3). However, these were not consistent features across replicate sediment cores or across profile duplicates and were detected randomly across all incubation experiments.

4.4.2 Sediment fluxes

Mangrove sediments demonstrated net O_2 uptake across all replicate profiles, with depth-integrated consumption rates ranging from 12.4 to 23.5 mmol-O_2 m^{-2} d^{-1} (15.4 ± 3.9 mmol-O_2 m^{-2} d^{-1}). Mean N_2O fluxes calculated across replicate profiles were also negative under all incubation conditions, reaching a maximum net consumption rate of -0.94 ± 0.28 μmol-N_2O m^{-2} d^{-1} in N_2O-amended cores (**Error! Reference source not found.**). Net sediment N_2O consumption rates were significantly elevated in N_2O-amended cores ($p < 0.0001$) but remained relatively constant across control and DIN-amended cores (-0.22 ± 0.15 to -0.30 ± 0.26 μmol-N_2O m^{-2} d^{-1}). Mean flux estimates calculated across individual profiles were in good agreement with those derived from the mean porewater profile. Small sediment N_2O effluxes (0.02 to 0.19 μmol-N_2O m^{-2} d^{-1}) were estimated for two control replicates and three replicates from NO_3^- -amended incubations.

Estimates of net N_2O efflux derived from individual profiles were not reproduced in duplicate profiles from the same core.

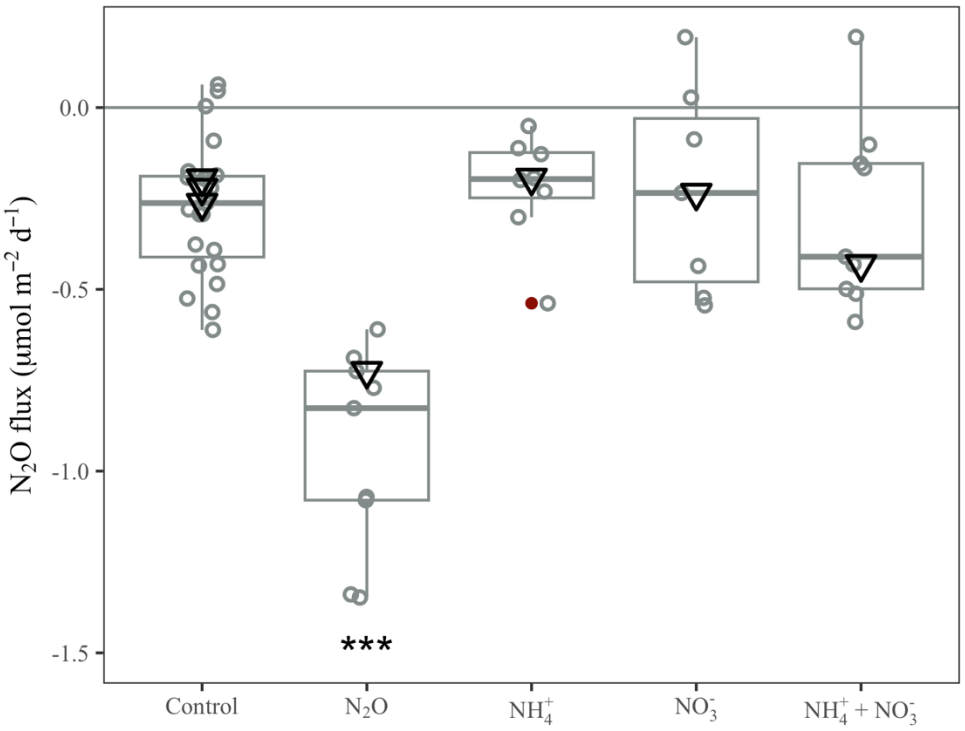

Fig. 4.4 Modelled sediment N2O fluxes.

Open circles represent fluxes (µmol-N_2O m-2 d-1) modelled from individual porewater concentration profiles in mangroves sediments. Control grouping contains pooled estimates across all DIN-amendment experiments. Black triangles represent fluxes modelled from the mean profiles shown in Fig. 4.3. Fluxes N_2O -amended cores were significantly greater (***) than control and DIN-amended cores ($p < 0.0001$). Negative values correspond to net sediment N_2O uptake

4.4.3 Variability in nosZ gene abundance & activity between N_2O sources & sinks

Logistical constraints precluded replicate sampling of nucleic acids from mangrove sediments, except for the N_2O-amendment experiments in which duplicate DNA and RNA samples were obtained. However, 16S-normalized *nosZI* and *nosZII* gene and transcript copy abundances were relatively consistent across all mangrove samples aside from a few statistical outliers (Fig. 4.10). To understand variability in microbial community dynamics between N_2O source and sink

sediments, I contrasted mangrove microbial communities with those surveyed in sediments from the NESAP continental margin. Corresponding flux estimates from these samples indicate a net source of N_2O to the overlying water column (Jameson et al., 2021). Mean sediment N_2O effluxes increased with slope depth and corresponding decreases in bottom water O_2 concentrations in the NESAP, ranging from 0.11 ± 0.03 μmol-N_2O m^{-2} d^{-1} at 200 m depth to 0.69 ± 0.41 μmol-N_2O m^{-2} d^{-1} at 850 m depth. Maximum sediment N_2O effluxes were observed in outer shelf sediments (200m) exposed to simulated upwelling conditions (0.81 ± 0.61 μmol-N_2O m^{-2} d^{-1}). Normalized *nosZ* gene and transcript copy abundances and nosZII gene and transcript ratios estimated in NESAP initial cores (pre-incubation) were consistent with those estimated in post-incubation cores, and are included in downstream analyses.

Proportional abundances of *nosZII* gene copies relative to total *nosZ* copies (*nosZI* + *nosZII*) ranged from 82.5 to 95.4% (91.8 ± 4.3%) across all mangrove samples and from 75.0 to 90.6% (84.5 ± 5.6%) across all NESAP samples (**Error! Reference source not found.**a). Contributions of *nosZII* copies to the total *nosZ* gene pool were significantly higher in mangrove sediments compared to 200 m ambient and simulated upwelling cores (p = 0.004–0.009). Comparisons between mangrove sediments and deeper slopes sediments were not statistically significant at the 95% confidence level. Normalized *nosZI* gene copy abundances were relatively consistent across sampling depths in the NESAP and were roughly twice as abundant in NESAP sediments than in the mangrove sediments (**Error! Reference source not found.**a). Conversely, mean normalized *nosZII* gene copy abundances were comparable across mangrove and NESAP sediments (Fig. 4.10b). Mangrove sediment *nosZ* transcript pools were overwhelmingly dominated by *nosZII* transcripts (84.8 ± 7.0%), while contributions from *nosZI* transcripts were significantly higher in NESAP sediments (40.5 ± 10.0%) (**Error! Reference source not found.**b). This was

ostensibly driven by low mangrove *nosZI* expression levels relative to the NESAP sediments and not by substantially elevated mangrove sediment community *nosZII* expression (Fig. 4.10d).

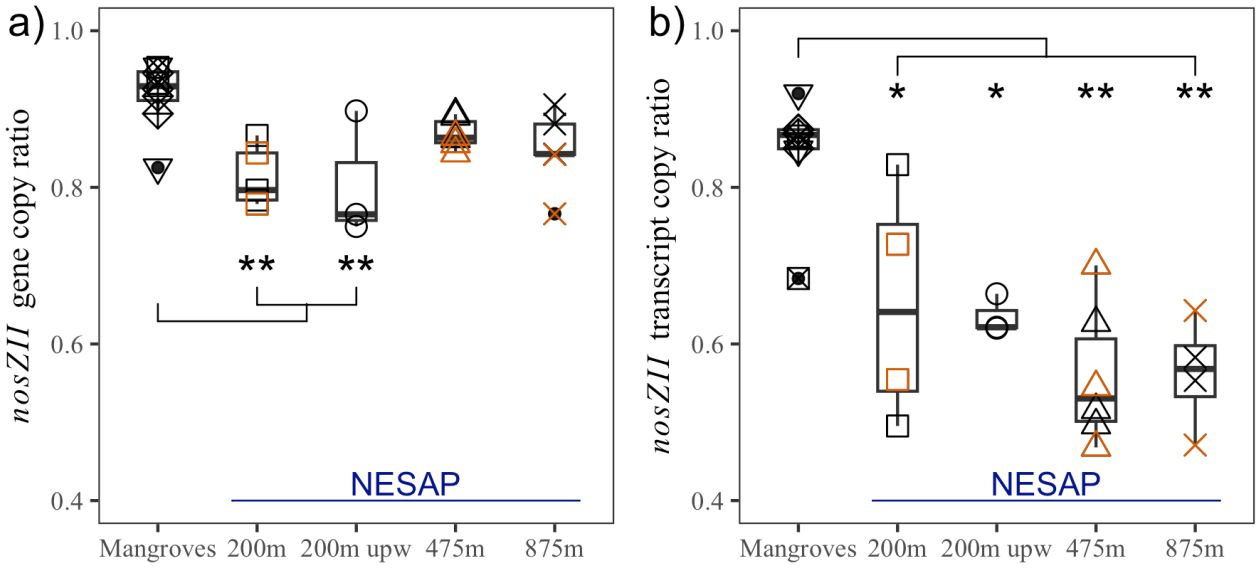

Fig. 4.5 Relative abundances of *nosZII* genes & transcripts.

NosZII gene (a) and transcript (b) copies as the ratio of *nosZII* copies to the total sum of *nosZ* copies (*nosZI* + *nosZII*). Mangrove sediment samples were obtained from control, DIN-amended, and N_2O-amended cores. Slope sediments were sampled from 200 m ambient and 200 m simulated upwelling, 475 m ambient, and 850 m ambient incubations. Initial samples were obtained in separate cores at each station prior to incubation and are indicated in orange. Asterisks denote significant differences ($p < 0.05$* or $p < 0.01$ (**).

4.4.4 Microbial community structure

Amplicon sequencing of prokaryote 16S rRNA genes in the top 5 mm of sediment produced 1.8 million paired-end reads from eight mangrove samples and 19 NESAP continental margin samples. A total of 888,582 bacterial and 388,521 archaeal reads were retained following merging and quality filtering. Denoising of filtered reads obtained in mangrove sediments generated 412 archaeal ASVs and 1210 bacterial ASVs from 164 Families while 385 archaeal ASVs and 4042 bacterial ASVs from 222 Families were detected in samples from the NESAP continental margin. Bacterial community diversity was relatively consistent across mangroves and NESAP sediments while archaeal diversity was significantly higher in NESAP sediments (**Error!**

Reference source not found.a). Simulated upwelling conditions did not have an appreciable effect on microbial community structure, and pre-incubation samples also agreed well with post-incubation samples at discrete slope sampling depths (Fig. 4.6; Fig. 4.11b). Similarly, microbial community structure was highly consistent across all mangrove sediment manipulation experiments.

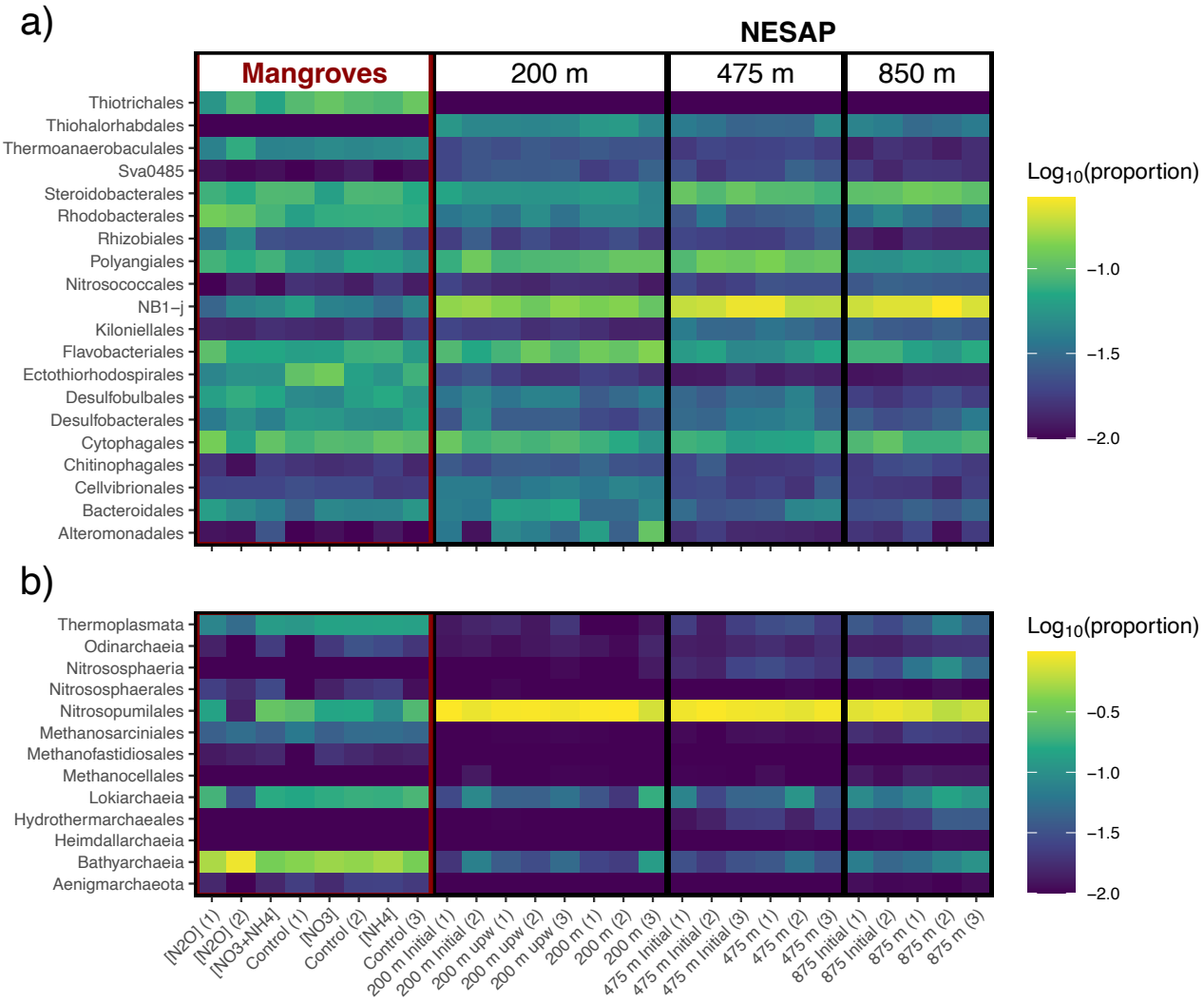

Fig. 4.6 Sediment bacterial and archaeal community structure.

Community structure heatmap depicts proportional abundances (log_{10}-transformed) of order-level taxonomic groupings for (a) the top 20 bacterial taxa and (b) all archaeal taxa. Mangrove sediment samples representing sediment N_2O sinks are highlighted in red on the left side of the figure. NESAP slope sediment samples are grouped left to right in order of increasing depth and N_2O efflux. Mangrove sediment samples were obtained from control, DIN-amended, and N_2O-amended cores. Slope sediments were sampled from

200 m ambient and 200 m simulated upwelling, 475 m ambient, and 850 m ambient incubations. Initial samples were obtained in separate cores at each station prior to incubation.

Approximately one third of mangrove sediment bacterial communities was constituted by ASVs mapped to the Cytophagales (8.8 ± 1.9%), Thiotrichales (8.0 ± 2.1%), Rhodobacterales (7.7 ± 2.1%), and Steroidobacterales (7.1 ± 1.1%) (**Error! Reference source not found.**a). A further third of the mangrove communities consisted of ASVs from the Flavobacteriales (6.3 ± 1.4%), Ectothiorhodospirales (6.2 ± 2.9%), Polyangiales (5.6 ± 1.3%), Desulfobulbales (5.1 ± 1.1%), Desulfobacterales (4.1 ± 0.8%), and Bacteroidales (3.6 ± 1.0 %). In contrast, NESAP sediments were dominated by ASVs from the uncultured Deltaproteobacteria order NB1-j (12.8 ± 1.6% to 21.5 ± 2.3%), which increased in relative abundance with slope depth along with members of the Steroidobacterales (4.4 ± 0.1%) (Fig. 4.6a). Increases in relative abundances of putative ammonia oxidizing bacteria (AOB) ASVs from the Nitrosococcales order were also observed along the NESAP slope depth gradient. Substantial contributions to community structure were also observed for members of the Thiohalorhabdales, Flavobacterales, Polyangiales, and Cytophagales despite no clear depth-related trends. ASVs belonging to putative sulfate-reducing groups, including the Desulfobacterales, Desulfobulbales, and Ectothiorhodospirales, accounted for less than 5% of all NESAP sequence reads combined.

Bathyarchaeia ASVs accounted for approximately half of the mangrove sediment Archaea community across samples (49.2 ± 16.3%) (**Error! Reference source not found.**b). The remaining half consisted primarily of ASVs mapped to the Nitrosopumilales (15.5 ± 9.0%), Lokiarchaeia (15.0 ± 5.6%), Thermoplasmata (10.5 ± 3.3 %), and Methanosarcinales (3.8 ± 0.8 %). Taxonomic evenness at the order level was substantially lower in NESAP sediments where Archaea communities were largely dominated by putative ammonia oxidizing archaea (AOA)

belonging to the Nitrosopumilales. Nitrosopumilales ASVs accounted for 73.2 ± 10.2% of all archaeal reads in sediments from 850 m and increased to a maximum of 90.2 ± 8.9% in outer shelf sediments at 200 m (Fig. 4.6b). Opposite trends were observed for putative AOA from the Nitrososphaeria order, which increased progressively from <0.1% to 4.3 ± 2.8% between 200.m and 850 m. Members of the Bathyarchaeia (2.5 ± 1.2%) and Lokiarchaeia (6.0 ± 2.3%) were also prominent across all continental slope depths, albeit at substantially lower abundances compared to the mangrove sediments (Fig. 4.6b).

4.5 Discussion

The present study builds on previous work using trace-level microelectrodes and applied numerical modelling to quantify N_2O production rates and vertical fluxes in Bermudian mangrove sediments with low DIN loads (Jameson et al., 2021). Mean seawater N_2O concentrations across control and nutrient-amended incubations was roughly two times higher than expected assuming equilibrium with the atmosphere and an atmospheric dry air mole fraction of 333 ppb (Dlugokencky et al. 2020). This is unlikely an issue with the calibration curves, given the high accuracy of measurements obtained above the sediment interface in N_2O-amended seawater following sensor calibration. Supersaturation of N_2O in surface waters of the Sargasso Sea has been reported previously, although most surface measurements trend toward slight undersaturation (Meyer et al., 2022). It is possible that local conditions on the Bermuda platform reflected slightly supersaturated surface waters, however, it is not possible to evaluate this possibility in the absence of discrete surface water N_2O measurements. Regardless, while N_2O fluxes estimated for the control and DIN-amended cores may be biased slightly high, the overall trends reported in the present study are in good agreement with those reported in other low-nutrient estuarine, coastal, and terrestrial system (Foster & Fulweiler, 2016; Murray et al., 2015; Syakila et al., 2010).

The N_2O sink capacity of Bermudian mangrove sediments suggests the ability of N_2O-reducing microbes to buffer against modest, short-term increases in seawater N_2O and DIN concentrations. Net sediment N_2O consumption was observed across control and experimentally manipulated mangrove sediments and was significantly greater in cores amended with 30 nmol L^{-1} N_2O. Interestingly, mean N_2O consumption rates were comparable between control sediments and those amended with 50 μmol L^{-1} NO_3^-, despite observable subsurface production below oxycline depths. In some systems, experimental DIN-enrichment has been sufficient to switch sediments from a net sink to a net source of N_2O (Kreuzwieser et al., 2003; Muñoz-Hincapié et al., 2002). However, such nutrient enrichment experiments often involve millimolar DIN amendments that far exceed concentrations observed in even the most hypernutrified estuaries (Robinson et al., 1998). Results of presented here suggest that some minimally impacted sediments may be capable of mitigating the acute effects of nutrient enrichment under more realistic enrichment scenarios.

The persistent N_2O sink capacity of DIN-amended sediments appears linked to zones of net consumption estimated in surface layers. The processes responsible for the apparent consumption in oxygenated sediments are not immediately clear, however; previous work has also shown similar bands of net consumption in the top two millimetres of Australian mangrove sediments following nutrient additions (Meyer et al., 2008). The potential for denitrification at anoxic, particle-associated microsites provides one possible explanation (Bianchi et al., 2018), although this does not necessarily explain why net N_2O consumption was still favored following NO_3^- enrichment. Recent work has provided experimental evidence for appreciable N_2O consumption rates in fully oxygenated waters of the high-latitude Atlantic Ocean and Eastern Tropical North Pacific (Rees et al., 2021; Sun et al., 2021). The potential for N_2O reduction in

oxygenated environments can also been inferred from the widespread prevalence of nitrous oxide reductase (*nosZ*) genes and transcripts in the upper water column (Sun et al., 2017). Indeed, the high incidence of *nosZII*-type (atypical) variants associated with non-denitrifying organisms may present a mechanism for N_2O scavenging across oxycline depths.

Sharp contrasts in the community structure of N_2O-reducing microorganisms were detected between mangrove sediments and N_2O sourse sediments of the NESAP continental shelf. Normalized *nosZII gene* copy abundances were roughly an order of magnitude higher than that of *nosZI* variants across all samples, consistent with molecular surveys demonstrating *nosZII* dominance in other marine microbiomes (Bertagnolli et al., 2020). However, mean normalized *nosZII* gene and transcript copy abundances were highest in mangrove sediments, accounting for over 90% of total *nosZ* genes and over 80% of total *nosZ* transcripts. This supports previous reports of correlations between microbial community N_2O sink capacity and atypical *nosZII* variants in terrestrial soils (Jones et al., 2014). Sediment *nosZII* gene copy ratios were comparable across continental slope depths in the NESAP, while relative *nosZII* expression levels decreased with decreases in bottom water O_2 concentrations and OPDs, and increases in sediment N_2O effluxes (Jameson et al., 2021). Elevated *nosZI* transcript abundances also followed a gradient of increasing bottom water NO_3^- concentrations, suggesting that denitrifying organisms with typical *nosZI* variants may contribute more to sediment N_2O effluxes in regions with shallow OPDs and high DIN availability.

Nitrogen limitation in minimally impacted mangrove systems has been previously linked to elevated rates from nitrogen conservation pathways such as dissimilatory nitrate reduction to ammonium (DNRA) (Fernandes et al., 2012). Interestingly, organisms that perform DNRA generally possess atypical *nosZII* variants and have been implicated as mediators of sediment N_2O

consumption through direct N_2O consumption and competition with typical denitrifiers for nitrogen substrates (Maher et al., 2016; Sanford et al., 2012). Mangrove bacterial community surveys reported here revealed high abundances of ASVs from the Thiotrichales, an order that contains known sediment-associated taxa capable of DNRA coupled to sulfide oxidation, including *Beggiatoa* and *Thioploca* (Otte et al., 1999; Preisler et al., 2007). Several additional orders that have been associated with atypical *nosZII* variants were also highly abundant in mangrove sediments, including the Cytophagales, Ectothiorhodospirales, and Bacteroidales (Bertagnolli et al., 2020; Sanford et al., 2012). Conversely, NESAP sediments were characterized by comparatively high relative abundances of ASVs from the uncultured Gammaproteobacteria order NB1-j and Thiohalorhabdales. These groups are commonly detected in marine sediments and have been implicated as potential contributors to N_2O production based on the presence of genes encoding respiratory nitric oxide reductases (de Voogd et al., 2015; Pushpakumara et al., 2023). Additional sequencing of *nosZI* and *nosZII* genes and transcript will help to further elucidate specific microbial taxa that contribute to pools of atypical versus typical N_2O reductases.

ASVs belonging to prominent sulfate-reducing bacterial groups such as the Desulfobulbales and Desulfobacterales were also more abundant in mangrove sediments compared to those from the NESAP continental margin. Organisms belonging to these groups have not been directly implicated in N_2O cycling, however; sulfide production from sulfate reduction may facilitate N_2O reduction by sulfide-oxidizing DNRA organisms such as Thiotrichales. Indeed, previous work has also reported correlations between putative sulfur-cycling ASVs, including members of the Desulfobacterales and Ectothiorhodospirales, and net N_2O consumption in the anoxic waters of Saanich inlet (Jameson et al., 2023). Similar trends were observed for putative methane-cycling groups such as the Bathyarchaeia (methanotrophs capable of DNRA) and

Methanosarcinales (methanogens), which were also highly enriched in mangrove sediments (Angelidaki et al., 2011; Zhou et al., 2018). Although some methanogenic bacteria have been shown to produce N_2O via ammonia oxidation (Campbell et al., 2011), the role of methane-cycling Archaea in the marine N_2O cycle is not well understood.

Net N_2O efflux from NESAP sediments was associated with archaeal communities dominated by putative AOA belonging to the Nitrosopumilales and Nitrososphaerales orders (Alves et al., 2018). Increases in the relative abundance of Nitrosococcales ASVs with depth also implicate putative AOB as a potential contributor to N_2O production. In contrast, AOA and AOB abundances were comparably low in mangrove sediments and N_2O consumption rates were unaffected by short-term exposure to elevated NH_4^+ concentrations. Competition with NH_4^+-assimilating epiphytobenthos and macrophytes may constrain the sediment nitrifying community through competitive mechanisms, leading to low overall nitrification rates and limited N_2O production near the sediment interfaces (Rysgaard et al., 1996; Ward, 2008). Sedimentary nitrification and denitrification have both been implicated as contributors to N_2O production in coastal sediments (Allen et al., 2007; Bauza et al., 2002; Muñoz-Hincapié et al., 2002). The results presented here provide further evidence that both pathways contribute to sediment N_2O efflux in source sediments, and suggest that sediment N_2O sink capacities may be facilitated by reduced AOA and AOB abundances.

4.6 Conclusions and outlook

In contrast with open ocean OMZs, coastal sediments bring anoxic, reducing environments in close proximity to the atmosphere, allowing for appreciable atmospheric N_2O drawdown in nitrogen-limited systems. Our results suggest that minimally impacted mangrove environments can drive net sediment N_2O uptake mediated by a diverse community of atypical

N_2O scavengers, and that the N_2O sink capacity of these communities is resilient against modest increases in DIN and seawater N_2O concentrations. Whether or not these environments contribute meaningfully to global N_2O budgets will require a complete inventory of the geographic extent of natural N_2O sinks, including information about the seasonal and inter-annual variability in N_2O consumption rates. Note also that these results represent the *functional capacity* of N_2O-reducing microorganisms to compensate for short-term increases in sedimentary N_2O production. Sustained chronic eutrophication of minimally impacted systems will also lead to *structural shifts* in sediment microbial community composition, and thus affect the balance between N_2O production and consumption processes over longer timescales.

Sharp contrasts in the community structure of N_2O-reducing bacteria were detected between mangrove sediments and N_2O source sediments from the NESAP continental shelf. Contributions from both denitrification and ammonia oxidation to sediment N_2O effluxes in the NESAP were demonstrated by high abundances and transcriptional activities of typical *nosZI*-type N_2O reductases, and archaeal communities dominated by putative AOA. In contrast, higher atypical *nosZII* gene and transcript copy abundances in Bermudian mangrove sediments were linked to taxa that may contribute to nitrogen conservations pathways such as DNRA in nitrogen-limiting systems. These results provide further scientific justification for the conservation and restoration of coastal wetland ecosystems in areas with substantial anthropogenic influence.

4.7 Acknowledgements

This research was supported by the Canadian Healthy Oceans Network (CHONe II), the Univeristy of Victoria, the Bermuda Institute of Ocean Sciences (BIOS), and the Canadian Associates of BIOS (CABIOS). Validation and execution of the qPCR analyses was funded in part by Genome Canada, Genome British Columbia, and Genome Québec large-scale applied research

project #312ITD to CCH. I would like to thank Dr. Yvonne Sawall for support during use of the BIOS mesocosm facility and Dr. Peter Berg for his advice on profile modelling. I would also like to thank co-authors Matthew Bonderud and Dr. Mark Louie Lopez, who were instrumental in the validation and execution of the qPCR assays. Thank you to all co-authors, as well as Drs. Roberta Hamme and Réal Roy for providing feedback on the first manuscript drafts. Finally, I would like to thank Moronke Harris for making the map of the Bermuda platform for this manuscript. All samples were collected under the authority of and in compliance with Special Permit #SP200801 issued by the Bermuda Government Department of Environment and Natural Resources.

4.8 Article Supplementary Material

Table 4.1 Supplement: Primer & probe sequences.

Primer and probe sequences used for qPCR assays and high-throughput sequencing of bacterial and archaeal 16S rRNA genes.

Primer/probe	Forward primer	Target	Reference
	qPCR assays		
ePlant5-150134F	5'-TCTAGGGATAACAGGCTGAT-3'	Chloroplast 23S rRNA	Veldhoen et al. (2016)
ePlant5-150135R	5'-TGAACCCAGCTCACGTAC-3'	Chloroplast 23S rRNA	Veldhoen et al. (2016)
ePlant5-150139 Probe	5'-TTTGGCACCTCGATGTCGG-3'	Chloroplast 23S rRNA	Veldhoen et al. (2016)
Bac1055YF	5'-ATGGYTGTCGTCAGCT-3'	Bacteria 16S rRNA	Ritalahti et al. (2006); Ferris et al. (1996)
Bac1392R	5'-ACGGGCGGTGTGTAC-3'	Bacteria 16S rRNA	Ritalahti et al. (2006); Lane (1991)
Bac1115Probe	5'-FAM-CAACGAGCGCAACCC-TAMRA-3'	Bacteria 16S rRNA	Ritalahti et al. (2006); Lane (1991); Harms et al. (2003)
nosZ-II-F	5'-CTI GGI CCI YTK CAY AC-3'	nosZII	Jones et al. (2013)
nosZ-II-R	5'-GCI GAR CAR AAI TCB GTR C-3'	nosZII	Jones et al. (2013)
nosZ1F	5'-WCSYTGTTCMTCGACAGCCAG-3'	nosZI	Henry et al. (2006)
nosZ1R	5'-ATGTCGATCARCTGVKCRTTYTC-3'	nosZI	Henry et al. (2006)
	MiSeq		
B969F	5'-ACGCGHNRAACCTTACC-3'	Bacteria 16S rRNA	Comeau et al. (2011)
BA1406R	5'-ACGGGCRGTGWGTRCAA-3'	Bacteria 16S rRNA	Comeau et al. (2011)
A956F	5'TYAATYGGANTCAACRCC-3'	Archaea 16S rRNA	Comeau et al. (2011)
A1401R	5'CRGTGWGTRCAAGGRGCA-3'	Archaea 16S rRNA	Comeau et al. (2011)

Table 4.2 Supplement: Amplification efficiencies for *nosZ* assays.

Calibration curve slopes, amplification efficiencies, threshold C_q values, and continuous limits of quantification (LOQ_{cont}) reported for *nosZI* and *nosZII* qPCR assays. LOD_{cont} represents the lowest detectable copy number per reaction.

Assay	Slope	Efficiency	C_q threshold	LOD_{cont}
nosZI	-3.54	92%	33	4
nosZII	-3.94	79%	38	4

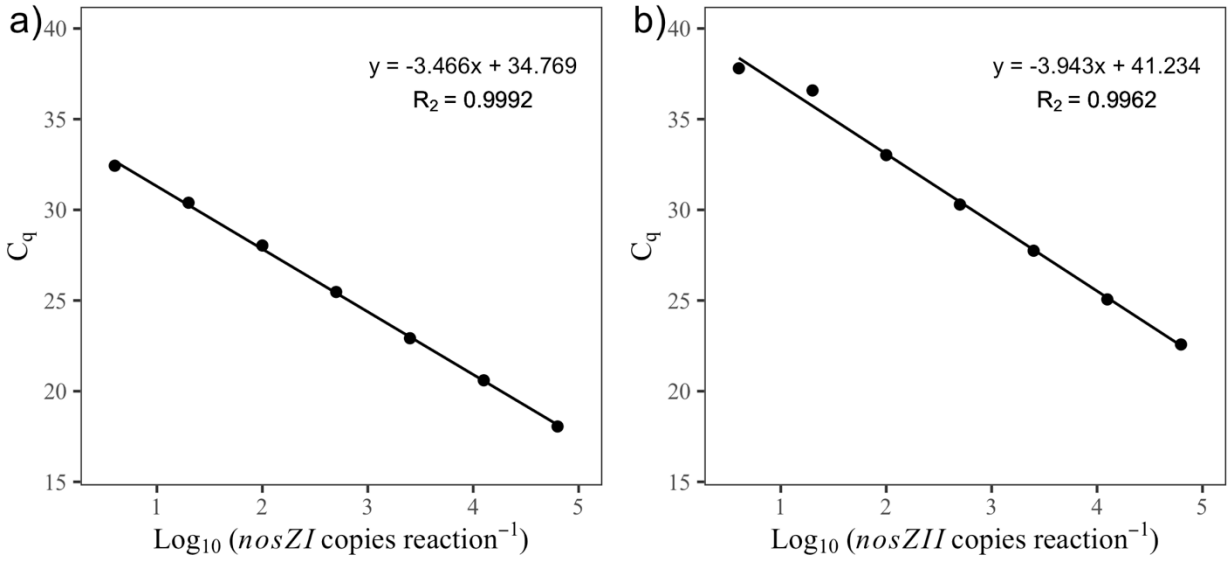

Fig. 4.7 Supplement: standard curves for *nosZI* and *nosZII* qPCR assays.

Standard curves generated using gBlocks® for quantification of (a) *nosZI* and (b) *nosZII* gene and transcript copy numbers in Bermudian mangroves and NESAP continental margin sediments. All technical replicates were positive at ≥ 4 copies per reaction (LOD_{cont}) and samples with mean C_q values greater than the LOD_{cont} were removed prior to downstream analyses.

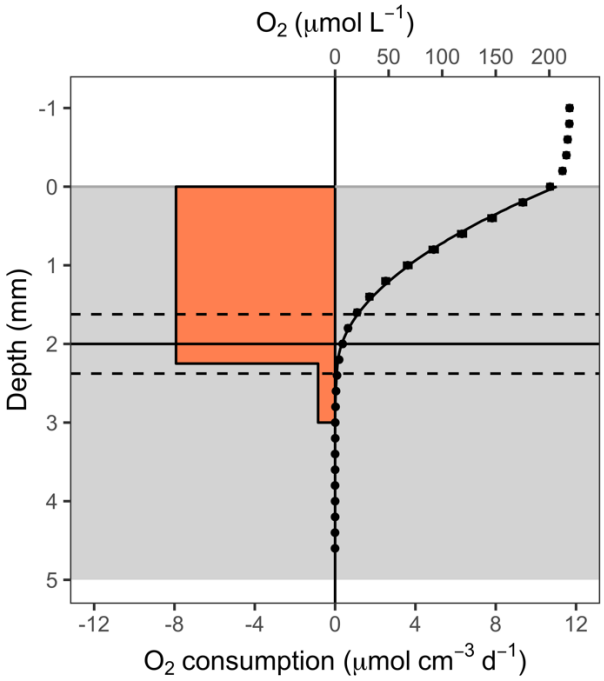

Fig. 4.8 Supplement: Mean porewater O_2 profile and modelled consumption rates.

Individual data points represent mean (± SE, n = 67) O_2 concentrations (µmol L^{-1}) obtained during dark incubations in mangrove sediments between 10 October and 01 November, 2020. Red boxes highlight to zones of O_2 consumption (µmol cm^{-3} d^{-1}) estimated from the mean concentration profile. The solid black profile line is the PROFILE model fit to the mean concentration profile. Horizontal black lines represent mean oxygen penetration depth (± SD, indicated by dashed lines). Oxygen penetration depths ranged from 1.2 to 2.8 mm across all replicates. Grey shading highlights the sample section depth for nucleic acids analyses.

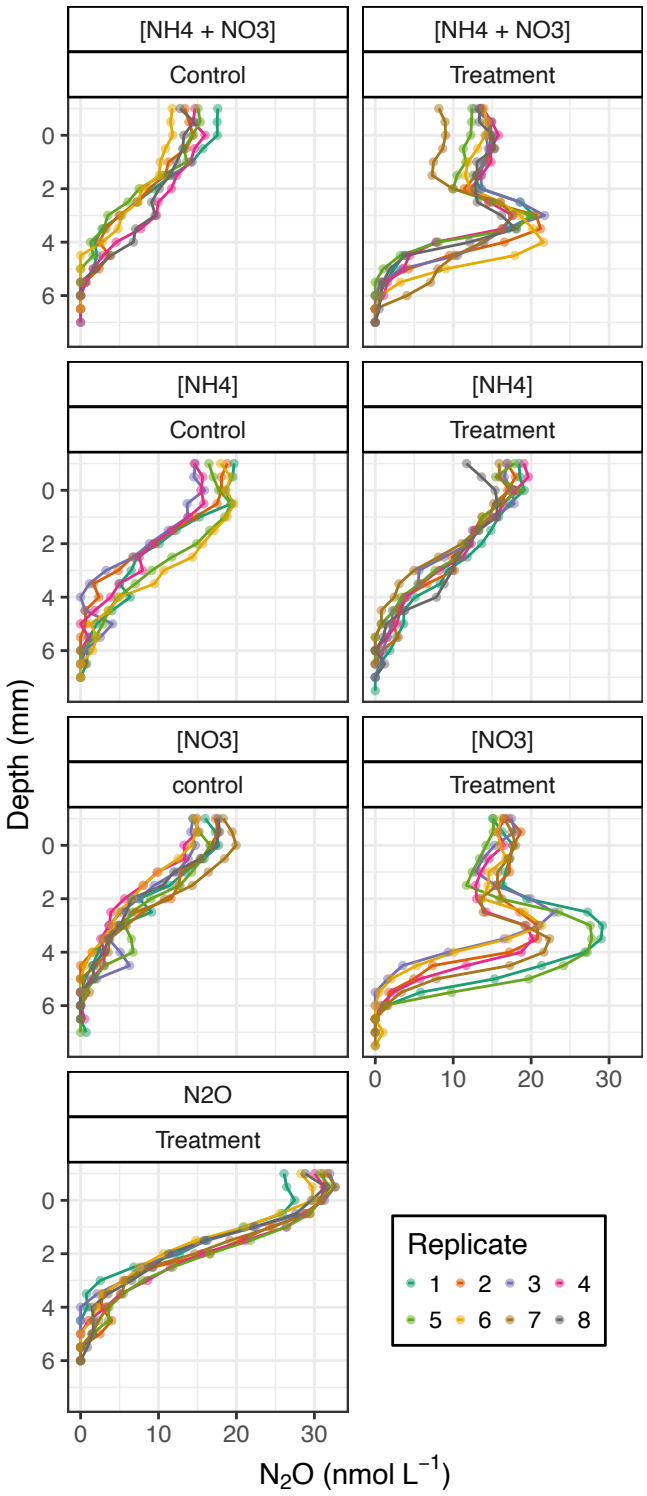

Fig. 4.9 Supplement: Mangrove sediment N_2O profiles.

Replicate drift-corrected porewater N_2O concentration (nmol L^{-1}) profiles obtained in post-incubation mangrove sediments from all experimental treatment and control groupings. Data reported here are used to construct the mean N_2O profiles depicted in Fig. 4.3 and for input to the PROFILE model.

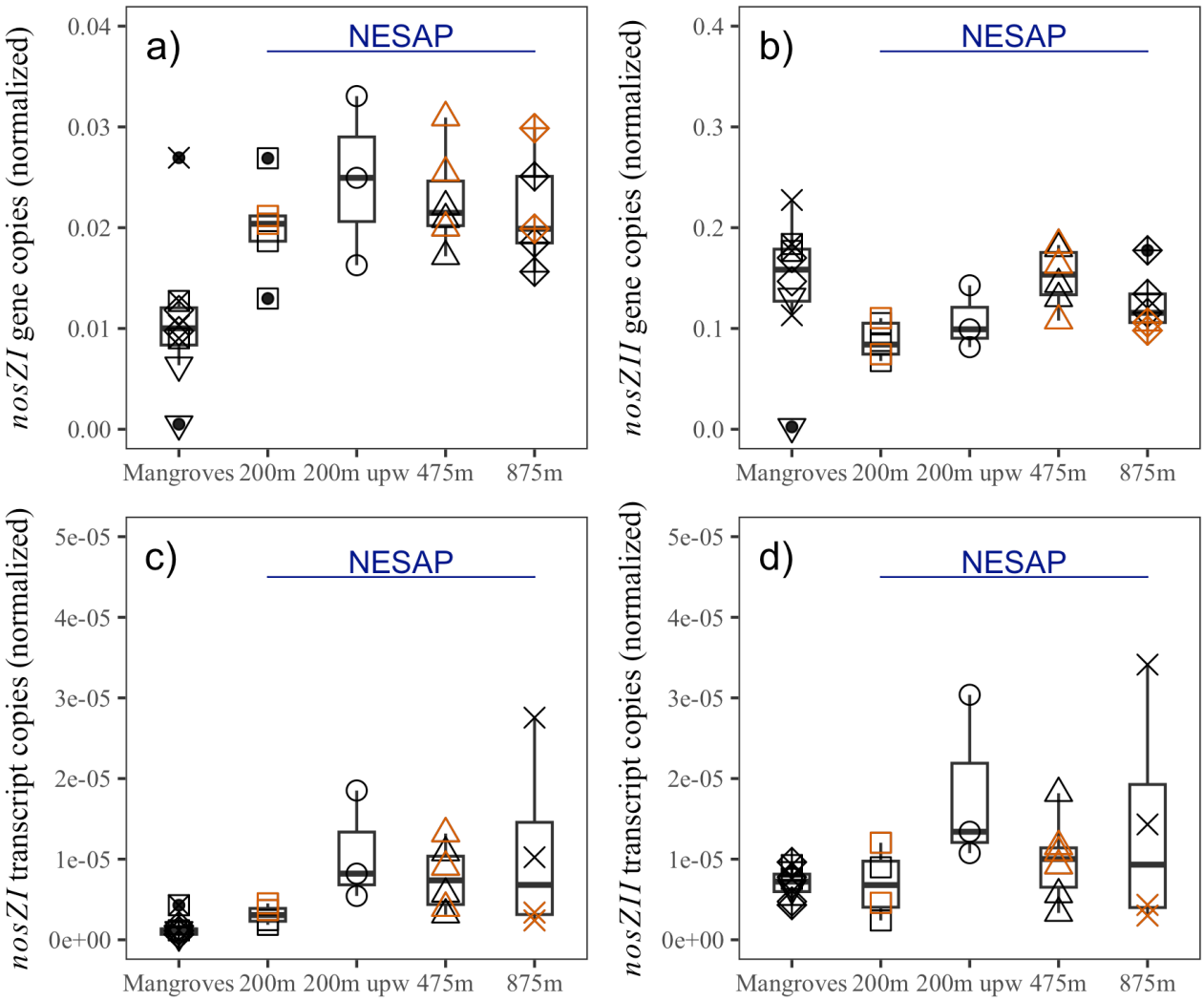

Fig. 4.10 Supplement: Boxplots of 16S-normalized *nosZ* gene and transcript copy abundances.

Bacteria *nosZI* and *nosZII* gene copy (gDNA) and transcript (cDNA) abundances are normalized to bacterial 16S rRNA (gDNA/cDNA) copy abundances and expressed as a ratio (nosZ:16S) for all samples. Mangrove sediment samples were obtained from control, DIN-amended, and N_2O-amended cores. NESAP slope sediments were sampled from 200 m ambient and 200 m simulated upwelling, 475 m ambient, and 850 m ambient incubations. Initial samples were obtained in separate cores at each station prior to incubation and are indicated in orange.

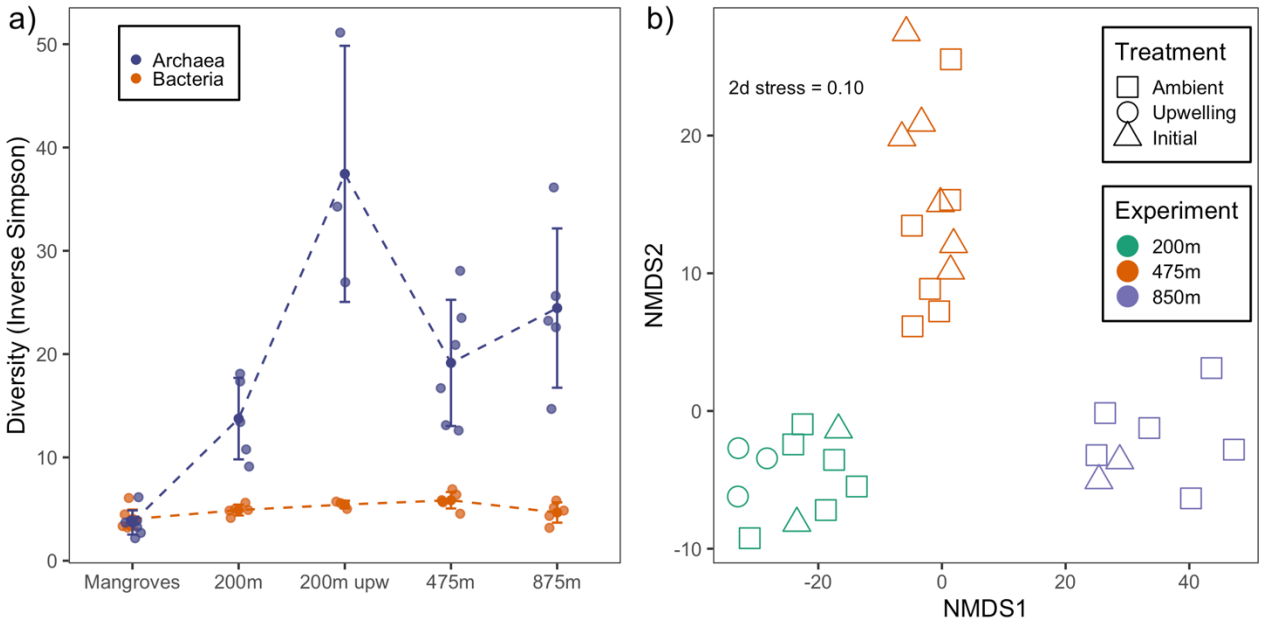

Fig. 4.11 Supplement: Community inverse Simpson diversities and bacterial NMDS biplot.

Inverse Simpson diversity indices calculated for sediment archaeal and bacterial communities in mangroves and NESAP continental margin sediments using ASV tables constructed from 16S rRNA amplicon sequences (a). Archaeal diversity is significantly lower in mangrove sediments than in slopes sediments (p = 0.030 – 0.005). Panel (b) shows nonmetric multidimensional scaling (NMDS) ordinations for Bacteria communities in NESAP continental margin sediments, used to assess community dissimilarities between sampling depths and between pre-incubation and post-incubation samples.

Chapter 5: Conclusions

5.1 Research summary and literature contributions

The main objective of this dissertation was to assess the relevance of microbial community structure to marine N_2O cycling through the interdisciplinary application of biogeochemical rate measurements and high-resolution microbial community profiling. In Chapter 2, I utilized the dynamic environmental conditions of Saanich Inlet to investigate patterns of microbial community assembly at the taxonomic level in relation to spatiotemporal variability in environmental conditions and N_2O production rates. This work, which was published in *Communications Biology* in 2023, provides circumstantial evidence for the presence of keystone microbial taxa that may regulate N_2O production and consumption through coupled metabolic exchanges. Water column N_2O accumulation driven by nitrifying processes across oxycline depths was closely linked to ubiquitous microbial groups, such as SAR11, implicated in the heterotrophic remineralization of organic matter. In contrast, N_2O production from denitrification was most prominent in N_2O-undersaturated anoxic waters containing important microbial players implicated in coupled carbon, nitrogen, and sulfur cycling. These data also provide further evidence for close coupling between N_2O production and consumption by elements of the denitrification pathway that are distributed across multiple taxonomic groups in the Saanich Inlet anoxic basin.

In Chapters 3 and 4, I direct attention toward understudied marine sediments of the NESAP outer continental margin and minimally impacted Bermudian mangroves. Previous approaches to studying N_2O fluxes from marine sediments have relied on whole-core squeezing, sealed-core incubations, or slurry incubations. Each of these methods carry methodological limitations that may bias N_2O production (or consumption) estimates. Porewater profiles obtained from whole-core squeezing suffer from poor vertical resolution that can mask near-surface

gradients while non-steady state conditions associated with sealed-core incubations may alter sedimentary redox gradients. On the other hand, sediment slurry incubations destroy sediment vertical structure entirely, and thus do not accurately reflect microbial activities *in situ*. Chapter 3 presents an improved method for constraining sediment N_2O fluxes in sedimented environments using trace-level microsensors and applied numerical modelling. This work, published in *Limnology and Oceanography Letters* in 2021, reports the first sub-millimeter resolution profiles of N_2O under ambient conditions and the first estimates of N_2O efflux from outer continental margin sediments underlying the NESAP ODZ.

Chapter 4 builds on this work first by quantifying the N_2O sink capacity of sediment microbial communities in a minimally impacted mangrove system and testing the resilience of this sink to modest increases in seawater N_2O and DIN concentrations. Mangrove and continental margin sediments were then compared to understand variability in microbial community dynamics between sedimentary N_2O sources and sinks. Targeting of two phylogenetically distinct *nosZ* gene clusters for quantification of gene and transcript copy abundances via qPCR indicated higher abundance and activity of 'atypical' *nosZII*-type N_2O reducers in mangrove sediments. These organisms typically lack additional denitrification genes and are implicated as important N_2O scavengers in marine and terrestrial environments. Parallel sequencing of bacterial and archaeal 16S rRNA amplicons implicated putative DNRA organisms as potentially important N_2O reducers in mangrove sediments. Similar to my findings in the Saanich Inlet anoxic basin, net N_2O consumption in mangrove sediments was associated with higher relative abundances of putative anaerobic sulfur cycling taxa from the Ectothiorhodospirales and Desulfobacterota. N_2O source sediments from the NESAP contained higher abundances of putative AOA and AOB, and were

associated with elevated expression levels of typical *nosZI* variants, suggesting likely contributions from nitrification and denitrification.

5.2 Research limitations

Several limitations became evident throughout the course of this research, the first of which relates to estimations of N_2O cycling rate processes in sedimented environments. Although trace-level microsensors combined with profile interpretation models present a preferred method in this sense, this work is presently constrained by the relatively high detection limits of commercially available sensors. This is less of a concern when working in systems with high ambient N_2O concentrations, such as those found in bottom waters overlying the NESAP continental margin. However, obtaining accurate measurements of porewater N_2O concentrations at high vertical resolutions is difficult when ambient N_2O concentrations are near atmospheric equilibrium. Recent advances in microsensor technology have now achieved N_2O sensors with automatic drift compensation and sensitivities as low as 2 nmol L^{-1} (Damgaard et al., 2020). Once commercially available, these sensors will hopefully facilitate further research across diverse sediment environments using similar approaches.

Additional limitations to the research presented in this dissertation are broadly related to the logistical constraints associated with surveying natural microbial communities. At present, high-throughput sequencing of the 16S rRNA genes provides the best approach for high-resolution taxonomic profiling and cataloguing of microbial diversity. The recent transition away from clustering of sequences into operational taxonomic units based on arbitrary similarity thresholds toward delineating amplicon sequence variants that differ at the single nucleotide level presents a considerable advancement. Chapter 2 demonstrates the utility of such approaches with respect to identifying patterns of co-variance between individual taxa, yet interpretations are restricted by the

fact that taxonomic affiliations can only provide circumstantial evidence of microbial functional capacities and potential ecological interaction. Integration of high-resolution taxonomic surveys with meta-omics sequencing will undoubtedly help to resolve some of these functional ambiguities moving forward and may also shed light on the level of taxonomic resolution that is necessary for investigations of ecosystem function at broad scales.

Inferences regarding the roles of specific organisms in regulating the biogeochemical transformations that produce and consume N_2O are based primarily on correlations between environmental variables, experimentally derived rate measurements, and pools of relevant biomolecules (i.e. genes, transcripts, or proteins). Multivariate statistical analyses can be useful for identifying patterns of co-variance across a wide range of biological organizations and for generating interesting hypotheses when paired with corresponding environmental characterizations and rate measurements. Direct contributions from individual taxa and potential ecological interactions must therefore be inferred *a posteriori* based on contextual information provided by taxonomic affiliation or functional capacity. The most pressing limitation of this research is that causal links between potentially important microbial groups and N_2O cycling rate processes cannot be determined empirically based on correlational relationships alone. Continued advancements in this domain will require careful experimentation guided by previous work of the sort presented in this dissertation.

5.3 Suggestions for future research

Biogeochemical rate measurements estimated from environmental samples represent the cumulative activities of diverse communities that contain active and inactive populations. Further to this, molecular surveys of natural microbial communities cannot distinguish inactive organisms from those that are either contributing directly to a given process or exerting influence over those

that are. In the macroscopic world, an ecologist might choose to remove a potential keystone species or functional group from a controlled system and observe the subsequent impacts to ecosystem function. This is obviously not a feasible line of inquiry for microbial communities. In this section, I propose a tractable research program that may help to address some of these limitations by borrowing methodologies that have been applied to studies of carbon cycling in the surface ocean.

Single-cell Raman spectroscopy provides a non-invasive means of obtaining molecular 'fingerprints' of individual cells *in vivo*, with each spectrum providing detailed information on cellular phenotypes and physiological states (Li et al., 2012). Intracellular molecules demonstrate detectable shifts in the corresponding Raman spectra following incorporation of stable isotopes such as ^{13}C and ^{15}N (Fig. 5.1), allowing for the tracing of labelled substrates into viable cellular biomass via Raman-stable isotope probing (Raman-SIP) (Wang et al., 2016). For example, incubations of mixed microbial communities with ^{13}C-labelled substrates have been used to quantitatively assess the metabolic activities of photoautotrophic and heterotrophic cells (Li et al., 2012; Wang et al., 2016). Pairing Raman-SIP with Raman-activated cell sorting (RACS) techniques allow researchers to isolate individual cells demonstrating ^{13}C-incorporation and extract nucleic acids for subsequent molecular analyses (Fig. 5.1) (Jing et al., 2018). These methods, collectively referred to as next-generation physiology, permit detailed characterizations of specific genotypes that contribute explicitly to ecosystem processes (Hatzenpichler et al., 2020).

The application of next-generation physiology to the study of marine microbial communities has shown its utility in the surface ocean (Jing et al., 2018), and is ready to be applied to investigations of microbial processes in the ocean interior. Although these methods do not directly apply to the tracing of ^{15}N from substrate to reactant pools in the environment (i.e. ^{15}N-

NO_3^- to ^{15}N-N_2O), nitrogen transformation processes are inextricably connected to the marine carbon cycle. For example, AOA couple ammonia oxidation to inorganic carbon fixation while autotrophic denitrifiers such as SUP05 couple carbon fixation to NO_x reduction and sulfide or elemental sulfur oxidation. Similarly, heterotrophic denitrifiers assimilate organic carbon using energy generated by organic carbon oxidation coupled to NO_x reduction. Future research may be able to utilize carbon assimilation processes as metabolic proxies for identifying quantitative links between microbial organisms and N_2O cycling processes using next generation physiology techniques.

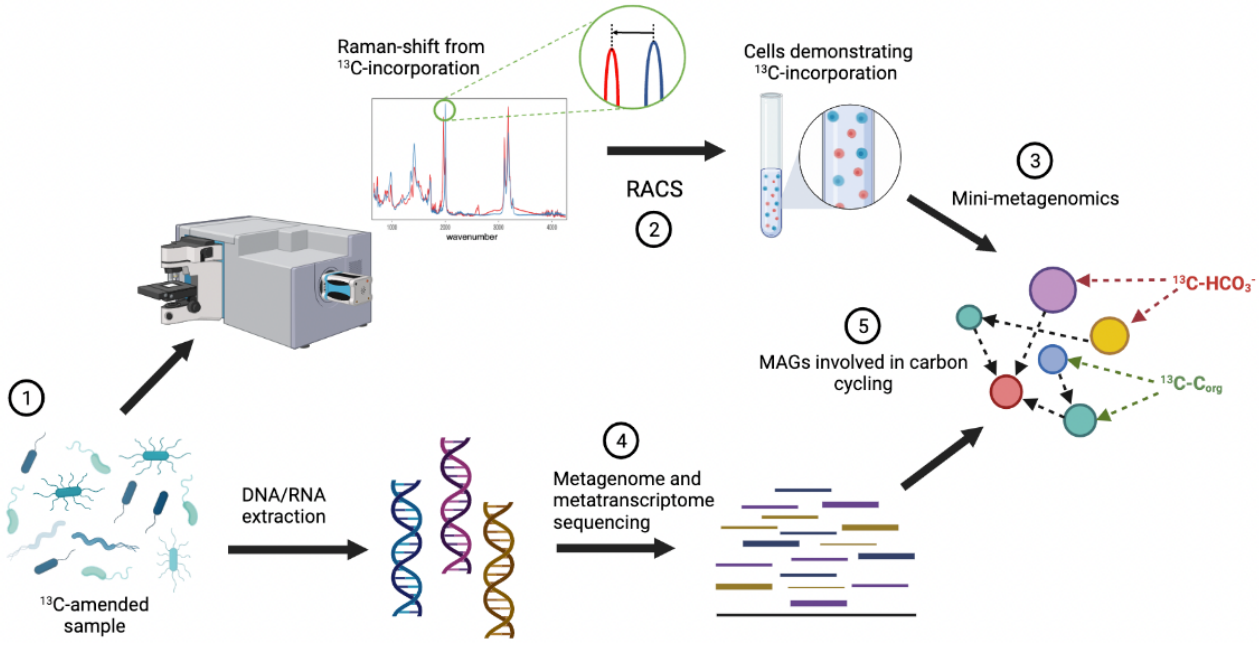

Fig. 5.1 Example workflow for identifying microbial carbon & nitrogen cycling groups.

Seawater samples incubated with ^{13}C-labelled substrate (1) are first analyzed using SCRS and RACS to isolate individual cells demonstrating incorporation of ^{13}C into viable biomass (2). Metagenomic sequencing of isolated cells (3) is augmented with shotgun metagenomic and metatranscriptomic sequencing of separate subsamples (4) to reconstruct metagenome-assembled genomes (MAGs) with confirmed roles in dark carbon fixation and heterotrophic carbon utilization (5). Workflow was adapted from Jing et al. (2018) and the diagram was created using BioRender.

This work will serve two primary functions. The first component will help to resolve fundamental questions regarding specific organisms responsible for regulating dark carbon fixation and organic carbon utilization in ODZ water columns. This would involve amendment of seawater samples from within and above marine ODZs with either ^{13}C-labelled bicarbonate or a complex ^{13}C-labelled organic substrate. Microbes demonstrating incorporation of ^{13}C into cellular structures can then be isolated using a high-throughput RACS method that leverages microfluidics and optical tweezing to sort individual cells for downstream sequencing via mini-metagenomics (Lee et al., 2019). Mini-metagenomics combines the advantages of shotgun and single-cell metagenomics by providing relatively high throughput while preserving single-cell resolution for low amounts of template DNA (Lee et al., 2019; Yu et al., 2017). For samples amended with ^{13}C-labelled organic carbon, isolated cells would reflect solely allochthonous carbon utilization via heterotrophic pathways. In contrast, cells isolated from samples amended with ^{13}C-labelled bicarbonate may reflect chemoautotrophic carbon fixation or heterotrophic incorporation of autochthonous carbon liberated through viral lysis or cellular exudates. Taxonomic annotation of functional gene profiles within the assembled mini-metagenomes will help to differentiate these two processes by linking gene orthologues corresponding to dark carbon fixation pathways to specific taxa.

The second component involves parallel amendments of separate samples with ^{15}N-labelled substrates to elucidate overall N_2O production rates and relative contributions from discrete pathways. Mini-metagenomes constructed from RACS-isolated cells can then be used as reference guides to construct single-cell genomes from shotgun metagenomic sequencing of whole-community DNA isolated from both *in situ* and *in vitro* communities. This would ideally improve the resolution of low-coverage regions missed by mini-metagenomic sequencing of

isolated cells and permit the reconstruction of complete metabolic pathways. Deep-sequencing of microbial metatranscriptomes will further aid interpretations by confirming transcriptional activity of candidate genes and pathways. By focusing analyses on populations with confirmed ^{13}C-incorporation, it will be possible to eliminate many of the confounding variables associated with community-wide profiling. Most importantly, this would allow for the identification of mechanistic links between cellular genotypes and ecosystem function with respect to coupled biogeochemical transformations that drive N_2O cycling in the ocean.

References

Allen, D., Dalal, R. C., Rennenberg, H., & Schmidt, S. (2011). Seasonal variation in nitrous oxide and methane emissions from subtropical estuary and coastal mangrove sediments, Australia. *Plant Biology*, *13*(1), 126–133. https://doi.org/10.1111/j.1438-8677.2010.00331.x

Allen, D. E., Dalal, R. C., Rennenberg, H., Meyer, R. L., Reeves, S., & Schmidt, S. (2007). Spatial and temporal variation of nitrous oxide and methane flux between subtropical mangrove sediments and the atmosphere. *Soil Biology and Biochemistry*, *39*(2), 622–631. https://doi.org/10.1016/j.soilbio.2006.09.013

Aller, R. C., & Aller, J. Y. (1992). Meiofauna and solute transport in marine muds. *Limnology and Oceanography*, *37*(5), 1018–1033. https://doi.org/10.4319/lo.1992.37.5.1018

Alves, R. J. E., Minh, B. Q., Urich, T., von Haeseler, A., & Schleper, C. (2018). Unifying the global phylogeny and environmental distribution of ammonia-oxidising archaea based on amoA genes. *Nature Communications*, *9*(1), Article 1. https://doi.org/10.1038/s41467-018-03861-1

Amir, A., McDonald, D., Navas-Molina, J. A., Kopylova, E., Morton, J. T., Zech Xu, Z., Kightley, E. P., Thompson, L. R., Hyde, E. R., Gonzalez, A., & Knight, R. (2017). Deblur Rapidly Resolves Single-Nucleotide Community Sequence Patterns. *MSystems*, *2*(2), e00191-16. https://doi.org/10.1128/mSystems.00191-16

Anderson, J. J., & Devol, A. H. (1973). Deep water renewal in Saanich Inlet, an intermittently anoxic basin. *Estuarine and Coastal Marine Science*, *1*(1), 1–10. https://doi.org/10.1016/0302-3524(73)90052-2

Angelidaki, I., Karakashev, D., Batstone, D. J., Plugge, C. M., & Stams, A. J. M. (2011). Chapter sixteen—Biomethanation and Its Potential. In A. C. Rosenzweig & S. W. Ragsdale (Eds.), *Methods in Enzymology* (Vol. 494, pp. 327–351). Academic Press. https://doi.org/10.1016/B978-0-12-385112-3.00016-0

Arévalo-Martínez, D. L., Kock, A., Löscher, C. R., Schmitz, R. A., & Bange, H. W. (2015). Massive nitrous oxide emissions from the tropical South Pacific Ocean. *Nature Geoscience*, *8*(7), Article 7. https://doi.org/10.1038/ngeo2469

Arias, P. A., et al. (2021). Technical Summary. *In Climate Change 2021: The Physical Science Basis. Contribution of Working Group I to the Sixth Assessment Report of the Intergovernmental Panel on Climate Change [Masson-Delmotte, V., P. Zhai, A. Pirani, S.L. Connors, C. Péan, S. Berger, N. Caud, Y. Chen, L. Goldfarb, M.I. Gomis, M. Huang, K. Leitzell, E. Lonnoy, J.B.R. Matthews, T.K. Maycock, T. Waterfield, O. Yelekçi, R. Yu, and B. Zhou (eds.)]. Cambridge University Press, Cambridge, United Kingdom and New York, NY, USA, pp. 33−144. doi:10.1017/9781009157896.002.*

Arrigo, K. R. (2005). Marine microorganisms and global nutrient cycles. *Nature*, *437*(7057), Article 7057. https://doi.org/10.1038/nature04159

Auladell, A., Barberán, A., Logares, R., Garcés, E., Gasol, J. M., & Ferrera, I. (2022). Seasonal niche differentiation among closely related marine bacteria. *The ISME Journal*, *16*(1), Article 1. https://doi.org/10.1038/s41396-021-01053-2

Auladell, A., Sánchez, P., Sánchez, O., Gasol, J. M., & Ferrera, I. (2019). Long-term seasonal and interannual variability of marine aerobic anoxygenic photoheterotrophic bacteria. *The ISME Journal*, *13*(8), Article 8. https://doi.org/10.1038/s41396-019-0401-4

Babbin, A. R., Bianchi, D., Jayakumar, A., & Ward, B. B. (2015). Rapid nitrous oxide cycling in the suboxic ocean. *Science*, *348*(6239), 1127–1129. https://doi.org/10.1126/science.aaa8380

Bahram, M., Espenberg, M., Pärn, J., Lehtovirta-Morley, L., Anslan, S., Kasak, K., Kõljalg, U., Liira, J., Maddison, M., Moora, M., Niinemets, Ü., Öpik, M., Pärtel, M., Soosaar, K., Zobel, M., Hildebrand, F., Tedersoo, L., & Mander, Ü. (2022). Structure and function of the soil microbiome underlying N2O emissions from global wetlands. *Nature Communications*, *13*(1), Article 1. https://doi.org/10.1038/s41467-022-29161-3

Bakenhus, I., Dlugosch, L., Billerbeck, S., Giebel, H.-A., Milke, F., & Simon, M. (2017). Composition of Total and Cell-Proliferating Bacterioplankton Community in Early Summer in the North Sea – Roseobacters Are the Most Active Component. *Frontiers in Microbiology*, *8*. https://www.frontiersin.org/article/10.3389/fmicb.2017.01771

Bálint, M., Bahram, M., Eren, A. M., Faust, K., Fuhrman, J. A., Lindahl, B., O'Hara, R. B., Öpik, M., Sogin, M. L., Unterseher, M., & Tedersoo, L. (2016). Millions of reads, thousands of taxa: Microbial community structure and associations analyzed via marker genes. *FEMS Microbiology Reviews*, *40*(5), 686–700. https://doi.org/10.1093/femsre/fuw017

Banerjee, S., Kirkby, C. A., Schmutter, D., Bissett, A., Kirkegaard, J. A., & Richardson, A. E. (2016). Network analysis reveals functional redundancy and keystone taxa amongst bacterial and fungal communities during organic matter decomposition in an arable soil. *Soil Biology and Biochemistry*, *97*, 188–198. https://doi.org/10.1016/j.soilbio.2016.03.017

Banerjee, S., Schlaeppi, K., & van der Heijden, M. G. A. (2018). Keystone taxa as drivers of microbiome structure and functioning. *Nature Reviews Microbiology*, *16*(9), 567–576. https://doi.org/10.1038/s41579-018-0024-1

Bange, H. W. (2008). Gaseous Nitrogen Compounds in the Ocean. *In* D. G. Capone, D. A. Bronk, M. R. Mulholland, & E. J. Carpenter (Eds.), *Nitrogen in the Marine Environment (Second Edition)* (pp. 51–94). Academic Press. https://doi.org/10.1016/B978-0-12-372522-6.00002-5

Bange, H. W., & Andreae, M. O. (1999). Nitrous oxide in the deep waters of the world's oceans. *Global Biogeochemical Cycles*, *13*(4), 1127–1135. https://doi.org/10.1029/1999GB900082

Bange, H. W., Arévalo-Martínez, D. L., de la Paz, M., Farías, L., Kaiser, J., Kock, A., Law, C. S., Rees, A. P., Rehder, G., Tortell, P. D., Upstill-Goddard, R. C., & Wilson, S. T. (2019). A Harmonized Nitrous Oxide (N_2O) Ocean Observation Network for the 21st Century. *Frontiers in Marine Science*, *6*. https://www.frontiersin.org/article/10.3389/fmars.2019.00157

Bange, H. W., Freing, A., Kock, A., & Löscher, C. R. (2010). Marine Pathways to Nitrous Oxide. *In* Smith, K. A. (Ed.), *Nitrous Oxide and Climate Change* (pp. 40-66) Routledge. https://doi.org/10.4324/9781849775113.

Barbera, P., Kozlov, A. M., Czech, L., Morel, B., Darriba, D., Flouri, T., & Stamatakis, A. (2019). EPA-ng: Massively Parallel Evolutionary Placement of Genetic Sequences. *Systematic Biology*, *68*(2), 365–369. https://doi.org/10.1093/sysbio/syy054

Barberán, A., Bates, S. T., Casamayor, E. O., & Fierer, N. (2012). Using network analysis to explore co-occurrence patterns in soil microbial communities. *The ISME Journal*, *6*(2), Article 2. https://doi.org/10.1038/ismej.2011.119

Barnes, J., & Owens, N. J. P. (1999). Denitrification and Nitrous Oxide Concentrations in the Humber Estuary, UK, and Adjacent Coastal Zones. *Marine Pollution Bulletin*, *37*(3), 247–260. https://doi.org/10.1016/S0025-326X(99)00079-X

Barnes, J., & Upstill-Goddard, R. C. (2018). The denitrification paradox: The role of O2 in sediment N2O production. *Estuarine, Coastal and Shelf Science*, *200*, 270–276. https://doi.org/10.1016/j.ecss.2017.11.018

Battaglia, G., & Joos, F. (2018). Marine N2O Emissions From Nitrification and Denitrification Constrained by Modern Observations and Projected in Multimillennial Global Warming Simulations. *Global Biogeochemical Cycles*, *32*(1), 92–121. https://doi.org/10.1002/2017GB005671

Bauza, J. F., Morell, J. M., & Corredor, J. E. (2002). Biogeochemistry of Nitrous Oxide Production in the Red Mangrove (Rhizophora mangle) Forest Sediments. *Estuarine, Coastal and Shelf Science*, *55*(5), 697–704. https://doi.org/10.1006/ecss.2001.0913

Bayer, B., Hansman, R. L., Bittner, M. J., Noriega-Ortega, B. E., Niggemann, J., Dittmar, T., & Herndl, G. J. (2019). Ammonia-oxidizing archaea release a suite of organic compounds potentially fueling prokaryotic heterotrophy in the ocean. *Environmental Microbiology*, *21*(11), 4062–4075. https://doi.org/10.1111/1462-2920.14755

Bayer, B., Vojvoda, J., Offre, P., Alves, R. J. E., Elisabeth, N. H., Garcia, J. A., Volland, J.-M., Srivastava, A., Schleper, C., & Herndl, G. J. (2016). Physiological and genomic characterization of two novel marine thaumarchaeal strains indicates niche

differentiation. *The ISME Journal*, *10*(5), Article 5. https://doi.org/10.1038/ismej.2015.200

Belley, R., Snelgrove, P. V. R., Archambault, P., & Juniper, S. K. (2016). Environmental Drivers of Benthic Flux Variation and Ecosystem Functioning in Salish Sea and Northeast Pacific Sediments. *PLOS ONE*, *11*(3), e0151110. https://doi.org/10.1371/journal.pone.0151110

Beman, J. M., Bertics, V. J., Braunschweiler, T., & Wilson, J. M. (2012). Quantification of ammonia oxidation rates and the distribution of ammonia-oxidizing Archaea and Bacteria in marine sediment depth profiles from Catalina Island, California. *Frontiers in Microbiology*, *3*, 263. https://doi.org/10.3389/fmicb.2012.00263

Beman, J. M., & Carolan, M. T. (2013). Deoxygenation alters bacterial diversity and community composition in the ocean's largest oxygen minimum zone. *Nature Communications*, *4*(1), 2705. https://doi.org/10.1038/ncomms3705

Bender, M., Martin, W., Hess, J., Sayles, F., Ball, L., & Lambert, C. (1987). A whole-core squeezer for interfacial pore-water sampling1. *Limnology and Oceanography*, *32*(6), 1214–1225. https://doi.org/10.4319/lo.1987.32.6.1214

Berg, P., Risgaard-Petersen, N., & Rysgaard, S. (1998). Interpretation of measured concentration profiles in sediment pore water. *Limnology and Oceanography*, *43*(7), 1500–1510. https://doi.org/10.4319/lo.1998.43.7.1500

Berg, P., Rysgaard, S., Funch, P., & Sejr, M. (2001). Effects of bioturbation on solutes and solids in marine sediments. *Aquatic Microbial Ecology*, *26*, 81–94. https://doi.org/10.3354/ame026081

Berry, D., & Widder, S. (2014). Deciphering microbial interactions and detecting keystone species with co-occurrence networks. *Frontiers in Microbiology*, *5*. https://www.frontiersin.org/article/10.3389/fmicb.2014.00219

Bertagnolli, A. D., Konstantinidis, K. T., & Stewart, F. J. (2020). Non-denitrifier nitrous oxide reductases dominate marine biomes. *Environmental Microbiology Reports*, *12*(6), 681–692. https://doi.org/10.1111/1758-2229.12879

Bertagnolli, A. D., & Stewart, F. J. (2018). Microbial niches in marine oxygen minimum zones. *Nature Reviews Microbiology*, *16*(12), Article 12. https://doi.org/10.1038/s41579-018-0087-z

Bertagnolli, A. D., Treusch, A. H., Mason, O. U., Stingl, U., Vergin, K. L., Chan, F., Beszteri, B., & Giovannoni, S. J. (2011). Bacterial diversity in the bottom boundary layer of the inner continental shelf of Oregon, USA. *Aquatic Microbial Ecology*, *64*(1), 15–25. https://doi.org/10.3354/ame01504

Bianchi, D., Weber, T. S., Kiko, R., & Deutsch, C. (2018). Global niche of marine anaerobic metabolisms expanded by particle microenvironments. *Nature Geoscience*, *11*(4), Article 4. https://doi.org/10.1038/s41561-018-0081-0

Bolyen, E., Rideout, J. R., Dillon, M. R., Bokulich, N. A., Abnet, C. C., Al-Ghalith, G. A., Alexander, H., Alm, E. J., Arumugam, M., Asnicar, F., Bai, Y., Bisanz, J. E., Bittinger, K., Brejnrod, A., Brislawn, C. J., Brown, C. T., Callahan, B. J., Caraballo-Rodríguez, A. M., Chase, J., … Caporaso, J. G. (2019). Reproducible, interactive, scalable and extensible microbiome data science using QIIME 2. *Nature Biotechnology*, *37*(8), Article 8. https://doi.org/10.1038/s41587-019-0209-9

Bonin, P., Gilewicz, M., & Bertrand, J. C. (1989). Effects of oxygen on each step of denitrification on Pseudomonas nautica. *Canadian Journal of Microbiology*, *35*(11), 1061–1064. https://doi.org/10.1139/m89-177

Breitburg, D., Levin, L. A., Oschlies, A., Grégoire, M., Chavez, F. P., Conley, D. J., Garçon, V., Gilbert, D., Gutiérrez, D., Isensee, K., Jacinto, G. S., Limburg, K. E., Montes, I., Naqvi, S. W. A., Pitcher, G. C., Rabalais, N. N., Roman, M. R., Rose, K. A., Seibel, B. A., … Zhang, J. (2018). Declining oxygen in the global ocean and coastal waters. *Science*, *359*(6371), eaam7240. https://doi.org/10.1126/science.aam7240

Bristow, L. A., Dalsgaard, T., Tiano, L., Mills, D. B., Bertagnolli, A. D., Wright, J. J., Hallam, S. J., Ulloa, O., Canfield, D. E., Revsbech, N. P., & Thamdrup, B. (2016). Ammonium and nitrite oxidation at nanomolar oxygen concentrations in oxygen minimum zone waters. *Proceedings of the National Academy of Sciences*, *113*(38), 10601–10606. https://doi.org/10.1073/pnas.1600359113

Callahan, B. J., McMurdie, P. J., Rosen, M. J., Han, A. W., Johnson, A. J. A., & Holmes, S. P. (2016). DADA2: High-resolution sample inference from Illumina amplicon data. *Nature Methods*, *13*(7), Article 7. https://doi.org/10.1038/nmeth.3869

Callbeck, C. M., Canfield, D. E., Kuypers, M. M. M., Yilmaz, P., Lavik, G., Thamdrup, B., Schubert, C. J., & Bristow, L. A. (2021). Sulfur cycling in oceanic oxygen minimum zones. *Limnology and Oceanography*, *66*(6), 2360–2392. https://doi.org/10.1002/lno.11759

Callbeck, C. M., Lavik, G., Ferdelman, T. G., Fuchs, B., Gruber-Vodicka, H. R., Hach, P. F., Littmann, S., Schoffelen, N. J., Kalvelage, T., Thomsen, S., Schunck, H., Löscher, C. R., Schmitz, R. A., & Kuypers, M. M. M. (2018). Oxygen minimum zone cryptic sulfur

cycling sustained by offshore transport of key sulfur oxidizing bacteria. *Nature Communications*, *9*(1), 1729. https://doi.org/10.1038/s41467-018-04041-x

Callbeck, C. M., Pelzer, C., Lavik, G., Ferdelman, T. G., Graf, J. S., Vekeman, B., Schunck, H., Littmann, S., Fuchs, B. M., Hach, P. F., Kalvelage, T., Schmitz, R. A., & Kuypers, M. M. M. (2019). *Arcobacter peruensis* sp. Nov., a Chemolithoheterotroph Isolated from Sulfide- and Organic-Rich Coastal Waters off Peru. *Applied and Environmental Microbiology*, *85*(24), e01344-19. https://doi.org/10.1128/AEM.01344-19

Campbell, M. A., Nyerges, G., Kozlowski, J. A., Poret-Peterson, A. T., Stein, L. Y., & Klotz, M. G. (2011). Model of the molecular basis for hydroxylamine oxidation and nitrous oxide production in methanotrophic bacteria. *FEMS Microbiology Letters*, *322*(1), 82–89. https://doi.org/10.1111/j.1574-6968.2011.02340.x

Canfield, D. E., Stewart, F. J., Thamdrup, B., De Brabandere, L., Dalsgaard, T., Delong, E. F., Revsbech, N. P., & Ulloa, O. (2010). A Cryptic Sulfur Cycle in Oxygen-Minimum–Zone Waters off the Chilean Coast. *Science*, *330*(6009), 1375–1378. https://doi.org/10.1126/science.1196889

Cao, K.-A. L., Rossouw, D., Robert-Granié, C., & Besse, P. (2008). A Sparse PLS for Variable Selection when Integrating Omics Data. *Statistical Applications in Genetics and Molecular Biology*, *7*(1). https://doi.org/10.2202/1544-6115.1390

Capelle, D. W., Hawley, A. K., Hallam, S. J., & Tortell, P. D. (2018). A multi-year time-series of N_2O dynamics in a seasonally anoxic fjord: Saanich Inlet, British Columbia. *Limnology and Oceanography*, *63*(2), 524–539. https://doi.org/10.1002/lno.10645

Capelle, D. W., & Tortell, P. D. (2016). Factors controlling methane and nitrous-oxide variability in the southern British Columbia coastal upwelling system. *Marine Chemistry*, *179*, 56–67. https://doi.org/10.1016/j.marchem.2016.01.011

Caranto, J. D., & Lancaster, K. M. (2017). Nitric oxide is an obligate bacterial nitrification intermediate produced by hydroxylamine oxidoreductase. *Proceedings of the National Academy of Sciences*, *114*(31), 8217–8222. https://doi.org/10.1073/pnas.1704504114

Cardman, Z., Arnosti, C., Durbin, A., Ziervogel, K., Cox, C., Steen, A. D., & Teske, A. (2014). Verrucomicrobia Are Candidates for Polysaccharide-Degrading Bacterioplankton in an Arctic Fjord of Svalbard. *Applied and Environmental Microbiology*, *80*(12), 3749–3756. https://doi.org/10.1128/AEM.00899-14

Cavigelli, M. A., & Robertson, G. P. (2000). The Functional Significance of Denitrifier Community Composition in a Terrestrial Ecosystem. *Ecology*, *81*(5), 1402–1414. https://doi.org/10.1890/0012-9658(2000)081[1402:TFSODC]2.0.CO;2

Christie-Oleza, J. A., Sousoni, D., Lloyd, M., Armengaud, J., & Scanlan, D. J. (2017). Nutrient recycling facilitates long-term stability of marine microbial phototroph–heterotroph interactions. *Nature Microbiology*, *2*(9), Article 9. https://doi.org/10.1038/nmicrobiol.2017.100

Codispoti, L. A. (2010). Interesting Times for Marine N_2O. *Science*, *327*(5971), 1339–1340. https://doi.org/10.1126/science.1184945

Codispoti, L. A., Brandes, J. A., Christensen, J. P., Devol, A. H., Naqvi, S. W. A., Paerl, H. W., & Yoshinari, T. (2001). The oceanic fixed nitrogen and nitrous oxide budgets: Moving targets as we enter the anthropocene? *Scientia Marina*, *65*(S2), Article S2. https://doi.org/10.3989/scimar.2001.65s285

Cohen, Y., & Gordon, L. I. (1979). Nitrous oxide production in the Ocean. *Journal of Geophysical Research: Oceans*, *84*(C1), 347–353. https://doi.org/10.1029/JC084iC01p00347

Comeau, A. M., Li, W. K. W., Tremblay, J.-É., Carmack, E. C., & Lovejoy, C. (2011). Arctic Ocean Microbial Community Structure before and after the 2007 Record Sea Ice Minimum. *PLOS ONE*, *6*(11), e27492. https://doi.org/10.1371/journal.pone.0027492

Conrad, R. (1996). Soil microorganisms as controllers of atmospheric trace gases (H_2, CO, CH_4, OCS, N_2O, and NO). *Microbiological Reviews*, *60*(4), 609–640. https://doi.org/10.1128/mr.60.4.609-640.1996

Cordero, O. X., & Polz, M. F. (2014). Explaining microbial genomic diversity in light of evolutionary ecology. *Nature Reviews Microbiology*, *12*(4), Article 4. https://doi.org/10.1038/nrmicro3218

Crawford, W. R., & Peña, M. A. (2013). Declining Oxygen on the British Columbia Continental Shelf. *Atmosphere-Ocean*, *51*(1), 88–103. https://doi.org/10.1080/07055900.2012.753028

Crump, B. C., Armbrust, E. V., & Baross, J. A. (1999). Phylogenetic Analysis of Particle-Attached and Free-Living Bacterial Communities in the Columbia River, Its Estuary, and the Adjacent Coastal Ocean. *Applied and Environmental Microbiology*, *65*(7), 3192–3204. https://doi.org/10.1128/AEM.65.7.3192-3204.1999

Czech, L., & Stamatakis, A. (2019). Scalable methods for analyzing and visualizing phylogenetic placement of metagenomic samples. *PLOS ONE*, *14*(5), e0217050. https://doi.org/10.1371/journal.pone.0217050

Dalsgaard, T., Underwood, J. C., Nedwell, D. B., Sundbäck, K., Rysgaard, S., Miles, A., Bartoli, M., Dong, L., Thornton, D. C. O., Ottosen, L. D. M., & Risgaard-Petersen, N. (2000).

Protocol handbook for NICE - Nitrogen Cycling in Estuaries: a project under the EU research programme: Marine Science and Technology (MAST III). *In* L. P. Nielsen, and others (eds.), National Environmental Research Institute, Silkeborg, Denmark.

Damgaard, L. R., Kelly, C., Casciotti, K., Ward, B. B., & Revsbech, N. P. (2020). Amperometric sensor for nanomolar nitrous oxide analysis. *Analytica Chimica Acta*, *1101*, 135–140. https://doi.org/10.1016/j.aca.2019.12.019

de Voogd, N. J., Cleary, D. F. R., Polónia, A. R. M., & Gomes, N. C. M. (2015). Bacterial community composition and predicted functional ecology of sponges, sediment and seawater from the thousand islands reef complex, West Java, Indonesia. *FEMS Microbiology Ecology*, *91*(4), fiv019. https://doi.org/10.1093/femsec/fiv019

Devol, A. H. (2008). Denitrification Including Anammox. *In* D. G. Capone, D. A. Bronk, M. R. Mulholland, & E. J. Carpenter (Eds.), *Nitrogen in the Marine Environment (Second Edition)* (pp. 263–301). Academic Press. https://doi.org/10.1016/B978-0-12-372522-6.00006-2

Devol, A. H. (2015). Denitrification, Anammox, and N_2 Production in Marine Sediments. *Annual Review of Marine Science*, *7*(1), 403–423. https://doi.org/10.1146/annurev-marine-010213-135040

Devol, A. H., & Christensen, J. P. (1993). Benthic fluxes and nitrogen cycling in sediments of the continental margin of the eastern North Pacific. *Journal of Marine Research*, *51*(2), 345–372. https://doi.org/10.1357/0022240933223765

Dixon, P. (2003). VEGAN, a package of R functions for community ecology. *Journal of Vegetation Science*, *14*(6), 927–930. https://doi.org/10.1111/j.1654-1103.2003.tb02228.x

Douglas, G. M., Maffei, V. J., Zaneveld, J. R., Yurgel, S. N., Brown, J. R., Taylor, C. M., Huttenhower, C., & Langille, M. G. I. (2020). PICRUSt2 for prediction of metagenome functions. *Nature Biotechnology*, *38*(6), Article 6. https://doi.org/10.1038/s41587-020-0548-6

Drescher, K., Nadell, C. D., Stone, H. A., Wingreen, N. S., & Bassler, B. L. (2014). Solutions to the public goods dilemma in bacterial biofilms. *Current Biology: CB*, *24*(1), 50–55. https://doi.org/10.1016/j.cub.2013.10.030

Dlugokencky, E.J., Crotwell, A.M. Mund, J.W. Crotwell, M.J. & Thoning, K.W. (2020). Atmospheric Nitrous Oxide Dry Air Mole Fractions from the NOAA GML Carbon Cycle Cooperative Global Air Sampling Network, 1997-2019, Version: 2020-07, https://doi.org/10.15138/53g1-x417

Edgar, R. C. (2010). Search and clustering orders of magnitude faster than BLAST. *Bioinformatics*, *26*(19), 2460–2461. https://doi.org/10.1093/bioinformatics/btq461

Edgar, R. C. (2016). UNOISE2: Improved error-correction for Illumina 16S and ITS amplicon sequencing. Preprint at bioRxiv. https://doi.org/10.1101/081257

Emerson, S., Cranston, R. E., & Liss, P. S. (1979). Redox species in a reducing fjord: Equilibrium and kinetic considerations. *Deep Sea Research Part A. Oceanographic Research Papers*, *26*(8), 859–878. https://doi.org/10.1016/0198-0149(79)90101-8

Falkowski, P. G., Fenchel, T., & Delong, E. F. (2008). The Microbial Engines That Drive Earth's Biogeochemical Cycles. *Science*, *320*(5879), 1034–1039. https://doi.org/10.1126/science.1153213

Fenwick, L., & Tortell, P. D. (2018). Methane and nitrous oxide distributions in coastal and open ocean waters of the Northeast Subarctic Pacific during 2015–2016. *Marine Chemistry*, *200*, 45–56. https://doi.org/10.1016/j.marchem.2018.01.008

Fernandes, S. O., Bonin, P. C., Michotey, V. D., Garcia, N., & LokaBharathi, P. A. (2012). Nitrogen-limited mangrove ecosystems conserve N through dissimilatory nitrate reduction to ammonium. *Scientific Reports*, *2*(1), Article 1. https://doi.org/10.1038/srep00419

Fernández-Gómez, B., Richter, M., Schüler, M., Pinhassi, J., Acinas, S. G., González, J. M., & Pedrós-Alió, C. (2013). Ecology of marine Bacteroidetes: A comparative genomics approach. *The ISME Journal*, *7*(5), 1026–1037. https://doi.org/10.1038/ismej.2012.169

Foster, S. Q., & Fulweiler, R. W. (2016). Sediment Nitrous Oxide Fluxes Are Dominated by Uptake in a Temperate Estuary. *Frontiers in Marine Science*, *3*. https://www.frontiersin.org/articles/10.3389/fmars.2016.00040

Frame, C. H., & Casciotti, K. L. (2010). Biogeochemical controls and isotopic signatures of nitrous oxide production by a marine ammonia-oxidizing bacterium. *Biogeosciences*, *7*(9), 2695–2709. https://doi.org/10.5194/bg-7-2695-2010

Freing, A., Wallace, D. W. R., & Bange, H. W. (2012). Global oceanic production of nitrous oxide. *Philosophical Transactions of the Royal Society B: Biological Sciences*, *367*(1593), 1245–1255. https://doi.org/10.1098/rstb.2011.0360

Fuhrman, J. A. (2009). Microbial community structure and its functional implications. *Nature*, *459*(7244), Article 7244. https://doi.org/10.1038/nature08058

Garcia, H. E., & Gordon, L. I. (1992). Oxygen solubility in seawater: Better fitting equations. *Limnology and Oceanography*, *37*(6), 1307–1312. https://doi.org/10.4319/lo.1992.37.6.1307

Garcia, H. E., & Gordon, L. I. (1993). Erratum: Oxygen solubility in seawater: Better fitting equations. *Limnology and Oceanography*, *38:* 656.

Gargett, A. E., Stucchi, D., & Whitney, F. (2003). Physical processes associated with high primary production in Saanich Inlet, British Columbia. *Estuarine, Coastal and Shelf Science*, *56*(5), 1141–1156. https://doi.org/10.1016/S0272-7714(02)00319-0

Giovannoni, S. J. (2017). SAR11 Bacteria: The Most Abundant Plankton in the Oceans. *Annual Review of Marine Science*, *9*(1), 231–255. https://doi.org/10.1146/annurev-marine-010814-015934

Gloor, G. B., Macklaim, J. M., Pawlowsky-Glahn, V., & Egozcue, J. J. (2017). Microbiome Datasets Are Compositional: And This Is Not Optional. *Frontiers in Microbiology*, *8*. https://www.frontiersin.org/article/10.3389/fmicb.2017.02224

Goldford, J. E., Lu, N., Bajić, D., Estrela, S., Tikhonov, M., Sanchez-Gorostiaga, A., Segrè, D., Mehta, P., & Sanchez, A. (2018). Emergent simplicity in microbial community assembly. *Science (New York, N.Y.)*, *361*(6401), 469–474. https://doi.org/10.1126/science.aat1168

Graf, D. R. H., Jones, C. M., & Hallin, S. (2014). Intergenomic Comparisons Highlight Modularity of the Denitrification Pathway and Underpin the Importance of Community Structure for N2O Emissions. *PLOS ONE*, *9*(12), e114118. https://doi.org/10.1371/journal.pone.0114118

Graham, E. B., Knelman, J. E., Schindlbacher, A., Siciliano, S., Breulmann, M., Yannarell, A., Beman, J. M., Abell, G., Philippot, L., Prosser, J., Foulquier, A., Yuste, J. C., Glanville,

H. C., Jones, D. L., Angel, R., Salminen, J., Newton, R. J., Bürgmann, H., Ingram, L. J., … Nemergut, D. R. (2016). Microbes as Engines of Ecosystem Function: When Does Community Structure Enhance Predictions of Ecosystem Processes? *Frontiers in Microbiology*, *7*. https://www.frontiersin.org/articles/10.3389/fmicb.2016.00214

Grantham, B. A., Chan, F., Nielsen, K. J., Fox, D. S., Barth, J. A., Huyer, A., Lubchenco, J., & Menge, B. A. (2004). Upwelling-driven nearshore hypoxia signals ecosystem and oceanographic changes in the northeast Pacific. *Nature*, *429*(6993), 749–754. https://doi.org/10.1038/nature02605

Grundle, D. S., Löscher, C. R., Krahmann, G., Altabet, M. A., Bange, H. W., Karstensen, J., Körtzinger, A., & Fiedler, B. (2017). Low oxygen eddies in the eastern tropical North Atlantic: Implications for N 2 O cycling. *Scientific Reports*, *7*(1), 4806. https://doi.org/10.1038/s41598-017-04745-y

Grundle, D. S., Maranger, R., & Juniper, S. K. (2012). Upper Water Column Nitrous Oxide Distributions in the Northeast Subarctic Pacific Ocean. *Atmosphere-Ocean*, *50*(4), 475–486. https://doi.org/10.1080/07055900.2012.727779

Grundle, D. S., Timothy, D. A., & Varela, D. E. (2009). Variations of phytoplankton productivity and biomass over an annual cycle in Saanich Inlet, a British Columbia fjord. *Continental Shelf Research*, *29*(19), 2257–2269. https://doi.org/10.1016/j.csr.2009.08.013

Guidi, L., Chaffron, S., Bittner, L., Eveillard, D., Larhlimi, A., Roux, S., Darzi, Y., Audic, S., Berline, L., Brum, J. R., Coelho, L. P., Espinoza, J. C. I., Malviya, S., Sunagawa, S., Dimier, C., Kandels-Lewis, S., Picheral, M., Poulain, J., Searson, S., … Gorsky, G. (2016). Plankton networks driving carbon export in the oligotrophic ocean. *Nature*, *532*(7600), 465–470. https://doi.org/10.1038/nature16942

Hatzenpichler, R. (2012). Diversity, Physiology, and Niche Differentiation of Ammonia-Oxidizing Archaea. *Applied and Environmental Microbiology*, *78*(21), 7501–7510. https://doi.org/10.1128/AEM.01960-12

Hatzenpichler, R., Krukenberg, V., Spietz, R. L., & Jay, Z. J. (2020). Next-generation physiology approaches to study microbiome function at single cell level. *Nature Reviews Microbiology*, *18*(4), Article 4. https://doi.org/10.1038/s41579-020-0323-1

Hawley, A. K., Brewer, H. M., Norbeck, A. D., Paša-Tolić, L., & Hallam, S. J. (2014). Metaproteomics reveals differential modes of metabolic coupling among ubiquitous oxygen minimum zone microbes. *Proceedings of the National Academy of Sciences*, *111*(31), 11395–11400. https://doi.org/10.1073/pnas.1322132111

Hawley, A. K., Nobu, M. K., Wright, J. J., Durno, W. E., Morgan-Lang, C., Sage, B., Schwientek, P., Swan, B. K., Rinke, C., Torres-Beltrán, M., Mewis, K., Liu, W.-T., Stepanauskas, R., Woyke, T., & Hallam, S. J. (2017). Diverse Marinimicrobia bacteria may mediate coupled biogeochemical cycles along eco-thermodynamic gradients. *Nature Communications*, *8*(1), 1507. https://doi.org/10.1038/s41467-017-01376-9

Heijden, M. G. A. van der, & Hartmann, M. (2016). Networking in the Plant Microbiome. *PLOS Biology*, *14*(2), e1002378. https://doi.org/10.1371/journal.pbio.1002378

Herren, C. M., & McMahon, K. D. (2018). Keystone taxa predict compositional change in microbial communities. *Environmental Microbiology*, *20*(6), 2207–2217. https://doi.org/10.1111/1462-2920.14257

Hink, L., Lycus, P., Gubry-Rangin, C., Frostegård, Å., Nicol, G. W., Prosser, J. I., & Bakken, L. R. (2017). Kinetics of NH3-oxidation, NO-turnover, N2O-production and electron flow during oxygen depletion in model bacterial and archaeal ammonia oxidisers.

Environmental Microbiology, *19*(12), 4882–4896. https://doi.org/10.1111/1462-2920.13914

Hu, J., Liu, S., Yang, W., He, Z., Wang, J., Liu, H., Zheng, P., Xi, C., Ma, F., & Hu, B. (2019). Ecological Success of the Nitrosopumilus and Nitrosospira Clusters in the Intertidal Zone. *Microbial Ecology*, *78*(3), 555–564. https://doi.org/10.1007/s00248-019-01359-x

Huber, J. A., Butterfield, D. A., & Baross, J. A. (2002). Temporal Changes in Archaeal Diversity and Chemistry in a Mid-Ocean Ridge Subseafloor Habitat. *Applied and Environmental Microbiology*, *68*(4), 1585–1594. https://doi.org/10.1128/AEM.68.4.1585-1594.2002

Huettel, M., Berg, P., & Kostka, J. E. (2014). Benthic Exchange and Biogeochemical Cycling in Permeable Sediments. *Annual Review of Marine Science*, *6*(1), 23–51. https://doi.org/10.1146/annurev-marine-051413-012706

IPCC. (2021). Global Carbon and other Biogeochemical Cycles and Feedbacks. *In* Masson-Delmotte, V., P. Zhai, A. Pirani, S.L. Connors, C. Péan, S. Berger, N. Caud, Y. Chen, L. Goldfarb, M.I. Gomis, M. Huang, K. Leitzell, E. Lonnoy, J.B.R. Matthews, T.K. Maycock, T. Waterfield, O. Yelekçi, R. Yu, and B. Zhou (eds.)*, Climate Change 2021: The Physical Science Basis. Contribution of Working Group I to the Sixth Assessment Report of the Intergovernmental Panel on Climate Change.* Cambridge University Press, Cambridge, United Kingdom and New York, NY, USA, pp*. 673−816.* doi:10.1017/9781009157896.007.

Jain, A. K., Briegleb, B. P., Minschwaner, K., & Wuebbles, D. J. (2000). Radiative forcings and global warming potentials of 39 greenhouse gases. *Journal of Geophysical Research: Atmospheres*, *105*(D16), 20773–20790. https://doi.org/10.1029/2000JD900241

Jameson, B. D., Berg, P., Grundle, D. S., Stevens, C. J., & Juniper, S. K. (2021). Continental margin sediments underlying the NE Pacific oxygen minimum zone are a source of nitrous oxide to the water column. *Limnology and Oceanography Letters*, *6*(2), 68–76. https://doi.org/10.1002/lol2.10174

Jameson, B. D., Murdock, S. A., Ji, Q., Stevens, C. J., Grundle, D. S., & Kim Juniper, S. (2023). Network analysis of 16S rRNA sequences suggests microbial keystone taxa contribute to marine N2O cycling. *Communications Biology*, *6*(1), Article 1. https://doi.org/10.1038/s42003-023-04597-5

Jensen, H. B., Jørgensen, K. S., & Sørensen, J. (1984). Diurnal variation of nitrogen cycling in coastal, marine sediments. *Marine Biology*, *83*(2), 177–183. https://doi.org/10.1007/BF00394726

Ji, Q., Babbin, A. R., Jayakumar, A., Oleynik, S., & Ward, B. B. (2015). Nitrous oxide production by nitrification and denitrification in the Eastern Tropical South Pacific oxygen minimum zone. *Geophysical Research Letters*, *42*(24), 10,755-10,764. https://doi.org/10.1002/2015GL066853

Ji, Q., Buitenhuis, E., Suntharalingam, P., Sarmiento, J. L., & Ward, B. B. (2018). Global Nitrous Oxide Production Determined by Oxygen Sensitivity of Nitrification and Denitrification. *Global Biogeochemical Cycles*, *32*(12), 1790–1802. https://doi.org/10.1029/2018GB005887

Ji, Q., Jameson, B. D., Juniper, S. K., & Grundle, D. S. (2020). Temporal and Vertical Oxygen Gradients Modulate Nitrous Oxide Production in a Seasonally Anoxic Fjord: Saanich Inlet, British Columbia. *Journal of Geophysical Research: Biogeosciences*, *125*(9), e2020JG005631. https://doi.org/10.1029/2020JG005631

Ji, Q., & Ward, B. B. (2017). Nitrous oxide production in surface waters of the mid-latitude North Atlantic Ocean. *Journal of Geophysical Research: Oceans*, *122*(3), 2612–2621. https://doi.org/10.1002/2016JC012467

Jing, X., Gou, H., Gong, Y., Su, X., Xu, L., Ji, Y., Song, Y., Thompson, I. P., Xu, J., & Huang, W. E. (2018). Raman-activated cell sorting and metagenomic sequencing revealing carbon-fixing bacteria in the ocean. *Environmental Microbiology*, *20*(6), 2241–2255. https://doi.org/10.1111/1462-2920.14268

Johnson, J. S., Spakowicz, D. J., Hong, B.-Y., Petersen, L. M., Demkowicz, P., Chen, L., Leopold, S. R., Hanson, B. M., Agresta, H. O., Gerstein, M., Sodergren, E., & Weinstock, G. M. (2019). Evaluation of 16S rRNA gene sequencing for species and strain-level microbiome analysis. *Nature Communications*, *10*(1), Article 1. https://doi.org/10.1038/s41467-019-13036-1

Jones, C. M., Graf, D. R., Bru, D., Philippot, L., & Hallin, S. (2013). The unaccounted yet abundant nitrous oxide-reducing microbial community: A potential nitrous oxide sink. *The ISME Journal*, *7*(2), 417–426. https://doi.org/10.1038/ismej.2012.125

Jones, C. M., Spor, A., Brennan, F. P., Breuil, M.-C., Bru, D., Lemanceau, P., Griffiths, B., Hallin, S., & Philippot, L. (2014). Recently identified microbial guild mediates soil N2O sink capacity. *Nature Climate Change*, *4*(9), Article 9. https://doi.org/10.1038/nclimate2301

Jung, M.-Y., Sedlacek, C. J., Kits, K. D., Mueller, A. J., Rhee, S.-K., Hink, L., Nicol, G. W., Bayer, B., Lehtovirta-Morley, L., Wright, C., de la Torre, J. R., Herbold, C. W., Pjevac, P., Daims, H., & Wagner, M. (2022). Ammonia-oxidizing archaea possess a wide range

of cellular ammonia affinities. *The ISME Journal*, *16*(1), Article 1. https://doi.org/10.1038/s41396-021-01064-z

Jung, M.-Y., Well, R., Min, D., Giesemann, A., Park, S.-J., Kim, J.-G., Kim, S.-J., & Rhee, S.-K. (2014). Isotopic signatures of N_2O produced by ammonia-oxidizing archaea from soils. *The ISME Journal*, *8*(5), Article 5. https://doi.org/10.1038/ismej.2013.205

Kalvelage, T., Lavik, G., Lam, P., Contreras, S., Arteaga, L., Löscher, C. R., Oschlies, A., Paulmier, A., Stramma, L., & Kuypers, M. M. M. (2013). Nitrogen cycling driven by organic matter export in the South Pacific oxygen minimum zone. *Nature Geoscience*, *6*(3), Article 3. https://doi.org/10.1038/ngeo1739

Knowles, R. (1982). Denitrification. *Microbiological Reviews*, *46*(1), 43–70. https://doi.org/10.1128/mr.46.1.43-70.1982

Könneke, M., Bernhard, A. E., de la Torre, J. R., Walker, C. B., Waterbury, J. B., & Stahl, D. A. (2005). Isolation of an autotrophic ammonia-oxidizing marine archaeon. *Nature*, *437*(7058), Article 7058. https://doi.org/10.1038/nature03911

Kozlowski, J. A., Kits, K. D., & Stein, L. Y. (2016a). Comparison of Nitrogen Oxide Metabolism among Diverse Ammonia-Oxidizing Bacteria. *Frontiers in Microbiology*, *7*. https://doi.org/10.3389/fmicb.2016.01090

Kozlowski, J. A., Stieglmeier, M., Schleper, C., Klotz, M. G., & Stein, L. Y. (2016b). Pathways and key intermediates required for obligate aerobic ammonia-dependent chemolithotrophy in bacteria and Thaumarchaeota. *The ISME Journal*, *10*(8), 1836–1845. https://doi.org/10.1038/ismej.2016.2

Kraft, B., Jehmlich, N., Larsen, M., Bristow, L. A., Könneke, M., Thamdrup, B., & Canfield, D. E. (2022). Oxygen and nitrogen production by an ammonia-oxidizing archaeon. *Science*, *375*(6576), 97–100. https://doi.org/10.1126/science.abe6733

Kreuzwieser, J., Buchholz, J., & Rennenberg, H. (2003). Emission of Methane and Nitrous Oxide by Australian Mangrove Ecosystems. *Plant Biology*, *5*(4), 423–431. https://doi.org/10.1055/s-2003-42712

Labrenz, M., Sintes, E., Toetzke, F., Zumsteg, A., Herndl, G. J., Seidler, M., & Jürgens, K. (2010). Relevance of a crenarchaeotal subcluster related to Candidatus *Nitrosopumilus maritimus* to ammonia oxidation in the suboxic zone of the central Baltic Sea. *The ISME Journal*, *4*(12), Article 12. https://doi.org/10.1038/ismej.2010.78

Lam, P., Lavik, G., Jensen, M. M., Vossenberg, J. van de, Schmid, M., Woebken, D., Gutiérrez, D., Amann, R., Jetten, M. S. M., & Kuypers, M. M. M. (2009). Revising the nitrogen cycle in the Peruvian oxygen minimum zone. *Proceedings of the National Academy of Sciences*, *106*(12), 4752–4757. https://doi.org/10.1073/pnas.0812444106

Landolfi, A., Somes, C. J., Koeve, W., Zamora, L. M., & Oschlies, A. (2017). Oceanic nitrogen cycling and N_2O flux perturbations in the Anthropocene. *Global Biogeochemical Cycles*, *31*(8), 1236–1255. https://doi.org/10.1002/2017GB005633

Langfelder, P., & Horvath, S. (2008). WGCNA: An R package for weighted correlation network analysis. *BMC Bioinformatics*, *9*, 559. https://doi.org/10.1186/1471-2105-9-559

Langille, M. G. I., Zaneveld, J., Caporaso, J. G., McDonald, D., Knights, D., Reyes, J. A., Clemente, J. C., Burkepile, D. E., Vega Thurber, R. L., Knight, R., Beiko, R. G., & Huttenhower, C. (2013). Predictive functional profiling of microbial communities using

16S rRNA marker gene sequences. *Nature Biotechnology*, *31*(9), Article 9. https://doi.org/10.1038/nbt.2676

Langlois, V. S., Allison, M. J., Bergman, L. C., To, T. A., & Helbing, C. C. (2021). The need for robust qPCR-based eDNA detection assays in environmental monitoring and species inventories. *Environmental DNA*, *3*(3), 519–527. https://doi.org/10.1002/edn3.164

Lavik, G., Stührmann, T., Brüchert, V., Van der Plas, A., Mohrholz, V., Lam, P., Mußmann, M., Fuchs, B. M., Amann, R., Lass, U., & Kuypers, M. M. M. (2009). Detoxification of sulphidic African shelf waters by blooming chemolithotrophs. *Nature*, *457*(7229), Article 7229. https://doi.org/10.1038/nature07588

Leão, P. N., Ramos, V., Vale, M., Machado, J. P., & Vasconcelos, V. M. (2012). Microbial Community Changes Elicited by Exposure to Cyanobacterial Allelochemicals. *Microbial Ecology*, *63*(1), 85–95. https://doi.org/10.1007/s00248-011-9939-z

Lee, K. S., Palatinszky, M., Pereira, F. C., Nguyen, J., Fernandez, V. I., Mueller, A. J., Menolascina, F., Daims, H., Berry, D., Wagner, M., & Stocker, R. (2019). An automated Raman-based platform for the sorting of live cells by functional properties. *Nature Microbiology*, *4*(6), 1035–1048. https://doi.org/10.1038/s41564-019-0394-9

Li, F., Chen, L., Zhang, J., Yin, J., & Huang, S. (2017). Bacterial Community Structure after Long-term Organic and Inorganic Fertilization Reveals Important Associations between Soil Nutrients and Specific Taxa Involved in Nutrient Transformations. *Frontiers in Microbiology*, *8*. https://www.frontiersin.org/article/10.3389/fmicb.2017.00187

Li, M., Canniffe, D. P., Jackson, P. J., Davison, P. A., FitzGerald, S., Dickman, M. J., Burgess, J. G., Hunter, C. N., & Huang, W. E. (2012). Rapid resonance Raman microspectroscopy to

probe carbon dioxide fixation by single cells in microbial communities. *The ISME Journal*, *6*(4), Article 4. https://doi.org/10.1038/ismej.2011.150

Li, M., Xu, J., Romero-Gonzalez, M., Banwart, S. A., & Huang, W. E. (2012). Single cell Raman spectroscopy for cell sorting and imaging. *Current Opinion in Biotechnology*, *23*(1), 56–63. https://doi.org/10.1016/j.copbio.2011.11.019

Löscher, C. R., Kock, A., Könneke, M., LaRoche, J., Bange, H. W., & Schmitz, R. A. (2012). Production of oceanic nitrous oxide by ammonia-oxidizing archaea. *Biogeosciences*, *9*(7), 2419–2429. https://doi.org/10.5194/bg-9-2419-2012

Louca, S., & Doebeli, M. (2018). Efficient comparative phylogenetics on large trees. *Bioinformatics*, *34*(6), 1053–1055. https://doi.org/10.1093/bioinformatics/btx701

Louca, S., Hawley, A. K., Katsev, S., Torres-Beltran, M., Bhatia, M. P., Kheirandish, S., Michiels, C. C., Capelle, D., Lavik, G., Doebeli, M., Crowe, S. A., & Hallam, S. J. (2016a). Integrating biogeochemistry with multiomic sequence information in a model oxygen minimum zone. *Proceedings of the National Academy of Sciences*, *113*(40), E5925–E5933. https://doi.org/10.1073/pnas.1602897113

Louca, S., Jacques, S. M. S., Pires, A. P. F., Leal, J. S., Srivastava, D. S., Parfrey, L. W., Farjalla, V. F., & Doebeli, M. (2016b). High taxonomic variability despite stable functional structure across microbial communities. *Nature Ecology & Evolution*, *1*(1), Article 1. https://doi.org/10.1038/s41559-016-0015

Louca, S., Parfrey, L. W., & Doebeli, M. (2016c). Decoupling function and taxonomy in the global ocean microbiome. *Science*, *353*(6305), 1272–1277. https://doi.org/10.1126/science.aaf4507

Louca, S., Polz, M. F., Mazel, F., Albright, M. B. N., Huber, J. A., O'Connor, M. I., Ackermann, M., Hahn, A. S., Srivastava, D. S., Crowe, S. A., Doebeli, M., & Parfrey, L. W. (2018). Function and functional redundancy in microbial systems. *Nature Ecology & Evolution*, *2*(6), Article 6. https://doi.org/10.1038/s41559-018-0519-1

Lu, Y., Xia, X., Cheung, S., Jing, H., & Liu, H. (2019). Differential Distribution and Determinants of Ammonia Oxidizing Archaea Sublineages in the Oxygen Minimum Zone off Costa Rica. *Microorganisms*, *7*(10), Article 10. https://doi.org/10.3390/microorganisms7100453

MacLean, C. R., Dickson, A., & Bell, G. (2005). Resource competition and adaptive radiation in a microbial microcosm. *Ecology Letters*, *8*(1), 38–46. https://doi.org/10.1111/j.1461-0248.2004.00689.x

Maher, D. T., Sippo, J. Z., Tait, D. R., Holloway, C., & Santos, I. R. (2016). Pristine mangrove creek waters are a sink of nitrous oxide. *Scientific Reports*, *6*(1), Article 1. https://doi.org/10.1038/srep25701

Martens-Habbena, W., Qin, W., Horak, R. E. A., Urakawa, H., Schauer, A. J., Moffett, J. W., Armbrust, E. V., Ingalls, A. E., Devol, A. H., & Stahl, D. A. (2015). The production of nitric oxide by marine ammonia-oxidizing archaea and inhibition of archaeal ammonia oxidation by a nitric oxide scavenger. *Environmental Microbiology*, *17*(7), 2261–2274. https://doi.org/10.1111/1462-2920.12677

Martin, M. (2011). Cutadapt removes adapter sequences from high-throughput sequencing reads. *EMBnet.Journal*, *17*(1), Article 1. https://doi.org/10.14806/ej.17.1.200

Martinez-Rey, J., Bopp, L., Gehlen, M., Tagliabue, A., & Gruber, N. (2015). Projections of oceanic N₂O emissions in the 21st century using the IPSL Earth

system model. *Biogeosciences*, *12*(13), 4133–4148. https://doi.org/10.5194/bg-12-4133-2015

Meyer, A. C. S., Cullen, J. T., & Grundle, D. S. (2022). Nitrous Oxide Distributions in the Oxygenated Water Column of the Sargasso Sea. *Atmosphere-Ocean*, *0*(0), 1–13. https://doi.org/10.1080/07055900.2022.2153325

Meyer, R. L., Allen, D. E., & Schmidt, S. (2008). Nitrification and denitrification as sources of sediment nitrous oxide production: A microsensor approach. *Marine Chemistry*, *110*(1), 68–76. https://doi.org/10.1016/j.marchem.2008.02.004

Michiels, C. C., Huggins, J. A., Giesbrecht, K. E., Spence, J. S., Simister, R. L., Varela, D. E., Hallam, S. J., & Crowe, S. A. (2019). Rates and Pathways of N2 Production in a Persistently Anoxic Fjord: Saanich Inlet, British Columbia. *Frontiers in Marine Science*, *0*. https://doi.org/10.3389/fmars.2019.00027

Middelburg, J. J., Klaver, G., Nieuwenhuize, J., Markusse, R. M., Vlug, T., & van der Nat, F. J. W. A. (1995). Nitrous oxide emissions from estuarine intertidal sediments. *Hydrobiologia*, *311*(1), 43–55. https://doi.org/10.1007/BF00008570

Mincer, T. J., Church, M. J., Taylor, L. T., Preston, C., Karl, D. M., & DeLong, E. F. (2007). Quantitative distribution of presumptive archaeal and bacterial nitrifiers in Monterey Bay and the North Pacific Subtropical Gyre. *Environmental Microbiology*, *9*(5), 1162–1175. https://doi.org/10.1111/j.1462-2920.2007.01239.x

Muck, S., De Corte, D., Clifford, E. L., Bayer, B., Herndl, G. J., & Sintes, E. (2019). Niche Differentiation of Aerobic and Anaerobic Ammonia Oxidizers in a High Latitude Deep Oxygen Minimum Zone. *Frontiers in Microbiology*, *10*, 2141. https://doi.org/10.3389/fmicb.2019.02141

Müller, O., Wilson, B., Paulsen, M. L., Rumińska, A., Armo, H. R., Bratbak, G., & Øvreås, L. (2018). Spatiotemporal Dynamics of Ammonia-Oxidizing Thaumarchaeota in Distinct Arctic Water Masses. *Frontiers in Microbiology*, *9*. https://www.frontiersin.org/articles/10.3389/fmicb.2018.00024

Muñoz-Hincapié, M., Morell, J. M., & Corredor, J. E. (2002). Increase of nitrous oxide flux to the atmosphere upon nitrogen addition to red mangroves sediments. *Marine Pollution Bulletin*, *44*(10), 992–996. https://doi.org/10.1016/S0025-326X(02)00132-7

Murdock, S. A., Tunnicliffe, V., Boschen-Rose, R. E., & Juniper, S. K. (2021). Emergent "core communities" of microbes, meiofauna and macrofauna at hydrothermal vents. *ISME Communications*, *1*(1), Article 1. https://doi.org/10.1038/s43705-021-00031-1

Murillo, A. A., Ramírez-Flandes, S., DeLong, E. F., & Ulloa, O. (2014). Enhanced metabolic versatility of planktonic sulfur-oxidizing γ-proteobacteria in an oxygen-deficient coastal ecosystem. *Frontiers in Marine Science*, *1*. https://www.frontiersin.org/article/10.3389/fmars.2014.00018

Murray, R. H., Erler, D. V., & Eyre, B. D. (2015). Nitrous oxide fluxes in estuarine environments: Response to global change. *Global Change Biology*, *21*(9), 3219–3245. https://doi.org/10.1111/gcb.12923

Nevison, C., Butler, J. H., & Elkins, J. W. (2003). Global distribution of N2O and the ΔN2O-AOU yield in the subsurface ocean. *Global Biogeochemical Cycles*, *17*(4). https://doi.org/10.1029/2003GB002068

Nielsen, M., Gieseke, A., Beer, D. de, & Revsbech, N. P. (2009). Nitrate, nitrite, and nitrous oxide transformations in sediments along a salinity gradient in the Weser Estuary. *Aquatic Microbial Ecology*, *55*(1), 39–52. https://doi.org/10.3354/ame01275

ONC. 2020. Folger Passage - Folger Deep dissolved oxygen data. Oceans Networks Canada, University of Victoria, Canada, [accessed 2020 June 30]. Available from https://www.oceannetworks.ca/observatories/pacific/folgerpassage#SOO-FP

Orellana, L. H., Francis, T. B., Ferraro, M., Hehemann, J.-H., Fuchs, B. M., & Amann, R. I. (2022). Verrucomicrobiota are specialist consumers of sulfated methyl pentoses during diatom blooms. *The ISME Journal*, *16*(3), Article 3. https://doi.org/10.1038/s41396-021-01105-7

Orellana, L. H., Rodriguez-R, L. M., Higgins, S., Chee-Sanford, J. C., Sanford, R. A., Ritalahti, K. M., Löffler, F. E., & Konstantinidis, K. T. (2014). Detecting Nitrous Oxide Reductase (nosZ) Genes in Soil Metagenomes: Method Development and Implications for the Nitrogen Cycle. *MBio*, *5*(3), e01193-14. https://doi.org/10.1128/mBio.01193-14

Otte, S., Kuenen, J. G., Nielsen, L. P., Paerl, H. W., Zopfi, J., Schulz, H. N., Teske, A., Strotmann, B., Gallardo, V. A., & Jørgensen, B. B. (1999). Nitrogen, Carbon, and Sulfur Metabolism in NaturalThioploca Samples. *Applied and Environmental Microbiology*, *65*(7), 3148–3157. https://doi.org/10.1128/AEM.65.7.3148-3157.1999

Palarea-Albaladejo, J., & Martín-Fernández, J. A. (2015). zCompositions—R package for multivariate imputation of left-censored data under a compositional approach. *Chemometrics and Intelligent Laboratory Systems*, *143*, 85–96. https://doi.org/10.1016/j.chemolab.2015.02.019

Parada, A. E., & Fuhrman, J. A. (2017). Marine archaeal dynamics and interactions with the microbial community over 5 years from surface to seafloor. *The ISME Journal*, *11*(11), Article 11. https://doi.org/10.1038/ismej.2017.104

Paulmier, A., & Ruiz-Pino, D. (2009). Oxygen minimum zones (OMZs) in the modern ocean. *Progress in Oceanography*, *80*(3), 113–128. https://doi.org/10.1016/j.pocean.2008.08.001

Peng, X., Fuchsman, C. A., Jayakumar, A., Oleynik, S., Martens-Habbena, W., Devol, A. H., & Ward, B. B. (2015). Ammonia and nitrite oxidation in the Eastern Tropical North Pacific. *Global Biogeochemical Cycles*, *29*(12), 2034–2049. https://doi.org/10.1002/2015GB005278

Pereira, O., Hochart, C., Auguet, J. C., Debroas, D., & Galand, P. E. (2019). Genomic ecology of Marine Group II, the most common marine planktonic Archaea across the surface ocean. *MicrobiologyOpen*, *8*(9), e00852. https://doi.org/10.1002/mbo3.852

Porter, K. G., & Feig, Y. S. (1980). The use of DAPI for identifying and counting aquatic microflora1. *Limnology and Oceanography*, *25*(5), 943–948. https://doi.org/10.4319/lo.1980.25.5.0943

Preisler, A., de Beer, D., Lichtschlag, A., Lavik, G., Boetius, A., & Jørgensen, B. B. (2007). Biological and chemical sulfide oxidation in a Beggiatoa inhabited marine sediment. *The ISME Journal*, *1*(4), Article 4. https://doi.org/10.1038/ismej.2007.50

Prinn, R. G., Weiss, R. F., Arduini, J., Arnold, T., DeWitt, H. L., Fraser, P. J., Ganesan, A. L., Gasore, J., Harth, C. M., Hermansen, O., Kim, J., Krummel, P. B., Li, S., Loh, Z. M., Lunder, C. R., Maione, M., Manning, A. J., Miller, B. R., Mitrevski, B., … Zhou, L. (2018). History of chemically and radiatively important atmospheric gases from the Advanced Global Atmospheric Gases Experiment (AGAGE). *Earth System Science Data*, *10*(2), 985–1018. https://doi.org/10.5194/essd-10-985-2018

Pushpakumara, B. L. D. U., Tandon, K., Willis, A., & Verbruggen, H. (2023). Unravelling microalgal-bacterial interactions in aquatic ecosystems through 16S rRNA gene-based co-occurrence networks. *Scientific Reports*, *13*(1), Article 1. https://doi.org/10.1038/s41598-023-27816-9

Quast, C., Pruesse, E., Yilmaz, P., Gerken, J., Schweer, T., Yarza, P., Peplies, J., & Glöckner, F. O. (2013). The SILVA ribosomal RNA gene database project: Improved data processing and web-based tools. *Nucleic Acids Research*, *41*(D1), D590–D596. https://doi.org/10.1093/nar/gks1219

Quinn, T. P., Richardson, M. F., Lovell, D., & Crowley, T. M. (2017). propr: An R-package for Identifying Proportionally Abundant Features Using Compositional Data Analysis. *Scientific Reports*, *7*(1), Article 1. https://doi.org/10.1038/s41598-017-16520-0

R Core Team. (2019). R: *A language and environment for statistical* computing. Vienna, Austria: R Foundation for Statistical Computing, available from https://www.r-project.org/

Rabus, R., Venceslau, S. S., Wöhlbrand, L., Voordouw, G., Wall, J. D., & Pereira, I. A. C. (2015). Chapter Two—A Post-Genomic View of the Ecophysiology, Catabolism and Biotechnological Relevance of Sulphate-Reducing Prokaryotes. In R. K. Poole (Ed.), *Advances in Microbial Physiology* (Vol. 66, pp. 55–321). Academic Press. https://doi.org/10.1016/bs.ampbs.2015.05.002

Ramsing, N., and J. Gundersen (1994), Seawater and gases: Tabulated physical parameters of interest to people working with microsensors in marine systems, Version 2.0, Unisense internal report, accessed from www.unisense.com

Ravishankara, A. R., Daniel, J. S., & Portmann, R. W. (2009). Nitrous Oxide (N_2O): The Dominant Ozone-Depleting Substance Emitted in the 21st Century. *Science*, *326*(5949), 123–125. https://doi.org/10.1126/science.1176985

Rees, A. P., Brown, I. J., Jayakumar, A., Lessin, G., Somerfield, P. J., & Ward, B. B. (2021). Biological nitrous oxide consumption in oxygenated waters of the high latitude Atlantic Ocean. *Communications Earth & Environment*, *2*(1), Article 1. https://doi.org/10.1038/s43247-021-00104-y

Reji, L., Tolar, B. B., Smith, J. M., Chavez, F. P., & Francis, C. A. (2019a). Depth distributions of nitrite reductase (nirK) gene variants reveal spatial dynamics of thaumarchaeal ecotype populations in coastal Monterey Bay. *Environmental Microbiology*, *21*(11), 4032–4045. https://doi.org/10.1111/1462-2920.14753

Reji, L., Tolar, B. B., Smith, J. M., Chavez, F. P., & Francis, C. A. (2019b). Differential co-occurrence relationships shaping ecotype diversification within Thaumarchaeota populations in the coastal ocean water column. *The ISME Journal*, *13*(5), Article 5. https://doi.org/10.1038/s41396-018-0311-x

Ritalahti, K. M., Amos, B. K., Sung, Y., Wu, Q., Koenigsberg, S. S., & Löffler, F. E. (2006). Quantitative PCR targeting 16S rRNA and reductive dehalogenase genes simultaneously monitors multiple Dehalococcoides strains. *Applied and Environmental Microbiology*, *72*(4), 2765–2774. https://doi.org/10.1128/AEM.72.4.2765-2774.2006

Robertson, G. P., & Groffman, P. M. (2015). Chapter 14—Nitrogen Transformations. In E. A. Paul (Ed.), *Soil Microbiology, Ecology and Biochemistry (Fourth Edition)* (pp. 421–446). Academic Press. https://doi.org/10.1016/B978-0-12-415955-6.00014-1

Robinson, A. D., Nedwell, D. B., Harrison, R. M., & Ogilvie, B. G. (1998). Hypernutrified estuaries as sources of N_2O emission to the atmosphere: The estuary of the River Colne, Essex, UK. *Marine Ecology Progress Series*, *164*, 59–71. https://doi.org/10.3354/meps164059

Rocca, J. D., Hall, E. K., Lennon, J. T., Evans, S. E., Waldrop, M. P., Cotner, J. B., Nemergut, D. R., Graham, E. B., & Wallenstein, M. D. (2015). Relationships between protein-encoding gene abundance and corresponding process are commonly assumed yet rarely observed. *The ISME Journal*, *9*(8), 1693–1699. https://doi.org/10.1038/ismej.2014.252

Rognes, T., Flouri, T., Nichols, B., Quince, C., & Mahé, F. (2016). VSEARCH: A versatile open source tool for metagenomics. *PeerJ*, *4*, e2584. https://doi.org/10.7717/peerj.2584

Rohart, F., Gautier, B., Singh, A., & Lê Cao, K.-A. (2017). mixOmics: An R package for 'omics feature selection and multiple data integration. *PLOS Computational Biology*, *13*(11), e1005752. https://doi.org/10.1371/journal.pcbi.1005752

Rysgaard, S., Risgaard-Petersen, N., & Sloth, N. P. (1996). Nitrification, denitrification, and nitrate ammonification in sediments of two coastal lagoons in Southern France. *Hydrobiologia*, *329*(1), 133–141. https://doi.org/10.1007/BF00034553

Salter, S. J., Cox, M. J., Turek, E. M., Calus, S. T., Cookson, W. O., Moffatt, M. F., Turner, P., Parkhill, J., Loman, N. J., & Walker, A. W. (2014). Reagent and laboratory contamination can critically impact sequence-based microbiome analyses. *BMC Biology*, *12*(1), 87. https://doi.org/10.1186/s12915-014-0087-z

Sanders, R. J., Jickells, T., Malcolm, S., Brown, J., Kirkwood, D., Reeve, A., Taylor, J., Horrobin, T., & Ashcroft, C. (1997). Nutrient fluxes through the Humber estuary. *Journal of Sea Research*, *37*(1), 3–23. https://doi.org/10.1016/S1385-1101(96)00002-0

Sanford, R. A., Wagner, D. D., Wu, Q., Chee-Sanford, J. C., Thomas, S. H., Cruz-García, C., Rodríguez, G., Massol-Deyá, A., Krishnani, K. K., Ritalahti, K. M., Nissen, S., Konstantinidis, K. T., & Löffler, F. E. (2012). Unexpected nondenitrifier nitrous oxide reductase gene diversity and abundance in soils. *Proceedings of the National Academy of Sciences*, *109*(48), 19709–19714. https://doi.org/10.1073/pnas.1211238109

Santoro, A. E., Buchwald, C., Knapp, A. N., Berelson, W. M., Capone, D. G., & Casciotti, K. L. (2021). Nitrification and Nitrous Oxide Production in the Offshore Waters of the Eastern Tropical South Pacific. *Global Biogeochemical Cycles*, *35*(2), e2020GB006716. https://doi.org/10.1029/2020GB006716

Santoro, A. E., Dupont, C. L., Richter, R. A., Craig, M. T., Carini, P., McIlvin, M. R., Yang, Y., Orsi, W. D., Moran, D. M., & Saito, M. A. (2015). Genomic and proteomic characterization of "Candidatus Nitrosopelagicus brevis": An ammonia-oxidizing archaeon from the open ocean. *Proceedings of the National Academy of Sciences*, *112*(4), 1173–1178. https://doi.org/10.1073/pnas.1416223112

Santoro, A. E., Saito, M. A., Goepfert, T. J., Lamborg, C. H., Dupont, C. L., & DiTullio, G. R. (2017). Thaumarchaeal ecotype distributions across the equatorial Pacific Ocean and their potential roles in nitrification and sinking flux attenuation. *Limnology and Oceanography*, *62*(5), 1984–2003. https://doi.org/10.1002/lno.10547

Sayavedra-Soto, L. A., & Arp, D. J. (2011). Ammonia-Oxidizing Bacteria: Their Biochemistry and Molecular Biology. In *Nitrification* (pp. 9–37). John Wiley & Sons, Ltd. https://doi.org/10.1128/9781555817145.ch2

Schloss, P. D., Westcott, S. L., Ryabin, T., Hall, J. R., Hartmann, M., Hollister, E. B., Lesniewski, R. A., Oakley, B. B., Parks, D. H., Robinson, C. J., Sahl, J. W., Stres, B.,

Thallinger, G. G., Van Horn, D. J., & Weber, C. F. (2009). Introducing mothur: Open-Source, Platform-Independent, Community-Supported Software for Describing and Comparing Microbial Communities. *Applied and Environmental Microbiology*, *75*(23), 7537–7541. https://doi.org/10.1128/AEM.01541-09

Schmidt, J. L., Deming, J. W., Jumars, P. A., & Keil, R. G. (1998). Constancy of bacterial abundance in surficial marine sediments. *Limnology and Oceanography*, *43*(5), 976–982. https://doi.org/10.4319/lo.1998.43.5.0976

Schunck, H., Lavik, G., Desai, D. K., Großkopf, T., Kalvelage, T., Löscher, C. R., Paulmier, A., Contreras, S., Siegel, H., Holtappels, M., Rosenstiel, P., Schilhabel, M. B., Graco, M., Schmitz, R. A., Kuypers, M. M. M., & LaRoche, J. (2013). Giant Hydrogen Sulfide Plume in the Oxygen Minimum Zone off Peru Supports Chemolithoautotrophy. *PLoS ONE*, *8*(8), e68661. https://doi.org/10.1371/journal.pone.0068661

Seitzinger, S. P., & Giblin, A. E. (1996). Estimating denitrification in North Atlantic continental shelf sediments. In R. W. Howarth (Ed.), *Nitrogen Cycling in the North Atlantic Ocean and its Watersheds* (pp. 235–260). Springer Netherlands. https://doi.org/10.1007/978-94-009-1776-7_7

Shah, V., Zhao, X., Lundeen, R. A., Ingalls, A. E., Nicastro, D., & Morris, R. M. (2019). Morphological Plasticity in a Sulfur-Oxidizing Marine Bacterium from the SUP05 Clade Enhances Dark Carbon Fixation. *MBio*, *10*(3), e00216-19. https://doi.org/10.1128/mBio.00216-19

Shannon, P., Markiel, A., Ozier, O., Baliga, N. S., Wang, J. T., Ramage, D., Amin, N., Schwikowski, B., & Ideker, T. (2003). Cytoscape: A Software Environment for

Integrated Models of Biomolecular Interaction Networks. *Genome Research*, *13*(11), 2498–2504. https://doi.org/10.1101/gr.1239303

Soetaert, G., Hamme, R. C., & Raftery, E. (2022). Renewal of seasonally anoxic Saanich Inlet is temporally and spatially dynamic. *Frontiers in Marine Science*, *9*. https://www.frontiersin.org/articles/10.3389/fmars.2022.1001146

Sogin, M. L., Morrison, H. G., Huber, J. A., Mark Welch, D., Huse, S. M., Neal, P. R., Arrieta, J. M., & Herndl, G. J. (2006). Microbial diversity in the deep sea and the underexplored "rare biosphere." *Proceedings of the National Academy of Sciences of the United States of America*, *103*(32), 12115–12120. https://doi.org/10.1073/pnas.0605127103

Sollai, M., Hopmans, E. C., Schouten, S., Keil, R. G., & Sinninghe Damsté, J. S. (2015). *Intact polar lipids of Thaumarchaeota and anammox bacteria as indicators of N-cycling in the Eastern Tropical North Pacific oxygen deficient zone* [Preprint]. Biogeochemistry: Environmental Microbiology. https://doi.org/10.5194/bgd-12-4833-2015

Sollai, M., Villanueva, L., Hopmans, E. C., Keil, R. G., & Sinninghe Damsté, J. S. (2019). Archaeal Sources of Intact Membrane Lipid Biomarkers in the Oxygen Deficient Zone of the Eastern Tropical South Pacific. *Frontiers in Microbiology*, *10*, 765. https://doi.org/10.3389/fmicb.2019.00765

Spiro, S. (2012). Nitrous oxide production and consumption: Regulation of gene expression by gas-sensitive transcription factors. *Philosophical Transactions of the Royal Society B: Biological Sciences*, *367*(1593), 1213–1225. https://doi.org/10.1098/rstb.2011.0309

Steele, J. A., Countway, P. D., Xia, L., Vigil, P. D., Beman, J. M., Kim, D. Y., Chow, C.-E. T., Sachdeva, R., Jones, A. C., Schwalbach, M. S., Rose, J. M., Hewson, I., Patel, A., Sun, F., Caron, D. A., & Fuhrman, J. A. (2011). Marine bacterial, archaeal and protistan

association networks reveal ecological linkages. *The ISME Journal*, *5*(9), Article 9. https://doi.org/10.1038/ismej.2011.24

Stein, L. Y. (2011). Surveying N_2O-Producing Pathways in Bacteria. *In* M. G. Klotz (Ed.), *Methods in Enzymology* (Vol. 486, pp. 131–152). Academic Press. https://doi.org/10.1016/B978-0-12-381294-0.00006-7

Stewart, F. J., Ulloa, O., & DeLong, E. F. (2012). Microbial metatranscriptomics in a permanent marine oxygen minimum zone. *Environmental Microbiology*, *14*(1), 23–40. https://doi.org/10.1111/j.1462-2920.2010.02400.x

Stieglmeier, M., Mooshammer, M., Kitzler, B., Wanek, W., Zechmeister-Boltenstern, S., Richter, A., & Schleper, C. (2014). Aerobic nitrous oxide production through N-nitrosating hybrid formation in ammonia-oxidizing archaea. *The ISME Journal*, *8*(5), Article 5. https://doi.org/10.1038/ismej.2013.220

Stramma, L., Johnson, G. C., Sprintall, J., & Mohrholz, V. (2008). Expanding oxygen-minimum zones in the tropical oceans. *Science (New York, N.Y.)*, *320*(5876), 655–658. https://doi.org/10.1126/science.1153847

Sun, X., Frey, C., Garcia-Robledo, E., Jayakumar, A., & Ward, B. B. (2021). Microbial niche differentiation explains nitrite oxidation in marine oxygen minimum zones. *The ISME Journal*, *15*(5), 1317–1329. https://doi.org/10.1038/s41396-020-00852-3

Sun, X., Jayakumar, A., Tracey, J. C., Wallace, E., Kelly, C. L., Casciotti, K. L., & Ward, B. B. (2021). Microbial N_2O consumption in and above marine N_2O production hotspots. *The ISME Journal*, *15*(5), Article 5. https://doi.org/10.1038/s41396-020-00861-2

Sun, X., Jayakumar, A., & Ward, B. B. (2017). Community Composition of Nitrous Oxide Consuming Bacteria in the Oxygen Minimum Zone of the Eastern Tropical South Pacific. *Frontiers in Microbiology*, *8*. https://doi.org/10.3389/fmicb.2017.01183

Sunagawa, S., Coelho, L. P., Chaffron, S., Kultima, J. R., Labadie, K., Salazar, G., Djahanschiri, B., Zeller, G., Mende, D. R., Alberti, A., Cornejo-Castillo, F. M., Costea, P. I., Cruaud, C., d'Ovidio, F., Engelen, S., Ferrera, I., Gasol, J. M., Guidi, L., Hildebrand, F., … Bork, P. (2015). Structure and function of the global ocean microbiome. *Science*, *348*(6237), 1261359. https://doi.org/10.1126/science.1261359

Suntharalingam, P., & Sarmiento, J. L. (2000). Factors governing the oceanic nitrous oxide distribution: Simulations with an ocean general circulation model. *Global Biogeochemical Cycles*, *14*(1), 429–454. https://doi.org/10.1029/1999GB900032

Syakila, A., Kroeze, C., & Slomp, C. P. (2010). Neglecting sinks for N_2O at the earth's surface: Does it matter? *Journal of Integrative Environmental Sciences*, *7*(sup1), 79–87. https://doi.org/10.1080/1943815X.2010.497492

Tamimi, A., Rinker, E. B., & Sandall, O. C. (1994). Diffusion Coefficients for Hydrogen Sulfide, Carbon Dioxide, and Nitrous Oxide in Water over the Temperature Range 293-368 K. *Journal of Chemical & Engineering Data*, *39*(2), 330–332. https://doi.org/10.1021/je00014a031

Teeling, H., Fuchs, B. M., Bennke, C. M., Krüger, K., Chafee, M., Kappelmann, L., Reintjes, G., Waldmann, J., Quast, C., Glöckner, F. O., Lucas, J., Wichels, A., Gerdts, G., Wiltshire, K. H., & Amann, R. I. (2016). Recurring patterns in bacterioplankton dynamics during coastal spring algae blooms. *ELife*, *5*, e11888. https://doi.org/10.7554/eLife.11888

Tian, H., Xu, R., Canadell, J. G., Thompson, R. L., Winiwarter, W., Suntharalingam, P., Davidson, E. A., Ciais, P., Jackson, R. B., Janssens-Maenhout, G., Prather, M. J., Regnier, P., Pan, N., Pan, S., Peters, G. P., Shi, H., Tubiello, F. N., Zaehle, S., Zhou, F., … Yao, Y. (2020). A comprehensive quantification of global nitrous oxide sources and sinks. *Nature*, *586*(7828), Article 7828. https://doi.org/10.1038/s41586-020-2780-0

Tourna, M., Stieglmeier, M., Spang, A., Könneke, M., Schintlmeister, A., Urich, T., Engel, M., Schloter, M., Wagner, M., Richter, A., & Schleper, C. (2011). Nitrososphaera viennensis, an ammonia oxidizing archaeon from soil. *Proceedings of the National Academy of Sciences of the United States of America*, *108*(20), 8420–8425. https://doi.org/10.1073/pnas.1013488108

Townsend-Small, A., Prokopenko, M. G., & Berelson, W. M. (2014). Nitrous oxide cycling in the water column and sediments of the oxygen minimum zone, eastern subtropical North Pacific, Southern California, and Northern Mexico (23°N–34°N). *Journal of Geophysical Research: Oceans*, *119*(5), 3158–3170. https://doi.org/10.1002/2013JC009580

Toyoda, S., Yoshida, O., Yamagishi, H., Fujii, A., Yoshida, N., & Watanabe, S. (2019). Identifying the origin of nitrous oxide dissolved in deep ocean by concentration and isotopocule analyses. *Scientific Reports*, *9*(1), Article 1. https://doi.org/10.1038/s41598-019-44224-0

Trimmer, M., Chronopoulou, P.-M., Maanoja, S. T., Upstill-Goddard, R. C., Kitidis, V., & Purdy, K. J. (2016). Nitrous oxide as a function of oxygen and archaeal gene abundance in the North Pacific. *Nature Communications*, *7*(1), 13451. https://doi.org/10.1038/ncomms13451

Tsementzi, D., Wu, J., Deutsch, S., Nath, S., Rodriguez-R, L. M., Burns, A. S., Ranjan, P., Sarode, N., Malmstrom, R. R., Padilla, C. C., Stone, B. K., Bristow, L. A., Larsen, M., Glass, J. B., Thamdrup, B., Woyke, T., Konstantinidis, K. T., & Stewart, F. J. (2016). SAR11 bacteria linked to ocean anoxia and nitrogen loss. *Nature*, *536*(7615), Article 7615. https://doi.org/10.1038/nature19068

Ulloa, O., Canfield, D. E., DeLong, E. F., Letelier, R. M., & Stewart, F. J. (2012). Microbial oceanography of anoxic oxygen minimum zones. *Proceedings of the National Academy of Sciences*, *109*(40), 15996–16003. https://doi.org/10.1073/pnas.1205009109

Usui, T., Koike, I., & Ogura, N. (1998). Vertical profiles of nitrous oxide and dissolved oxygen in marine sediments. *Marine Chemistry*, *59*(3), 253–270. https://doi.org/10.1016/S0304-4203(97)00091-1

Usui, T., Koike, I., & Ogura, N. (2001). N_2O Production, Nitrification and Denitrification in an Estuarine Sediment. *Estuarine, Coastal and Shelf Science*, *52*(6), 769–781. https://doi.org/10.1006/ecss.2000.0765

Vajrala, N., Martens-Habbena, W., Sayavedra-Soto, L. A., Schauer, A., Bottomley, P. J., Stahl, D. A., & Arp, D. J. (2013). Hydroxylamine as an intermediate in ammonia oxidation by globally abundant marine archaea. *Proceedings of the National Academy of Sciences*, *110*(3), 1006–1011. https://doi.org/10.1073/pnas.1214272110

Walker, C. B., Torre, J. R. de la, Klotz, M. G., Urakawa, H., Pinel, N., Arp, D. J., Brochier-Armanet, C., Chain, P. S. G., Chan, P. P., Gollabgir, A., Hemp, J., Hügler, M., Karr, E. A., Könneke, M., Shin, M., Lawton, T. J., Lowe, T., Martens-Habbena, W., Sayavedra-Soto, L. A., … Stahl, D. A. (2010). *Nitrosopumilus maritimus* genome reveals unique mechanisms for nitrification and autotrophy in globally distributed marine crenarchaea.

Proceedings of the National Academy of Sciences, *107*(19), 8818–8823. https://doi.org/10.1073/pnas.0913533107

Wallenstein, M. D., Myrold, D. D., Firestone, M., & Voytek, M. (2006). Environmental Controls on Denitrifying Communities and Denitrification Rates: Insights from Molecular Methods. *Ecological Applications*, *16*(6), 2143–2152. https://doi.org/10.1890/1051-0761(2006)016[2143:ECODCA]2.0.CO;2

Walsh, D. A., Zaikova, E., Howes, C. G., Song, Y. C., Wright, J. J., Tringe, S. G., Tortell, P. D., & Hallam, S. J. (2009). Metagenome of a Versatile Chemolithoautotroph from Expanding Oceanic Dead Zones. *Science*, *326*(5952), 578–582. https://doi.org/10.1126/science.1175309

Wang, C., Shan, B., Zhang, H., & Rong, N. (2014). Analyzing sediment dissolved oxygen based on microprofile modeling. *Environmental Science and Pollution Research*, *21*(17), 10320–10328. https://doi.org/10.1007/s11356-014-2875-y

Wang, S., Tang, W., Delage, E., Gifford, S., Whitby, H., González, A. G., Eveillard, D., Planquette, H., & Cassar, N. (2021). Investigating the microbial ecology of coastal hotspots of marine nitrogen fixation in the western North Atlantic. *Scientific Reports*, *11*(1), 5508. https://doi.org/10.1038/s41598-021-84969-1

Wang, Y., Huang, W. E., Cui, L., & Wagner, M. (2016). Single cell stable isotope probing in microbiology using Raman microspectroscopy. *Current Opinion in Biotechnology*, *41*, 34–42. https://doi.org/10.1016/j.copbio.2016.04.018

Ward, B. B. (2002). Nitrification in Aquatic Systems. In *Encyclopedia of Environmental Microbiology*. John Wiley & Sons, Ltd. https://doi.org/10.1002/0471263397.env287

Ward, B. B. (2008). Nitrification in Marine Systems. In *Nitrogen in the Marine Environment* (pp. 199–261). Elsevier. https://doi.org/10.1016/B978-0-12-372522-6.00005-0

Wei, W., Isobe, K., Nishizawa, T., Zhu, L., Shiratori, Y., Ohte, N., Koba, K., Otsuka, S., & Senoo, K. (2015). Higher diversity and abundance of denitrifying microorganisms in environments than considered previously. *The ISME Journal*, *9*(9), Article 9. https://doi.org/10.1038/ismej.2015.9

Weiss, R. F., & Price, B. A. (1980). Nitrous oxide solubility in water and seawater. *Marine Chemistry*, *8*(4), 347–359. https://doi.org/10.1016/0304-4203(80)90024-9

Westley, M. B., Yamagishi, H., Popp, B. N., & Yoshida, N. (2006). Nitrous oxide cycling in the Black Sea inferred from stable isotope and isotopomer distributions. *Deep Sea Research Part II: Topical Studies in Oceanography*, *53*(17), 1802–1816. https://doi.org/10.1016/j.dsr2.2006.03.012

Whitman, W. B., Coleman, D. C., & Wiebe, W. J. (1998). Prokaryotes: The unseen majority. *Proceedings of the National Academy of Sciences*, *95*(12), 6578–6583. https://doi.org/10.1073/pnas.95.12.6578

Wright, J. J., Konwar, K. M., & Hallam, S. J. (2012). Microbial ecology of expanding oxygen minimum zones. *Nature Reviews Microbiology*, *10*(6), 381–394. https://doi.org/10.1038/nrmicro2778

Wuchter, C., Abbas, B., Coolen, M. J. L., Herfort, L., van Bleijswijk, J., Timmers, P., Strous, M., Teira, E., Herndl, G. J., Middelburg, J. J., Schouten, S., & Sinninghe Damsté, J. S. (2006). Archaeal nitrification in the ocean. *Proceedings of the National Academy of Sciences*, *103*(33), 12317–12322. https://doi.org/10.1073/pnas.0600756103

Xie, H., Hong, Y., Liu, H., Jiao, L., Wu, J., & Wang, L. (2020). Spatio-temporal shifts in community structure and activity of nirS-type denitrifiers in the sediment cores of Pearl River Estuary. *PLOS ONE*, *15*(4), e0231271. https://doi.org/10.1371/journal.pone.0231271

Yang, S., Chang, B. X., Warner, M. J., Weber, T. S., Bourbonnais, A. M., Santoro, A. E., Kock, A., Sonnerup, R. E., Bullister, J. L., Wilson, S. T., & Bianchi, D. (2020). Global reconstruction reduces the uncertainty of oceanic nitrous oxide emissions and reveals a vigorous seasonal cycle. *Proceedings of the National Academy of Sciences*, *117*(22), 11954–11960. https://doi.org/10.1073/pnas.1921914117

Yoon, S., Nissen, S., Park, D., Sanford, R. A., & Löffler, F. E. (2016). Nitrous Oxide Reduction Kinetics Distinguish Bacteria Harboring Clade I NosZ from Those Harboring Clade II NosZ. *Applied and Environmental Microbiology*, *82*(13), 3793–3800. https://doi.org/10.1128/AEM.00409-16

Yoshinari, T. (1976). Nitrous oxide in the sea. *Marine Chemistry*, *4*(2), 189–202. https://doi.org/10.1016/0304-4203(76)90007-4

Yu, F. B., Blainey, P. C., Schulz, F., Woyke, T., Horowitz, M. A., & Quake, S. R. (2017). Microfluidic-based mini-metagenomics enables discovery of novel microbial lineages from complex environmental samples. *ELife*, *6*, e26580. https://doi.org/10.7554/eLife.26580

Zaikova, E., Walsh, D. A., Stilwell, C. P., Mohn, W. W., Tortell, P. D., & Hallam, S. J. (2010). Microbial community dynamics in a seasonally anoxic fjord: Saanich Inlet, British Columbia. *Environmental Microbiology*, *12*(1), 172–191. https://doi.org/10.1111/j.1462-2920.2009.02058.x

Zecher, K., Hayes, K. R., & Philipp, B. (2020). Evidence of Interdomain Ammonium Cross-Feeding From Methylamine- and Glycine Betaine-Degrading Rhodobacteraceae to Diatoms as a Widespread Interaction in the Marine Phycosphere. *Frontiers in Microbiology*, *11*. https://www.frontiersin.org/article/10.3389/fmicb.2020.533894

Zhou, Z., Pan, J., Wang, F., Gu, J.-D., & Li, M. (2018). Bathyarchaeota: Globally distributed metabolic generalists in anoxic environments. *FEMS Microbiology Reviews*, *42*(5), 639–655. https://doi.org/10.1093/femsre/fuy023

Zumft, W. G. (1997). Cell biology and molecular basis of denitrification. *Microbiology and Molecular Biology Reviews*, *61*(4), 533–616. https://doi.org/10.1128/mmbr.61.4.533-616.1997

Appendices

Appendix A. Supplementary Data: Saanich ASV taxonomic predictions

Taxonomic predictions for individual bacterial and archaeal ASVs inferred from the silva_nr_132 reference database using Mothur v1.42.3. Table includes only variants included in WGCNA and sPLSR analyses following removal of rare taxa.

ASV ID	Phylum	Class	Order	Family	Genus
ARCH1	Thaumarchaeota	Nitrososphaeria	Nitrosopumilales	Nitrosopumilaceae	Candidatus_Nitrosopumilus
ARCH10	Euryarchaeota	Thermoplasmata	Marine_Group_II	Marine_Group_II_fa	Marine_Group_II_ge
ARCH11	Euryarchaeota	Thermoplasmata	Marine_Group_II	Marine_Group_II_fa	Marine_Group_II_ge
ARCH13	Euryarchaeota	Thermoplasmata	Marine_Group_II	Marine_Group_II_fa	Marine_Group_II_ge
ARCH130	Euryarchaeota	Thermoplasmata	Marine_Group_II	Marine_Group_II_fa	Marine_Group_II_ge
ARCH14	Thaumarchaeota	Nitrososphaeria	Nitrosopumilales	Nitrosopumilaceae	Candidatus_Nitrosopelagicus
ARCH15	Euryarchaeota	Thermoplasmata	Marine_Group_II	Marine_Group_II_fa	Marine_Group_II_ge
ARCH16	Euryarchaeota	Thermoplasmata	Marine_Group_II	Marine_Group_II_fa	Marine_Group_II_ge
ARCH18	Euryarchaeota	Thermoplasmata	Marine_Group_II	Marine_Group_II_fa	Marine_Group_II_ge
ARCH19	Euryarchaeota	Thermoplasmata	Marine_Group_II	Marine_Group_II_fa	Marine_Group_II_ge
ARCH2	Thaumarchaeota	Nitrososphaeria	Nitrosopumilales	Nitrosopumilaceae	Candidatus_Nitrosopumilus
ARCH20	Euryarchaeota	Thermoplasmata	Marine_Group_II	Marine_Group_II_fa	Marine_Group_II_ge
ARCH22	Euryarchaeota	Thermoplasmata	Marine_Group_III	Marine_Group_III_fa	Marine_Group_III_ge
ARCH24	Euryarchaeota	Thermoplasmata	Marine_Group_II	Marine_Group_II_fa	Marine_Group_II_ge
ARCH26	Euryarchaeota	Thermoplasmata	Marine_Group_II	Marine_Group_II_fa	Marine_Group_II_ge
ARCH28	Crenarchaeota	Bathyarchaeia	Bathyarchaeia_or	Bathyarchaeia_fa	Bathyarchaeia_ge
ARCH29	Thaumarchaeota	Nitrososphaeria	Nitrosopumilales	Nitrosopumilaceae	Candidatus_Nitrosopelagicus
ARCH3	Thaumarchaeota	Nitrososphaeria	Nitrosopumilales	Nitrosopumilaceae	Candidatus_Nitrosopumilus
ARCH30	Euryarchaeota	Thermoplasmata	Marine_Group_II	Marine_Group_II_fa	Marine_Group_II_ge
ARCH32	Thaumarchaeota	Nitrososphaeria	Nitrosopumilales	Nitrosopumilaceae	Candidatus_Nitrosopelagicus

ASV ID	Phylum	Class	Order	Family	Genus
ARCH34	Euryarchaeota	Thermoplasmata	Marine_Group_II	Marine_Group_II_fa	Marine_Group_II_ge
ARCH35	Thaumarchaeota	Nitrososphaeria	Nitrosopumilales	Nitrosopumilaceae	Candidatus_Nitrosopelagicus
ARCH36	Euryarchaeota	Thermoplasmata	Marine_Group_II	Marine_Group_II_fa	Marine_Group_II_ge
ARCH37	Euryarchaeota	Thermoplasmata	uncultured	uncultured_fa	uncultured_ge
ARCH4	Thaumarchaeota	Nitrososphaeria	Nitrosopumilales	Nitrosopumilaceae	Candidatus_Nitrosopumilus
ARCH40	Crenarchaeota	Bathyarchaeia	Bathyarchaeia_or	Bathyarchaeia_fa	Bathyarchaeia_ge
ARCH42	Euryarchaeota	Thermoplasmata	uncultured	uncultured_fa	uncultured_ge
ARCH50	Thaumarchaeota	Nitrososphaeria	Nitrosopumilales	Nitrosopumilaceae	Nitrosopumilaceae
ARCH51	Thaumarchaeota	Nitrososphaeria	Nitrosopumilales	Nitrosopumilaceae	Candidatus_Nitrosopelagicus
ARCH52	Euryarchaeota	Thermoplasmata	Thermoplasmata_unclassified	Thermoplasmata_unclassified	Thermoplasmata_unclassified
ARCH57	Thaumarchaeota	Nitrososphaeria	Nitrosopumilales	Nitrosopumilaceae	Candidatus_Nitrosopelagicus
ARCH6	Euryarchaeota	Thermoplasmata	Marine_Group_II	Marine_Group_II_fa	Marine_Group_II_ge
ARCH61	Euryarchaeota	Thermoplasmata	Marine_Group_II	Marine_Group_II_fa	Marine_Group_II_ge
ARCH63	Asgardaeota	Asgardaeota_unclassified	Asgardaeota_unclassified	Asgardaeota_unclassified	Asgardaeota_unclassified
ARCH65	Thaumarchaeota	Nitrososphaeria	Nitrosopumilales	Nitrosopumilaceae	Nitrosopumilaceae
ARCH7	Euryarchaeota	Thermoplasmata	Marine_Group_II	Marine_Group_II_fa	Marine_Group_II_ge
ARCH8	Euryarchaeota	Thermoplasmata	Marine_Group_II	Marine_Group_II_fa	Marine_Group_II_ge
ARCH9	Euryarchaeota	Thermoplasmata	Marine_Group_II	Marine_Group_II_fa	Marine_Group_II_ge
BACT1	Proteobacteria	Gammaproteobacteria	Thiomicrospirales	Thioglobaceae	SUP05_cluster
BACT10	Proteobacteria	Alphaproteobacteria	Rhodobacterales	Rhodobacteraceae	Rhodobacteraceae_unclassified
BACT101	Verrucomicrobia	Verrucomicrobiae	Verrucomicrobiae_unclassified	Verrucomicrobiae_unclassified	Verrucomicrobiae_unclassified
BACT102	Nitrospinae	Nitrospinia	Nitrospinales	Nitrospinaceae	Nitrospina
BACT103	Proteobacteria	Gammaproteobacteria	SAR86_clade	SAR86_clade_fa	SAR86_clade_ge
BACT104	Bacteroidetes	Bacteroidia	Flavobacteriales	NS9_marine_group	NS9_marine_group_ge
BACT105	Bacteroidetes	Bacteroidia	Flavobacteriales	Flavobacteriales_unclassified	Flavobacteriales_unclassified
BACT106	Proteobacteria	Gammaproteobacteria	Oceanospirillales	Pseudohongiellaceae	Pseudohongiella
BACT107	Proteobacteria	Gammaproteobacteria	Alteromonadales	Pseudoalteromonadaceae	Pseudoalteromonas
BACT108	Proteobacteria	Alphaproteobacteria	Rhodobacterales	Rhodobacteraceae	Ascidiaceihabitans

ASV ID	Phylum	Class	Order	Family	Genus
BACT109	Nitrospinae	Nitrospinia	Nitrospinales	Nitrospinaceae	Nitrospina
BACT11	Proteobacteria	Gammaproteobacteria	Gammaproteobacteria_unclassified	Gammaproteobacteria_unclassified	Gammaproteobacteria_unclassified
BACT110	Verrucomicrobia	Verrucomicrobiae	Opitutales	Puniceicoccaceae	MB11C04_marine_group
BACT1103	Proteobacteria	Gammaproteobacteria	Thiomicrospirales	Thioglobaceae	SUP05_cluster
BACT111	Nitrospinae	Nitrospinia	Nitrospinales	Nitrospinaceae	Nitrospina
BACT112	Nitrospinae	Nitrospinia	Nitrospinales	Nitrospinaceae	Nitrospina
BACT113	Bacteria_unclassified	Bacteria_unclassified	Bacteria_unclassified	Bacteria_unclassified	Bacteria_unclassified
BACT1131	Proteobacteria	Gammaproteobacteria	Gammaproteobacteria_unclassified	Gammaproteobacteria_unclassified	Gammaproteobacteria_unclassified
BACT114	Proteobacteria	Alphaproteobacteria	Alphaproteobacteria_unclassified	Alphaproteobacteria_unclassified	Alphaproteobacteria_unclassified
BACT115	Bacteria_unclassified	Bacteria_unclassified	Bacteria_unclassified	Bacteria_unclassified	Bacteria_unclassified
BACT116	Proteobacteria	Alphaproteobacteria	Alphaproteobacteria_unclassified	Alphaproteobacteria_unclassified	Alphaproteobacteria_unclassified
BACT118	Proteobacteria	Gammaproteobacteria	Gammaproteobacteria_unclassified	Gammaproteobacteria_unclassified	Gammaproteobacteria_unclassified
BACT119	Proteobacteria	Alphaproteobacteria	SAR11_clade	Clade_II	SAR11
BACT12	Proteobacteria	Alphaproteobacteria	Rhodobacterales	Rhodobacteraceae	Planktomarina
BACT121	Bacteria_unclassified	Bacteria_unclassified	Bacteria_unclassified	Bacteria_unclassified	Bacteria_unclassified
BACT122	Verrucomicrobia	Verrucomicrobiae	Verrucomicrobiae_unclassified	Verrucomicrobiae_unclassified	Verrucomicrobiae_unclassified
BACT123	Bacteria_unclassified	Bacteria_unclassified	Bacteria_unclassified	Bacteria_unclassified	Bacteria_unclassified
BACT124	Bacteroidetes	Bacteroidia	Flavobacteriales	NS9_marine_group	NS9_marine_group_ge
BACT1253	Proteobacteria	Gammaproteobacteria	Gammaproteobacteria_unclassified	Gammaproteobacteria_unclassified	Gammaproteobacteria_unclassified
BACT126	Bacteria_unclassified	Bacteria_unclassified	Bacteria_unclassified	Bacteria_unclassified	Bacteria_unclassified
BACT127	Bacteria_unclassified	Bacteria_unclassified	Bacteria_unclassified	Bacteria_unclassified	Bacteria_unclassified
BACT128	Proteobacteria	Gammaproteobacteria	Oceanospirillales	Pseudohongiellaceae	Pseudohongiella
BACT129	Bacteria_unclassified	Bacteria_unclassified	Bacteria_unclassified	Bacteria_unclassified	Bacteria_unclassified
BACT13	Proteobacteria	Alphaproteobacteria	Rhodobacterales	Rhodobacteraceae	Rhodobacteraceae_unclassified
BACT131	Proteobacteria	Proteobacteria_unclassified	Proteobacteria_unclassified	Proteobacteria_unclassified	Proteobacteria_unclassified
BACT132	Proteobacteria	Alphaproteobacteria	Alphaproteobacteria_unclassified	Alphaproteobacteria_unclassified	Alphaproteobacteria_unclassified
BACT133	Proteobacteria	Gammaproteobacteria	Oceanospirillales	Pseudohongiellaceae	Pseudohongiella
BACT134	Bacteroidetes	Bacteroidia	Flavobacteriales	NS9_marine_group	NS9_marine_group_ge

ASV ID	Phylum	Class	Order	Family	Genus
BACT135	Marinimicrobia_	Marinimicrobia__cl	Marinimicrobia__or	Marinimicrobia__fa	Marinimicrobia__ge
BACT137	Bacteroidetes	Bacteroidia	Chitinophagales	Saprospiraceae	Saprospiraceae_unclassified
BACT138	Proteobacteria	Gammaproteobacteria	UBA10353_marine_group	UBA10353_marine_group_fa	UBA10353_marine_group_ge
BACT1384	Proteobacteria	Gammaproteobacteria	Thiomicrospirales	Thioglobaceae	SUP05_cluster
BACT139	Planctomycetes	OM190	OM190_or	OM190_fa	OM190_ge
BACT14	Proteobacteria	Alphaproteobacteria	SAR11_clade	Clade_I	SAR11
BACT140	Nitrospinae	Nitrospinia	Nitrospinales	Nitrospinaceae	Nitrospina
BACT141	Bacteria_unclassified	Bacteria_unclassified	Bacteria_unclassified	Bacteria_unclassified	Bacteria_unclassified
BACT142	Marinimicrobia_	Marinimicrobia__cl	Marinimicrobia__or	Marinimicrobia__fa	Marinimicrobia__ge
BACT143	Proteobacteria	Alphaproteobacteria	SAR11_clade	Clade_II	SAR11
BACT1445	Proteobacteria	Gammaproteobacteria	Thiomicrospirales	Thioglobaceae	SUP05_cluster
BACT145	Proteobacteria	Gammaproteobacteria	SAR86_clade	SAR86_clade_fa	SAR86_clade_ge
BACT146	Proteobacteria	Alphaproteobacteria	SAR11_clade	Clade_II	SAR11
BACT148	Bacteroidetes	Bacteroidia	Flavobacteriales	Flavobacteriaceae	Flavobacteriaceae_unclassified
BACT149	Proteobacteria	Alphaproteobacteria	SAR11_clade	Clade_II	SAR11
BACT15	Proteobacteria	Alphaproteobacteria	SAR11_clade	Clade_II	SAR11
BACT1504	Proteobacteria	Gammaproteobacteria	Thiomicrospirales	Thioglobaceae	SUP05_cluster
BACT1529	Proteobacteria	Gammaproteobacteria	Thiomicrospirales	Thioglobaceae	SUP05_cluster
BACT153	Bacteria_unclassified	Bacteria_unclassified	Bacteria_unclassified	Bacteria_unclassified	Bacteria_unclassified
BACT154	Proteobacteria	Alphaproteobacteria	Alphaproteobacteria_unclassified	Alphaproteobacteria_unclassified	Alphaproteobacteria_unclassified
BACT155	Proteobacteria	Alphaproteobacteria	SAR11_clade	Clade_I	SAR11
BACT156	Bacteria_unclassified	Bacteria_unclassified	Bacteria_unclassified	Bacteria_unclassified	Bacteria_unclassified
BACT1564	Proteobacteria	Gammaproteobacteria	Thiomicrospirales	Thioglobaceae	SUP05_cluster
BACT1569	Proteobacteria	Gammaproteobacteria	Thiomicrospirales	Thioglobaceae	SUP05_cluster
BACT157	Actinobacteria	Actinobacteria	Micrococcales	Microbacteriaceae	Microbacterium
BACT159	Bacteroidetes	Bacteroidia	Flavobacteriales	Flavobacteriaceae	Polaribacter
BACT16	Proteobacteria	Alphaproteobacteria	Rhodobacterales	Rhodobacteraceae	Ascidiaceihabitans
BACT160	Proteobacteria	Gammaproteobacteria	Gammaproteobacteria_unclassified	Gammaproteobacteria_unclassified	Gammaproteobacteria_unclassified

ASV ID	Phylum	Class	Order	Family	Genus
BACT161	Proteobacteria	Alphaproteobacteria	Rhodospirillales	AEGEAN-169_marine_group	AEGEAN-169_marine_group_ge
BACT162	Planctomycetes	OM190	OM190_or	OM190_fa	OM190_ge
BACT163	Bacteria_unclassified	Bacteria_unclassified	Bacteria_unclassified	Bacteria_unclassified	Bacteria_unclassified
BACT164	Bacteroidetes	Bacteroidia	Flavobacteriales	Flavobacteriaceae	Flavobacteriaceae_unclassified
BACT1644	Proteobacteria	Gammaproteobacteria	Thiomicrospirales	Thioglobaceae	SUP05_cluster
BACT165	Proteobacteria	Alphaproteobacteria	Alphaproteobacteria_unclassified	Alphaproteobacteria_unclassified	Alphaproteobacteria_unclassified
BACT166	Bacteria_unclassified	Bacteria_unclassified	Bacteria_unclassified	Bacteria_unclassified	Bacteria_unclassified
BACT167	Verrucomicrobia	Verrucomicrobiae	Verrucomicrobiales	Verrucomicrobiales_unclassified	Verrucomicrobiales_unclassified
BACT168	Bacteria_unclassified	Bacteria_unclassified	Bacteria_unclassified	Bacteria_unclassified	Bacteria_unclassified
BACT1684	Proteobacteria	Gammaproteobacteria	Thiomicrospirales	Thioglobaceae	SUP05_cluster
BACT17	Bacteroidetes	Bacteroidia	Flavobacteriales	Flavobacteriaceae	NS5_marine_group
BACT170	Proteobacteria	Proteobacteria_unclassified	Proteobacteria_unclassified	Proteobacteria_unclassified	Proteobacteria_unclassified
BACT171	Bacteria_unclassified	Bacteria_unclassified	Bacteria_unclassified	Bacteria_unclassified	Bacteria_unclassified
BACT172	Bacteria_unclassified	Bacteria_unclassified	Bacteria_unclassified	Bacteria_unclassified	Bacteria_unclassified
BACT1722	Proteobacteria	Gammaproteobacteria	Thiomicrospirales	Thioglobaceae	SUP05_cluster
BACT173	Proteobacteria	Alphaproteobacteria	Alphaproteobacteria_unclassified	Alphaproteobacteria_unclassified	Alphaproteobacteria_unclassified
BACT174	Bacteria_unclassified	Bacteria_unclassified	Bacteria_unclassified	Bacteria_unclassified	Bacteria_unclassified
BACT175	Proteobacteria	Gammaproteobacteria	Gammaproteobacteria_unclassified	Gammaproteobacteria_unclassified	Gammaproteobacteria_unclassified
BACT1752	Proteobacteria	Gammaproteobacteria	Gammaproteobacteria_unclassified	Gammaproteobacteria_unclassified	Gammaproteobacteria_unclassified
BACT1759	Proteobacteria	Gammaproteobacteria	Thiomicrospirales	Thioglobaceae	SUP05_cluster
BACT176	Bacteroidetes	Bacteroidia	Bacteroidia_unclassified	Bacteroidia_unclassified	Bacteroidia_unclassified
BACT1765	Proteobacteria	Proteobacteria_unclassified	Proteobacteria_unclassified	Proteobacteria_unclassified	Proteobacteria_unclassified
BACT177	Bacteria_unclassified	Bacteria_unclassified	Bacteria_unclassified	Bacteria_unclassified	Bacteria_unclassified
BACT179	Proteobacteria	Alphaproteobacteria	Alphaproteobacteria_unclassified	Alphaproteobacteria_unclassified	Alphaproteobacteria_unclassified
BACT18	Bacteroidetes	Bacteroidia	Bacteroidales	Bacteroidales_unclassified	Bacteroidales_unclassified
BACT180	Verrucomicrobia	Verrucomicrobiae	Opitutales	Puniceicoccaceae	MB11C04_marine_group
BACT181	Proteobacteria	Alphaproteobacteria	uncultured	uncultured_fa	uncultured_ge
BACT182	Nitrospinae	Nitrospinia	Nitrospinales	Nitrospinaceae	Nitrospina

ASV ID	Phylum	Class	Order	Family	Genus
BACT184	Bacteria_unclassified	Bacteria_unclassified	Bacteria_unclassified	Bacteria_unclassified	Bacteria_unclassified
BACT1845	Proteobacteria	Alphaproteobacteria	SAR11_clade	Clade_II	SAR11
BACT185	Bacteria_unclassified	Bacteria_unclassified	Bacteria_unclassified	Bacteria_unclassified	Bacteria_unclassified
BACT186	Proteobacteria	Proteobacteria_unclassified	Proteobacteria_unclassified	Proteobacteria_unclassified	Proteobacteria_unclassified
BACT188	Proteobacteria	Gammaproteobacteria	Gammaproteobacteria_unclassified	Gammaproteobacteria_unclassified	Gammaproteobacteria_unclassified
BACT189	Proteobacteria	Alphaproteobacteria	Rhodospirillales	Magnetospiraceae	uncultured
BACT19	Proteobacteria	Alphaproteobacteria	Rhodobacterales	Rhodobacteraceae	Rhodobacteraceae_unclassified
BACT190	Bacteroidetes	Bacteroidia	Flavobacteriales	NS9_marine_group	NS9_marine_group_ge
BACT192	Proteobacteria	Gammaproteobacteria	Gammaproteobacteria_unclassified	Gammaproteobacteria_unclassified	Gammaproteobacteria_unclassified
BACT1937	Proteobacteria	Gammaproteobacteria	Thiomicrospirales	Thioglobaceae	SUP05_cluster
BACT195	Nitrospinae	Nitrospinia	Nitrospinales	Nitrospinaceae	Nitrospina
BACT1952	Proteobacteria	Gammaproteobacteria	Thiomicrospirales	Thioglobaceae	SUP05_cluster
BACT196	Bacteroidetes	Bacteroidia	Flavobacteriales	Flavobacteriales_unclassified	Flavobacteriales_unclassified
BACT1970	Proteobacteria	Gammaproteobacteria	Gammaproteobacteria_unclassified	Gammaproteobacteria_unclassified	Gammaproteobacteria_unclassified
BACT199	Bacteria_unclassified	Bacteria_unclassified	Bacteria_unclassified	Bacteria_unclassified	Bacteria_unclassified
BACT2	Proteobacteria	Alphaproteobacteria	SAR11_clade	Clade_I	SAR11
BACT20	Proteobacteria	Gammaproteobacteria	Gammaproteobacteria_unclassified	Gammaproteobacteria_unclassified	Gammaproteobacteria_unclassified
BACT200	Bacteroidetes	Bacteroidia	Flavobacteriales	Flavobacteriaceae	Flavobacteriaceae_unclassified
BACT201	Proteobacteria	Alphaproteobacteria	Caulobacterales	Caulobacteraceae	Brevundimonas
BACT202	Bacteria_unclassified	Bacteria_unclassified	Bacteria_unclassified	Bacteria_unclassified	Bacteria_unclassified
BACT203	Proteobacteria	Alphaproteobacteria	Alphaproteobacteria_unclassified	Alphaproteobacteria_unclassified	Alphaproteobacteria_unclassified
BACT2030	Proteobacteria	Alphaproteobacteria	SAR11_clade	Clade_I	SAR11
BACT204	Proteobacteria	Alphaproteobacteria	Alphaproteobacteria_unclassified	Alphaproteobacteria_unclassified	Alphaproteobacteria_unclassified
BACT2043	Proteobacteria	Gammaproteobacteria	Gammaproteobacteria_unclassified	Gammaproteobacteria_unclassified	Gammaproteobacteria_unclassified
BACT2047	Proteobacteria	Gammaproteobacteria	Gammaproteobacteria_unclassified	Gammaproteobacteria_unclassified	Gammaproteobacteria_unclassified
BACT206	Bacteria_unclassified	Bacteria_unclassified	Bacteria_unclassified	Bacteria_unclassified	Bacteria_unclassified
BACT208	Proteobacteria	Proteobacteria_unclassified	Proteobacteria_unclassified	Proteobacteria_unclassified	Proteobacteria_unclassified
BACT21	Proteobacteria	Gammaproteobacteria	Gammaproteobacteria_unclassified	Gammaproteobacteria_unclassified	Gammaproteobacteria_unclassified

ASV ID	Phylum	Class	Order	Family	Genus
BACT211	Marinimicrobia_	Marinimicrobia__cl	Marinimicrobia__or	Marinimicrobia__fa	Marinimicrobia__ge
BACT212	Nitrospinae	Nitrospinia	Nitrospinales	Nitrospinaceae	Nitrospina
BACT213	Proteobacteria	Gammaproteobacteria	OM182_clade	OM182_clade_fa	OM182_clade_ge
BACT214	Bacteroidetes	Bacteroidia	Flavobacteriales	Flavobacteriaceae	Flavobacteriaceae_unclassified
BACT215	Proteobacteria	Gammaproteobacteria	Gammaproteobacteria_unclassified	Gammaproteobacteria_unclassified	Gammaproteobacteria_unclassified
BACT216	Proteobacteria	Alphaproteobacteria	Alphaproteobacteria_unclassified	Alphaproteobacteria_unclassified	Alphaproteobacteria_unclassified
BACT217	Bacteria_unclassified	Bacteria_unclassified	Bacteria_unclassified	Bacteria_unclassified	Bacteria_unclassified
BACT218	Bacteroidetes	Bacteroidia	Flavobacteriales	NS9_marine_group	NS9_marine_group_ge
BACT219	Proteobacteria	Alphaproteobacteria	Alphaproteobacteria_unclassified	Alphaproteobacteria_unclassified	Alphaproteobacteria_unclassified
BACT22	Bacteroidetes	Bacteroidia	Flavobacteriales	Flavobacteriales_unclassified	Flavobacteriales_unclassified
BACT220	Bacteria_unclassified	Bacteria_unclassified	Bacteria_unclassified	Bacteria_unclassified	Bacteria_unclassified
BACT221	Bacteroidetes	Bacteroidia	Flavobacteriales	NS9_marine_group	NS9_marine_group_ge
BACT222	Bacteroidetes	Bacteroidia	Flavobacteriales	NS9_marine_group	NS9_marine_group_ge
BACT224	Proteobacteria	Alphaproteobacteria	Alphaproteobacteria_unclassified	Alphaproteobacteria_unclassified	Alphaproteobacteria_unclassified
BACT225	Proteobacteria	Gammaproteobacteria	Cellvibrionales	Porticoccaceae	SAR92_clade
BACT2257	Proteobacteria	Alphaproteobacteria	SAR11_clade	Clade_I	SAR11
BACT228	Bacteria_unclassified	Bacteria_unclassified	Bacteria_unclassified	Bacteria_unclassified	Bacteria_unclassified
BACT229	Bacteroidetes	Bacteroidia	Flavobacteriales	NS9_marine_group	NS9_marine_group_ge
BACT23	Proteobacteria	Alphaproteobacteria	SAR11_clade	Clade_II	SAR11
BACT230	Proteobacteria	Proteobacteria_unclassified	Proteobacteria_unclassified	Proteobacteria_unclassified	Proteobacteria_unclassified
BACT231	Proteobacteria	Alphaproteobacteria	Emcibacterales	Emcibacteraceae	Emcibacter
BACT233	Proteobacteria	Alphaproteobacteria	Alphaproteobacteria_unclassified	Alphaproteobacteria_unclassified	Alphaproteobacteria_unclassified
BACT234	Bacteroidetes	Bacteroidia	Bacteroidia_unclassified	Bacteroidia_unclassified	Bacteroidia_unclassified
BACT235	Planctomycetes	OM190	OM190_or	OM190_fa	OM190_ge
BACT236	Bacteria_unclassified	Bacteria_unclassified	Bacteria_unclassified	Bacteria_unclassified	Bacteria_unclassified
BACT237	Nitrospinae	Nitrospinia	Nitrospinales	Nitrospinaceae	Nitrospina
BACT2383	Proteobacteria	Alphaproteobacteria	SAR11_clade	Clade_I	SAR11
BACT24	Bacteroidetes	Bacteroidia	Flavobacteriales	Flavobacteriaceae	NS4_marine_group

ASV ID	Phylum	Class	Order	Family	Genus
BACT241	Verrucomicrobia	Verrucomicrobiae	Verrucomicrobiales	DEV007	DEV007_ge
BACT242	Verrucomicrobia	Verrucomicrobiae	Opitutales	Puniceicoccaceae	Puniceicoccaceae_unclassified
BACT243	Bacteroidetes	Bacteroidia	Chitinophagales	Saprospiraceae	Saprospiraceae_unclassified
BACT244	Proteobacteria	Gammaproteobacteria	Cellvibrionales	Porticoccaceae	SAR92_clade
BACT2440	Proteobacteria	Gammaproteobacteria	Gammaproteobacteria_unclassified	Gammaproteobacteria_unclassified	Gammaproteobacteria_unclassified
BACT2453	Epsilonbacteraeota	Campylobacteria	Campylobacterales	Arcobacteraceae	Arcobacter
BACT2458	Proteobacteria	Gammaproteobacteria	Gammaproteobacteria_unclassified	Gammaproteobacteria_unclassified	Gammaproteobacteria_unclassified
BACT246	Marinimicrobia_	Marinimicrobia__cl	Marinimicrobia__or	Marinimicrobia__fa	Marinimicrobia__ge
BACT247	Proteobacteria	Gammaproteobacteria	OM182_clade	OM182_clade_fa	OM182_clade_ge
BACT25	Proteobacteria	Alphaproteobacteria	SAR11_clade	Clade_I	SAR11
BACT250	Nitrospinae	Nitrospinia	Nitrospinales	Nitrospinaceae	Nitrospina
BACT251	Bacteroidetes	Bacteroidia	Bacteroidales	Bacteroidales_unclassified	Bacteroidales_unclassified
BACT253	Chloroflexi	Dehalococcoidia	Dehalococcoidia_unclassified	Dehalococcoidia_unclassified	Dehalococcoidia_unclassified
BACT254	Proteobacteria	Proteobacteria_unclassified	Proteobacteria_unclassified	Proteobacteria_unclassified	Proteobacteria_unclassified
BACT256	Proteobacteria	Gammaproteobacteria	Gammaproteobacteria_unclassified	Gammaproteobacteria_unclassified	Gammaproteobacteria_unclassified
BACT257	Proteobacteria	Deltaproteobacteria	PB19	PB19_fa	PB19_ge
BACT259	Proteobacteria	Alphaproteobacteria	Caulobacterales	Caulobacteraceae	Brevundimonas
BACT26	Bacteria_unclassified	Bacteria_unclassified	Bacteria_unclassified	Bacteria_unclassified	Bacteria_unclassified
BACT260	Proteobacteria	Deltaproteobacteria	Desulfobacterales	Desulfobacterales_unclassified	Desulfobacterales_unclassified
BACT261	Bacteria_unclassified	Bacteria_unclassified	Bacteria_unclassified	Bacteria_unclassified	Bacteria_unclassified
BACT262	Proteobacteria	Alphaproteobacteria	SAR11_clade	Clade_II	SAR11
BACT264	Proteobacteria	Alphaproteobacteria	Rhodobacterales	Rhodobacteraceae	uncultured
BACT265	Proteobacteria	Gammaproteobacteria	Betaproteobacteriales	Betaproteobacteriales_unclassified	Betaproteobacteriales_unclassified
BACT268	Proteobacteria	Proteobacteria_unclassified	Proteobacteria_unclassified	Proteobacteria_unclassified	Proteobacteria_unclassified
BACT27	Proteobacteria	Alphaproteobacteria	Rhizobiales	Rhizobiales_unclassified	Rhizobiales_unclassified
BACT270	Proteobacteria	Gammaproteobacteria	SAR86_clade	SAR86_clade_fa	SAR86_clade_ge
BACT2714	Proteobacteria	Gammaproteobacteria	Thiomicrospirales	Thioglobaceae	SUP05_cluster
BACT2723	Proteobacteria	Gammaproteobacteria	Oceanospirillales	Nitrincolaceae	Marinobacterium

ASV ID	Phylum	Class	Order	Family	Genus
BACT273	Proteobacteria	Alphaproteobacteria	Alphaproteobacteria_unclassified	Alphaproteobacteria_unclassified	Alphaproteobacteria_unclassified
BACT274	Proteobacteria	Gammaproteobacteria	OM182_clade	OM182_clade_fa	OM182_clade_ge
BACT2746	Proteobacteria	Gammaproteobacteria	Ectothiorhodospirales	Ectothiorhodospiraceae	uncultured
BACT276	Proteobacteria	Alphaproteobacteria	Alphaproteobacteria_unclassified	Alphaproteobacteria_unclassified	Alphaproteobacteria_unclassified
BACT28	Proteobacteria	Alphaproteobacteria	Alphaproteobacteria_unclassified	Alphaproteobacteria_unclassified	Alphaproteobacteria_unclassified
BACT280	Bacteroidetes	Bacteroidia	Bacteroidales	Bacteroidetes_BD2-2	Bacteroidetes_BD2-2_ge
BACT2802	Proteobacteria	Gammaproteobacteria	Thiomicrospirales	Thioglobaceae	SUP05_cluster
BACT281	Bacteroidetes	Bacteroidetes_unclassified	Bacteroidetes_unclassified	Bacteroidetes_unclassified	Bacteroidetes_unclassified
BACT283	Bacteria_unclassified	Bacteria_unclassified	Bacteria_unclassified	Bacteria_unclassified	Bacteria_unclassified
BACT284	Bacteroidetes	Bacteroidia	Bacteroidia_unclassified	Bacteroidia_unclassified	Bacteroidia_unclassified
BACT285	Bacteria_unclassified	Bacteria_unclassified	Bacteria_unclassified	Bacteria_unclassified	Bacteria_unclassified
BACT2857	Proteobacteria	Gammaproteobacteria	Thiomicrospirales	Thioglobaceae	SUP05_cluster
BACT286	Proteobacteria	Deltaproteobacteria	PB19	PB19_fa	PB19_ge
BACT287	Bacteria_unclassified	Bacteria_unclassified	Bacteria_unclassified	Bacteria_unclassified	Bacteria_unclassified
BACT289	Bacteroidetes	Bacteroidia	Bacteroidia_unclassified	Bacteroidia_unclassified	Bacteroidia_unclassified
BACT29	Marinimicrobia_	Marinimicrobia__cl	Marinimicrobia__or	Marinimicrobia__fa	Marinimicrobia__ge
BACT290	Bacteria_unclassified	Bacteria_unclassified	Bacteria_unclassified	Bacteria_unclassified	Bacteria_unclassified
BACT291	Verrucomicrobia	Verrucomicrobiae	Opitutales	Puniceicoccaceae	MB11C04_marine_group
BACT292	Bacteroidetes	Bacteroidia	Flavobacteriales	Flavobacteriaceae	NS4_marine_group
BACT298	Proteobacteria	Alphaproteobacteria	SAR11_clade	Clade_II	SAR11
BACT299	Proteobacteria	Alphaproteobacteria	Alphaproteobacteria_unclassified	Alphaproteobacteria_unclassified	Alphaproteobacteria_unclassified
BACT3	Proteobacteria	Gammaproteobacteria	Thiomicrospirales	Thioglobaceae	SUP05_cluster
BACT30	Marinimicrobia_	Marinimicrobia__cl	Marinimicrobia__or	Marinimicrobia__fa	Marinimicrobia__ge
BACT301	Proteobacteria	Proteobacteria_unclassified	Proteobacteria_unclassified	Proteobacteria_unclassified	Proteobacteria_unclassified
BACT302	Bacteria_unclassified	Bacteria_unclassified	Bacteria_unclassified	Bacteria_unclassified	Bacteria_unclassified
BACT304	Proteobacteria	Gammaproteobacteria	Gammaproteobacteria_unclassified	Gammaproteobacteria_unclassified	Gammaproteobacteria_unclassified
BACT31	Proteobacteria	Alphaproteobacteria	Alphaproteobacteria_unclassified	Alphaproteobacteria_unclassified	Alphaproteobacteria_unclassified
BACT311	Proteobacteria	Alphaproteobacteria	Alphaproteobacteria_unclassified	Alphaproteobacteria_unclassified	Alphaproteobacteria_unclassified

ASV ID	Phylum	Class	Order	Family	Genus
BACT315	Proteobacteria	Deltaproteobacteria	Deltaproteobacteria_unclassified	Deltaproteobacteria_unclassified	Deltaproteobacteria_unclassified
BACT317	Bacteroidetes	Bacteroidia	Flavobacteriales	Flavobacteriaceae	Flavobacteriaceae_unclassified
BACT318	Bacteria_unclassified	Bacteria_unclassified	Bacteria_unclassified	Bacteria_unclassified	Bacteria_unclassified
BACT319	Proteobacteria	Deltaproteobacteria	SAR324_clade	SAR324_clade_fa	SAR324_clade_ge
BACT32	Bacteria_unclassified	Bacteria_unclassified	Bacteria_unclassified	Bacteria_unclassified	Bacteria_unclassified
BACT3201	Proteobacteria	Gammaproteobacteria	Thiomicrospirales	Thioglobaceae	SUP05_cluster
BACT321	Proteobacteria	Gammaproteobacteria	Alteromonadales	Pseudoalteromonadaceae	Pseudoalteromonas
BACT3229	Proteobacteria	Gammaproteobacteria	Gammaproteobacteria_unclassified	Gammaproteobacteria_unclassified	Gammaproteobacteria_unclassified
BACT325	Bacteria_unclassified	Bacteria_unclassified	Bacteria_unclassified	Bacteria_unclassified	Bacteria_unclassified
BACT327	Bacteria_unclassified	Bacteria_unclassified	Bacteria_unclassified	Bacteria_unclassified	Bacteria_unclassified
BACT328	Proteobacteria	Alphaproteobacteria	Alphaproteobacteria_unclassified	Alphaproteobacteria_unclassified	Alphaproteobacteria_unclassified
BACT33	Proteobacteria	Alphaproteobacteria	SAR11_clade	Clade_I	SAR11
BACT332	Proteobacteria	Deltaproteobacteria	Oligoflexales	053A03-B-DI-P58	053A03-B-DI-P58_ge
BACT336	Nitrospinae	Nitrospinia	Nitrospinales	Nitrospinaceae	Nitrospina
BACT338	Bacteria_unclassified	Bacteria_unclassified	Bacteria_unclassified	Bacteria_unclassified	Bacteria_unclassified
BACT34	Proteobacteria	Alphaproteobacteria	Rhodobacterales	Rhodobacteraceae	Rhodobacteraceae_unclassified
BACT340	Bacteroidetes	Bacteroidia	Bacteroidia_unclassified	Bacteroidia_unclassified	Bacteroidia_unclassified
BACT3415	Proteobacteria	Gammaproteobacteria	Thiomicrospirales	Thioglobaceae	SUP05_cluster
BACT3459	Proteobacteria	Alphaproteobacteria	Rhodobacterales	Rhodobacteraceae	Rhodobacteraceae_unclassified
BACT350	Proteobacteria	Alphaproteobacteria	Alphaproteobacteria_unclassified	Alphaproteobacteria_unclassified	Alphaproteobacteria_unclassified
BACT3503	Proteobacteria	Gammaproteobacteria	Thiomicrospirales	Thioglobaceae	SUP05_cluster
BACT354	Bacteria_unclassified	Bacteria_unclassified	Bacteria_unclassified	Bacteria_unclassified	Bacteria_unclassified
BACT356	Proteobacteria	Alphaproteobacteria	Rhizobiales	Xanthobacteraceae	Bradyrhizobium
BACT357	Proteobacteria	Alphaproteobacteria	Alphaproteobacteria_unclassified	Alphaproteobacteria_unclassified	Alphaproteobacteria_unclassified
BACT358	Proteobacteria	Alphaproteobacteria	SAR11_clade	SAR11_clade_unclassified	SAR11
BACT36	Marinimicrobia_	Marinimicrobia__cl	Marinimicrobia__or	Marinimicrobia__fa	Marinimicrobia__ge
BACT360	Proteobacteria	Gammaproteobacteria	Gammaproteobacteria_unclassified	Gammaproteobacteria_unclassified	Gammaproteobacteria_unclassified
BACT361	Cyanobacteria	Oxyphotobacteria	Synechococcales	Cyanobiaceae	Synechococcus_CC9902

ASV ID	Phylum	Class	Order	Family	Genus
BACT37	Proteobacteria	Alphaproteobacteria	SAR11_clade	Clade_II	SAR11
BACT379	Bacteroidetes	Bacteroidia	Flavobacteriales	Flavobacteriaceae	Flavobacteriaceae_unclassified
BACT38	Proteobacteria	Gammaproteobacteria	Gammaproteobacteria_unclassified	Gammaproteobacteria_unclassified	Gammaproteobacteria_unclassified
BACT387	Proteobacteria	Alphaproteobacteria	Rhodospirillales	Magnetospiraceae	uncultured
BACT39	Proteobacteria	Gammaproteobacteria	Betaproteobacteriales	Methylophilaceae	OM43_clade
BACT396	Proteobacteria	Alphaproteobacteria	SAR11_clade	Clade_I	SAR11
BACT397	Proteobacteria	Alphaproteobacteria	SAR11_clade	Clade_I	SAR11
BACT4	Proteobacteria	Alphaproteobacteria	SAR11_clade	Clade_I	SAR11
BACT40	Proteobacteria	Alphaproteobacteria	Alphaproteobacteria_unclassified	Alphaproteobacteria_unclassified	Alphaproteobacteria_unclassified
BACT400	Proteobacteria	Gammaproteobacteria	Gammaproteobacteria_unclassified	Gammaproteobacteria_unclassified	Gammaproteobacteria_unclassified
BACT41	Proteobacteria	Deltaproteobacteria	Desulfobacterales	Desulfobacteraceae	uncultured
BACT411	Bacteria_unclassified	Bacteria_unclassified	Bacteria_unclassified	Bacteria_unclassified	Bacteria_unclassified
BACT416	Proteobacteria	Alphaproteobacteria	SAR11_clade	Clade_II	SAR11
BACT42	Verrucomicrobia	Verrucomicrobiae	Verrucomicrobiales	Rubritaleaceae	Roseibacillus
BACT43	Proteobacteria	Gammaproteobacteria	SAR86_clade	SAR86_clade_fa	SAR86_clade_ge
BACT430	Proteobacteria	Alphaproteobacteria	SAR11_clade	Clade_II	SAR11
BACT4309	Proteobacteria	Alphaproteobacteria	Rhodobacterales	Rhodobacteraceae	Amylibacter
BACT4344	Proteobacteria	Alphaproteobacteria	SAR11_clade	Clade_I	SAR11
BACT44	Planctomycetes	Planctomycetes_unclassified	Planctomycetes_unclassified	Planctomycetes_unclassified	Planctomycetes_unclassified
BACT443	Verrucomicrobia	Verrucomicrobiae	Opitutales	Puniceicoccaceae	MB11C04_marine_group
BACT45	Bacteroidetes	Bacteroidia	Flavobacteriales	Flavobacteriales_unclassified	Flavobacteriales_unclassified
BACT455	Proteobacteria	Proteobacteria_unclassified	Proteobacteria_unclassified	Proteobacteria_unclassified	Proteobacteria_unclassified
BACT46	Proteobacteria	Alphaproteobacteria	Rhodobacterales	Rhodobacteraceae	Tateyamaria
BACT4625	Proteobacteria	Gammaproteobacteria	Thiomicrospirales	Thioglobaceae	SUP05_cluster
BACT465	Proteobacteria	Deltaproteobacteria	Desulfobacterales	Desulfobulbaceae	Desulfobulbaceae_unclassified
BACT47	Proteobacteria	Gammaproteobacteria	UBA10353_marine_group	UBA10353_marine_group_fa	UBA10353_marine_group_ge
BACT474	Bacteria_unclassified	Bacteria_unclassified	Bacteria_unclassified	Bacteria_unclassified	Bacteria_unclassified
BACT475	Bacteroidetes	Bacteroidia	Flavobacteriales	NS9_marine_group	NS9_marine_group_ge

ASV ID	Phylum	Class	Order	Family	Genus
BACT478	Bacteria_unclassified	Bacteria_unclassified	Bacteria_unclassified	Bacteria_unclassified	Bacteria_unclassified
BACT48	Proteobacteria	Proteobacteria_unclassified	Proteobacteria_unclassified	Proteobacteria_unclassified	Proteobacteria_unclassified
BACT49	Verrucomicrobia	Verrucomicrobiae	Verrucomicrobiae_unclassified	Verrucomicrobiae_unclassified	Verrucomicrobiae_unclassified
BACT491	Bacteria_unclassified	Bacteria_unclassified	Bacteria_unclassified	Bacteria_unclassified	Bacteria_unclassified
BACT5	Proteobacteria	Alphaproteobacteria	Rhodobacterales	Rhodobacteraceae	Amylibacter
BACT50	Bacteria_unclassified	Bacteria_unclassified	Bacteria_unclassified	Bacteria_unclassified	Bacteria_unclassified
BACT508	Bacteroidetes	Bacteroidia	Flavobacteriales	NS9_marine_group	NS9_marine_group_ge
BACT51	Proteobacteria	Proteobacteria_unclassified	Proteobacteria_unclassified	Proteobacteria_unclassified	Proteobacteria_unclassified
BACT52	Proteobacteria	Alphaproteobacteria	Alphaproteobacteria_unclassified	Alphaproteobacteria_unclassified	Alphaproteobacteria_unclassified
BACT53	Verrucomicrobia	Verrucomicrobiae	Arctic97B-4_marine_group	Arctic97B-4_marine_group_fa	Arctic97B-4_marine_group_ge
BACT54	Proteobacteria	Deltaproteobacteria	Deltaproteobacteria_unclassified	Deltaproteobacteria_unclassified	Deltaproteobacteria_unclassified
BACT55	Proteobacteria	Alphaproteobacteria	Rhodobacterales	Rhodobacteraceae	Rhodobacteraceae_unclassified
BACT56	Proteobacteria	Alphaproteobacteria	Rhizobiales	Beijerinckiaceae	Methylobacterium
BACT57	Proteobacteria	Gammaproteobacteria	SAR86_clade	SAR86_clade_fa	SAR86_clade_ge
BACT58	Actinobacteria	Acidimicrobiia	Microtrichales	Microtrichaceae	Sva0996_marine_group
BACT59	Proteobacteria	Alphaproteobacteria	Rhodobacterales	Rhodobacteraceae	Rhodobacteraceae_unclassified
BACT6	Epsilonbacteraeota	Campylobacteria	Campylobacterales	Arcobacteraceae	Arcobacter
BACT60	Proteobacteria	Gammaproteobacteria	Oceanospirillales	Pseudohongiellaceae	Pseudohongiella
BACT61	Proteobacteria	Deltaproteobacteria	Desulfobacterales	Desulfobacteraceae	uncultured
BACT62	Planctomycetes	Planctomycetes_unclassified	Planctomycetes_unclassified	Planctomycetes_unclassified	Planctomycetes_unclassified
BACT63	Proteobacteria	Proteobacteria_unclassified	Proteobacteria_unclassified	Proteobacteria_unclassified	Proteobacteria_unclassified
BACT636	Proteobacteria	Alphaproteobacteria	Rhodobacterales	Rhodobacteraceae	Amylibacter
BACT64	Proteobacteria	Gammaproteobacteria	UBA10353_marine_group	UBA10353_marine_group_fa	UBA10353_marine_group_ge
BACT644	Proteobacteria	Alphaproteobacteria	Alphaproteobacteria_unclassified	Alphaproteobacteria_unclassified	Alphaproteobacteria_unclassified
BACT65	Verrucomicrobia	Verrucomicrobiae	Verrucomicrobiales	Verrucomicrobiales_unclassified	Verrucomicrobiales_unclassified
BACT66	Bacteroidetes	Bacteroidia	Flavobacteriales	Flavobacteriaceae	Flavobacteriaceae_unclassified
BACT661	Proteobacteria	Gammaproteobacteria	Thiomicrospirales	Thioglobaceae	SUP05_cluster
BACT67	Proteobacteria	Alphaproteobacteria	Alphaproteobacteria_unclassified	Alphaproteobacteria_unclassified	Alphaproteobacteria_unclassified

ASV ID	Phylum	Class	Order	Family	Genus
BACT68	Marinimicrobia_	Marinimicrobia__cl	Marinimicrobia__or	Marinimicrobia__fa	Marinimicrobia__ge
BACT7	Proteobacteria	Gammaproteobacteria	Ectothiorhodospirales	Ectothiorhodospiraceae	uncultured
BACT70	Bacteroidetes	Bacteroidia	Cytophagales	Cytophagales_unclassified	Cytophagales_unclassified
BACT71	Bacteroidetes	Bacteroidia	Flavobacteriales	Flavobacteriaceae	NS5_marine_group
BACT72	Nitrospinae	Nitrospinia	Nitrospinales	Nitrospinaceae	Nitrospina
BACT73	Bacteroidetes	Bacteroidia	Flavobacteriales	NS9_marine_group	NS9_marine_group_ge
BACT736	Proteobacteria	Gammaproteobacteria	Alteromonadales	Colwelliaceae	Colwellia
BACT74	Bacteroidetes	Bacteroidia	Bacteroidia_unclassified	Bacteroidia_unclassified	Bacteroidia_unclassified
BACT75	Bacteria_unclassified	Bacteria_unclassified	Bacteria_unclassified	Bacteria_unclassified	Bacteria_unclassified
BACT76	Actinobacteria	Acidimicrobiia	Microtrichales	Microtrichaceae	Sva0996_marine_group
BACT761	Proteobacteria	Alphaproteobacteria	SAR11_clade	Clade_I	SAR11
BACT77	Proteobacteria	Deltaproteobacteria	Desulfobacterales	Desulfobacteraceae	uncultured
BACT79	Bacteroidetes	Bacteroidia	Flavobacteriales	Flavobacteriaceae	Flavobacterium
BACT8	Proteobacteria	Gammaproteobacteria	Gammaproteobacteria_unclassified	Gammaproteobacteria_unclassified	Gammaproteobacteria_unclassified
BACT80	Bacteroidetes	Bacteroidia	Flavobacteriales	Flavobacteriaceae	Flavobacteriaceae_unclassified
BACT81	Proteobacteria	Gammaproteobacteria	Ectothiorhodospirales	Ectothiorhodospiraceae	uncultured
BACT82	Proteobacteria	Alphaproteobacteria	SAR11_clade	Clade_I	SAR11
BACT84	Bacteria_unclassified	Bacteria_unclassified	Bacteria_unclassified	Bacteria_unclassified	Bacteria_unclassified
BACT86	Verrucomicrobia	Verrucomicrobiae	Opitutales	Puniceicoccaceae	MB11C04_marine_group
BACT87	Bacteroidetes	Bacteroidia	Bacteroidales	Bacteroidales_unclassified	Bacteroidales_unclassified
BACT88	Proteobacteria	Alphaproteobacteria	Alphaproteobacteria_unclassified	Alphaproteobacteria_unclassified	Alphaproteobacteria_unclassified
BACT89	Marinimicrobia_	Marinimicrobia__cl	Marinimicrobia__or	Marinimicrobia__fa	Marinimicrobia__ge
BACT9	Bacteria_unclassified	Bacteria_unclassified	Bacteria_unclassified	Bacteria_unclassified	Bacteria_unclassified
BACT90	Bacteroidetes	Bacteroidia	Flavobacteriales	Flavobacteriaceae	Flavobacteriaceae_unclassified
BACT906	Proteobacteria	Alphaproteobacteria	SAR11_clade	Clade_II	SAR11
BACT91	Proteobacteria	Gammaproteobacteria	Betaproteobacteriales	Betaproteobacteriales_unclassified	Betaproteobacteriales_unclassified
BACT92	Bacteria_unclassified	Bacteria_unclassified	Bacteria_unclassified	Bacteria_unclassified	Bacteria_unclassified
BACT93	Nitrospinae	Nitrospinia	Nitrospinales	Nitrospinaceae	Nitrospina

ASV ID	Phylum	Class	Order	Family	Genus
BACT94	Marinimicrobia_	Marinimicrobia__cl	Marinimicrobia__or	Marinimicrobia__fa	Marinimicrobia__ge
BACT95	Proteobacteria	Alphaproteobacteria	SAR11_clade	Clade_II	SAR11
BACT97	Proteobacteria	Alphaproteobacteria	Alphaproteobacteria_unclassified	Alphaproteobacteria_unclassified	Alphaproteobacteria_unclassified
BACT98	Proteobacteria	Alphaproteobacteria	Alphaproteobacteria_unclassified	Alphaproteobacteria_unclassified	Alphaproteobacteria_unclassified
BACT99	Proteobacteria	Deltaproteobacteria	Deltaproteobacteria_unclassified	Deltaproteobacteria_unclassified	Deltaproteobacteria_unclassified
BACT998	Proteobacteria	Alphaproteobacteria	SAR11_clade	SAR11_clade_unclassified	SAR11
BACT998	Proteobacteria	Alphaproteobacteria	SAR11_clade	SAR11_clade_unclassified	SAR11

Appendix B. Supplementary Data: Results of WGCNA

Correlations between prokaryotic ASVs and sample traits determined through weighted gene correlational network analyses (WGCNA). Pearson correlation coefficients (GS) and corresponding p values (p) are reported for pairwise correlations between ALL prokaryotic ASVs and sample traits calculated by Weighted Gene Correlational Network Analysis (WGCNA). Variables kTotal, kIn and kOut define whole-network connectivity, intra-subnetwork connectivity and extra-subnetwork connectivity, respectively. Subnetwork membership (SM) estimates for SNET1, SNET2, and SNET3 are also reported. Sample traits considered include nitrification rates, delta N_2O values, N_2O yields from nitrification, and N_2O production rates from NO3 reduction and NH4 oxidation.

ASV	Subtnet	SM1	SM2	SM3	kTotal	kIn	kOut	GS.Nit	p.Nit	GS. N2O	p. N2O	GS.NO3	p.NO3	GS.NH4	p.NH4	GS.Yld	p.Yld
ARCH1	SNET1	0.51	-0.11	-0.64	10.91	10.14	0.77	-0.29	0.2388	-0.08	0.7630	0.33	0.1776	-0.03	0.9064	0.20	0.4361
ARCH10	SNET3	-0.64	0.24	0.75	25.89	23.94	1.94	0.21	0.3989	0.26	0.3049	-0.39	0.1118	-0.19	0.4546	-0.35	0.1587
ARCH11	SNET3	-0.53	0.23	0.58	16.31	14.39	1.92	0.10	0.6801	0.54	0.0218	-0.45	0.0638	0.06	0.8129	-0.31	0.2051
ARCH13	SNET2	-0.32	0.46	0.20	10.58	5.25	5.33	0.33	0.1833	0.61	0.0072	-0.11	0.6609	0.16	0.5382	-0.46	0.0544
ARCH130	SNET3	-0.40	-0.08	0.57	14.38	13.82	0.55	0.09	0.7206	-0.18	0.4838	-0.16	0.5323	-0.13	0.6052	-0.09	0.7193
ARCH14	SNET2	-0.47	0.52	0.40	14.12	6.28	7.85	0.35	0.1562	0.04	0.8697	0.05	0.8454	-0.19	0.4471	-0.29	0.2483
ARCH15	SNET3	-0.57	0.22	0.62	16.63	14.81	1.82	0.09	0.7089	0.46	0.0565	-0.48	0.0443	-0.31	0.2159	-0.33	0.1862
ARCH16	SNET3	-0.45	0.27	0.42	10.39	8.06	2.32	0.07	0.7762	0.67	0.0025	-0.54	0.0213	0.05	0.8459	-0.29	0.2418
ARCH18	SNET3	-0.81	0.46	0.87	42.25	37.11	5.14	0.39	0.1061	0.36	0.1443	-0.61	0.0067	0.00	0.9944	-0.46	0.0554
ARCH19	SNET3	-0.76	0.40	0.83	34.12	30.76	3.36	0.18	0.4695	0.48	0.0420	-0.59	0.0107	-0.43	0.0774	-0.49	0.0413
ARCH2	SNET3	-0.54	0.45	0.47	16.99	11.41	5.58	0.03	0.9073	0.48	0.0434	-0.50	0.0335	-0.24	0.3316	-0.46	0.0556
ARCH20	SNET3	-0.53	0.49	0.52	19.21	12.77	6.44	0.54	0.0198	0.20	0.4293	0.07	0.7745	0.07	0.7674	-0.31	0.2179
ARCH22	SNET3	-0.36	-0.09	0.52	13.00	12.31	0.69	0.31	0.2099	-0.09	0.7239	-0.30	0.2268	-0.04	0.8836	-0.24	0.3378
ARCH24	SNET3	-0.37	-0.16	0.51	12.28	11.47	0.81	-0.21	0.4101	0.16	0.5228	-0.31	0.2035	-0.30	0.2338	-0.20	0.4201
ARCH26	SNET2	-0.44	0.64	0.33	14.76	7.76	7.00	0.35	0.1526	0.51	0.0306	-0.18	0.4863	0.08	0.7377	-0.25	0.3245
ARCH28	SNET1	0.86	-0.67	-0.83	37.25	37.17	0.08	-0.39	0.1100	-0.75	0.0004	0.63	0.0055	0.17	0.4889	0.61	0.0075
ARCH29	SNET2	-0.67	0.83	0.53	27.04	14.44	12.60	0.32	0.1900	0.51	0.0311	-0.23	0.3523	-0.33	0.1844	-0.21	0.4009
ARCH3	SNET1	0.75	-0.27	-0.86	24.99	24.53	0.46	-0.28	0.2540	-0.32	0.1935	0.56	0.0160	0.08	0.7658	0.35	0.1514
ARCH30	SNET1	0.10	0.18	-0.20	5.68	3.63	2.04	0.30	0.2250	0.19	0.4424	0.18	0.4627	0.48	0.0431	-0.21	0.3959
ARCH32	SNET2	-0.66	0.78	0.54	23.85	11.94	11.92	0.26	0.2910	0.58	0.0111	-0.24	0.3308	-0.35	0.1546	-0.43	0.0759

ASV	Subtnet	SM1	SM2	SM3	kTotal	kIn	kOut	GS.Nit	p.Nit	GS. N2O	p. N2O	GS.NO3	p.NO3	GS.NH4	p.NH4	GS.Yld	p.Yld
ARCH34	SNET3	-0.71	0.37	0.79	31.29	27.92	3.37	0.41	0.0905	0.29	0.2446	-0.61	0.0075	-0.13	0.6080	-0.42	0.0842
ARCH35	SNET2	-0.67	0.74	0.54	23.82	10.92	12.90	0.34	0.1640	0.58	0.0112	-0.29	0.2368	-0.26	0.2978	-0.59	0.0100
ARCH36	SNET1	0.25	0.21	-0.44	11.36	9.04	2.32	-0.13	0.6098	0.36	0.1463	0.21	0.3929	0.17	0.5061	-0.16	0.5380
ARCH37	SNET1	0.90	-0.75	-0.84	42.26	42.20	0.07	-0.48	0.0416	-0.73	0.0006	0.50	0.0357	0.11	0.6663	0.65	0.0032
ARCH4	SNET1	0.67	-0.25	-0.78	18.31	17.86	0.45	-0.24	0.3476	-0.18	0.4660	0.36	0.1376	0.10	0.6875	0.32	0.1895
ARCH40	SNET1	0.90	-0.76	-0.85	41.75	41.68	0.06	-0.54	0.0219	-0.70	0.0012	0.49	0.0403	0.11	0.6732	0.61	0.0067
ARCH42	SNET1	0.88	-0.74	-0.83	40.55	40.49	0.06	-0.52	0.0265	-0.68	0.0019	0.52	0.0262	0.03	0.9074	0.62	0.0061
ARCH50	SNET1	0.20	-0.26	-0.12	3.80	2.37	1.43	0.02	0.9344	-0.42	0.0835	-0.06	0.8283	-0.03	0.8996	0.03	0.9087
ARCH51	SNET2	-0.39	0.72	0.20	13.53	9.37	4.17	0.28	0.2535	0.64	0.0046	-0.23	0.3594	0.09	0.7137	-0.25	0.3167
ARCH52	SNET1	0.85	-0.76	-0.78	36.58	36.50	0.08	-0.51	0.0295	-0.72	0.0008	0.38	0.1210	0.07	0.7696	0.63	0.0053
ARCH57	SNET2	-0.24	0.38	0.15	6.76	3.51	3.24	0.32	0.1979	-0.16	0.5382	0.22	0.3800	-0.05	0.8407	-0.05	0.8478
ARCH6	SNET2	-0.53	0.55	0.44	16.31	7.08	9.23	0.37	0.1253	0.63	0.0050	-0.22	0.3790	0.19	0.4498	-0.29	0.2489
ARCH61	SNET3	-0.31	-0.21	0.49	11.71	11.30	0.42	0.02	0.9426	-0.12	0.6265	-0.18	0.4749	-0.20	0.4345	-0.11	0.6621
ARCH63	SNET1	0.85	-0.73	-0.79	35.97	35.90	0.07	-0.38	0.1182	-0.73	0.0005	0.37	0.1270	0.12	0.6412	0.59	0.0107
ARCH65	SNET1	0.11	-0.30	0.00	3.21	1.62	1.59	0.02	0.9488	-0.41	0.0939	-0.31	0.2172	-0.25	0.3117	0.21	0.3998
ARCH7	SNET1	0.34	0.13	-0.50	12.61	11.09	1.52	0.08	0.7551	0.11	0.6749	0.37	0.1346	0.29	0.2381	0.07	0.7927
ARCH8	SNET3	-0.70	0.30	0.79	30.11	27.55	2.56	0.25	0.3245	0.34	0.1660	-0.45	0.0631	-0.04	0.8680	-0.34	0.1679
ARCH9	SNET2	-0.65	0.61	0.57	24.39	9.50	14.90	0.52	0.0267	0.57	0.0131	-0.20	0.4257	0.11	0.6746	-0.57	0.0140
BACT1	SNET1	0.92	-0.65	-0.94	43.96	43.87	0.09	-0.37	0.1256	-0.41	0.0898	0.45	0.0583	0.21	0.4002	0.39	0.1139
BACT10	SNET3	-0.95	0.77	0.89	54.53	41.43	13.09	0.27	0.2791	0.78	0.0001	-0.73	0.0006	-0.26	0.2931	-0.57	0.0144
BACT101	SNET2	-0.80	0.94	0.65	39.51	19.45	20.07	0.25	0.3079	0.82	0.0000	-0.41	0.0904	-0.26	0.3009	-0.52	0.0283
BACT102	SNET1	0.72	-0.29	-0.79	22.97	22.41	0.57	-0.33	0.1794	-0.37	0.1266	0.59	0.0093	-0.09	0.7283	0.42	0.0825
BACT103	SNET2	-0.80	0.86	0.69	37.58	16.49	21.08	0.56	0.0151	0.54	0.0208	-0.18	0.4666	0.16	0.5212	-0.50	0.0334
BACT104	SNET3	-0.79	0.39	0.86	40.41	35.80	4.60	0.36	0.1440	0.17	0.5092	-0.42	0.0829	-0.22	0.3869	-0.39	0.1089
BACT105	SNET3	-0.67	0.71	0.59	26.99	16.08	10.91	0.18	0.4850	0.39	0.1057	-0.50	0.0352	-0.19	0.4598	-0.25	0.3075
BACT106	SNET3	-0.58	0.23	0.69	22.66	20.40	2.26	0.27	0.2871	0.08	0.7594	-0.27	0.2782	-0.17	0.4933	-0.30	0.2325
BACT107	SNET2	-0.28	0.53	0.15	11.05	6.39	4.67	0.00	0.9986	0.50	0.0348	-0.23	0.3663	-0.06	0.8039	-0.13	0.5969
BACT108	SNET3	-0.87	0.60	0.88	44.44	36.99	7.44	0.16	0.5343	0.61	0.0070	-0.70	0.0012	-0.40	0.0961	-0.45	0.0597

ASV	Subtnet	SM1	SM2	SM3	kTotal	kIn	kOut	GS.Nit	p.Nit	GS. N2O	p. N2O	GS.NO3	p.NO3	GS.NH4	p.NH4	GS.Yld	p.Yld
BACT109	SNET2	-0.25	0.71	0.02	14.45	9.67	4.79	0.06	0.8033	0.61	0.0071	-0.10	0.6993	-0.13	0.6153	-0.20	0.4189
BACT11	SNET1	-0.34	0.46	0.20	10.96	2.90	8.06	0.15	0.5424	0.59	0.0100	-0.18	0.4770	-0.01	0.9693	-0.24	0.3419
BACT110	SNET3	-0.85	0.82	0.75	41.56	27.36	14.19	0.23	0.3638	0.89	0.0000	-0.69	0.0016	-0.26	0.2907	-0.47	0.0501
BACT1103	SNET1	0.19	0.05	-0.31	11.64	10.21	1.43	-0.01	0.9668	0.29	0.2409	-0.02	0.9354	0.14	0.5700	-0.29	0.2515
BACT111	SNET1	0.64	-0.24	-0.72	17.38	16.94	0.44	-0.24	0.3364	-0.38	0.1229	0.46	0.0556	-0.02	0.9506	0.48	0.0422
BACT112	SNET3	-0.81	0.75	0.74	38.03	26.20	11.83	0.37	0.1295	0.76	0.0003	-0.76	0.0002	-0.11	0.6589	-0.49	0.0394
BACT113	SNET2	-0.10	0.60	-0.11	9.63	6.63	3.00	0.08	0.7660	0.32	0.1999	0.25	0.3141	0.17	0.5037	-0.09	0.7171
BACT1131	SNET1	0.91	-0.80	-0.85	43.39	43.35	0.04	-0.44	0.0644	-0.52	0.0284	0.47	0.0464	0.30	0.2276	0.47	0.0504
BACT114	SNET1	0.43	0.11	-0.59	12.15	10.04	2.11	-0.20	0.4222	-0.01	0.9540	0.43	0.0780	-0.13	0.5992	0.26	0.3028
BACT115	SNET1	0.95	-0.79	-0.89	48.57	48.52	0.05	-0.48	0.0435	-0.58	0.0112	0.55	0.0190	0.22	0.3711	0.54	0.0199
BACT116	SNET2	-0.89	0.87	0.80	46.87	16.53	30.34	0.34	0.1729	0.66	0.0031	-0.38	0.1164	-0.35	0.1596	-0.47	0.0490
BACT118	SNET1	0.97	-0.89	-0.89	52.62	52.59	0.04	-0.48	0.0419	-0.66	0.0030	0.53	0.0224	0.17	0.5021	0.49	0.0396
BACT119	SNET3	-0.91	0.63	0.91	52.55	42.22	10.33	0.49	0.0391	0.49	0.0397	-0.49	0.0392	-0.12	0.6487	-0.56	0.0163
BACT12	SNET3	-0.91	0.59	0.90	49.92	41.62	8.30	0.28	0.2688	0.62	0.0061	-0.63	0.0048	-0.26	0.2902	-0.49	0.0389
BACT121	SNET1	0.93	-0.82	-0.85	46.05	45.99	0.07	-0.36	0.1392	-0.78	0.0001	0.67	0.0024	0.13	0.6188	0.55	0.0177
BACT122	SNET2	-0.27	0.60	0.10	10.34	6.47	3.87	-0.08	0.7503	0.47	0.0484	0.02	0.9487	-0.25	0.3227	0.13	0.6053
BACT123	SNET3	-0.71	0.48	0.74	29.36	23.81	5.55	0.47	0.0508	0.14	0.5798	-0.13	0.6186	-0.14	0.5902	-0.37	0.1282
BACT124	SNET3	-0.39	0.12	0.51	11.82	10.46	1.36	0.20	0.4175	-0.22	0.3737	-0.06	0.8071	-0.38	0.1197	-0.09	0.7077
BACT1253	SNET1	0.92	-0.81	-0.87	45.07	45.03	0.04	-0.37	0.1272	-0.59	0.0094	0.52	0.0279	0.34	0.1695	0.45	0.0639
BACT126	SNET1	0.95	-0.77	-0.90	47.12	47.05	0.07	-0.35	0.1594	-0.61	0.0067	0.67	0.0024	0.09	0.7272	0.49	0.0381
BACT127	SNET2	-0.67	0.90	0.52	29.37	16.47	12.90	0.41	0.0880	0.64	0.0043	-0.14	0.5713	-0.15	0.5443	-0.45	0.0600
BACT128	SNET3	-0.65	0.34	0.69	23.37	19.24	4.13	0.33	0.1838	0.32	0.1940	-0.25	0.3230	-0.10	0.6822	-0.17	0.5081
BACT129	SNET1	0.29	0.20	-0.46	7.88	5.78	2.10	0.12	0.6312	0.06	0.8049	0.54	0.0206	0.31	0.2045	0.21	0.4058
BACT13	SNET2	-0.78	0.91	0.63	36.40	17.92	18.48	0.37	0.1352	0.73	0.0006	-0.43	0.0732	-0.22	0.3712	-0.59	0.0093
BACT131	SNET2	-0.80	0.86	0.69	36.62	15.96	20.67	0.50	0.0328	0.41	0.0948	-0.18	0.4810	-0.03	0.9129	-0.39	0.1067
BACT132	SNET3	-0.89	0.65	0.88	45.86	37.84	8.01	0.19	0.4547	0.68	0.0019	-0.66	0.0027	-0.40	0.1026	-0.52	0.0280
BACT133	SNET3	-0.86	0.65	0.86	43.14	34.65	8.49	0.36	0.1441	0.51	0.0303	-0.68	0.0017	-0.09	0.7201	-0.35	0.1518
BACT134	SNET2	-0.45	0.78	0.27	19.29	12.81	6.48	0.30	0.2307	0.58	0.0111	-0.35	0.1520	0.07	0.7790	-0.23	0.3544

ASV	Subtnet	SM1	SM2	SM3	kTotal	kIn	kOut	GS.Nit	p.Nit	GS. N2O	p. N2O	GS.NO3	p.NO3	GS.NH4	p.NH4	GS.Yld	p.Yld
BACT135	SNET1	0.91	-0.89	-0.82	43.56	43.52	0.04	-0.35	0.1497	-0.62	0.0056	0.49	0.0376	0.20	0.4204	0.55	0.0169
BACT137	SNET3	-0.45	0.39	0.38	10.88	7.46	3.42	-0.06	0.8249	0.63	0.0047	-0.42	0.0860	-0.25	0.3226	-0.23	0.3587
BACT138	SNET2	-0.82	0.89	0.72	41.03	17.74	23.29	0.39	0.1087	0.63	0.0049	-0.23	0.3578	-0.24	0.3374	-0.51	0.0289
BACT1384	SNET1	0.90	-0.81	-0.83	42.10	42.06	0.04	-0.40	0.0981	-0.54	0.0199	0.51	0.0298	0.32	0.1897	0.45	0.0630
BACT139	SNET1	0.18	0.28	-0.35	5.79	3.42	2.37	0.30	0.2319	0.09	0.7286	0.29	0.2360	0.26	0.3022	0.02	0.9277
BACT14	SNET3	-0.85	0.66	0.84	44.67	34.11	10.56	0.49	0.0370	0.48	0.0443	-0.37	0.1358	-0.13	0.6184	-0.51	0.0307
BACT140	SNET2	-0.46	0.60	0.35	14.33	7.15	7.18	0.13	0.5944	0.56	0.0157	-0.50	0.0360	0.02	0.9229	-0.58	0.0117
BACT141	SNET1	0.83	-0.76	-0.74	36.97	36.87	0.09	-0.38	0.1164	-0.75	0.0004	0.53	0.0241	0.15	0.5587	0.61	0.0077
BACT142	SNET1	0.90	-0.59	-0.92	39.62	39.49	0.13	-0.21	0.4096	-0.40	0.1046	0.57	0.0136	0.28	0.2597	0.43	0.0756
BACT143	SNET3	-0.91	0.65	0.92	51.37	42.79	8.58	0.40	0.0982	0.54	0.0200	-0.63	0.0048	-0.25	0.3077	-0.40	0.0981
BACT1445	SNET1	0.92	-0.63	-0.94	43.54	43.44	0.10	-0.36	0.1442	-0.39	0.1103	0.48	0.0457	0.27	0.2871	0.40	0.1005
BACT145	SNET3	-0.50	0.34	0.51	15.06	11.87	3.19	-0.10	0.6966	0.35	0.1538	-0.51	0.0288	-0.21	0.4136	-0.29	0.2423
BACT146	SNET3	-0.83	0.55	0.86	41.17	35.33	5.84	0.15	0.5505	0.67	0.0024	-0.70	0.0013	-0.26	0.2972	-0.39	0.1083
BACT148	SNET3	-0.71	0.40	0.77	29.10	25.67	3.44	0.38	0.1171	0.15	0.5489	-0.45	0.0601	-0.22	0.3784	-0.26	0.3024
BACT149	SNET3	-0.84	0.48	0.89	44.29	38.48	5.82	0.34	0.1642	0.44	0.0703	-0.44	0.0706	-0.24	0.3313	-0.55	0.0170
BACT15	SNET3	-0.94	0.77	0.89	54.93	40.61	14.32	0.47	0.0506	0.69	0.0014	-0.54	0.0199	-0.07	0.7683	-0.51	0.0318
BACT1504	SNET1	0.87	-0.66	-0.87	38.82	38.75	0.07	-0.28	0.2594	-0.44	0.0711	0.49	0.0394	0.27	0.2714	0.41	0.0944
BACT1529	SNET1	0.88	-0.65	-0.89	37.03	36.95	0.08	-0.33	0.1782	-0.39	0.1055	0.46	0.0529	0.17	0.4988	0.37	0.1355
BACT153	SNET2	-0.53	0.56	0.43	17.66	6.21	11.45	-0.02	0.9511	0.38	0.1204	-0.43	0.0717	-0.26	0.3021	-0.24	0.3368
BACT154	SNET2	0.10	0.42	-0.30	9.20	3.78	5.41	-0.01	0.9791	0.22	0.3786	0.39	0.1076	-0.15	0.5496	-0.12	0.6375
BACT155	SNET3	-0.80	0.47	0.83	37.12	31.83	5.28	0.49	0.0406	0.37	0.1320	-0.50	0.0334	-0.19	0.4538	-0.52	0.0259
BACT156	SNET1	0.78	-0.70	-0.74	27.50	27.38	0.11	-0.53	0.0252	-0.61	0.0070	0.62	0.0060	-0.19	0.4567	0.53	0.0245
BACT1564	SNET1	0.89	-0.74	-0.87	41.70	41.65	0.05	-0.37	0.1268	-0.42	0.0792	0.47	0.0492	0.36	0.1473	0.40	0.0968
BACT1569	SNET1	0.49	-0.32	-0.55	14.92	14.53	0.39	-0.18	0.4769	-0.04	0.8609	0.18	0.4722	0.07	0.7824	0.13	0.6039
BACT157	SNET1	0.10	-0.23	-0.10	5.33	3.72	1.60	-0.29	0.2352	0.15	0.5564	-0.06	0.8056	-0.19	0.4587	0.00	0.9964
BACT159	SNET3	-0.54	0.20	0.58	14.22	12.54	1.69	0.18	0.4696	0.17	0.5072	-0.34	0.1642	-0.17	0.5014	-0.29	0.2355
BACT16	SNET3	-0.86	0.77	0.77	42.21	29.77	12.44	0.17	0.4945	0.83	0.0000	-0.73	0.0006	-0.19	0.4432	-0.57	0.0141
BACT160	SNET3	-0.70	0.41	0.71	28.19	23.38	4.81	0.18	0.4645	0.36	0.1436	-0.47	0.0484	-0.37	0.1316	-0.40	0.1016

ASV	Subtnet	SM1	SM2	SM3	kTotal	kIn	kOut	GS.Nit	p.Nit	GS. N2O	p. N2O	GS.NO3	p.NO3	GS.NH4	p.NH4	GS.Yld	p.Yld
BACT161	SNET2	-0.87	0.85	0.77	43.42	15.64	27.78	0.41	0.0949	0.77	0.0002	-0.43	0.0724	0.09	0.7104	-0.56	0.0154
BACT162	SNET3	-0.49	0.25	0.50	14.49	11.67	2.82	0.06	0.8130	0.14	0.5927	-0.38	0.1188	-0.35	0.1548	-0.25	0.3101
BACT163	SNET1	0.06	-0.22	-0.05	6.31	3.09	3.22	-0.31	0.2040	-0.03	0.9062	-0.18	0.4635	-0.27	0.2787	-0.07	0.7718
BACT164	SNET3	-0.54	0.29	0.59	19.43	15.80	3.62	0.30	0.2325	0.08	0.7391	-0.04	0.8701	-0.23	0.3682	-0.02	0.9342
BACT1644	SNET1	0.91	-0.89	-0.81	45.41	45.35	0.06	-0.49	0.0376	-0.75	0.0004	0.48	0.0450	0.18	0.4666	0.53	0.0230
BACT165	SNET2	-0.08	0.33	-0.01	5.67	2.58	3.09	0.21	0.4132	0.19	0.4422	0.34	0.1640	-0.01	0.9747	-0.30	0.2226
BACT166	SNET3	-0.63	0.32	0.70	24.28	21.28	3.00	0.50	0.0360	0.31	0.2156	-0.40	0.1013	0.11	0.6593	-0.22	0.3888
BACT167	SNET3	-0.37	-0.02	0.47	12.67	11.26	1.42	-0.09	0.7347	-0.07	0.7884	-0.24	0.3376	-0.35	0.1578	-0.13	0.6186
BACT168	SNET3	-0.62	0.27	0.65	21.33	19.01	2.32	0.02	0.9397	0.49	0.0388	-0.66	0.0030	-0.26	0.2895	-0.40	0.1044
BACT1684	SNET1	0.91	-0.83	-0.85	43.60	43.56	0.04	-0.48	0.0457	-0.61	0.0068	0.58	0.0124	0.31	0.2049	0.41	0.0908
BACT17	SNET2	-0.89	0.91	0.78	46.35	18.46	27.89	0.42	0.0828	0.60	0.0084	-0.31	0.2165	-0.09	0.7088	-0.55	0.0183
BACT170	SNET2	-0.40	0.53	0.27	11.91	5.91	6.00	0.16	0.5222	0.59	0.0105	-0.10	0.6788	-0.17	0.4933	-0.48	0.0463
BACT171	SNET1	0.80	-0.69	-0.73	28.46	28.31	0.16	-0.22	0.3876	-0.78	0.0001	0.75	0.0003	-0.03	0.9213	0.45	0.0590
BACT172	SNET1	0.89	-0.85	-0.79	42.42	42.35	0.07	-0.47	0.0518	-0.75	0.0003	0.59	0.0098	-0.03	0.9159	0.58	0.0117
BACT1722	SNET1	0.94	-0.75	-0.91	46.68	46.63	0.05	-0.35	0.1531	-0.54	0.0198	0.51	0.0315	0.20	0.4276	0.50	0.0334
BACT173	SNET1	0.91	-0.65	-0.90	40.59	40.51	0.08	-0.26	0.3064	-0.55	0.0187	0.62	0.0063	0.24	0.3476	0.44	0.0669
BACT174	SNET1	0.86	-0.84	-0.75	41.97	41.90	0.07	-0.43	0.0766	-0.71	0.0010	0.46	0.0569	0.19	0.4430	0.58	0.0111
BACT175	SNET2	-0.42	0.61	0.32	12.87	6.97	5.89	0.38	0.1166	0.19	0.4515	-0.25	0.3210	0.23	0.3540	0.03	0.9056
BACT1752	SNET1	0.89	-0.92	-0.78	42.48	42.42	0.06	-0.47	0.0473	-0.72	0.0007	0.49	0.0392	0.11	0.6558	0.55	0.0180
BACT1759	SNET1	0.92	-0.88	-0.82	46.15	46.11	0.04	-0.40	0.1020	-0.73	0.0006	0.44	0.0687	0.21	0.3948	0.55	0.0175
BACT176	SNET3	-0.51	0.33	0.55	18.03	14.31	3.72	0.55	0.0193	-0.01	0.9793	0.03	0.9081	0.01	0.9652	-0.15	0.5655
BACT1765	SNET1	0.89	-0.68	-0.88	39.17	39.09	0.09	-0.36	0.1428	-0.44	0.0693	0.53	0.0231	0.13	0.6012	0.43	0.0721
BACT177	SNET1	0.96	-0.80	-0.91	51.14	51.09	0.05	-0.35	0.1541	-0.66	0.0028	0.57	0.0130	0.32	0.1954	0.54	0.0211
BACT179	SNET1	0.14	0.34	-0.29	6.63	2.96	3.66	-0.11	0.6517	0.20	0.4305	0.45	0.0635	-0.02	0.9444	0.19	0.4402
BACT18	SNET1	0.88	-0.54	-0.91	36.16	36.00	0.16	-0.39	0.1121	-0.47	0.0499	0.55	0.0190	0.13	0.6197	0.48	0.0426
BACT180	SNET2	-0.53	0.73	0.40	19.71	10.48	9.23	0.27	0.2847	0.72	0.0007	-0.46	0.0555	-0.09	0.7358	-0.23	0.3568
BACT181	SNET3	-0.85	0.51	0.89	44.52	39.05	5.47	0.22	0.3755	0.49	0.0398	-0.75	0.0003	-0.37	0.1317	-0.44	0.0698
BACT182	SNET2	-0.55	0.75	0.43	20.01	10.62	9.38	0.35	0.1582	0.33	0.1836	-0.29	0.2407	-0.24	0.3307	-0.06	0.8048

ASV	Subtnet	SM1	SM2	SM3	kTotal	kIn	kOut	GS.Nit	p.Nit	GS. N2O	p. N2O	GS.NO3	p.NO3	GS.NH4	p.NH4	GS.Yld	p.Yld
BACT184	SNET1	0.81	-0.81	-0.70	36.20	36.11	0.09	-0.43	0.0731	-0.68	0.0020	0.35	0.1502	0.17	0.4884	0.56	0.0155
BACT1845	SNET3	-0.68	0.44	0.73	26.14	22.23	3.91	0.45	0.0635	0.30	0.2336	-0.53	0.0234	0.07	0.7691	-0.29	0.2497
BACT185	SNET2	-0.66	0.73	0.57	23.34	10.21	13.13	0.42	0.0789	0.29	0.2350	-0.16	0.5243	0.18	0.4635	-0.33	0.1880
BACT186	SNET2	-0.60	0.60	0.51	20.50	8.66	11.84	0.41	0.0924	0.39	0.1077	0.02	0.9349	-0.13	0.6071	-0.46	0.0572
BACT188	SNET3	-0.58	0.37	0.59	21.27	16.01	5.26	0.42	0.0825	0.13	0.6108	-0.18	0.4782	-0.16	0.5367	-0.23	0.3663
BACT189	SNET1	0.27	0.13	-0.36	7.28	5.17	2.11	0.13	0.5984	-0.15	0.5532	0.48	0.0436	-0.07	0.7894	0.16	0.5276
BACT19	SNET3	-0.95	0.75	0.91	56.30	42.49	13.81	0.44	0.0678	0.66	0.0031	-0.56	0.0148	-0.10	0.7029	-0.61	0.0069
BACT190	SNET3	-0.76	0.59	0.76	31.24	24.61	6.63	0.24	0.3388	0.44	0.0687	-0.51	0.0325	-0.22	0.3710	-0.50	0.0366
BACT192	SNET1	0.61	-0.37	-0.66	16.44	15.97	0.47	-0.08	0.7491	-0.22	0.3781	0.61	0.0069	0.21	0.3926	0.19	0.4517
BACT1937	SNET1	0.65	-0.65	-0.59	18.24	18.14	0.10	-0.33	0.1760	-0.41	0.0953	0.20	0.4293	0.46	0.0561	0.35	0.1515
BACT195	SNET2	-0.52	0.70	0.37	16.52	8.72	7.81	-0.05	0.8567	0.48	0.0437	-0.24	0.3448	-0.39	0.1103	-0.15	0.5585
BACT1952	SNET1	0.01	0.25	-0.16	11.85	8.80	3.04	0.05	0.8349	0.42	0.0800	-0.19	0.4581	0.09	0.7314	-0.27	0.2836
BACT196	SNET3	-0.75	0.35	0.82	33.02	30.13	2.89	0.30	0.2325	0.22	0.3721	-0.54	0.0204	-0.26	0.2927	-0.34	0.1616
BACT1970	SNET2	-0.75	0.84	0.62	32.52	14.70	17.82	0.40	0.1011	0.57	0.0139	-0.43	0.0757	-0.27	0.2705	-0.48	0.0448
BACT199	SNET3	-0.59	0.23	0.68	24.22	21.32	2.90	0.40	0.0981	-0.04	0.8849	-0.28	0.2679	-0.09	0.7239	-0.20	0.4291
BACT2	SNET3	-0.92	0.74	0.87	51.00	37.18	13.82	0.46	0.0548	0.65	0.0038	-0.54	0.0217	-0.09	0.7109	-0.69	0.0015
BACT20	SNET2	-0.49	0.79	0.30	19.95	12.07	7.88	0.35	0.1511	0.59	0.0093	-0.30	0.2337	-0.04	0.8813	-0.25	0.3144
BACT200	SNET3	-0.85	0.55	0.87	41.84	35.50	6.34	0.32	0.2004	0.44	0.0700	-0.63	0.0050	-0.03	0.9099	-0.37	0.1360
BACT201	SNET1	0.08	-0.34	-0.02	4.81	2.96	1.85	-0.15	0.5613	0.02	0.9436	-0.14	0.5728	-0.06	0.8116	-0.04	0.8621
BACT202	SNET3	-0.53	0.35	0.57	17.87	14.07	3.80	0.45	0.0589	0.11	0.6556	-0.08	0.7521	0.14	0.5903	-0.38	0.1226
BACT203	SNET2	-0.44	0.70	0.29	17.57	10.51	7.07	0.22	0.3845	0.56	0.0155	-0.43	0.0715	-0.14	0.5858	-0.33	0.1814
BACT2030	SNET3	-0.75	0.65	0.74	31.81	23.74	8.06	0.30	0.2186	0.44	0.0668	-0.49	0.0385	-0.17	0.4955	-0.31	0.2146
BACT204	SNET1	0.82	-0.48	-0.86	30.67	30.36	0.31	-0.26	0.2998	-0.52	0.0266	0.73	0.0005	0.15	0.5572	0.47	0.0473
BACT2043	SNET1	-0.05	0.26	-0.08	10.27	7.10	3.17	0.16	0.5177	0.36	0.1473	-0.10	0.7034	-0.13	0.6156	-0.25	0.3108
BACT2047	SNET1	0.91	-0.73	-0.88	42.86	42.81	0.05	-0.28	0.2526	-0.55	0.0183	0.52	0.0255	0.39	0.1112	0.44	0.0680
BACT206	SNET1	0.95	-0.84	-0.88	50.24	50.20	0.04	-0.49	0.0398	-0.61	0.0074	0.54	0.0209	0.20	0.4167	0.54	0.0206
BACT208	SNET2	-0.40	0.54	0.34	13.34	5.71	7.64	0.06	0.8084	0.28	0.2561	-0.30	0.2257	-0.06	0.8016	-0.21	0.3963
BACT21	SNET1	0.93	-0.85	-0.87	45.73	45.68	0.05	-0.39	0.1101	-0.69	0.0017	0.48	0.0451	0.17	0.5037	0.48	0.0440

ASV	Subtnet	SM1	SM2	SM3	kTotal	kIn	kOut	GS.Nit	p.Nit	GS. N2O	p. N2O	GS.NO3	p.NO3	GS.NH4	p.NH4	GS.Yld	p.Yld
BACT211	SNET1	0.78	-0.37	-0.85	27.77	27.40	0.37	-0.27	0.2764	-0.33	0.1764	0.63	0.0047	0.12	0.6461	0.37	0.1304
BACT212	SNET3	-0.79	0.80	0.70	36.97	23.02	13.95	0.23	0.3669	0.55	0.0189	-0.52	0.0269	-0.25	0.3201	-0.50	0.0361
BACT213	SNET3	-0.65	0.23	0.77	27.39	25.61	1.78	0.10	0.6924	0.28	0.2622	-0.48	0.0448	-0.27	0.2767	-0.30	0.2259
BACT214	SNET3	-0.44	0.07	0.56	14.47	13.30	1.18	0.39	0.1146	-0.02	0.9252	-0.27	0.2850	0.10	0.6893	-0.13	0.6202
BACT215	SNET3	-0.60	0.20	0.67	21.71	19.54	2.17	0.08	0.7593	0.28	0.2548	-0.59	0.0103	-0.28	0.2691	-0.40	0.1017
BACT216	SNET3	-0.24	0.01	0.26	7.95	5.35	2.59	-0.04	0.8713	-0.04	0.8882	-0.28	0.2570	-0.31	0.2141	-0.25	0.3247
BACT217	SNET1	0.85	-0.83	-0.74	39.57	39.49	0.08	-0.46	0.0522	-0.71	0.0009	0.52	0.0254	0.00	0.9986	0.60	0.0080
BACT218	SNET3	-0.59	0.34	0.66	21.30	18.40	2.91	0.28	0.2599	0.11	0.6548	-0.48	0.0426	-0.09	0.7202	-0.24	0.3274
BACT219	SNET1	0.86	-0.48	-0.91	34.45	34.19	0.26	-0.35	0.1489	-0.36	0.1405	0.55	0.0191	0.21	0.4027	0.41	0.0888
BACT22	SNET3	-0.69	0.69	0.64	27.05	16.80	10.25	0.31	0.2140	0.24	0.3276	-0.35	0.1506	-0.29	0.2394	-0.28	0.2682
BACT220	SNET3	-0.76	0.32	0.86	36.52	33.80	2.72	0.43	0.0747	0.24	0.3451	-0.71	0.0009	0.02	0.9401	-0.39	0.1143
BACT221	SNET2	-0.43	0.55	0.37	15.29	7.03	8.26	0.36	0.1431	0.45	0.0632	-0.38	0.1229	0.22	0.3749	-0.17	0.5028
BACT222	SNET3	-0.57	0.52	0.52	19.85	13.23	6.62	0.03	0.9104	0.42	0.0811	-0.51	0.0309	-0.29	0.2465	-0.31	0.2035
BACT224	SNET3	-0.77	0.48	0.78	30.18	25.35	4.84	0.19	0.4569	0.42	0.0853	-0.52	0.0255	-0.16	0.5361	-0.40	0.0997
BACT225	SNET3	-0.81	0.56	0.84	39.51	32.45	7.06	0.40	0.0987	0.50	0.0353	-0.46	0.0570	-0.22	0.3712	-0.42	0.0856
BACT2257	SNET1	0.37	-0.09	-0.49	14.07	13.34	0.73	-0.05	0.8306	0.14	0.5927	0.12	0.6363	0.21	0.3981	-0.10	0.7052
BACT228	SNET1	0.87	-0.85	-0.75	41.67	41.60	0.07	-0.36	0.1368	-0.71	0.0011	0.50	0.0348	0.24	0.3377	0.60	0.0079
BACT229	SNET3	-0.88	0.60	0.92	49.18	41.79	7.39	0.29	0.2415	0.37	0.1309	-0.58	0.0113	-0.34	0.1715	-0.33	0.1773
BACT23	SNET3	-0.65	0.42	0.67	21.58	17.85	3.73	0.62	0.0061	0.20	0.4359	-0.29	0.2418	-0.14	0.5669	-0.40	0.0988
BACT230	SNET3	-0.66	0.57	0.61	24.98	17.76	7.22	0.11	0.6779	0.56	0.0156	-0.73	0.0005	-0.27	0.2829	-0.43	0.0745
BACT231	SNET1	0.19	0.21	-0.35	9.24	7.18	2.06	0.20	0.4321	0.02	0.9277	0.39	0.1078	-0.03	0.9021	-0.07	0.7883
BACT233	SNET1	0.95	-0.83	-0.88	49.80	49.76	0.04	-0.36	0.1457	-0.73	0.0006	0.62	0.0057	0.20	0.4354	0.59	0.0107
BACT234	SNET2	-0.38	0.58	0.23	10.26	5.97	4.29	0.07	0.7680	0.32	0.1937	-0.01	0.9793	-0.14	0.5730	-0.28	0.2655
BACT235	SNET2	-0.78	0.83	0.68	36.06	14.35	21.71	0.40	0.1039	0.59	0.0107	-0.56	0.0163	-0.11	0.6654	-0.34	0.1725
BACT236	SNET2	-0.18	0.34	0.10	9.03	4.48	4.54	-0.07	0.7953	0.45	0.0608	-0.43	0.0764	0.08	0.7518	-0.19	0.4384
BACT237	SNET2	-0.51	0.70	0.40	19.91	10.30	9.60	0.21	0.4093	0.35	0.1550	-0.41	0.0873	-0.09	0.7368	-0.17	0.5016
BACT2383	SNET3	-0.69	0.38	0.75	26.45	23.35	3.10	0.24	0.3378	0.30	0.2187	-0.48	0.0445	-0.21	0.4031	-0.29	0.2363
BACT24	SNET3	-0.95	0.66	0.96	57.45	47.86	9.59	0.39	0.1102	0.61	0.0074	-0.69	0.0017	-0.15	0.5442	-0.43	0.0770

ASV	Subtnet	SM1	SM2	SM3	kTotal	kIn	kOut	GS.Nit	p.Nit	GS. N2O	p. N2O	GS.NO3	p.NO3	GS.NH4	p.NH4	GS.Yld	p.Yld
BACT241	SNET3	-0.40	0.07	0.51	11.22	10.25	0.97	-0.23	0.3614	0.06	0.8242	-0.37	0.1335	-0.30	0.2241	0.10	0.6823
BACT242	SNET2	-0.57	0.82	0.43	25.12	14.39	10.73	0.24	0.3359	0.68	0.0018	-0.33	0.1850	-0.07	0.7875	-0.22	0.3802
BACT243	SNET3	-0.28	0.07	0.30	8.87	6.44	2.43	-0.18	0.4868	0.01	0.9575	-0.33	0.1824	-0.32	0.2013	-0.20	0.4233
BACT244	SNET3	-0.71	0.25	0.82	32.55	30.62	1.93	0.00	0.9867	0.36	0.1410	-0.63	0.0049	-0.29	0.2347	-0.37	0.1254
BACT2440	SNET1	-0.08	0.29	-0.06	10.63	6.75	3.88	0.03	0.9175	0.42	0.0834	-0.20	0.4224	-0.25	0.3233	-0.34	0.1667
BACT2453	SNET1	0.73	-0.75	-0.66	25.10	25.02	0.08	-0.41	0.0918	-0.42	0.0794	0.21	0.3973	0.42	0.0805	0.32	0.1953
BACT2458	SNET1	0.91	-0.89	-0.80	44.77	44.73	0.05	-0.49	0.0403	-0.73	0.0005	0.51	0.0306	0.17	0.4968	0.55	0.0175
BACT246	SNET3	-0.70	0.30	0.81	31.92	29.35	2.57	0.25	0.3181	0.13	0.6154	-0.45	0.0593	-0.36	0.1435	-0.12	0.6403
BACT247	SNET3	-0.25	0.14	0.26	5.53	3.65	1.87	0.35	0.1594	-0.01	0.9774	-0.07	0.7808	-0.16	0.5255	-0.08	0.7475
BACT25	SNET2	-0.61	0.88	0.42	26.79	16.75	10.04	0.41	0.0938	0.69	0.0015	-0.18	0.4756	0.01	0.9820	-0.53	0.0226
BACT250	SNET1	0.84	-0.50	-0.86	31.63	31.41	0.22	-0.43	0.0771	-0.39	0.1053	0.52	0.0279	0.06	0.8015	0.41	0.0941
BACT251	SNET1	0.88	-0.83	-0.78	43.00	42.94	0.06	-0.32	0.1989	-0.74	0.0005	0.47	0.0484	0.27	0.2732	0.60	0.0086
BACT253	SNET2	-0.36	0.76	0.18	15.03	10.75	4.28	0.31	0.2145	0.37	0.1269	0.08	0.7498	0.29	0.2468	-0.29	0.2393
BACT254	SNET2	-0.57	0.74	0.43	21.03	11.32	9.71	0.25	0.3255	0.55	0.0174	-0.57	0.0139	0.08	0.7476	-0.29	0.2448
BACT256	SNET3	-0.68	0.53	0.68	23.21	17.75	5.46	0.17	0.5015	0.36	0.1482	-0.22	0.3729	-0.18	0.4872	-0.25	0.3169
BACT257	SNET2	-0.30	0.66	0.15	13.37	8.94	4.43	0.09	0.7315	0.50	0.0337	0.03	0.8955	0.06	0.8001	-0.25	0.3160
BACT259	SNET1	0.31	-0.49	-0.25	5.75	4.95	0.80	-0.37	0.1358	-0.03	0.9148	0.01	0.9815	-0.10	0.6835	0.05	0.8550
BACT26	SNET2	-0.76	0.87	0.62	34.65	17.97	16.68	0.60	0.0084	0.49	0.0379	-0.16	0.5330	-0.03	0.9074	-0.50	0.0334
BACT260	SNET1	0.89	-0.85	-0.79	44.32	44.26	0.06	-0.33	0.1861	-0.78	0.0001	0.52	0.0274	0.32	0.2007	0.58	0.0112
BACT261	SNET2	-0.76	0.76	0.69	33.46	12.47	20.99	0.41	0.0951	0.49	0.0401	-0.23	0.3486	-0.27	0.2716	-0.34	0.1705
BACT262	SNET3	-0.69	0.57	0.67	25.06	18.55	6.51	0.54	0.0203	0.46	0.0537	-0.35	0.1574	0.26	0.3050	-0.38	0.1218
BACT264	SNET3	-0.53	0.55	0.50	19.90	12.19	7.71	0.29	0.2394	0.46	0.0532	-0.35	0.1572	0.14	0.5914	-0.17	0.5019
BACT265	SNET3	-0.88	0.55	0.89	45.39	39.08	6.31	0.23	0.3496	0.64	0.0042	-0.69	0.0014	-0.26	0.2982	-0.53	0.0251
BACT268	SNET1	0.84	-0.77	-0.76	39.06	38.98	0.08	-0.36	0.1388	-0.73	0.0006	0.49	0.0380	0.29	0.2406	0.61	0.0068
BACT27	SNET3	-0.93	0.73	0.92	55.39	43.38	12.02	0.41	0.0934	0.67	0.0021	-0.60	0.0089	-0.10	0.6940	-0.53	0.0240
BACT270	SNET3	-0.85	0.61	0.86	41.17	33.64	7.53	0.27	0.2779	0.44	0.0643	-0.57	0.0129	-0.26	0.3068	-0.36	0.1410
BACT2714	SNET1	0.82	-0.81	-0.74	32.97	32.92	0.06	-0.47	0.0467	-0.43	0.0726	0.30	0.2185	0.35	0.1567	0.36	0.1441
BACT2723	SNET2	-0.49	0.63	0.36	14.83	7.30	7.53	0.46	0.0568	0.43	0.0746	-0.30	0.2343	-0.23	0.3490	-0.40	0.0967

ASV	Subtnet	SM1	SM2	SM3	kTotal	kIn	kOut	GS.Nit	p.Nit	GS. N2O	p. N2O	GS.NO3	p.NO3	GS.NH4	p.NH4	GS.Yld	p.Yld
BACT273	SNET1	0.24	0.00	-0.28	5.42	3.93	1.48	-0.05	0.8579	-0.17	0.5094	0.43	0.0775	-0.18	0.4842	0.37	0.1322
BACT274	SNET3	-0.82	0.58	0.86	41.13	34.57	6.56	0.31	0.2181	0.45	0.0578	-0.59	0.0095	-0.17	0.4895	-0.34	0.1734
BACT2746	SNET1	0.94	-0.83	-0.88	47.95	47.92	0.04	-0.42	0.0813	-0.61	0.0076	0.53	0.0251	0.30	0.2303	0.45	0.0590
BACT276	SNET1	0.79	-0.50	-0.78	27.15	26.93	0.22	-0.27	0.2855	-0.65	0.0038	0.75	0.0004	-0.07	0.7712	0.58	0.0116
BACT28	SNET1	0.86	-0.49	-0.90	35.06	34.87	0.19	-0.26	0.2944	-0.47	0.0492	0.67	0.0026	-0.01	0.9562	0.46	0.0574
BACT280	SNET1	0.89	-0.84	-0.80	45.41	45.35	0.06	-0.42	0.0867	-0.72	0.0008	0.56	0.0153	0.23	0.3542	0.60	0.0091
BACT2802	SNET1	0.89	-0.66	-0.89	37.95	37.88	0.07	-0.36	0.1444	-0.55	0.0189	0.62	0.0060	0.11	0.6673	0.44	0.0661
BACT281	SNET2	-0.40	0.53	0.31	11.68	5.39	6.29	0.28	0.2659	0.50	0.0365	0.04	0.8863	0.08	0.7537	-0.22	0.3841
BACT283	SNET3	-0.06	0.09	-0.01	5.47	1.96	3.51	-0.23	0.3484	0.26	0.3002	-0.30	0.2195	-0.34	0.1670	-0.18	0.4671
BACT284	SNET1	0.90	-0.85	-0.81	44.40	44.35	0.05	-0.45	0.0613	-0.61	0.0072	0.50	0.0326	0.26	0.2942	0.55	0.0183
BACT285	SNET3	-0.72	0.54	0.71	26.57	20.54	6.04	0.25	0.3131	0.34	0.1651	-0.38	0.1174	-0.14	0.5887	-0.23	0.3596
BACT2857	SNET3	-0.84	0.66	0.82	38.94	30.22	8.73	0.52	0.0256	0.43	0.0745	-0.64	0.0043	-0.20	0.4200	-0.40	0.0999
BACT286	SNET1	0.12	0.09	-0.22	7.88	6.34	1.53	-0.11	0.6739	0.17	0.5116	0.23	0.3544	-0.19	0.4528	-0.27	0.2813
BACT287	SNET2	-0.65	0.61	0.60	22.46	8.11	14.34	0.54	0.0221	0.11	0.6667	-0.08	0.7520	0.09	0.7153	-0.37	0.1300
BACT289	SNET3	-0.25	0.18	0.30	9.43	6.88	2.55	0.31	0.2126	-0.02	0.9381	0.20	0.4167	0.02	0.9330	-0.03	0.8914
BACT29	SNET1	0.93	-0.60	-0.96	43.56	43.43	0.13	-0.30	0.2205	-0.50	0.0360	0.66	0.0031	0.16	0.5287	0.45	0.0592
BACT290	SNET1	0.93	-0.84	-0.86	48.67	48.62	0.05	-0.48	0.0432	-0.72	0.0008	0.60	0.0091	0.11	0.6650	0.56	0.0158
BACT291	SNET3	-0.68	0.32	0.76	27.03	24.47	2.57	0.15	0.5403	0.16	0.5182	-0.44	0.0660	-0.27	0.2832	-0.28	0.2641
BACT292	SNET2	-0.77	0.87	0.65	33.96	15.39	18.58	0.55	0.0192	0.50	0.0328	-0.35	0.1518	-0.01	0.9705	-0.46	0.0528
BACT298	SNET3	-0.82	0.64	0.83	40.95	32.65	8.30	0.33	0.1877	0.57	0.0139	-0.41	0.0898	-0.20	0.4171	-0.40	0.0974
BACT299	SNET2	-0.84	0.83	0.76	40.75	15.03	25.72	0.36	0.1373	0.64	0.0043	-0.30	0.2238	-0.19	0.4469	-0.45	0.0641
BACT3	SNET1	0.90	-0.66	-0.91	41.71	41.62	0.09	-0.38	0.1232	-0.42	0.0851	0.41	0.0928	0.22	0.3904	0.37	0.1306
BACT30	SNET1	0.93	-0.65	-0.93	44.58	44.49	0.09	-0.29	0.2464	-0.51	0.0292	0.53	0.0251	0.23	0.3575	0.47	0.0516
BACT301	SNET2	-0.11	0.12	0.07	5.09	1.98	3.11	0.19	0.4509	0.09	0.7178	0.18	0.4822	-0.04	0.8796	-0.29	0.2464
BACT302	SNET1	0.83	-0.64	-0.82	32.52	32.45	0.08	-0.35	0.1543	-0.57	0.0144	0.59	0.0096	0.16	0.5340	0.46	0.0542
BACT304	SNET3	-0.63	0.35	0.66	20.39	17.41	2.99	-0.19	0.4552	0.51	0.0314	-0.33	0.1767	-0.39	0.1113	-0.33	0.1811
BACT31	SNET3	-0.92	0.54	0.96	55.43	49.03	6.40	0.36	0.1437	0.57	0.0143	-0.73	0.0006	-0.14	0.5811	-0.44	0.0673
BACT311	SNET3	-0.67	0.19	0.77	29.37	27.54	1.83	0.01	0.9795	0.34	0.1663	-0.61	0.0071	-0.44	0.0674	-0.39	0.1070

ASV	Subtnet	SM1	SM2	SM3	kTotal	kIn	kOut	GS.Nit	p.Nit	GS. N2O	p. N2O	GS.NO3	p.NO3	GS.NH4	p.NH4	GS.Yld	p.Yld
BACT315	SNET1	0.75	-0.72	-0.66	28.17	28.03	0.14	-0.28	0.2566	-0.61	0.0074	0.27	0.2768	0.49	0.0402	0.53	0.0233
BACT317	SNET3	-0.69	0.24	0.79	29.18	27.24	1.95	-0.01	0.9710	0.28	0.2568	-0.39	0.1078	-0.37	0.1273	-0.42	0.0845
BACT318	SNET2	-0.45	0.47	0.39	12.43	4.21	8.22	0.03	0.8972	0.10	0.6900	-0.26	0.2950	-0.21	0.4000	-0.30	0.2344
BACT319	SNET3	-0.70	0.69	0.67	29.65	19.72	9.93	0.33	0.1755	0.33	0.1852	-0.54	0.0207	-0.02	0.9284	-0.30	0.2300
BACT32	SNET1	0.94	-0.88	-0.86	49.79	49.75	0.04	-0.46	0.0523	-0.68	0.0018	0.54	0.0207	0.19	0.4439	0.56	0.0149
BACT3201	SNET1	0.90	-0.80	-0.85	41.48	41.43	0.06	-0.40	0.1008	-0.54	0.0220	0.40	0.0968	0.26	0.3011	0.44	0.0644
BACT321	SNET2	-0.10	0.33	0.00	7.51	4.41	3.10	0.06	0.8272	0.50	0.0329	-0.27	0.2713	0.34	0.1632	-0.07	0.7808
BACT3229	SNET1	0.65	-0.45	-0.69	21.84	21.66	0.18	-0.19	0.4512	-0.20	0.4282	0.34	0.1735	0.19	0.4608	0.25	0.3169
BACT325	SNET1	0.06	-0.20	-0.05	6.15	2.89	3.26	-0.30	0.2290	-0.02	0.9308	-0.20	0.4261	-0.30	0.2318	-0.12	0.6464
BACT327	SNET3	-0.82	0.78	0.74	36.11	23.75	12.36	0.41	0.0950	0.55	0.0190	-0.52	0.0284	-0.29	0.2390	-0.52	0.0255
BACT328	SNET1	0.92	-0.76	-0.87	42.31	42.25	0.06	-0.37	0.1329	-0.53	0.0232	0.56	0.0167	0.18	0.4631	0.46	0.0567
BACT33	SNET3	-0.83	0.61	0.84	43.59	34.52	9.07	0.57	0.0132	0.40	0.0999	-0.33	0.1851	-0.17	0.4888	-0.50	0.0346
BACT332	SNET2	-0.47	0.58	0.42	16.61	6.86	9.76	0.28	0.2588	0.37	0.1321	-0.17	0.5071	-0.03	0.9077	-0.05	0.8571
BACT336	SNET1	0.71	-0.38	-0.73	20.65	20.26	0.39	-0.26	0.3057	-0.50	0.0336	0.37	0.1285	0.08	0.7588	0.46	0.0575
BACT338	SNET2	-0.09	0.49	-0.06	8.34	5.04	3.30	0.36	0.1443	0.34	0.1633	0.26	0.3054	0.29	0.2390	-0.19	0.4405
BACT34	SNET3	-0.32	-0.04	0.44	12.01	10.74	1.27	0.28	0.2690	-0.12	0.6330	0.04	0.8660	-0.18	0.4643	-0.18	0.4759
BACT340	SNET3	-0.04	0.14	0.01	4.75	2.19	2.55	-0.15	0.5499	-0.15	0.5627	-0.10	0.6932	-0.15	0.5636	0.02	0.9393
BACT3415	SNET1	-0.01	0.26	-0.14	9.13	5.98	3.14	0.05	0.8339	0.40	0.0983	-0.03	0.9109	-0.25	0.3240	-0.33	0.1822
BACT3459	SNET3	-0.80	0.78	0.71	34.98	22.75	12.23	0.14	0.5682	0.74	0.0004	-0.42	0.0853	-0.36	0.1383	-0.45	0.0589
BACT350	SNET2	0.00	0.27	-0.08	5.07	1.96	3.11	0.13	0.6104	-0.03	0.9022	0.49	0.0382	-0.18	0.4725	-0.04	0.8838
BACT3503	SNET1	0.38	-0.21	-0.46	12.78	12.18	0.59	-0.08	0.7535	0.10	0.6873	0.09	0.7262	0.10	0.6945	-0.03	0.9181
BACT354	SNET1	0.02	0.34	-0.18	8.42	5.06	3.37	0.09	0.7293	0.15	0.5562	0.24	0.3277	-0.12	0.6398	-0.22	0.3715
BACT356	SNET1	0.04	-0.12	-0.05	4.55	2.90	1.65	-0.21	0.3959	0.05	0.8297	-0.02	0.9398	-0.09	0.7213	0.01	0.9529
BACT357	SNET1	0.84	-0.49	-0.86	30.87	30.70	0.17	-0.24	0.3419	-0.59	0.0099	0.59	0.0107	0.29	0.2501	0.57	0.0131
BACT358	SNET3	-0.85	0.44	0.91	45.20	40.57	4.63	0.39	0.1073	0.44	0.0688	-0.59	0.0107	-0.23	0.3581	-0.39	0.1145
BACT36	SNET1	0.41	0.09	-0.58	13.91	12.52	1.39	0.03	0.8950	-0.02	0.9332	0.41	0.0937	0.11	0.6552	0.17	0.5093
BACT360	SNET3	-0.51	0.28	0.55	14.76	12.06	2.70	0.39	0.1143	-0.11	0.6585	-0.32	0.1884	0.10	0.6792	-0.25	0.3179
BACT361	SNET3	-0.40	0.38	0.40	13.49	8.57	4.92	0.16	0.5373	0.33	0.1827	-0.45	0.0633	0.08	0.7396	-0.09	0.7371

ASV	Subtnet	SM1	SM2	SM3	kTotal	kIn	kOut	GS.Nit	p.Nit	GS. N2O	p. N2O	GS.NO3	p.NO3	GS.NH4	p.NH4	GS.Yld	p.Yld
BACT37	SNET3	-0.86	0.73	0.84	44.78	33.87	10.91	0.43	0.0737	0.56	0.0147	-0.50	0.0339	0.02	0.9404	-0.40	0.1000
BACT379	SNET3	-0.55	0.39	0.54	17.13	13.21	3.92	0.11	0.6738	0.15	0.5441	-0.39	0.1142	-0.23	0.3579	-0.23	0.3535
BACT38	SNET1	0.88	-0.62	-0.90	38.54	38.43	0.11	-0.29	0.2425	-0.40	0.0976	0.43	0.0718	0.27	0.2745	0.39	0.1087
BACT387	SNET1	0.40	-0.40	-0.31	6.12	5.46	0.66	-0.04	0.8754	-0.56	0.0146	0.66	0.0029	-0.22	0.3789	0.34	0.1614
BACT39	SNET3	-0.18	0.06	0.22	4.38	3.20	1.18	0.16	0.5316	-0.17	0.5099	0.28	0.2647	0.13	0.5939	-0.15	0.5463
BACT396	SNET3	-0.75	0.62	0.72	31.22	22.84	8.38	0.48	0.0437	0.30	0.2300	-0.28	0.2561	-0.01	0.9724	-0.43	0.0732
BACT397	SNET3	-0.79	0.49	0.82	35.80	30.11	5.69	0.45	0.0628	0.42	0.0848	-0.41	0.0889	-0.27	0.2706	-0.53	0.0249
BACT4	SNET2	-0.88	0.88	0.77	47.20	18.14	29.06	0.50	0.0362	0.72	0.0007	-0.43	0.0736	-0.03	0.9108	-0.64	0.0042
BACT40	SNET1	0.73	-0.36	-0.78	23.68	23.26	0.42	-0.34	0.1623	-0.40	0.0979	0.72	0.0008	-0.19	0.4618	0.43	0.0748
BACT400	SNET2	-0.03	0.22	-0.03	6.39	3.18	3.21	0.09	0.7227	0.33	0.1873	-0.16	0.5373	0.52	0.0271	0.02	0.9217
BACT41	SNET1	0.94	-0.87	-0.87	49.41	49.37	0.04	-0.39	0.1110	-0.71	0.0009	0.58	0.0120	0.17	0.5107	0.59	0.0106
BACT411	SNET3	-0.68	0.51	0.72	28.31	22.83	5.48	0.40	0.0955	0.12	0.6475	-0.42	0.0844	-0.11	0.6745	-0.25	0.3149
BACT416	SNET3	-0.54	0.38	0.58	19.04	15.38	3.66	0.48	0.0444	0.07	0.7945	-0.14	0.5882	-0.14	0.5768	-0.11	0.6763
BACT42	SNET3	-0.83	0.48	0.84	40.17	35.04	5.13	0.15	0.5588	0.54	0.0212	-0.72	0.0007	-0.20	0.4325	-0.47	0.0508
BACT43	SNET3	-0.85	0.44	0.93	46.62	42.58	4.04	0.24	0.3390	0.48	0.0433	-0.66	0.0027	-0.34	0.1628	-0.55	0.0180
BACT430	SNET3	-0.41	-0.01	0.54	13.36	12.52	0.84	0.25	0.3243	0.12	0.6297	-0.44	0.0670	-0.25	0.3230	-0.28	0.2606
BACT4309	SNET3	-0.79	0.56	0.80	34.72	28.58	6.14	0.29	0.2513	0.47	0.0478	-0.51	0.0291	-0.24	0.3444	-0.33	0.1864
BACT4344	SNET1	0.19	-0.12	-0.24	9.41	8.43	0.98	0.09	0.7318	0.15	0.5545	-0.17	0.5080	0.12	0.6262	-0.24	0.3371
BACT44	SNET3	-0.85	0.76	0.79	40.86	27.77	13.10	0.42	0.0789	0.43	0.0765	-0.49	0.0393	-0.02	0.9461	-0.36	0.1404
BACT443	SNET3	-0.81	0.72	0.76	39.05	28.13	10.92	0.18	0.4873	0.72	0.0008	-0.69	0.0015	-0.18	0.4805	-0.40	0.0961
BACT45	SNET3	-0.89	0.64	0.89	49.17	38.32	10.85	0.48	0.0431	0.49	0.0398	-0.39	0.1140	-0.02	0.9306	-0.51	0.0300
BACT455	SNET2	-0.17	0.24	0.08	6.51	3.26	3.24	0.09	0.7263	0.32	0.1994	0.13	0.5999	0.05	0.8461	-0.39	0.1124
BACT46	SNET3	-0.50	0.47	0.46	13.53	9.38	4.16	-0.21	0.3967	0.49	0.0405	-0.15	0.5557	-0.57	0.0145	-0.12	0.6442
BACT4625	SNET1	-0.01	0.29	-0.16	12.14	8.79	3.34	0.15	0.5588	0.41	0.0871	-0.19	0.4598	0.02	0.9440	-0.26	0.3012
BACT465	SNET1	0.86	-0.84	-0.76	41.60	41.54	0.06	-0.39	0.1061	-0.68	0.0018	0.46	0.0577	0.33	0.1869	0.50	0.0327
BACT47	SNET2	-0.48	0.80	0.29	19.66	13.30	6.36	0.32	0.1958	0.52	0.0253	0.11	0.6590	-0.24	0.3455	-0.45	0.0584
BACT474	SNET1	0.81	-0.60	-0.79	28.63	28.43	0.20	-0.24	0.3453	-0.56	0.0148	0.71	0.0009	-0.05	0.8510	0.41	0.0889
BACT475	SNET3	-0.61	0.55	0.57	21.32	15.22	6.10	-0.06	0.8101	0.62	0.0057	-0.44	0.0669	-0.23	0.3585	-0.27	0.2750

ASV	Subtnet	SM1	SM2	SM3	kTotal	kIn	kOut	GS.Nit	p.Nit	GS. N2O	p. N2O	GS.NO3	p.NO3	GS.NH4	p.NH4	GS.Yld	p.Yld
BACT478	SNET1	0.79	-0.68	-0.73	27.53	27.45	0.08	-0.37	0.1300	-0.62	0.0058	0.43	0.0752	0.44	0.0679	0.43	0.0773
BACT48	SNET1	0.94	-0.86	-0.87	49.57	49.54	0.04	-0.41	0.0906	-0.66	0.0030	0.59	0.0108	0.23	0.3554	0.56	0.0155
BACT49	SNET3	-0.70	0.55	0.68	24.70	18.65	6.05	0.03	0.9081	0.45	0.0620	-0.30	0.2191	-0.55	0.0172	-0.59	0.0102
BACT491	SNET3	-0.31	0.22	0.31	8.27	5.86	2.42	0.22	0.3876	0.34	0.1716	-0.25	0.3128	0.23	0.3642	-0.09	0.7159
BACT5	SNET3	-0.94	0.64	0.95	57.40	47.28	10.12	0.42	0.0817	0.59	0.0092	-0.60	0.0092	-0.12	0.6324	-0.62	0.0062
BACT50	SNET3	-0.82	0.41	0.89	44.67	40.25	4.42	0.45	0.0602	0.37	0.1309	-0.66	0.0031	-0.20	0.4313	-0.45	0.0621
BACT508	SNET3	-0.17	-0.34	0.35	8.29	7.44	0.85	-0.19	0.4469	-0.32	0.1932	-0.14	0.5731	-0.31	0.2145	-0.18	0.4673
BACT51	SNET2	-0.72	0.79	0.61	30.73	14.82	15.91	0.44	0.0696	0.49	0.0392	-0.12	0.6237	-0.22	0.3713	-0.36	0.1480
BACT52	SNET3	-0.96	0.74	0.94	58.72	46.04	12.68	0.31	0.2127	0.64	0.0041	-0.63	0.0054	-0.31	0.2140	-0.56	0.0160
BACT53	SNET2	-0.82	0.88	0.69	40.22	18.21	22.00	0.35	0.1526	0.69	0.0015	-0.34	0.1668	-0.15	0.5532	-0.61	0.0067
BACT54	SNET1	0.92	-0.80	-0.86	46.50	46.43	0.07	-0.44	0.0655	-0.67	0.0022	0.57	0.0127	0.25	0.3226	0.57	0.0145
BACT55	SNET3	-0.93	0.60	0.96	56.70	48.41	8.29	0.40	0.0990	0.49	0.0381	-0.65	0.0038	-0.25	0.3209	-0.44	0.0686
BACT56	SNET1	0.03	-0.13	-0.03	4.87	3.04	1.83	-0.24	0.3315	0.07	0.7952	0.01	0.9552	-0.12	0.6415	0.00	0.9920
BACT57	SNET3	-0.92	0.67	0.92	53.33	42.66	10.67	0.46	0.0563	0.37	0.1291	-0.42	0.0829	-0.28	0.2574	-0.50	0.0348
BACT58	SNET1	0.62	-0.21	-0.74	17.82	17.18	0.64	-0.10	0.6908	-0.20	0.4315	0.62	0.0062	0.08	0.7431	0.19	0.4534
BACT59	SNET3	-0.76	0.37	0.81	36.18	31.98	4.20	0.20	0.4357	0.39	0.1088	-0.59	0.0097	-0.39	0.1056	-0.43	0.0764
BACT6	SNET1	0.81	-0.73	-0.78	31.96	31.84	0.11	-0.40	0.1037	-0.43	0.0775	0.25	0.3154	0.25	0.3235	0.35	0.1588
BACT60	SNET1	0.34	0.12	-0.52	12.60	10.90	1.70	-0.06	0.8189	0.22	0.3816	0.22	0.3730	0.37	0.1268	-0.13	0.5967
BACT61	SNET1	0.88	-0.88	-0.78	43.58	43.52	0.06	-0.51	0.0302	-0.68	0.0020	0.49	0.0413	0.13	0.6009	0.60	0.0087
BACT62	SNET2	-0.71	0.79	0.62	27.90	12.06	15.84	0.65	0.0038	0.38	0.1179	-0.34	0.1615	0.31	0.2117	-0.45	0.0606
BACT63	SNET2	-0.84	0.79	0.76	41.48	15.09	26.40	0.50	0.0334	0.51	0.0322	-0.30	0.2216	0.04	0.8860	-0.52	0.0266
BACT636	SNET3	-0.90	0.52	0.95	53.82	47.61	6.22	0.40	0.1043	0.47	0.0504	-0.68	0.0018	-0.14	0.5850	-0.44	0.0656
BACT64	SNET2	-0.74	0.93	0.59	34.17	18.37	15.80	0.47	0.0481	0.68	0.0020	-0.26	0.3023	-0.02	0.9502	-0.48	0.0441
BACT644	SNET3	-0.83	0.57	0.86	41.90	35.26	6.63	0.29	0.2436	0.39	0.1142	-0.59	0.0098	-0.11	0.6626	-0.35	0.1594
BACT65	SNET3	-0.19	0.26	0.17	8.39	4.33	4.06	0.01	0.9608	0.30	0.2304	-0.12	0.6439	0.20	0.4150	0.00	0.9918
BACT66	SNET3	-0.81	0.46	0.86	38.27	34.01	4.26	0.21	0.3946	0.54	0.0221	-0.65	0.0034	-0.17	0.4961	-0.23	0.3585
BACT661	SNET1	0.91	-0.77	-0.87	43.90	43.85	0.05	-0.32	0.1893	-0.54	0.0201	0.49	0.0376	0.37	0.1305	0.41	0.0940
BACT67	SNET3	-0.91	0.57	0.94	54.55	46.45	8.10	0.35	0.1529	0.52	0.0281	-0.54	0.0200	-0.31	0.2069	-0.50	0.0355

ASV	Subtnet	SM1	SM2	SM3	kTotal	kIn	kOut	GS.Nit	p.Nit	GS. N2O	p. N2O	GS.NO3	p.NO3	GS.NH4	p.NH4	GS.Yld	p.Yld
BACT68	SNET1	0.79	-0.48	-0.80	27.11	26.88	0.23	-0.11	0.6759	-0.49	0.0369	0.48	0.0441	0.26	0.2925	0.38	0.1170
BACT7	SNET1	0.93	-0.67	-0.95	46.14	46.07	0.07	-0.35	0.1532	-0.44	0.0682	0.49	0.0374	0.30	0.2320	0.40	0.1011
BACT70	SNET3	-0.93	0.61	0.95	54.91	47.26	7.65	0.27	0.2840	0.65	0.0036	-0.73	0.0006	-0.25	0.3247	-0.48	0.0420
BACT71	SNET3	-0.78	0.42	0.84	36.70	32.85	3.85	0.31	0.2161	0.38	0.1191	-0.68	0.0017	0.04	0.8637	-0.40	0.0974
BACT72	SNET3	-0.83	0.78	0.75	38.53	25.48	13.05	0.08	0.7417	0.66	0.0029	-0.53	0.0232	-0.52	0.0263	-0.37	0.1325
BACT73	SNET3	-0.85	0.66	0.86	44.58	35.55	9.03	0.43	0.0767	0.41	0.0912	-0.55	0.0191	-0.01	0.9553	-0.34	0.1656
BACT736	SNET3	-0.09	0.00	0.17	5.18	3.67	1.52	0.32	0.1883	-0.32	0.1921	0.24	0.3319	0.00	0.9901	0.19	0.4606
BACT74	SNET2	-0.72	0.84	0.59	31.05	15.27	15.78	0.44	0.0679	0.40	0.1039	-0.19	0.4545	-0.13	0.6093	-0.50	0.0357
BACT75	SNET1	0.94	-0.88	-0.86	49.28	49.24	0.04	-0.52	0.0283	-0.63	0.0051	0.54	0.0209	0.21	0.4055	0.59	0.0102
BACT76	SNET2	-0.30	0.59	0.14	10.40	6.02	4.39	0.42	0.0798	0.43	0.0780	-0.10	0.7070	0.24	0.3293	-0.53	0.0243
BACT761	SNET3	-0.86	0.59	0.89	47.30	39.21	8.09	0.51	0.0305	0.36	0.1410	-0.45	0.0609	-0.24	0.3372	-0.49	0.0390
BACT77	SNET1	0.91	-0.86	-0.82	46.75	46.70	0.05	-0.38	0.1190	-0.72	0.0007	0.51	0.0304	0.24	0.3334	0.56	0.0152
BACT79	SNET3	-0.59	0.21	0.68	22.82	20.53	2.29	0.35	0.1598	0.18	0.4801	-0.20	0.4336	-0.16	0.5386	-0.33	0.1771
BACT8	SNET2	-0.92	0.84	0.83	51.92	16.67	35.25	0.46	0.0527	0.68	0.0018	-0.52	0.0261	-0.11	0.6732	-0.59	0.0096
BACT80	SNET3	-0.74	0.51	0.78	33.47	27.93	5.54	0.34	0.1715	0.26	0.2891	-0.53	0.0252	0.01	0.9751	-0.29	0.2501
BACT81	SNET1	0.96	-0.85	-0.90	51.84	51.79	0.04	-0.49	0.0397	-0.66	0.0032	0.54	0.0204	0.20	0.4326	0.53	0.0243
BACT82	SNET3	-0.92	0.73	0.89	52.67	39.76	12.91	0.49	0.0384	0.57	0.0134	-0.49	0.0374	-0.29	0.2516	-0.52	0.0255
BACT84	SNET1	0.93	-0.76	-0.89	45.34	45.28	0.07	-0.32	0.1933	-0.58	0.0120	0.51	0.0322	0.33	0.1848	0.51	0.0314
BACT86	SNET3	-0.59	0.04	0.74	26.19	25.12	1.07	0.16	0.5347	0.01	0.9588	-0.40	0.1018	-0.23	0.3537	-0.24	0.3321
BACT87	SNET1	0.92	-0.86	-0.84	47.60	47.55	0.05	-0.34	0.1724	-0.72	0.0007	0.49	0.0376	0.26	0.2981	0.59	0.0103
BACT88	SNET3	-0.86	0.51	0.89	44.69	39.05	5.63	0.29	0.2502	0.48	0.0435	-0.71	0.0010	-0.33	0.1846	-0.40	0.0983
BACT89	SNET3	-0.89	0.59	0.92	49.50	42.81	6.69	0.26	0.2963	0.53	0.0251	-0.70	0.0011	-0.33	0.1842	-0.45	0.0625
BACT9	SNET1	0.90	-0.55	-0.94	41.04	40.89	0.15	-0.29	0.2501	-0.55	0.0188	0.71	0.0009	0.09	0.7346	0.50	0.0367
BACT90	SNET1	0.13	0.01	-0.18	4.58	2.84	1.74	-0.17	0.4953	0.08	0.7463	0.57	0.0140	-0.41	0.0871	0.16	0.5255
BACT906	SNET3	-0.79	0.48	0.84	38.16	33.43	4.73	0.45	0.0579	0.46	0.0547	-0.55	0.0184	-0.09	0.7167	-0.34	0.1735
BACT91	SNET2	-0.77	0.83	0.66	32.51	13.42	19.09	0.43	0.0780	0.60	0.0087	-0.44	0.0658	0.01	0.9836	-0.46	0.0568
BACT92	SNET1	0.92	-0.86	-0.84	46.61	46.56	0.05	-0.44	0.0703	-0.69	0.0015	0.56	0.0151	0.22	0.3825	0.57	0.0142
BACT93	SNET2	-0.12	0.27	0.08	7.44	3.85	3.59	-0.07	0.7849	0.29	0.2432	-0.52	0.0269	-0.13	0.6082	0.11	0.6639

ASV	Subtnet	SM1	SM2	SM3	kTotal	kIn	kOut	GS.Nit	p.Nit	GS. N2O	p. N2O	GS.NO3	p.NO3	GS.NH4	p.NH4	GS.Yld	p.Yld
BACT94	SNET3	-0.94	0.72	0.92	55.34	44.11	11.22	0.43	0.0781	0.63	0.0051	-0.70	0.0011	-0.33	0.1743	-0.50	0.0339
BACT95	SNET3	-0.60	0.43	0.62	19.62	15.52	4.09	0.30	0.2281	0.35	0.1532	-0.34	0.1708	-0.12	0.6407	-0.30	0.2315
BACT97	SNET1	0.44	-0.09	-0.51	9.34	8.16	1.18	0.15	0.5638	-0.20	0.4246	0.63	0.0046	-0.03	0.9054	0.20	0.4359
BACT98	SNET1	0.37	0.01	-0.47	9.30	8.00	1.30	-0.16	0.5308	-0.05	0.8543	0.55	0.0180	-0.36	0.1375	0.24	0.3479
BACT99	SNET2	-0.41	0.63	0.26	15.49	8.95	6.55	-0.02	0.9346	0.71	0.0010	-0.47	0.0490	0.13	0.6172	-0.30	0.2247
BACT998	SNET3	-0.81	0.68	0.80	39.56	30.29	9.27	0.45	0.0627	0.51	0.0316	-0.38	0.1167	-0.19	0.4542	-0.46	0.0522
BACT998	SNET3	39.58	30.32	9.27	0.45	0.06	0.51	-0.38	0.1167	-0.19	0.4542	-0.46	0.0522				

Appendix C. Supplementary Data: sPLSR Pearson Correlation Coefficients

Pearson correlation coefficients between SELECTED prokarytic ASVs and sample traits as calculated from the sparse partial least squares regression (sPLSR) model. Sample traits considered include nitrification rates, delta N_2O values, N_2O yields from nitrification, and N_2O production rates from NO_3^- reduction and NH_4^+ oxidation. Taxonomic predictions are listed for each ASV down to the genus level where possible.

ASV	delta_N2O	NO3_NO2	Nitrification	O2Mol	NH4_Prod	NO3_Prod	N2O_yield	NH4Mol
ARCH13	0.6312117	0.51388252	0.26468712	0.05988359	0.00021736	-0.2026063	-0.3775083	-0.5738443
ARCH130	-0.0802682	0.23793646	0.06191115	0.60778523	-0.1854238	-0.3475255	-0.1145434	-0.0239759
ARCH22	0.04559037	0.33996773	0.11455126	0.6188474	-0.1851159	-0.3873909	-0.1895836	-0.1382575
ARCH28	-0.7369754	-0.8971373	-0.4026744	-0.6728711	0.18139265	0.60229436	0.60002402	0.76498378
ARCH30	0.3159634	0.11145819	0.08655755	-0.2658175	0.08921976	0.07800455	-0.1108384	-0.2406486
ARCH36	0.33429199	-0.0033378	0.05336705	-0.5272912	0.16852176	0.23178113	-0.0522762	-0.2158454
ARCH37	-0.7654518	-0.9050568	-0.4098056	-0.6446007	0.17205218	0.59264768	0.60887406	0.78599286
ARCH4	-0.2776672	-0.5758285	-0.2266544	-0.7360754	0.21371924	0.51963591	0.35353018	0.36424141
ARCH40	-0.7474058	-0.8902211	-0.4021929	-0.6425963	0.1719703	0.58667791	0.59800407	0.7695409
ARCH61	-0.0850116	0.22419045	0.05680736	0.58727888	-0.1793832	-0.3338372	-0.1064089	-0.0165039
ARCH65	-0.3088858	-0.1835928	-0.1081362	0.10842727	-0.0415995	0.01560083	0.14835522	0.25911488
ARCH7	0.22594832	-0.0966065	0.00633938	-0.5478452	0.17158001	0.27279009	0.01523486	-0.1157298
BACT10	0.70651269	0.88697809	0.39451407	0.6996896	-0.1903531	-0.610537	-0.5896523	-0.7419699
BACT104	0.30613093	0.63712107	0.25060235	0.81612522	-0.2370118	-0.5756909	-0.3909842	-0.4023037
BACT106	0.16530651	0.47682639	0.17716616	0.71014268	-0.2091568	-0.4743061	-0.2822965	-0.2596865
BACT109	0.58399907	0.32607883	0.19782128	-0.2476788	0.09150829	-0.0036075	-0.2692167	-0.4831755
BACT11	0.60207252	0.50377441	0.25675836	0.08474498	-0.0081153	-0.2100105	-0.367378	-0.5517056
BACT110	0.72733022	0.80402258	0.37176222	0.49894847	-0.1292755	-0.4942554	-0.548558	-0.7289599
BACT113	0.34442316	0.08410851	0.08257211	-0.3656273	0.12011177	0.13105002	-0.1007828	-0.2503726
BACT114	-0.0434344	-0.374576	-0.125106	-0.6924287	0.20734543	0.43145601	0.20778369	0.14792153
BACT121	-0.7144332	-0.8562676	-0.386126	-0.6250414	0.16763546	0.56734343	0.57447359	0.73729228
BACT124	-0.0544796	0.19589764	0.05286206	0.48232869	-0.1468827	-0.2782196	-0.0961829	-0.027271
BACT129	0.13745437	-0.1769676	-0.0333896	-0.5731154	0.17663323	0.31143075	0.07261759	-0.0326201

ASV	delta_N2O	NO3_NO2	Nitrification	O2Mol	NH4_Prod	NO3_Prod	N2O_yield	NH4Mol
BACT139	0.15842725	-0.1101326	-0.0089146	-0.4701556	0.14622211	0.24345237	0.03340453	-0.0675935
BACT15	0.72375993	0.88833626	0.3977497	0.67559022	-0.1825941	-0.6004623	-0.5931696	-0.7535953
BACT154	0.29381432	-0.0115076	0.0442033	-0.480842	0.15335759	0.21426907	-0.041351	-0.186969
BACT162	0.16463556	0.39024722	0.14977436	0.53550791	-0.1565655	-0.3681992	-0.2357848	-0.2315749
BACT1644	-0.7683346	-0.8561804	-0.3948731	-0.5409359	0.14073864	0.53052604	0.58314433	0.77223942
BACT167	-0.067837	0.23541937	0.06314162	0.58332145	-0.1776942	-0.3359611	-0.1152049	-0.0312375
BACT170	0.6226165	0.5395661	0.27138126	0.12538202	-0.0197634	-0.2400721	-0.3898836	-0.5764772
BACT180	0.57860795	0.50026894	0.25183397	0.11416811	-0.017658	-0.2216766	-0.3617043	-0.5353595
BACT19	0.70627964	0.90368203	0.39973983	0.73394676	-0.2006802	-0.6312554	-0.5985673	-0.7471583
BACT199	0.11730247	0.43484328	0.15612207	0.69969995	-0.2073993	-0.4553259	-0.2520314	-0.2151176
BACT2	0.70884916	0.88682445	0.39484601	0.69573978	-0.1890956	-0.6087567	-0.5899478	-0.7434368
BACT20	0.65624152	0.53346237	0.27493163	0.06064008	0.00071345	-0.2096588	-0.3920505	-0.5963444
BACT2043	0.3907856	0.22883199	0.13572423	-0.144156	0.05473214	-0.0155036	-0.1858475	-0.3267186
BACT211	-0.273748	-0.5989584	-0.2333051	-0.7891112	0.22981021	0.55077394	0.3652931	0.36909213
BACT220	0.26538516	0.613291	0.23646014	0.83121548	-0.2427365	-0.5741105	-0.3716223	-0.3682473
BACT241	-0.0909421	0.17748551	0.04112443	0.50174311	-0.1537862	-0.2803906	-0.0804176	0.00227407
BACT244	0.25065611	0.58722923	0.22584992	0.80126731	-0.2341403	-0.5520644	-0.355272	-0.3503591
BACT246	0.19466491	0.53299021	0.19964355	0.77839247	-0.2288686	-0.5234391	-0.3171464	-0.2966898
BACT25	0.78323673	0.68344595	0.34286738	0.16723332	-0.0277256	-0.307771	-0.4929751	-0.7266921
BACT257	0.46127694	0.28631569	0.1653135	-0.1372751	0.05469819	-0.0382471	-0.2280572	-0.3908338
BACT260	-0.7831298	-0.8729658	-0.4025709	-0.5519583	0.14363129	0.54110955	0.59453356	0.78720532
BACT291	0.18286319	0.47293119	0.17879674	0.67490175	-0.1980322	-0.4575546	-0.2830483	-0.2698333
BACT338	0.41468442	0.18892146	0.12703819	-0.2623515	0.09103112	0.04989578	-0.168322	-0.3294679
BACT36	0.12831113	-0.2081903	-0.0447168	-0.6222333	0.19116605	0.34363332	0.09083054	-0.0167066
BACT360	0.06763327	0.32260302	0.11266766	0.54928982	-0.1635233	-0.3510055	-0.1838417	-0.1470096
BACT430	0.14618746	0.42800203	0.15866841	0.64084207	-0.1888322	-0.4272331	-0.2530364	-0.2316733
BACT4625	0.43679263	0.22667276	0.14253323	-0.2201738	0.07896411	0.01848757	-0.1921309	-0.355881
BACT47	0.66256679	0.53529633	0.27653922	0.05451246	0.00274243	-0.2076082	-0.3940564	-0.6010349

ASV	delta_N2O	NO3_NO2	Nitrification	O2Mol	NH4_Prod	NO3_Prod	N2O_yield	NH4Mol
BACT5	0.62101161	0.87316144	0.37624163	0.80478577	-0.2244877	-0.6517625	-0.568419	-0.682074
BACT508	-0.3124722	0.02791806	-0.0420694	0.54319242	-0.172681	-0.2471746	0.03557318	0.19382976
BACT52	0.6633637	0.87857731	0.38484269	0.74982972	-0.2067065	-0.6295842	-0.5781713	-0.7112863
BACT54	-0.7247726	-0.8837611	-0.3964728	-0.6647298	0.17929295	0.59414137	0.59088128	0.75278985
BACT58	-0.1017148	-0.419582	-0.1487755	-0.6930042	0.20583303	0.44715807	0.24133096	0.20012474
BACT60	0.22982862	-0.1067667	0.00376938	-0.5745034	0.17972333	0.28793825	0.0200528	-0.1149997
BACT86	0.03917012	0.42152602	0.13920653	0.79433574	-0.2381694	-0.4921475	-0.2322575	-0.1601627
BACT94	0.64209863	0.8515783	0.37287313	0.72815687	-0.2007924	-0.6108359	-0.5602616	-0.6888574